DISSECTING THE MECHANISMS UNDERLYING ADOLESCENT-ONSET SCHIZOPHRENIA USING PATIENT-DERIVED CELLS



A THESIS SUBMITTED TO
MEDICAL SCIENCE DIVISION, UNIVERSITY OF OXFORD
FOR THE DEGREE OF
DOCTOR OF PHILOSOPHY

BY YICHEN LI

ST. ANNE'S COLLEGE
SUPERVISOR: PROF FRANCIS SZELE
DEPARTMENT OF PHYSIOLOGY, ANATOMY AND GENETICS
Michaelmas term, 2018

Copyright 2018

Yichen Li

All rights reserved

ABSTRACT

Schizophrenia is a complex mental disorder with unknown causes. It is widely accepted that the disease has a strong genetic basis and a root in neurodevelopment. To investigate the mechanisms at the cellular and molecular levels of schizophrenia, blood samples, nasal tissues and skin tissues from a cohort of patients with adolescent-onset schizophrenia and healthy controls were collected. Whole exome sequencing revealed genetic variants associated with multiple pathways including cell adhesion and postsynaptic signalling. Patient-derived primary olfactory ecto-mesenchymal stem cells had significantly reduced adhesion and elevated levels of stress responses. Total protein expression profiling showed significantly downregulated EIF signalling, mTOR pathway and cytoskeleton regulation, resulting in reduced global protein synthesis, impaired stress response and dysregulated cytoskeleton dynamics. These observations highly agreed with previously studies on adult-onset schizophrenia, suggesting common disease mechanisms. Induced neurons, reprogrammed from skin fibroblasts via induced pluripotent stem cells, did not reveal obvious differences on neurite outgrowth and spine morphologies. Further studies are required to investigate the synaptic signal transmission of the induced neurons. This study demonstrated the use of human-specific systems to study disease mechanisms and highlighted the potential to discover dynamic disease-associated cellular and molecular phenotypes, as well as some technical challenges.

ACKNOWLEDGEMENTS

I would like to express my great appreciation to my principal supervisor Prof Francis Szele for initiating this project and for giving me the freedom to explore in science with his guidance. My deep gratitude also goes to Prof Anthony James, who is always enthusiastic about schizophrenia research and has spent tremendous efforts to obtain the ethic approvals and to recruit the invaluable study cohort. I would also like to thank Dr Pablo Devesa for his professionalism in operating the biopsy-taking surgical procedures, Prof Alan MacKay-Sim for sharing his experiences on olfactory stem cells, Prof Alex Cristino for careful analysis of the proteomics data, Prof David Cotter and Dr Melanie Focking for their excellent skills on mass spectrometry, Prof Jenny Taylor, Dr Alistair Pagnamenta and Mr Vassilis Ragoussis for their great helps on the genetics part of this study. My great appreciation also goes to Dr Sally Cowley who kindly hosted me in the James Martin Stem Cell Facility and Dr Walther Haenseler who taught me everything on reprogramming. My gratitude also extends to Dr Justin Ichida, Prof Francois Feron, Dr Emmanuel Nivet, Mrs Sarah Noujaim, Dr Sarah Newey, Dr Hannah Sleven, Prof Zameel Cader, Prof Kevin Talbot, Prof Noel Buckley and Prof Caleb Webber for their generous advices on my study and insightful scientific discussions.

I would like to offer my special thanks to Dr Siqi Ying, Miss Liwen Tu, Miss Erhui Cai, Dr Bin Sun, Mr Jie Yin, Dr Nidaa Ababneh, Dr Mei Ki Wong and Dr Cecelia Heyne Lee for sharing memorable moments with me in Oxford. I would also like to express my appreciation to Mr Michael Chickering for the enlightening conversations. Last, my deepest gratitude goes to my parents: Mrs Guijun Chen and Mr Guoliang Li for always doing their best to protect my dreams.

TABLE OF CONTENTS

	Page
ABSTRACTS	i
ACKNOWLEDGEMENTS	ii
TABLE OF CONTENTS	iii
LIST OF FIGURES	viii
LIST OF TABLES	xi
LIST OF ABBREVIATIONS	xiii
GENERAL INTRODUCTION	1
The symptoms and the epidemiology of schizophrenia	1
The neuropathology of schizophrenia	3
The neurodevelopmental hypothesis of schizophrenia	7
The rationale of this study and the study outline	9
CHAPTER 1 PARTICIPANT RECRUITMENT AND WHOLE EXOME SEQUENCING	11
1.1 Summary	11
1.2 Introduction	12
1.2.1 Complex disease	12
1.2.2 Common variants	14
1.2.3 The 108 loci GWAS study	16
1.2.4 Why study rare variants?	18
1.2.5 How to study rare variants?	19
1.2.6 *De novo* mutations	20
1.3 Aims	22
1.4 My roles in the study and contributions from collaborators	25
1.5 Materials and methods	26
1.5.1 Participants	26
1.5.2 DNA extraction and whole exome sequencing	27

1.5.3 Analysis of whole exome sequencing data 27
1.6 Results 29
1.6.1 Biometric data of participants 29
1.6.2 Schizophrenia-associated mutations in coding regions of participants 34
1.6.3 Variants contributing to multiple cellular functions 36
1.6.4 Each patient carries multiple variants 43
1.7 Discussion 44

CHAPTER 2 A COMPARISON OF IN VITRO BEHAVIOURS OF AN ADULT STEM CELL POPULATION; OLFACTORY ECTO-MESENCHYMAL STEM CELLS, BETWEEN PATIENTS WITH ADOLESCENT-ONSET SCHIZOPHRENIA AND HEALTHY CONTROLS

2.1 Summary 52
2.2 Introduction 54
2.2.1 Adult niche stem cells 54
2.2.2 OE-MSCs in the nasal cavity are adult niche stem cells 56
2.2.3 *In vitro* characterisation of OE-MSCs 58
2.2.4 OE-MSCs in schizophrenia research 63
2.3 Aims 66
2.4 My roles in the study and contributions from collaborators 67
2.5 Materials and methods 68
2.5.1 Nasal biopsy processing and primary cultures 68
2.5.2 Population doubling time assay 70
2.5.3 EdU incorporation assay 71
2.5.4 Sphere formation assay 72
2.5.5 Live/dead staining 73
2.5.6 'Wound closure' assay 74
2.5.7 Cell-to-substrate adhesion assay 75
2.5.8 Oxidative stress assay 76
2.5.9 Neuronal differentiation 77
2.5.10 Immunocytochemistry and microscopy 79
2.5.11 Harvesting total protein for proteomics study 81

2.5.12 Statistics 82
2.6 Results 83
2.6.1 Banking of OE-MSCs 83
2.6.2 OE-MSCs from patients and controls express the same panel of cell identity markers 85
2.6.3 The proliferation rate of OE-MSCs remains the same between patients and controls 88
2.6.4 Similar sphere-formation ability between patient cells and control cells 93
2.6.5 Cell death rate remains the same between patient cells and control cells 98
2.6.6 No difference between patients and controls shown in 'wound-closure' assay 101
2.6.7 Patient cells have reduced cell-to-substrate adhesion ability 103
2.6.8 Patient cells are more prone to oxidative stress 106
2.6.9 OE-MSCs can obtain neuron-like morphology in neuronal differentiation media 110
2.6.10 Proteomic expression profiling showed EIF2 signalling was significantly downregulated in patient OE-MSCs 113
2.7 Discussion 123
2.7.1 Summary of OE-MSC cellular behaviours 124
2.7.2 Molecular signatures of OE-MSCs and their links with cellular behaviours of OE-MSCs 129

CHAPTER 3 PHENOTYPIC COMPARISON BETWEEN REPROGRAMMED NEURONS DERIVED FROM PATIENTS WITH ADOLESCENT-ONSET SCHIZOPHRENIA AND HEALTHY CONTROLS

3.1 Summary 134

3.2 Introduction 136

3.2.1 Induced pluripotent stem cells: discovery, characterisations and cautions 136

3.2.2 Reprogrammed neural cells: directed differentiation and direct conversion 141

3.2.3 Post-synaptic signalling, *SYNGAP1* and *SHANK2* 147

3.2.3.1 The post-synaptic density 149

3.2.3.2 *SYNGAP1* 152

3.2.3.3 *SHANK2* 155

3.3 Aims 158

3.4 My roles in the study and contributions from collaborators 159

3.5 Materials and methods 160

3.5.1 Skin biopsy processing and primary cultures 160

3.5.2 Reprogramming 161

3.5.3 Freezing and thawing of iPSCs 163

3.5.4 Flow cytometry 164

3.5.5 RNA extraction and qRT-PCR 165

3.5.6 DNA extraction and genome integrity assay 166

3.5.7 Generation of lentiviruses 167

3.5.8 Inducing neurons with *NGN2* overexpression 169

3.5.9 Immunocytochemistry and microscopy 171

3.6 Results 172

3.6.1 *SYNGAP1* and *SHANK2* variants in patient 002 172

3.6.2 Generation of induced pluripotent stem cells 176

3.6.3 Generation of cortical glutamatergic neurons 184

3.6.3.1 *NGN2* protocol optimisation 184

3.6.3.2 Live imaging of induced neurons 189

3.6.3.3 Staining of *NGN2*-neurons and RNA sequencing 194

3.7 Discussion 197
3.7.1 Technical challenges in cellular reprogramming 198
3.7.2 Biological meanings of the obtained data 201
3.7.3 Previous studies on schizophrenia using iPSCs 204
3.7.4 Suggestions for future research 213

GENERAL DISCUSSION 215
CONCLUSIONS 220
REFERENCE 222
Appendix I: Speculations on the links between basic stem cell properties and the cellular neuropathology of schizophrenia 260
Appendix II: Additional results for genomic integrity assay 273
Appendix III: short description of clinical phenotypes (from Anthony James) 275

LIST OF FIGURES

Figure Number	Figure title	Page number
Figure 1	The multi-hit model in the neurodevelopmental hypothesis of schizophrenia.	8
Figure 1.1	Relationship between risk allele frequency and strength of genetic effect (odds ratio).	13
Figure 1.2	Manhattan plot for the 108 risk loci identified in the largest schizophrenia GWAS study to date.	17
Figure 2.1	The anatomy of the olfactory system.	57
Figure 2.2	Transcriptomic comparison of OE-MSCs with hypothetical relevant cell types in identity.	61
Figure 2.3	The maintenance of a sustainable cell bank of OE-MSCs and a summary of assays done at the corresponding stages.	69
Figure 2.4	Primary cultures from lamina propria and the initial banking strategy.	84
Figure 2.5	Expression patterns of cell identity markers on OE-MSCs when cultured as monolayer	86
Figure 2.6	Expression patterns of cell identity markers on OE-MSCs when cultured as spheres	87
Figure 2.7	Comparison of population doubling time (PDT) between 9 controls and 10 patients (SZ).	90
Figure 2.8	Comparison of the percentage of dividing cells using Edu-incorporation as an index between 5 controls and 7 patients (SZ).	91
Figure 2.9	sphere formation of OE-MSCs in the presence of mitogen is dependent on the initial seeding density.	95

Figure 2.10	Comparison of sphere-formation ability from OE-MSCs derived from 4 controls and 7 patients.	96
Figure 2.11	Comparison of percentage of dead cells in OE-MSC cultures derived from 5 controls and 8 patients.	99
Figure 2.12	Comparison of the 'wound' closure time between 6 control lines and 10 patient lines.	102
Figure 2.13	Comparison of the cell-to-substrate adhesion ability for OE-MSCs derived from 5 controls and 7 patients.	105
Figure 2.14	Comparison of oxidative stress response from OE-MSCs from 7 patient lines and 8 control lines.	107
Figure 2.15	Morphological comparison of membrane blebbing from 9 patient lines and 8 control lines.	109
Figure 2.16	Morphological changes of OE-MSCs during neuron differentiation.	112
Figure 2.17	Principal component analysis of total proteins from 6 patients (blue) and 6 controls (red).	118
Figure 2.18	Implicated pathways and the directions of changes from Ingenuity Pathway Analysis (IPA) of total proteins from 5 patient samples and 5 control samples.	122
Figure 3.1	Schematic illustration of stages in directed differentiation of neurons, comparing to the *in vivo* developmental stages.	144
Figure 3.2	Simplified schematic illustration of the synapsis and the molecular composition of the postsynaptic density.	151
Figure 3.3	Illustration of the *SYNGAP1* variant in patient 002 at the gene and protein levels.	174
Figure 3.4	Illustration of the *SHANK2* variant in patient 002 at the transcript and protein levels.	175
Figure 3.5	Primary cultures from skin biopsies and the banking strategy.	177
Figure 3.6	Morphological changes along the generation of induced pluripotent stem cells.	181
Figure 3.7	Vast majority of cells in iPSC master stocks highly express pluripotency markers.	182

Figure 3.8	Genomic integrity test results.	183
Figure 3.9	Morphological changes during the neuronal conversions mediated by *NGN2-EGFP* overexpression in induced pluripotent stem cells.	192
Figure 3.10	Neurite tracing results showed significant longer neurites on converting neurons from patient line 002S-9 than from control line 011S-16.	193
Figure 3.11	Immunostaining characterisation of *NGN2*-neurons at day 28.	195
Figure 3.12	Immunostaining of synapsin and SynGAP on adult mouse brain whole-mount sections.	196
Figure II.1	Additional genomic integrity test results.	274

LIST OF TABLES

Table number	Table title	Page number
Table 1.1	Biometrics of patients with adolescent onset schizophrenia recruited between 2014-18.	31
Table 1.2	Biometrics of adolescent healthy controls recruited between 2014-18.	33
Table 1.3	Summaries of biomaterials taken/derived from participants from 2014-18.	35
Table 1.4	Summaries of candidate variants identified in participants.	37
Table 1.5	Summaries of the functions of genes with candidate variants identified in them.	39
Table 1.6	Summaries of WES analysis results.	42
Table 1.7	Recently published rare variant studies in schizophrenia with positive results	46
Table 2.1	Published OE-MSC studies on schizophrenia.	64
Table 2.2	Medium composition of 3 published OE-MSC neuronal differentiation protocols.	78
Table 2.3	Antibodies used in this study.	80
Table 2.4	Percentages of Edu-incorporated cells after 6h Edu pause.	92
Table 2.5	The numbers of spheres raised from single-cell plated OE-MSCs cultured for 6 and 8 days with mitogens.	97
Table 2.6	The numbers of live cells and dead cells present in OE-MSC cultures.	100

Table 2.7	A list of False Discovery Rate (FDR) positive proteins that were significantly differentially expressed between patient group and control group and their corresponding functions.	119
Table 2.8	Pathway analysis using Kyoto Encyclopedia of Genes and Genomes (KEGG) of differentially expressed proteins identified with mass spectrometry between OE-MSCs derived from 5 patients and 5 controls.	120
Table 2.9	Ingenuity pathway analysis (IPA) of differentially expressed proteins identified with mass spectrometry between OE-MSCs derived from 5 patients and 5 controls.	121
Table 3.1	Recent studies that characterised human iPSCs.	139
Table 3.2	Summaries of plasmids used in the *NGN2* protocol.	168
Table 3.3	Primary antibodies used in the iPSC study.	171
Table 3.4	Summaries of *SYNGAP1* and *SHANK2* variants in patient 002.	173
Table 3.5	Summaries of the status of all iPSC lines generated in this study.	179
Table 3.6	Ct values from qRT-PCR Sendai virus clearance assay.	180
Table 3.7	Nanodrop results of plasmids for making *NGN2*-neurons.	186
Table 3.8	The optimal plating densities for *NGN2* induction varies between iPSC lines.	187
Table 3.9	Summaries of testing results for key chemical compounds.	188
Table 3.10	Recent published studies on schizophrenia using iPSCs grouped according to major findings.	208

LIST OF ABBREVIATIONS

3'UTR	3 prime untranslated region
A1BG	Alpha-1B-glycoprotein
aCGH	Array comparative genomic hybridization
ADP	Adenosine diphosphate
ADPRHL2	ADP-Ribosylhydrolase Like 2
AFP	Alpha-fetoprotein
AHSG	Alpha-2-HS-glycoprotein
AJ	Prof. Anthony James
AMPA	α-amino-3-hydroxy-5-methyl-4-isoxazolepropionic acid
AMPAR	α-amino-3-hydroxy-5-methyl-4-isoxazolepropionic acid receptor
Ank	Ankyrin repeat domain
AOS	Adolescent-onset schizophrenia
AP2	Apetala 2
APOA1	Apolipoprotein A-I
AR	Androgen receptor
ASCL1	Achaete-Scute Family BHLH Transcription Factor 2
ASD	Autism spectrum disorder
ASPM	Abnormal Spindle Microtubule Assembly
ara-c	Cytarabine
ATR	ATR Serine/Threonine Kinase
ATRIP	ATR Interacting Protein
B3GAT1	Beta-1,3-Glucuronyltransferase 1
BAM	*BRN2, ASCL2, MYT1L*
BCL11B/CTIP2	B Cell CLL/Lymphoma 11B
BDNF	Brain-derived neurotrophic factor
bHLH	Basic helix-loop-helix
BMP	Bone Morphogenetic Protein

BMP2	Bone Morphogenetic Protein 2
βIII-tublin/Tuj1	Class III β-tubulin
BRS	Brain-specific regions
BSA	Bovine serum albumin
CADD	Combined Annotation Dependent Depletion
CaMKII	Ca^{2+}/calmodulin-dependent protein kinase II
CC	Coiled-coil
CCDC88C	Coiled-Coil Domain Containing 88C
CCR5	C-C Motif Chemokine Receptor 5 (Gene/Pseudogene)
CDK5	Cyclin-dependent kinase 5
CD105/ENG	Endoglin
CDH11	Cadherin 11
CES4A	Carboxylesterase 4A
c-Myc	MYC proto-oncogene
CNS	Central nervous system
CNV	Copy number variant
CNBP	Cellular nucleic acid-binding protein
CPZEQ	Chlorpromazine equivalents
CS	Citrate Synthase
CUX1	Homeobox Protein Cut-like 1
CYBRD1	Cytochrome B Reductase 1
DAB2	Disabled homolog 2
DAPI	4',6-diamidino-2-phenylindole
DCX	Doublecortin
DISC1	Disrupted in Schizophrenia 1
DLG	Discs large
DLG1	Discs large homolog 1
DLGAP	Disk large associated guanylate-associated proteins
DLST	Dihydrolipoamide S-Succinyltransferase
DMEM	Dulbecco's Modified Eagle Medium
DMSO	Dimethyl sulfoxide

DNA	Deoxyribonucleic acid
DPYD	Dihydropyrimidine Dehydrogenase
DSM-5	Diagnostic and Statistical Manual version IV
E14	Embryonic day 14
ECM	Extracellular matrix
Edu	5-ethynyl-2´-deoxyuridine
EDTA	Ethylenediaminetetraacetic acid
EGFP	Enhanced green fluorescent protein
EIF	Eukaryotic initiation factor
EIF2	Eukaryotic initiation factor 2
EM	Electron microscopy
ER	Endoplasmic reticulum
erB	Receptor Tyrosine-protein Kinase erbB
ExAC	Exome Aggregation Consortium
FACS	Fluorescence activated cell sorting
FBS	Fetal bovine serum
FDR	False positive discovery rate
FEZ1	Elongation protein zeta-1
FGF2	Fibroblast Growth Factor 2
FGF8	Fibroblast Growth Factor 8
FOXA2	Forkhead Box A2
FOXG1B	Forkhead Box G1B
FXR	Farnesoid X receptor
GC	Vitamin D-binding protein
GDNF	Glial cell-derived neurotrophic factor
GFAP	Glial fibrillary acidic protein
GFR	Growth factor reduced
GKAP/DLGAP1	Guanylate-kinase-associated protein
GlyA	Hematopoietic cells
gnomAD	Genome Aggregation Database
GTP	Guanosine triphosphate

GWAS	Genome-wide association study
H_2O_2	Hydrogen peroxide
H3K27	Histone H3 lysine (K)27
HBB	Haemoglobin subunit beta
HEK293T	Human embryonic kidney 293 (with large T antigen)
hESC	Human embryonic stem cell
Iba1	Ionized calcium binding adaptor molecule 1
ID	Intellectual disability
IgG	Immunoglobulin G
IgM	Immunoglobulin M
IPA	Ingenuity Pathway Analysis
iPSC	Induced pluripotent stem cell
ITIH2	Inter-alpha-trypsin inhibitor heavy chain H2
JAKMIP1	Janus Kinase And Microtubule Interacting Protein 1
K	Lysine
KEGG	Kyoto Encyclopedia of Genes and Genomes
Ki67	Marker Of Proliferation Ki-67
Klf4	KLF4 Kruppel like factor 4
KO-DMEM	Knocked-out DMEM
K-SADS-PL	Kiddie Schedule for Affective Disorders and Schizophrenia
LB	Lysogeny broth
lncRNA	long non-coding RNA
LTD	Long term depression
LTP	Long term potentiation
LLPS	Liquid-liquid phase transition
LoF	Loss-of-function
LXR	Liver X receptor
MAGUK	Membrane-associated guanylate kinase
MAP2	Microtubule associated protein 2
MAP5	Microtubule associated protein 5
MBP	Myelin basic protein

MDH2	Malate Dehydrogenase 2
MEF	Mouse embryonic fibroblast
MECP2	Methyl-CpG Binding Protein 2
miRNA	MicroRNA
MMP10	Matrix Metallopeptidase 10
MPD	Membrane proximal domain
MRI	Magnetic resonance imaging
mRNA	Messenger ribonucleic acid
mTOR	Mechanistic target of rapamycin
MYT1L	Myelin Transcription Factor 1 Like
N	Nasal
NAA	N-acetyl-aspartate
Nanog	Homeobox Protein NANOG
NEAA	Non-essential amino acids
NES	Nestin
NDS	Normal donkey serum
NG2	Nerve/glia antigen 2
NGFR	Nerve Growth Factor Receptor
NGN2	Neurogenin 2
NLGN4X	Neuroligin 4 X-Linked
NMDA	N-Methyl-D-aspartic acid
NMDAR	N-Methyl-D-aspartic acid receptor
NNAT	Neonatin
NPC	Neural progenitor cell
NT-3	Neurotrophin-3
NR4A2	Nuclear Receptor Subfamily 4 Group A Member 2
NRG1	Neuregulin-1
OE-MSC	Olfactory ecto-mesenchymal stem cell
Oct3/4	Octamer-binding transcription factor 3/4
oRG	Outer radial glia
OTX2	Orthodenticle Homeobox 2

P7	Postnatal day 7
PANSS	Positive and Negative Syndrome Scale
PARP	Poly (ADP-ribose) polymerase
PAX6	Paired Box 6
PAX7	Paired Box 7
pb	Polybrene
PBS	Phosphate-buffered saline
PCA	principle component analysis
PCDH12	Protocadherin 12
PDT	population doubling time
PDZ	PSD95/DLG/ZO1
PEI	Polyethylenimine
PFA	Paraformaldehyde
PGC	Psychiatrics Genomics Consortium
PH	Pleckstrin homology
Pik2	Phosphatidylinositol 3-kinase 2
PITX3	Paired Like Homeodomain 3
PCK2	Phosphoenolpyruvate Carboxykinase 2, Mitochondrial
PLD3	Phospholipase D Family Member 3
PLL	Poly-L-lysine
PO	Poly-ornithine
PolyPhen-2	Polymorphism Phenotyping v2
POC	Periosteal cells
POU3F2/*BRN2*	POU Domain, Class 3, Transcription Factor 2
P/S	Penicillin-Streptomycin
PSD	Postsynaptic density
qRT-PCR	Quantitative reverse transcription polymerase chain reaction
RA	Retinoid Acid
Ri	ROCK inhibitor
SDHB	Succinate Dehydrogenase Complex Iron Sulfur Subunit B
SERPINF1	Serpin Family F Member 1

SIFT	Sorting Intolerant From Tolerant
SLCO1B7	Solute Carrier Organic Anion Transporter Family Member 1B7 (Putative)
RM-ANOVA	Repeated-measures analysis of variance
RNA	Ribonucleic acid
ROS	Reactive oxygen species
RPL7	Ribosomal Protein L7
RPS3A	Ribosomal Protein S3A
RPS6	Ribosomal Protein S6
RPS27L	Ribosomal Protein S27 Like
rtTA3	Reverse tetracycline-controlled transactivator 3
RXR	Retinoid X receptor
S	Skin
SAM	Sterile alpha motif
SATB2	DNA-binding Protein SATB2
SED1A	SET Domain Containing 1A
SGZ	Subgranular zone
SH3	Src homology
SHANK2	SH3 And Multiple Ankyrin Repeat Domains 2
SHH	Sonic Hedgehog
SNP	Single nucleotide polymorphism
Sox2	SRY (sex determining region Y)-box 2
SRY	Sex determining region Y
SVZ	Subventricular zone
SZ	Schizophrenia
SFb	Synovial fibroblasts
SGA	Second generation antipsychotic
SMAD	Mothers Against DPP Homolog 1
SNV	Single nucleotide variant
SYNGAP1	Synaptic Ras GTPase Activating Protein 1
TBR2	T-box Brain Protein 2

TCA	Tricarboxylic acid
TEAB	Triethylamonium bicarbonat
TGFβ	Transforming Growth Factor Beta
TP53	Cellular tumor antigen p53
TRE	Tet response element
vGlut1	Vascular Glutamate Transporter 1
VTN	Vitronectin
WARS	Tryptophanyl-TRNA Synthetase
WASI	The Wechsler Abbreviated Scale of Intelligence
WES	Whole exome sequencing
WNT	Wingless/Integrated
XCI	X-chromosome inactivation
XIST	X-inactive specific transcript
ZIC1	Zic Family Member 1
ZO1	Zonula Occludens-1
ZSCAN4	Zinc Finger And SCAN Domain Containing 4
ZSCAN10	Zinc Finger And SCAN Domain Containing 10

GENERAL INTRODUCTION

The symptoms and the epidemiology of schizophrenia

Schizophrenia is a severe mental disorder characterised by recurrent episodes of psychoses which hamper normal abilities to perceive and process information. Symptoms and duration of episodes vary among patients. In general, the disease causes positive symptoms such as delusions and hallucinations, negative symptoms such as concentration and motivation deficiencies, social withdrawals and a lack of emotions and cognitive impairments such as memory problems (American Psychiatric Association, 2013). Disability and mortality rate in patients with schizophrenia is substantially higher than in the general population (Drake & Cotton, 1986). Schizophrenia usually appears during late adolescence and young adulthood but can also manifest earlier. Patients with childhood-onset and adolescent-onset schizophrenia (AOS) generally suffer from more severe symptoms (Rapoport, Judith L., Addington, Frangou, & Psych, 2005; White, Ho, Ward, O'Leary, & Andreasen, 2006). Current medications for schizophrenia alleviate the positive symptoms but do not stop or reverse the disease; symptoms from about two-thirds of the patients remain persistent or fluctuating for decades (American Psychiatric Association, 2013).

Epidemiologic studies of schizophrenia have contributed to the understanding of the complex mental disorder by analysing the distribution patterns of the disease within populations and associating them with risk factors. Schizophrenia was estimated to affect 1% of the total population across the world (American Psychiatric Association, 2013) . Systematic review of large bodies of epidemiologic data showed the risks of getting schizophrenia were associated with factors including viral infections during pregnancy, advanced paternal age, cannabis use, economic status, urbanicity and social migration (Messias, Chen, & Eaton, 2007; Saha, Chant, Welham, & McGrath, 2005).

The neuropathology of schizophrenia

The most consistently reported brain structural change in schizophrenia is reduced brain volume and enlarged ventricles (Rapoport, J. L., Giedd, & Gogtay, 2012). Structural changes of the brain on macroscopic levels are best revealed by imaging of live patients and healthy individuals. To rule out the impact from prolonged disease duration and antipsychotic medication, as well as to understand the neurodevelopmental process involved in schizophrenia, neuroimaging studies have focused on young patients, non-psychotic siblings, ultra-high-risk groups and prenatal scans, using both cross-sectional and longitudinal designs.

Brain volume reduction was observed in both young patients and old patients. Cross-sectional neuroimaging studies reported that a reduction in the cortical thickness was already present in children with prodromal symptoms (Rapoport et al., 2012). Longitudinal imaging studies found young patients with psychosis reached a significant volume loss in prefrontal lobes and parietal lobes by age 20 (Greenstein et al., 2006), providing evidence for the continuity in the biological basis of schizophrenia from childhood-onset forms to adult illness. Similar to the developmental abnormalities observed in grey matter, a tensor based imaging study reported that the white matter of patients with childhood-onset schizophrenia had significantly reduced growth during their adolescence (Gogtay et al., 2008). Therefore, the brain volume reduction is rooted early in the disease process, before the onset of symptoms, and involves reductions in both the grey matter thickness and the white matter connectivity.

Brain volume reduction was also observed in unaffected siblings. Studying unaffected siblings offers a valuable comparison to the observed abnormal brain development in patients. The unaffected siblings share great similarity at the genetic levels with patients, yet remain asymptomatic (although some can exhibit mild cognitive impairments) and are untreated. In a longitudinal study, patients with childhood-onset schizophrenia and their unaffected siblings showed reduced grey matter thickness in temporal and prefrontal regions at age of 10, when compared to matched controls (Gogtay et al., 2007). In this study, the unaffected siblings gradually 'normalised' these reductions and showed no difference with healthy controls by the age of 17, while the brain abnormalities persisted in the patient group (Gogtay et al., 2007). This observation was replicated by another longitudinal study using healthy siblings of patients with childhood-onset schizophrenia and matched controls (Mattai et al., 2011). The connectivities within several regions of the white matter, including left inferior frontal gyrus and bilateral cingulate, were also found to be reduced in healthy siblings of patients with schizophrenia (Hao et al., 2009; Hoptman et al., 2008). Interestingly, grey matter thinning was generally not observed in the unaffected siblings from patients with adult-onset schizophrenia. Taken together, these data suggest brain volume reduction in schizophrenia is linked to family/genetic factors. Patients with early onset, and their unaffected siblings are more likely to carry genetic insults that lead to reduced volumes of prefrontal and temporal regions. The mechanisms underlying the ability to 'normalise' brain deficits of the unaffected siblings remain unclear. However, it is well known that adolescence is a critical period for neuroplasticity. For patients with early onset, whether the genetic variants (and their interactions with environments) that lead to the failure of neuroplasticity during adolescence, or the primary genetic insults *per se* that lead to the brain volume reduction in the first place played a greater role in the disease aetiology remains to be elucidated. Future longitudinal

studies combining high power neuroimaging methods and detailed genetic and environmental profiling may help to disentangle the remaining problems.

Brain structural abnormalities were observed in clinically defined ultra-high-risk individuals who later converted to psychosis. Reduced white matter connectivity was also observed in ultra-high-risk individuals who later developed psychosis (Walterfang et al., 2008). For the grey matter volumes, a longitudinal study using T2 images did not reveal any significant grey matter changes for ultra-high-risk individuals who later developed psychosis (converters) compared to ultra-high-risk individuals who did not develop psychosis (non-converters) (Pantelis et al., 2003). A more recent longitudinal study using higher resolution T1 images, allowing the detection of sub-voxel level changes, reported significantly greater prefrontal grey matter surface retractions for converters compared to non-converters around the time of psychosis onsets (Sun, D. et al., 2009). The authors correlated nicely regional brain surface retractions with regional brain volume reductions. The differences reported in this study were all below the size of a single voxel that was routinely used in conventional magnetic resonance imaging (MRI) studies, which explained the negative results obtained for converters and non-converters from previous studies. These results suggested that brain structure changes, especially the reduction of prefrontal lobe volumes, were present during the transition phases of the illness.

Surprisingly, genetically defined high-risk male infants but not female infants, born from mothers with schizophrenia or schizoaffective disorders, had increased total brain volumes (including grey matter thickness, ventricle size and cerebrospinal fluid volume) in the first 2 years after birth (Gilmore, Schmitt et al., 2010; Gilmore, Kang et al., 2010). This counterintuitive evidence suggested that the widely observed brain volume reductions in schizophrenia could be contributed to by gene and environment interactions, as no enlarged brain volumes were reported in male or female patients, who had apparently passed the infant phases (Rapoport et al., 2012). All this evidence together shows that psychosis-related brain volume abnormalities are likely to reflect the true disease processes, rather than to be merely a result of prolonged exposure to psychoses and antipsychotic medications.

The neurodevelopmental hypothesis of schizophrenia

About 30 years ago, the prototype of the neurodevelopmental hypothesis of schizophrenia was formulated to speculate the aetiology of the disease (Murray, R. M. & Lewis, 1987; Weinberger, 1987). This model initially postulated that brain developmental deficits during pregnancy manifested into clinical symptoms which emerged later in life. Multiple lines of evidence supported the neurodevelopmental model (*Chapter 2 Discussion*). However, the initial model suggested a 'single-hit' accounting for the disease aetiology which could not explain the dynamic changes involved in the disease processes such as the longitudinal brain volume changes in patients (McGrath, Féron, Burne, Mackay-Sim, & Eyles, 2003; Velakoulis, Wood, McGorry, & Pantelis, 2000). As a result, the '2-hit' model was formulated and it described that the first hit that happened during pregnancy made the brain vulnerable to a second hit that happened later in life (Mednick, Machon, Huttunen, & Bonett, 1988). However, with more studies addressing the 2-hit model, it was found that the model still could not fully explain the heterogeneity in the longitudinal changes (Gogtay, Vyas, Testa, Wood, & Pantelis, 2011; Pantelis et al., 2005). Recently, a multi-hit model (Figure 1) has been introduced which proposes that: multiple hits at various developmental stages synergise in individuals who are genetically primed and culminate into the(McGrath, Féron et al. 2003, Velakoulis, Wood et al. 2000) clinical features of schizophrenia (Davis et al., 2016; Murray, Robin M., Bhavsar, Tripoli, & Howes, 2017). Among multiple lines of research, the strongest evidence for neurodevelopmental hypothesis came from the largest schizophrenia genome-wide association study (GWAS) to date, pointing at many processes involved in the development of the brain. The genetics of schizophrenia will be elaborated in *Chapter 1*.

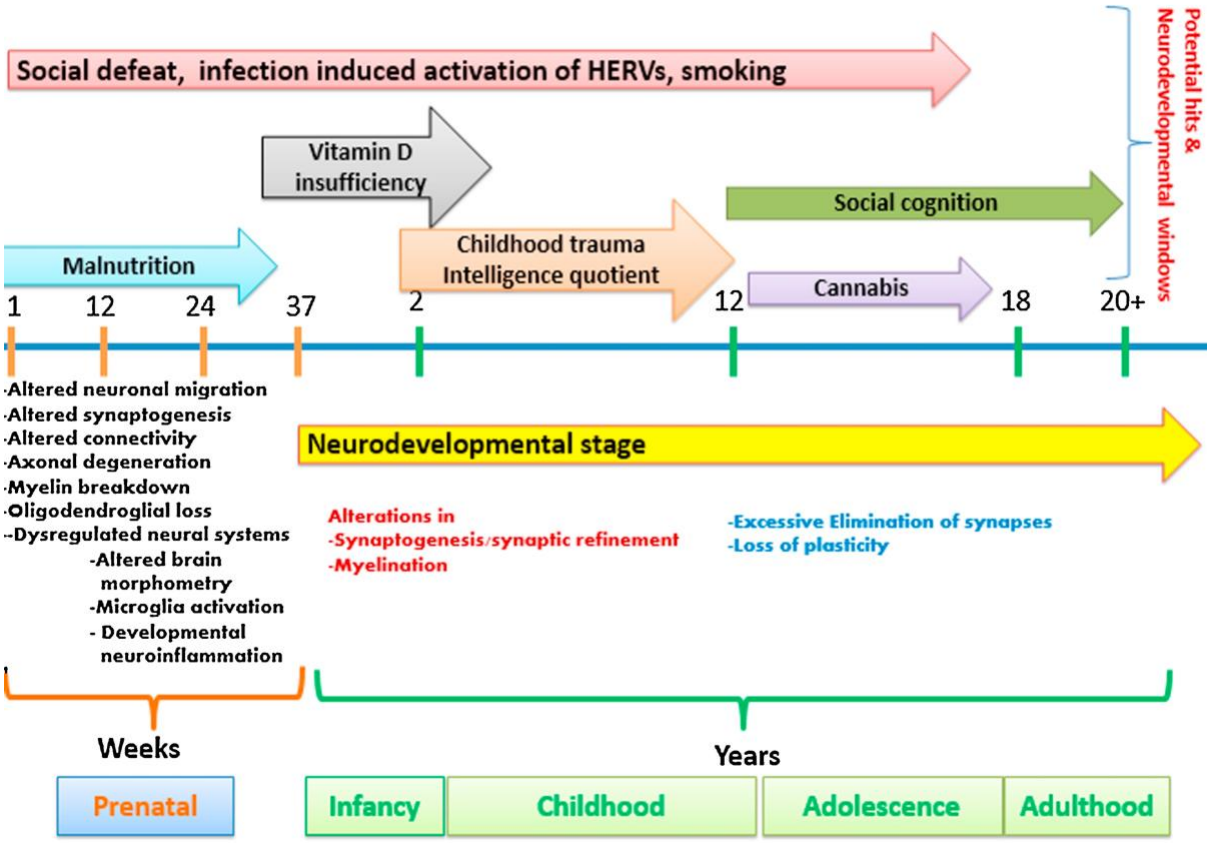


Figure 1. The multi-hit model in the neurodevelopmental hypothesis of schizophrenia. Along the neurodevelopment window, multiple hits falling at different developmental stages may interact with the corresponding biological developmental milestones and together with the first genetic hits that the patient carries, manifest into clinical features of schizophrenia. Figure adapted from (Davis et al., 2016).

The rationale of this study and the study outline

Despite decades of research on multiple levels that keep updating the hypotheses for the aetiology of schizophrenia, the disease mechanisms still remain unknown. It is difficult to replicate polygenic genetic predispositions in animal models and post-mortem studies cannot reveal dynamic pathological changes. In the present study, a group of adolescent-onset schizophrenia patients were recruited to study the disease mechanisms. The young onset age ought to enrich the cohort with genetic components and clinical severity. The patients recruited to this study do not suffer from prolonged untreated psychosis or prolonged antipsychotic medication, hence reducing possible confounding effects from disease durations or medications. Whole exome sequencing was performed to identify candidate variants that impact on protein functions (*Chapter 1*). The results from sequencing studies were used to select patients in which the disease was likely to be caused by protein loss-of-function. Those patients will be prioritised for future cell biology studies.

The olfactory functions in patients with schizophrenia are often impaired (Moberg et al., 1999; Nguyen, Shenton, & Levitt, 2010). In the present study, a type of adult stem cell in the nasal cavity whose roles are to replace olfactory sensory neurons were isolated. A series of cellular behaviours and the protein expression profiles of the adult nasal stem cells are carried out to look for cellular and molecular phenotypes that could be common disease mechanisms (*Chapter 2*). Based on sequencing results in *Chapter 1*, a small group of patients and controls were reprogrammed to obtain induced stem cells. The conversion of induced stem cells to induced neurons ought to reveal dynamic processes of neurite development and synaptic maturation. This is aiming at precise dissection of the disease mechanisms, as oppose to

common disease mechanisms in *Chapter 2*. By using patient-derived induced neurons, I hope to discover gene-associated developmental abnormalities and study the phenotypes with gene editing. A general discussion and a conclusion is carried out at the end of the thesis to evaluate the research approaches and data obtained in this study.

CHAPTER 1 PARTICIPANT RECRUITMENT AND WHOLE EXOME SEQUENCING

1.1 Summary

Schizophrenia has a strong genetic basis. The studies of the genetic basis for schizophrenia have applied GWAS to address common variants and deoxyribonucleic acid (DNA) sequencing or customised arrays to address rare variants. The trio study design is particularly useful to identify strong *de novo* disease-associating variants. Studying the functions of such variants would help to reveal the biological mechanisms behind schizophrenia. Parents of the patients were included when no family histories of schizophrenia were present in order to identity rare and possibly disease-associating *de novo* variants in patients. Only probands but not the parents were included when family histories of schizophrenia were present. WES was applied on DNA derived from blood cells to prioritise the study with coding regions of the genomes. Results of WES aalysis showed that the candidate variants identified from each patient were unique, in a way that no single candidate variant was over-represented by more than one patient. However, candidate variants appeared in genes involved in 'post-synaptic signalling' and 'cytoskeleton interactors and adhesion molecules' were recurrent in patients. This was in line with previous literatures on schizophrenia. However, the study was limited as the studied cohort was relatively small, the non-coding regions were not included in the sequencing and only the DNA from one type of tissues was used for sequencing.

1.2 Introduction

1.2.1 Complex disease

Schizophrenia is a complex disease in which the risk has been linked to more than 100 genomic loci and to various environmental factors. Although the inheritability of schizophrenia is high, the transmission patterns over generations do not follow a Mendelian model. This makes it difficult to identify the genetic elements that contribute to the observed strong inheritability. Studies of the genetic origins of schizophrenia can either address common variants with relatively weak effects but in aggregate increase the disease risks, or address rare variants with relatively strong individual effects (Figure 1.1). These rare variants with strong effects can be difficult to find due to their negative selections in the evolution. However, they can enlighten us on the possible mechanisms underlying the disease more directly. In recent decades, genomics approaches, which involve interpreting genetic information on the whole genome/exome levels, have been developed for both types of studies. In this chapter, I will introduce these approaches and discuss how the results have helped the field to start unravelling the aetiology of such a complex mental disorder.

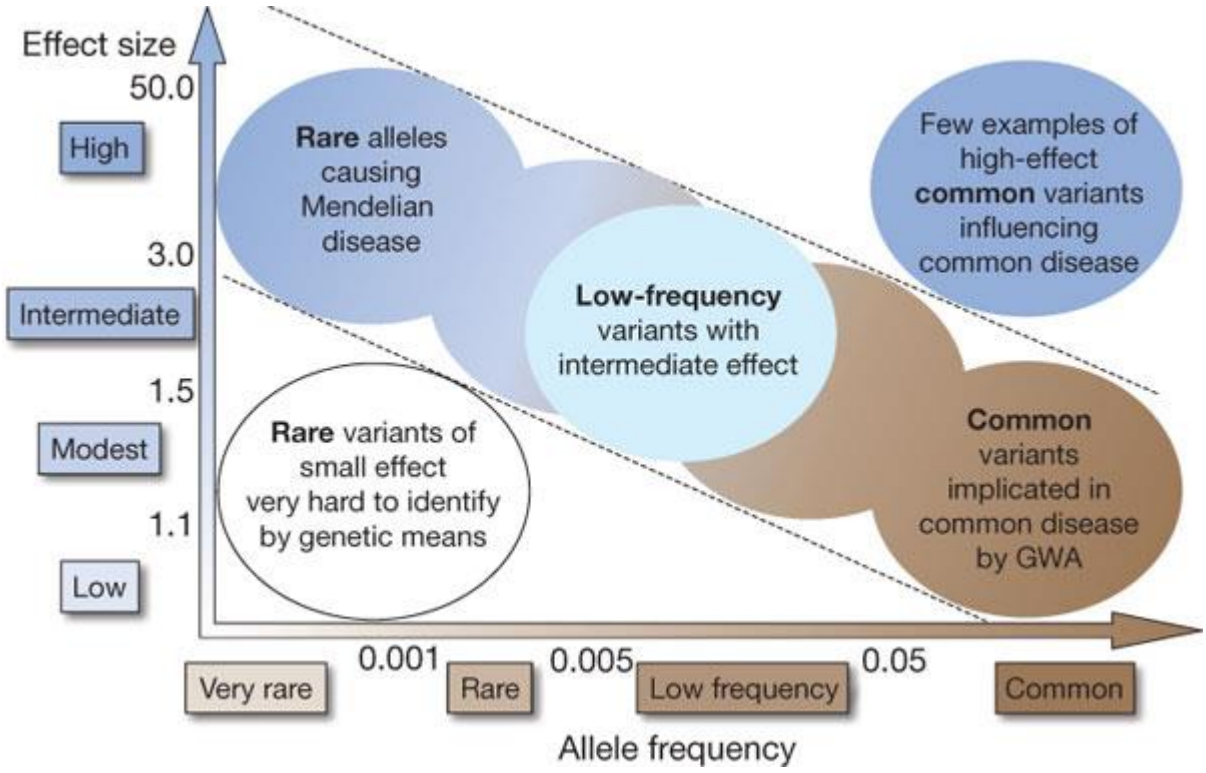


Figure 1.1 Relationship between risk allele frequency and strength of genetic effect (odds ratio). X-axis shows the allele frequencies of the genetic variants in the general population and y-axis shows the estimated effect sizes of the genetic variants. Extremely rare alleles of large effect sizes would result in inheritance patterns seen in Mendelian diseases. Common variants that collectively show modest effect sizes cause inheritance patterns seen in complex diseases and could be identified with genome-wide association studies (GWAS). Common variants with large effect sizes are generally very rare, possibly due to evolutionary negative selection power. Less common variants and rare variants with intermediate effect sizes contribute to complex diseases and could be studied with DNA sequencing. Rare variants with very small effect sizes are in turn very difficult to detect. Figure adapted from (Manolio et al., 2009).

1.2.2 Common variants

GWAS, which are based on the common-disease/common-variant (minor allele frequency > 1%) hypothesis, have shed light on the genetic architectures of schizophrenia. Common variants are estimated to explain one third to one half of the genetic liability of schizophrenia (Purcell et al., 2014). Before GWAS became available, identification of disease-linked genes was done with family linkage studies, karyotyping and candidate gene testing. For example, this led to the heralded discoveries of 22q11.2 chromosomal region and the Disrupted in Schizophrenia 1 (*DISC1*) gene, as risk candidates for schizophrenia (Dahoun, Trossbach, Brandon, Korth, & Howes, 2017; Ishizuka, Paek, Kamiya, & Sawa, 2006). However, a collection of 'schizophrenia genes' were later tested using a genotyping approach and no significant association was found (Sanders et al., 2008). The failure of replicating disease-associated risk variants in schizophrenia has reflected both the heterogeneity of the disease and the lack of power in assays that were used. Instead, the GWAS developed later have increased the coverage of sequencing from only targeted genes to the entire characterised portions of the genome by increasing the amount of single nucleotide polymorphism (SNP) tags. Meanwhile, the sample sizes also increased from a few thousands to dozens of thousands. Indeed, GWAS in 2009 using 3,000 cases resulted in the first identification of genomic locus that surpassed whole genome level significance (International Schizophrenia Consortium, 2009), and this number grew to 108 in 2014 using 36,989 cases and 113,075 controls, as the largest schizophrenia GWAS study to date (Schizophrenia Working Group of the Psychiatric Genomics Consortium, 2014). In 2018, 145 loci have been linked to schizophrenia risk based on a meta-analysis combining datasets from CLOZUK (individuals who were prescribed clozapine in UK) and the Psychiatrics Genomics Consortium (PGC) (together 105,318; 40,675 cases and 64,643

controls) (Pardiñas et al., 2018). The large numbers of associated risk loci identified emphasised the complexity and the heterogeneity of the disease, but studying pathways that the loci converge is likely to shed lights on convergent mechanisms of various and distinct genetic risks.

1.2.3 The 108 loci GWAS study

GWAS are a category of experimental designs in human genetics to address the common variants that statistically associate with a disease or a trait. Genome-wide genotype data are usually obtained from cohorts with large sample sizes, as the statistical power, directly related to the sample sizes, is the key limiting factor of identifying associated loci. The largest schizophrenia GWAS to date used data from 36,989 cases and 113.075 controls, identified 108 genomic loci as associated with schizophrenia (Figure 1.2) (International Schizophrenia Consortium, 2009). In this study, arrays containing SNPs and insertion-deletions identified from the 1000 Genomes Project were used. About 9.5 million variants were included in association testing in each case after quality control steps. From the results, glutamatergic neurotransmission, voltage-gated calcium channels, the immune system as well as the development of forebrain were re-confirmed as playing important roles (Schizophrenia Working Group of the Psychiatric Genomics Consortium, 2014). However, the majority of the significant loci were non-coding, including many known regulatory regions that were specifically active in the brain. This suggests the regulatory elements in brain development as a new direction of schizophrenia research.

Although the goal of GWAS is to understand the underlying biology and pave the ways to better treatments, the path from GWAS to disease mechanisms is not straightforward. First, showing the associations between genomic loci and disease status does not inform us on the process of how the affected genes manifest into diseases. Second, GWAS only cover what are already known as common variants in human genomes, which itself is likely to be population-sensitive and our knowledge on SNPs in the human genomes are also likely to evolve overtime.

Thirdly, the SNP-based and array-based GWAS are not purposed for detecting CNVs hence may miss important disease-associated CNVs due to the lack of SNP tags in those CNVs (although it is possible to call some CNVs from GWAS data). Last, GWAS are designed to specifically address common variants hence inevitably will miss rare variants whose importance in schizophrenia will be discussed in next subchapter. Overall, GWAS provide valuable knowledge on the possible disease mechanisms by associating common variants with schizophrenia, however it still has its limitations.

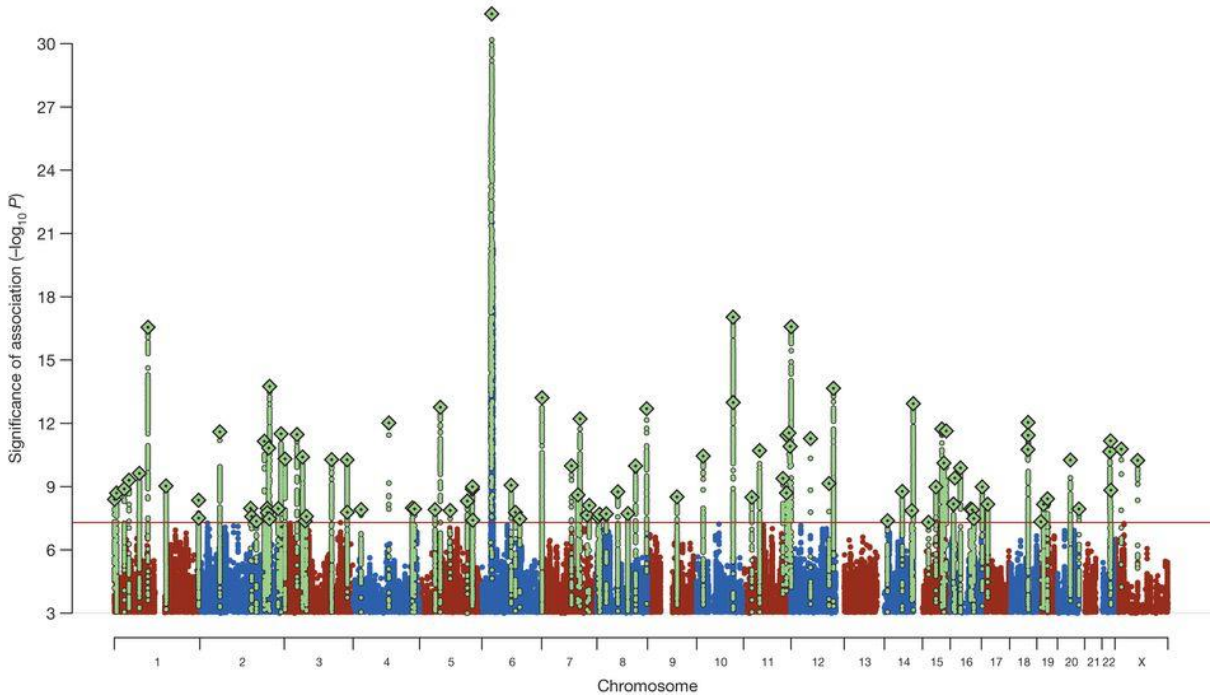


Figure 1.2 Manhattan plot for the 108 risk loci identified in the largest schizophrenia GWAS study to date. The highest signal comes from MHC regions and the four major implicated pathways are the immune system, forebrain development, glutamatergic neurotransmission and calcium channels. Figure adapted from (Schizophrenia Working Group of the Psychiatric Genomics Consortium, 2014).

1.2.4 Why study rare variants?

While the role of common variants is becoming more and more well characterised, there is still an unexplained fraction of the heritability observed in schizophrenia and other complex diseases (Loh et al., 2015; Maher, 2008). Therefore, the impact of rare variants needs to be addressed in addition to that of the common ones. Although common and rare is on a continuum rather than on two separated ends, the rare variants addressed in research usually have a minor allele frequency <1% (Auer & Lettre, 2015). Indeed, a growing body of evidence shows that rare variants can possess substantial individual risks with odds ratios of 2-60 (Fromer et al., 2014; Kirov et al., 2012; Rees et al., 2014; Singh et al., 2016; Zhu, Need, Petrovski, & Goldstein, 2014). This is much greater than that of common variants, which individually only have small effects with a median odd ratio of 1.08 in the 108 loci study (Ripke et al., 2014). Moreover, it is challenging to dissect out contributions from individual genes and pathways from the long list of loci identified via GWAS, and even more difficult to accurately find the sequence of biological events that manifests into the disease. The hope of finding rare variants with high disease penetrance is built on the possibility of pinpointing particular genes and pathways with clarity and genetically modifying such genes in *in vitro* and *in vivo* models to study them. Therefore, rare variants offer unique opportunities to study the biological mechanisms of the disease aetiology.

1.2.5 How to study rare variants?

Rare variants are usually not included in genotyping arrays so require specialised methods for analysis. GWAS may detect some of the 'common' rare variants on the spectrum of rareness, but will miss the extremely rare ones and the private ones due to the lack of specific tags for rare variants. Therefore, DNA sequencing approaches and customised arrays have been used to detect rare variants. Sequencing the whole genome at deep depth (>20x) can be very costly and is carried out the expense of sample size if the budget is limited. It was shown that sequencing more individuals at lower depth, compared to sequencing fewer samples at high coverage, gave stronger statistical power when looking for genetic associations (Li, D., Lewinger, Gauderman, Murcray, & Conti, 2011). For example, the 1000 Genomes Project built a human genome database by including data collected from 2,500 participants worldwide and performing whole genome sequencing at relatively low depth (<10x) (1000 Genomes Project Consortium, 2010; 1000 Genomes Project Consortium, 2012). This resulted in a haplotype map that contained 38 million SNPs and 1.4 million short insertion-deletions, and enabled analysis of common and relatively rare variants in individuals from diverse populations. Sequencing the whole exome will cut the cost down significantly but will inevitably miss non-coding information. This could be of particular concern given that a few studies have implicated long non-coding ribonucleic acids (lncRNAs) in neuropsychiatric disorders (Ng, Lin, Soh, & Stanton, 2013; Qureshi, Mattick, & Mehler, 2010). Nevertheless, the dilemma of reading depth versus sample size should always be considered based on the particular research question to be asked.

1.2.6 De novo variants

One powerful way to look for such disease-causing rare variants is to sequence the genomes of the affected individuals as well as the unaffected parents in a trio study. Variants that are only present in the proband but not in the parents are called *de novo* variants. In schizophrenia, these variants are usually random germline variants that have not yet been exposed to evolution long enough to be excluded. As the genetic background is highly similar between proband and parents, other than the *de novo* putative candidate variants, this method may allow smaller sample sizes than case control studies.

Duplications, deletions and insertions that involve genomic sequences longer than 1 kb and shorter than 500 kb are defined as copy number variants (CNVs). Methods to detect CNVs include chromosomal arrays and CNV calling from next-generation sequencing data. Similar as SNPs, a given CNV can be common or rare and the effects range from adaptive traits to disease-causing. The identification of putative disease-causing CNVs requires knowledge on CNVs present in healthy parents, siblings and control populations. Profiling of non-pathogenic CNVs at whole genome levels were first described more than 10 years ago and continued to grow (Conrad et al., 2010; Iafrate et al., 2004; Redon et al., 2006; Sebat et al., 2004; Zarrei et al, 2015) . To date, CNVs were estimated to take up 4.8-9.7% of the human genome in healthy populations (Zarrei et al., 2015) . CNVs could contribute to diseases by overlapping with genes hence disrupting the presence or the sequences of genes or overlapping with regulatory elements that affect the expression levels of genes. In schizophrenia, the largest systematic survey (6882 cases and 6316 controls, array-based) revealed 11 most strongly disease-associated CNVs and they were all >500 kb and spanned multiple regions (Kirov et al., 2012;

Rees et al., 2014). Each of the 11 strongly disease-associated CNVs, except for the *NRXN1* locus, contained a few dozens of genes whose roles remained unclear in schizophrenia. Exonic deletions in *NRXN1* have long been associated with schizophrenia (Kirov et al., 2007; Kirov et al., 2009; Levinson et al., 2011; Rujescu et al., 2008) . The gene encodes for a presynaptic adhesion molecule which act as the ligand for the post-synaptic neuroligins. The exact mechanisms by which *NRXN1* deletions increase the risks of schizophrenia remain unknown. Rodent models suggested impaired neurotransmitter release and reduced synaptic calcium channel functions being implicated in the *NRXN1* deletion pathophysiology (Etherton et al., 2009; Grayton et al., 2013; Missler et al., 2003). The identification of rare disease-associated CNVs can lead to downstream identifications of disease-associated genes and regulatory elements. However, the large size of currently identified risk CNVs and great numbers of genes involved remains as a bottle neck for CNV-linked disease mechanism studies.

Structural polymorphisms that only involves one nucleotide are termed single nucleotide variants (SNVs). The rate of ultra-rare disruptive SNVs is higher in patients compared to in controls in genes that are intolerant for loss-of-function (LoF) mutations as indicated in Exome Aggregation Consortium (ExAC) database (Fromer et al., 2014; Genovese et al., 2016; Zhu et al., 2014). No individual SNVs have been robustly associated with schizophrenia so far (Rees et al., 2014).

Other ways of studying rare variance include extreme phenotype sampling which works best when the studied phenotype follows a normal distribution (Kryukov, Shpunt, Stamatoyannopoulos, & Sunyaev, 2009; Li et al., 2011), and population isolation studies which requires historically isolated populations (Hatzikotoulas, Gilly, & Zeggini, 2014).

We do not yet know how much of schizophrenia is caused by common versus rare variants but it is more and more widely accepted that both contribute to the disease. There are also emerging literatures on pathways that are affected by both common variants and rare variants in schizophrenia (Pocklington et al., 2015; Singh et al., 2016). In the following chapters of this thesis, I will discuss some of those pathways and their possible roles in the patients that I study.

1.3 Aims

The primary aim of the study, that this chapter was part of, was to identify novel genetic variants that could potentially be risk candidates for schizophrenia. WES ought to be performed to enable functional interpretation of candidate genetic risk variants and to reduce the costs of DNA sequencing. The aims of performing WES on DNA were to identify *de novo* variants when there were no family histories of psychiatric disorders. In this case, DNA from patients with AOS as and DNA from both parents of the patients were sequenced. In the case of patients with family histories of psychiatric disorders, only DNA from patients were sequenced in order to identify rare variants that could potentially be risk factors for schizophrenia. The criteria used for identifying novel genetic variants were: 1) the candidate variants being rare (minor allele frequency <1% in genomAD or ExAC; 2) the candidate variants being likely deleterious to the functions of the encoded proteins based on *in silico* predictions and 3) the candidate variants being localised to genes that encodes for proteins that were likely to play roles in neurodevelopment.

The most relevant aims of the above study to my cell biology study was to select participants for cellular reprogramming and to understand the heterogeneity of the cohort in the perspective of the potential genetic risk factors that each individual patient carries. To this end, the likely impacts of identified candidate risk variants on the functions of their encoded proteins were predicted using *in silico* tools and summarised together with the functions of encoded proteins in tables. Therefore, the aims of analysing the identified candidate variants were to: 1) prioritise participants who carry rare genetic variants in genes play key roles in neurodevelopment as to be included in the cell biology studies, especially the cellular

reprogramming study given the time-consuming nature of cellular reprogramming; 2) understand the heterogeneity of potential genetic risk factors in the cohort so that patients with candidate variants that were likely to affect similar cellular pathways could be grouped together in assays that address the corresponding likely affected cellular pathways.

1.4 My roles in the study and contributions from collaborators

My role in this part of the study was to collect information on the biometrics and genetic variants from various collaborators, to summarise and document the information, to interpret the possible biological impacts on neurodevelopment based on the genes that they were localised to and their *in silico* prediction results, and finally to determine which patients to be included in future cell biology studies when the number of cell lines derived from patients that could be handled at a time is limited.

The recruitment of this cohort and the collection of blood cells was done at the Highfield Adolescent Inpatient Unit at Warneford Hospital by Anthony James. WES sequencing on DNA isolated from blood cells, as well as all downstream analysis was done by the Jenny Taylor lab at the Welcome Trust Centre for Human Genetics. A list of genes that candidate risk variants were identified in was kept updated by the Jenny Taylor lab and shared with me to discuss the possible functional impacts. The checking of candidate variants' minor allele frequencies on genomAD/ExAC and the *in silico* predictions were both done by the Jenny Taylor lab and by myself independently.

1.5 Materials and methods

1.5.1 Participants

Patients were diagnosed according to DSM-V-criteria. To determine the diagnosis of psychosis, the level of intelligence and cognitive functioning, participants were screened with the structured psychiatric interview (K-SADS-PL) (Kaufman et al., 1997) and the psychometric interview (The Wechsler Abbreviated Scale of Intelligence, WASI) (Wechsler, 1999) at the Highfield Unit, Warneford Hospital, Oxford. Control subjects who showed emotional, behavioural or psychiatric disorders were excluded. Participants with any of the following conditions were also excluded: infectious or other nasal conditions, coagulopathies, known systemic medical diseases and infections, neurological disorders including significant head injury, learning disability, substance abuse or poor understanding of English. All eligible participants, or in the case of younger participants (<18 years old) their parents, gave signed consent for participation in the study. The study was approved by the South Central-Oxford A Research Ethics Committee. Patients without family histories of schizophrenia and their parents, as well as adolescent healthy controls and their parents were included in the WES study. Patients with family histories of schizophrenia and their parents, except for patient 002 who I included in the WES study due to the presence of high risk variants, will be included in the next phase of the WES study.

1.5.2 DNA extraction and whole exome sequencing

The DNA extraction and WES were carried out by the laboratory of my collaborator Prof. Jenny Taylor (Wellcome Trust Centre for Human Genetics). The quality of DNA was assessed with Nanodrop. Briefly, the WES was performed using HiSeq4000 (Illumina) and the SeqCap EZ Human Exome Library v3.0 (NimbleGen) was used. In total, 64 Mb reads with 75 bp pair-end were generated, covering over 80% of the total exonic regions at 10x. The initial processing of the WES data was carried out by the laboratory of Prof. Jenny Taylor. Briefly, the 64Mb reads were mapped to reference human genomes, applying methods that allowed detection of variants even if they cover less than 50% reads for a gene therefore revealing the haplotypes of the samples. The Integrated Genome Viewer was applied to compare data from proband with data from parents. *De novo* variants were identified when the variants only present in the probands but not in parents.

1.5.3 Analysis of WES data

The Ingenuity Variant Analysis (IVA) was carried out to estimate the biological impacts of the previously identified variants based on available databases that were embedded in the software. Several filters were applied in this analysis. The first filter selected genes variants that were successfully mapped onto the reference exonic regions. The second layer kept variants that had higher than 10x read depth and greater than 20% allele ratio. The third filter revealed variants that were reported in 1000G, NHLBI exomes, ExAC and gnomAD as with less than 1% minor allele frequency, therefore reporting rare variants. The next layer further categorised the filtered variants into three groups; *de novo*, compound heterozygous (both copies of a gene were affected and one copy was inherited from each parent) and homozygous (both copies of a gene had the same mutations). Finally, the filter 'Biological Context' was applied which selected for genes that are associated with certain phenotypes or key terms based on the Ingenuity Knowledge Base. The key terms used in this analysis were 'schizophrenia', 'dendritic spine morphology', 'dendritic spine maturation', 'adhesion of neuronal cells', 'neocortical neuron excitation', 'microglia abnormalities', 'synaptogenesis of pyramidal cells', 'synaptogenesis of brain cells', and 'mTOR signalling pathway'. In an

additional analysis, the terms 'autism', 'intellectual disability' and 'epilepsy' were applied, however made no difference to the filtered results. *In silico* predictions were performed for all variants that passed the above-mentioned filters. The above-mentioned steps were carried out by the laboratory of Prof. Jenny Taylor. CADD scores (indicating how deleterious the variants are), SIFT and PolyPhen-2 (predicting impacts on protein functions) were calculated using corresponding online tools, the pLI scores for loss-of-function variants and the z-scores for missense variants were collected from ExAC database (*in silico* predictions of the candidate variants identified in *SYNGAP1* and *SHANK2*, collection of their allele frequencies in GenomAD/ExAC and all genes' pLI scores and z-scores were done by me, detailed information on other variants were not available at the time). The pLI scores and z-scores were computed by ExAC, which includes collected exome sequencing data from 60,706 individuals. The pLI scores were used to indicate a gene's tolerance of LoF mutations, with higher scores indicating higher intolerance. The z-scores showed the deviation of observed variant counts from the expected number, with positive z-scores indicating higher intolerance to variation (the gene had less variants than expected) and negative z-scores indicating lower intolerance to variation (the gene had more variants than expected). The sources for the *in silico* online tools are:

CADD: https://cadd.gs.washington.edu

SIFT: https://sift.bii.a-star.edu.sg

PolyPhen-2: http://genetics.bwh.harvard.edu/pph2/

1.6 Results

1.6.1 Biometric data of participants

Between years 2014 to 2018, 17 patients were recruited; they were 7 males and 10 females, averaging 16.61 ± 1.56 (standard deviation) years at the time of recruitment, 14.78 ± 2.19 years old at onset, with a 0.46 ± 0.28 years untreated period and 1.37 ± 1.70 years of medication history (Table 1.1). Ten healthy control subjects were recruited; 4 males and 6 females, average age of 14.92 ± 2.08 years at recruitment (Table 1.2). The control subjects were neurologically healthy and without any obvious signs of illness for their general condition. No significant difference of gender ratio or age was seen between patients and controls. All participants were recruited at the Highfield Adolescent Inpatient Unit at Warneford Hospital, Oxford, UK. A Semi-structured diagnostic instrument; Kiddie Schedule for Affective Disorders and Schizophrenia (K-SADS-PL) was used for psychiatric evaluation of all participants (Kaufman et al., 1997) by my collaborator the experienced adolescent psychiatrist Prof. Anthony James (AJ). The Positive and Negative Syndrome Scale (PANSS) has seven items. One to seven points can be given to each item so that in total 7 is the minimal score for no symptoms and 49 is the maximum score (Kay, Flszbein, & Opfer, 1987). As expected, the positive symptom scores (patient=20.00 ± 3.66, control=7.00 ± 0.00) and negative symptoms scores (patient=14.41 ± 3.39, control=7.00 ± 0.00) were both significantly higher (p<0.0001) in patients than in controls (Table 1.1 & Table 1.2). Disregarding the fact that a few patients and controls were not tested for IQ yet, the average IQ so far for patients was 88.00 ± 12.90, which was significantly lower (p<0.0001) than 120.00 ± 4.24 from controls (Table 1.1 & Table 1.2). As indicated by the high positive and high negative scores, as well as

their cognitive impairments, the patients were considered by the psychiatrist (AJ) as severely ill and clustered on the severe end of the spectrum of clinical phenotypes. All patients were receiving second generation antipsychotics (SGAs) at the time of recruitment (medication history at recruitment=1.37 ± 1.70 years) with an average dosage in chlorpromazine equivalents (CPZEQ) of 304.20 ± 81.30 mg (Leucht et al., 2015). Some treatment-resistant patients were receiving clozapine (Table 1.1). Although the vast majority of the patients were experiencing their first episode of psychosis, the duration of illness varied from 0.59 years to 7.59 years (average=1.83 ± 1.71 years). The duration of untreated psychosis varied from none to 1 year (average=0.46 ± 0.28 year). A short description of the clinical phenotypes was obatined from the psychiatrist Antony James and shown as Appendix III.

Table 1.1 Biometrics of patients with adolescent onset schizophrenia recruited between 2014-18.

Patient ID (n=17)	Sex	Age at recruitment (years)	Age at onset (years)	Un-treated (years)	Medicated (years)	Medication (mg)	CPZEQ	Positive symptom score	Negative symptom score	IQ
001	male	18.98	15.50	1.00	2.48	clozapine 350	275	19	20	84
002	male	17.09	16.50	0.00	0.59	clozapine 300	236	19	14	98
003	female	18.35	16.90	0.45	1.00	clozapine 300	236	16	17	87
004	female	17.97	16.50	0.50	0.97	clozapine 350, aripiprazole 200	840	23	18	77
005	female	17.31	16.50	0.30	0.51	risperidone 2 fluoxetine 20	194	20	9	100
006	female	15.56	15.00	0.20	0.36	risperidone 50	200	23	11	101
007	female	15.39	14.50	0.20	0.69	clozapine 150 olanzapine 5	291	23	13	85
009	female	17.28	16.00	0.20	1.08	aripiprazole 15 sertraline 150	416	23	11	94
015	male	14.87	13.30	0.30	1.27	aripiprazole 5 amisulpride 700	475	10	16	75
017	male	17.71	16.70	0.80	0.21	clozapine 375 sertraline 150	295	22	14	70

Patient ID (n=17)	Sex	Age at recruitment (years)	Age at onset (years)	Un-treated (years)	Medicated (years)	Medication (mg)	CPZEQ	Positive symptom score	Negative symptom score	IQ
018	female	16.92	16.02	0.40	0.50	clozapine 400 sertraline 150	313	21	11	106
019	male	17.76	16.60	0.90	0.26	clozapine 300	236	21	14	100
020	male	16.59	9.00	0.20	7.39	clozapine 450 aripiprazole 10	356	15	15	67
025	female	14.01	12.50	0.50	1.01	clozapine 250	196	23	21	N/A
026	male	14.99	12.00	0.80	2.19	clozapine 250	196	20	13	N/A
027	female	13.75	12.75	0.50	0.50	olanzapine 20	400	18	17	N/A
028	female	17.82	15.00	0.60	2.22	clozapine 550	432	24	11	N/A

*N/A means data not collected

Table 1.2 Biometrics of adolescent healthy controls recruited between 2014-18.

Control ID	Sex	Age at recruitment (years)	Positive symptom score	Negative symptom score	IQ
010	female	17.81	7	7	121
011	male	17.98	7	7	112
012	female	17.10	7	7	122
013	male	12.83	7	7	125
014	male	14.86	7	7	122
016	female	14.42	7	7	117
021	female	14.75	7	7	N/A*
022	female	14.50	7	7	N/A
023	female	12.50	7	7	121
024	male	12.49	7	7	N/A

*N/A means data not collecte

1.6.2 Variants identified in the coding regions of participants

In order to identify potential schizophrenia-associated rare genetic variants that could affect protein functions in patients, WES using DNA extracted from whole blood samples were performed. I collaborated with Prof. Jenny Taylor (Wellcome Trust Centre for Human Genetics) who carried out the WES sequencing. Analysis of the WES data was carried out by her group and myself. As summarised in Table 1.3, out of the 17 patients, 3 had family history of schizophrenia (001, 002 & 007) hence were initially recruited as singletons, 2 still needed to be surveyed (015 & 017), and the remaining 12 were without family history of schizophrenia and were recruited together with their parents as trios, to look for *de novo* variants. Blood samples were taken from all participants except for patients 015 and 017 and controls 010 and 012, as well as their parents, whose appointments for blood-taking have not been settled. Blood was sampled from all parents in trios. Patient 002 was recruited as a singleton due to family history but become a trio later on, as mutations that affect glutamatergic post-synaptic signalling were identified in him and the source of inheritance was confirmed with blood samples from both parents. Glutamatergic postsynaptic signalling is implicated in schizophrenia by both common variant studies and rare variant studies (Hall, J., Trent, Thomas, O'Donovan, & Owen, 2015). In total, blood samples from 15 patients (including 13 trios) and 8 controls (all trios) were processed for whole exome sequencing. Because non-coding regions of the genomes were not sequenced, from here on 'variants' will refer to variants in the protein coding regions.

Table 1.3 Summaries of biomaterials taken/derived from participants from 2014-18.

Patient ID (n=17)	Status	Family history	Blood from parents	Proband blood	Proband nasal biopsy	Proband skin biopsy	Proband iPSCs
001	Singleton	Yes	None	Yes	Yes	Yes	Yes
002	Trio	Yes	Yes	Yes	Yes	Yes	Yes
003	Trio	No	Yes	Yes	Yes	Yes	No
004	Trio	No	Yes	Yes	Yes	Yes	No
005	Trio	No	Yes	Yes	Yes	Yes	No
006	Trio	No	Yes	Yes	Yes	Yes	No
007	Singleton	Yes	None	Yes	Yes	Yes	Yes
009	Trio	No	Yes	Yes	Yes	Yes	No
015	NA	NA	None	No	Yes	Yes	No
017	NA	NA	None	No	No	Yes	No
018	Trio	No	Yes	Yes	Yes	Yes	No
019	Trio	No	Yes	Yes	Yes	Yes	No
020	Trio	No	Yes	Yes	Yes	Yes	No
025	Trio	No	Yes	Yes	No	No	No
026	Trio	No	Yes	Yes	No	No	No
027	Trio	No	Yes	Yes	No	No	No
028	Trio	No	Yes	Yes	No	No	No
control ID (n=10)							
010	NA	No	None	No	Yes	Yes	Yes
011	Trio	No	Yes	Yes	Yes	Yes	Yes
012	NA	No	None	No	Yes	No	No
013	Trio	No	Yes	Yes	Yes	No	No
014	Trio	No	Yes	Yes	Yes	Yes	Yes
016	Trio	No	Yes	Yes	Yes	Yes	No
021	Trio	No	Yes	Yes	Yes	Yes	No
022	Trio	No	Yes	Yes	Yes	Yes	No
023	Trio	No	Yes	Yes	Yes	Yes	No
024	Trio	No	Yes	Yes	No	Yes	No

1.6.3 Variants contributing to multiple cellular functions

As expected for a polygenic complex disease, candidate variants in multiple genes and pathways were identified in the patient cohort. In the sequencing data analysis pipeline, several layers of filters were applied (*Materials and Methods*) to rule out common variants and to annotate the candidate variants with biological meanings. A candidate variant should fit at least one of the following criteria: having a low allele frequency (<1%) in the general population based on the Genome Aggregation Database (gnomAD); being predicted *in silico* as damaging the function of the encoded protein by Sorting Intolerant From Tolerant (SIFT) and Polymorphism Phenotyping v2 (PolyPhen-2); having a relatively high Combined Annotation Dependent Depletion (CADD) score (>20). A CADD score higher than 20 indicates that a variant is within the top 1% of all deleterious variants and a CADD score higher than 30 indicates for top 0.1% of the deleterious variants. Some variants that satisfied the above criteria but were inherited from a healthy parent were considered as secondary candidate variants (shown in grey shading of the gene symbol e.g. SETD1A in Table 1.4-1.6). Those variants are very likely to have low penetrance as they did not lead to any noticeable clinical phenotypes in the neurologically healthy parents. Table 1.4 shows the candidate variants identified in patients, with the criteria that were used to define primary candidate variants (genes' names in black) and secondary candidate variants (genes' names in grey). Table 1.5 shows the functions of the genes in which candidate variants were identified and categorises them according to the cellular functions they most directly contribute to. Interestingly, 'adhesion molecule- and cytoskeleton-related functions' appeared to be the largest functional group among this cohort. Moreover, this group was made up of primary candidate variants only.

Table 1.4 Summaries of candidate variants identified in participants.

Patient ID	Candidate genes	mRNA	protein	Genotype	Transmission	Type	Frequency on gnomAD	SIFT	PolyPhen	CADD	pLI	z-score
002	*SYNGAP1*	2752G>A	A918T	heterozygous	father	missense	not found	tolerated	probably damaging	23.5		5.60
	SHANK2	1229C>T	T411M	heterozygous	mother	missense	0.0001934	damaging	probably damaging	28.9		2.32
004	*AR*	2533T>G	C845G	heterozygous	*de novo*	missense	not found	tolerated	benign	23.4		1.23
	SETD1A	1364_1366 del AAG	E455del	N/A	dominant	frameshift	N/A	N/A	N/A	11.26	1	
	DPYD	1257G>A	W419*	N/A	dominant	N/A	N/A	N/A	N/A	40	0	
005	*ATRIP*	1277C>T	T426I	heterozygous	*de novo*	missense	not found	tolerated	benign	22.8		1.05
006	*JAKMIP1*	1908G>T	L636F	heterozygous	*de novo*	missense	not found	damaging	probably damaging	26.5		2.89
	MECP2	587C>G	T196S	N/A	(x-linked)	N/A	0.041	N/A	N/A	N/A		
018	*CCR5*	569_575del GGAAGAA	W190fs*5	heterozygous	*de novo*	frameshift	-	-	-	-	0	
	ADPRHL2	491A>G	Y164C	heterozygous	mother	missense	0.048%	N/A	N/A	N/A		0.35
019	*CDH11*	2309A>G	D770G	heterozygous	*de novo*	3'UTR exonic	0 homo count 0.001% freq	tolerated	benign	24.8		1.59
020	*CYBRD1*	215C>T	P72L	heterozygous	mother	missense	0.001%	N/A	N/A			0.59
025	*PCDH12*	2389G>A	D797N	homozygous	both	missense	0 homo count 0.002% freq	tolerated	benign	20.9		0.78

	CCDC88C	3895C>T	R1299C	homozygous	both	missense	8 homo count 0.439% freq	damaging	probably damaging	34		0.71
026	*MMP10*	1340A>G	Y447C	compound heterozygous	father	missense	0 homo count 0% freq	damaging	probably damaging	25.5		-1.08
		frameshift	D130fs*5		mother	frameshift	0 homo count 0.04% freq	-	-	33	0	
027	*NLGN4X*	1573A>C	T526P	heterozygous	*de novo*	missense	N/A	damaging	probably damaging	21.7		2.7
	SLCO1B7	40A>G	I14V	compound heterozygous	father	missense	1 homo count 0.034% freq	damaging	probably damaging	18.2		-0.96
		493T>A	G137E		mother	missense	2 homo count 0.124% freq	damaging	probably damaging	24.2		

Note that patient 001 and 002 were not included due to the presence of family histories of schizophrenia. *'N/A' means not updated from collaborators. **'-'means not done due to frameshifts.

Table 1.5 Summaries of the functions of genes with candidate variants identified in them.

Gene (patient)	Protein Function
	Post-synaptic signalling:
SYNGAP1 (002)	synaptic Ras GTPase-activating protein 1, binds with PSD-95, a member of the NMDAR complex, transduces Ras signaling, intracellular Ca^{2+} signaling, negatively regulates Ras, Rap and AMPAR trafficking to the postsynaptic membrane, helps regulating synapse adaptions and promotes proper brain wiring
SHANK2 (002)	scaffolding protein at PSD of excitatory synapses, contains multiple domains for protein-protein interaction, binds with GKAP1/3 and Homer1, interconnects receptors at PSD including NMDA-type and metabotropic glutamate receptors, interacts with actin-based cytoskeleton, may play a role in the structural and functional organization of the dendritic spine and synaptic junction
	Cytoskeleton interactor and adhesion molecules:
JAKMIP1 (006)	Janus Kinase And Microtubule Interacting Protein 1, interacts with JAK1 and TYK2, may regulate microtubule cytoskeleton rearrangements, may regulate the transport of GABA-B receptor in a microtubule-dependent manner
CDH11 (019)	Cadherin 11, a type II cadherin, lacks HAV cell adhesion recognition sequence as to type I, facilitates Ca^{2+}dependent cell-cell adhesion, mostly interacts with each other in a homophilic way in connecting cells and hence may be used to sort heterogeneous cells.
PCDH12 (025)	Protocadherin 12, belongs to a subfamily of cadherins, a cellular adhesion molecule with un-determined function, may promote homotypic Ca^{2+}dependent aggregation at intercellular junctions, mouse ortholog show no impact on cell migration or growth, does not bind with catenins, interacts with cytoskeleton only weakly (by similarity)
MMP10 (026)	Matrix Metallopeptidase 10, breaks down extracellular matrix, a zinc-dependent endopeptidase, the major proteases for ECM degradation, involved in cancer metastasis (are FDA approved drug targets)
NLGN4X (027)	Neuroligin 4, X-Linked, a neuronal cell surface protein, may involve in cell-cell interactions, may interact with neurexins in a Ca^{2+}dependent way, may interact with DLG4/PSD-95, may regulate the development of synapses

	Epigenetic regulators:
SETD1A (004)	Histone methyltransferase, methylates Lys-4 of histone H3, regulates epigenetic transcriptional activation, contributes to epigenetic control of chromatin structure and gene expression
MECP2 (006)	Methyl-CpG Binding Protein 2, binds to methylated DNA, mediates transcription regression, essential for embryonic development, subject to X inactivation, dispensable in stem cells, mutations in *MECP2* can cause Rett syndrome
	DNA damage reponsors:
ATRIP (005)	ATR interacting protein, essential checkpoint signalling after DNA damage, may stabilise ATR (a DNA damage sensor, a serine/threonine kinase)
ADPRHL2 (018)	Poly(ADP-ribose) glycohydrolase ARH3, degrades PAR chain formed by poly(ADP-ribosome) poly (ADP-ribose) polymerase (=PARP) is expressed in cells under stress and/or DNA damage, over-activation of PARP can deplete ATP hence lead to cell death, mediates post-translational modification of regulators of DNA methylation, associates with parental imprinting, after attaching poly ADP-ribose chains it may directly regulate the amount of DNA methylation, some PARPs can help to maintain telomerase, mediates vesicular trafficking, participates in mitotic spindle assembly. PARP polymerises ADP-ribose to form a chain after detecting single-strand DNA breaks, this chain (called PAR chain) recruits other DNA-repairing enzymes to work on the DNA damage, after repairing, the PAR chain is degraded by Poly(ADP-ribose) glycohydrolase ARH3
	Ion metabolism:
SLCO1B7 (027)	Solute Carrier Organic Anion Transporter Family Member 1B7 (Putative), associates with Bile secretion pathway, linked to schizophrenia
CYBRD1 (020)	Cytochrome B Reductase 1, an iron-regulated protein, may regulate dietary iron absorption, linked to schizophrenia

	Others:
AR (004)	Androgen receptor, stimulates transcription of androgen responsive genes, expansion of polyglutamine repeats at the N-terminal causes spinal bulbar muscular atrophy, isoform 3 and isoform 4 can active gene transcription independently of steroid hormones, related Gene Ontology includes *DNA binding transcription factory activity and chromatin binding*
CCR5 (018)	C-C Motif Chemokine Receptor 5, a member of the beta chemokine receptor family (structurally similar to G protein-coupled receptor), expressed in T cells and macrophages, mediates some virus to enter immune cells, may regulate granulocytic lineage proliferation and differentiation, a co-receptor of CD4 for HIV-1
DPYD (004)	Dihydropyrimidine Dehydrogenase, a pyrimidine catabolic enzyme, regulates the initiation and the rate of uracil and thymidine catabolism, cancer patients who carry mutation in *DPYD* have higher risk of toxicity when receiving chemo drug F-fluorouracil
CCDC88C (025)	Coiled-coil Domain Containing 88C, ubiquitously expressed, interacts with dishevelled protein, a negative regulator of canonical Wnt signalling, may interact with JNK signalling pathway

Table 1.6 Summaries of WES analysis results.

Total	Group	patient ID	Description	Gene function and predicted impact of mutation
15 patients analysed	3 patients with family history	001	no candidate variants found	
		002	inherited	post-synaptic signalling, NA
		007	no candidate variants found	
	12 patients without family history	003	no candidate variants found	
		009	no candidate variants found	
		028	no candidate variants found	
		020	inherited	ion metabolism, NA
		025	inherited	adhesion molecule, tolerated;
				Wnt signalling, damaging
		026	inherited	ECM degradation, damaging
		005	*de novo*	DNA damage, tolerated
		019	*de novo*	adhesion molecule, tolerated
		004	inherited	epigenetic regulator, NA;
				uracil and thymidine catabolism, NA
			de novo	androgen receptor, tolerated
		006	inherited	epigenetic regulator, NA
			de novo	cytoskeleton interactor, damaging
		018	inherited	DNA damage response, NA
			de novo	chemokine receptor, NA (frameshift)
		027	inherited	anion transporter, damaging
			de novo	neurexin surface interactor, damaging

1.6.4 Each patient carries multiple variants

Although some patients shared similarities based on the cellular functions of the genes that their rare variants were identified in, most patients carried multiple candidate variants. As summarised in Table 1.6, for the 3 cases with family histories, candidate variants were only identified in 1 patient (002). As the candidate variants identified in patient 002 were biologically highly relevant to schizophrenia, the parents of proband were recruited and the candidate variants were confirmed as inherited from parents. No candidate variants were identified in patient 001 and patient 007, who also had family histories of schizophrenia. In the 12 cases without family histories, there were 3 cases (003, 009 & 028) that no candidate variants were identified in. Inherited candidate variants were found in 3 cases (020, 025 and 026), affecting ion metabolism, adhesion molecules, *Wnt* signalling and extracellular matrix (ECM) degradation. However, these variants were inherited from neurologically healthy parents hence were considered as with low disease penetrance. Interestingly, there were 2 cases in which only *de novo* candidate variants were identified (005 & 019), affecting DNA damage responses and adhesion molecules. The 4 cases (004, 006, 018 & 027) left in the no family history group had both inherited and *de novo* variants, affecting pathways including epigenetic regulation of gene expression, DNA damage response and cell surface interactors etc. (Table 1.6). The WES data was also used for CNV analysis, which reported no known risk CNVs in coding regions of all patients, but identified one CNV for control 014. Analysis using tags of the 108 loci in coding regions also did not result in any associations. The candidate variants identified here only represent a starting point to unravel the possible relationships between the affected genes and schizophrenia, much more evidences are required to conclude on the association of those genes and the disease.

1.7 Discussion

The aims of this chapter were to characterise the cohort used in this study, from the genetics perspectives, and to search for rare *de novo* candidate variants that may have high penetrance in schizophrenia. In this discussion, I will summarise the biometric and genetic information that I collected so far from the patients and controls, along with their possible impacts on the following molecular- and cellular-based studies using this cohort, with an emphasis of the limitations of this study.

The understanding of schizophrenia has evolved greatly from the days it was firstly defined as a psychotic reaction, to a disorder of the mind; to a disease of the brain; to a problem of the dopamine system; and to today's 108 risk loci. The more we learnt about this disease and other mental disorders, the greater we realise the blurriness of their boundaries—not only the boundaries between different mental disorders but also the boundaries between healthiness and illness. The current diagnosis of schizophrenia is under a unified guideline; the Diagnostic and Statistical Manual version IV (DSM-5). It has attempted to bring a unified diagnosis into the field, and has been widely accepted. However, one has to recognise the current limitations we face due to the lack of understanding of the fundamental disease mechanisms. For example, no biomarker of schizophrenia is available in general, let alone specific biomarkers that help to recognise different stages or progression trajectories of the disease. We also do not know if schizophrenia is one disease or a collection of symptoms that have distinct origins and biomarkers to distinguish subtypes of the disease would be very useful. Therefore, research that shed lights on the aetiology, progression and even diagnosis of schizophrenia is of utmost importance.

With the aim of reducing heterogeneity between patients, using currently available knowledge, a group of patients with AOS was recruited. These patients had the following clinical characteristics: young, severe illness, poor prognosis, no smoking history, short untreated psychosis and short medication history (AJ). These characteristics help to reduce the possibilities of finding cellular phenotypes caused merely by confounding factors, such as smoking status, untreated psychosis and prolonged duration of medication. By doing so, I ought to study cellular phenotypes that rooted to genetic factors.

Although enriched for disease severity and young ages of onset, the cohort expectedly still showed a considerable degree of genetic heterogeneity. The two groups of genes for 'post-synaptic signalling' and 'cytoskeleton interactors and adhesion molecules' stood out as they contained more than one example in patient group and were predicted to be likely highly deleterious and penetrating. The two variants that affect post-synaptic signalling, Synaptic Ras GTPase Activating Protein 1 (*SYNGAP1*) gene and (SH3 And Multiple Ankyrin Repeat Domains 2) *SHANK2* gene, were found in the same patient (002). To further study the causal relationship between these two mutations and the patient's clinical phenotypes, I reprogrammed the skin fibroblasts from this patient into induced pluripotent stem cells (iPSCs) (*Chapter 3*).

Table 1.7 Recently published rare variant studies in schizophrenia with positive results.

Year	Approach	Sample size	Major findings	Ref
2018	WES	4225 cases 5834 controls	no individual variants or genes were significantly enriched in cases; the gene (*FYN*) with the highest signed log p value regulates glutamate receptors.	Curtis et al., 2018
2017	WES	10,011 cases 13,791 controls	No individual variant/gene surpass genome-wide significance; candidate gene sets enriched for LoF intolerant genes and genes whose mRNAs bind to FMRP;	Leonenko et al., 2017
2016	WES	4,877 Swedish cases 45,376 controls	cases had high burdens of gene-disruptive ultra-rare variants (URVs) but not synonymous URVs; The elevated rate of URVs in cases was several times higher than that of *de novo* mutations; genes affected by disruptive URVs were enriched for synaptic protein interactors.	Genovese et al., 2016
2016	WES	1043 ASD cases 1021 SZ cases 731 controls	*De novo* synonymous variants within DNase I (frontal cortex-derived) hypersensitivity sites were enriches in SZ cases, *SED1A* was the most significant gene.	Takata et al., 2016
2016	WES	4,264 cases 9,343 controls	rare loss-of-function variants in *SETD1A* were significantly associated with schizophrenia	Singh et al., 2016
2014	WES	623 trios	small deleterious *de novo* variants affecting the NMDAR complexes and ARC were overrepresented in patients.	Fromer et al., 2014
2014	WES	2,536 cases 2,543 controls	polygenic burden of rare disruptive variants affecting voltage-gated calcium ion channel signalling and ARC signalling	Purcell et al., 2014

2014	WES	57 trios	Cases had elevated levels of nonsense *de novo* variants; affected genes overlapped with risk genes for autism and intellectual disability; several candidate genes converge on epigenetic regulation of transcription.	McCarthy et al., 2014
2013	WES	105 probands 84 unaffected siblings 210 unaffected parents	genes harbouring *de novo* mutations in patients from otherwise healthy families formed an inter-connected network within the transcriptomes of dorsolateral and ventrolateral prefrontal cortex during fetal development; the network functions include neuronal migration, synaptic signalling and transcriptional regulation.	Gulsuner et al., 2013
2012	WES	231 patient-proband trios 34 control trios	excess *de novo* nonsynonymous SNV and excess *de novo* gene-disruptive variants in cases, effecting genes in a wide range of functions but substantially early fetal development; recurrent de novo events occurred in *LAMA2*, *PDYD*, *TRRAP* and *VPS39*.	Xu et al., 2012
2012	genotyping arrays	662 trios	rare *de novo* CNVs were more frequent in cases; New risk CNVs identified spanned genes encoding components of the PSD; case *de novo* CNVs were enriched for PSD proteome that can be largely explained by NMDARs and ARC.	Kirov et al., 2012
2015	genotyping arrays	11,355 cases 16,416 controls	case CNVs were enriched for glutamatergic signalling and GABAergic signalling.	Pocklington et al., 2015

ARC: activity-regulated cytoskeleton-associated protein. FMRP: fragile X mental retardation protein.

Previous studies of rare variants showed the association of gene networks during early brain development, synaptic signalling and epigenetic regulation with schizophrenia (Table 1.7). By analysing exome data from trios, Xu et al., 2012 found that the genes affected by *de novo* disruptive variants in probands were substantially made of genes that were expressed during early brain development. This was confirmed a year later by Gulsuner et al., 2013; by analysing exome data from quads, the genes harbouring *de novo* mutations in patients could be mapped to the transcriptomes of the developing human dorsolateral and ventrolateral prefrontal cortex. The association of epigenetic regulators with schizophrenia was best illustrated with WES studies reporting variants in the gene *SET Domain Containing 1A* (*SETD1A*) (Singh et al., 2016; Takata et al., 2016). The protein product of *SETD1A* is a component of the histone methyltransferase complex that methylate histone H3 at lysine 4 (H3K4). The trimethylation of H3K4 is a mark for transcription starting sites. Therefore, *SETD1A* plays essential roles for epigenetic regulations of gene expressions, however, it remains unclear how such a ubiquitous mechanism could be impaired to increase the risk of schizophrenia.

Several studies showed the associations of variants within the genes involved in synaptic signalling. Using genotyping arrays and CNV calling, Kirov et al., 2012 and Pockling et al., 2015 independently showed that patient CNVs were enriched for genes involved in synaptic signalling, using trio design and case-control design, respectively. Kirov et al., 2012 reported elevated levels of CNVs in probands affecting members of the PSD complex, which could be largely explained by NMDARs and activity-regulated cytoskeleton-associated protein (ARC). Pockling et al., 2015 reported that case CNVs were enriched for genes involved in glutamatergic signalling, as well as genes for GABAergic signalling. The enrichment of CNVs that contained genes for GABAergic signalling showed genetic evidence for GABAergic

signalling being directed involved in the aetiology of schizophrenia, rather than being secondary responses. The importance of NMDAR complexes in schizophrenia genetics was validated later on by Fromer et al., 2014 and Curtis et al., 2018, using trio designs and a case-control designs, respectively. Beyond the post-synaptic glutamatergic signalling, Purcell et al., 2014 revealed polygenic burden of rare disruptive variants in genes governing voltage-gated calcium ion channel signalling and again the ARC signalling in patients using WES. Similarly, Genovese et al., 2016 used WES data from a larger cohort and revealed an elevated burden of ultra-rare disruptive variants that affected synaptic protein interactors in patients. These studies independently demonstrated the significance of synaptic signalling in the aetiology of schizophrenia by reporting the enrichment of rare and/or *de novo* variants that affected the same functional category. Although not specifically discusses, there were several genes related to cell adhesion and cytoskeleton regulation in the synaptic gene networks that Fromer et al., 2014 and Purcell et al., 2014 found as enriched for case rare variants, such as α-Actinin which was an actin-binding protein and Ankyrin-1 which links cytoskeleton with membrane proteins. However, so far there was no individual variants proven to be significantly associated with schizophrenia. This was best demonstrated by two recent WES studies using large numbers of cases and controls (Curtis, Coelewij, Liu, Humphrey, & Mott, 2018; Leonenko et al., 2017) . Perhaps this could be used to argue for that we should view the genetic liability of schizophrenia as disruptions of functional networks, rather than simply LoF of individual genes.

In summary, in a cohort of patients with adolescent-onset schizophrenia that were enriched by severity of clinical phenotypes, I found both genetic heterogeneity and some agreement in cellular pathways. The two most commonly revealed pathways in the studied cohort, post-

synaptic signalling and cytoskeletal and cellular adhesion molecules, were in agreement with past genetic studies on schizophrenia. The presence of rare variants in *SYNGAP1* and *SHANK2* in the same patient could serve as an interesting case for following-up biological studies, as the protein products of both genes are essential for glutamatergic post-synaptic signalling. The roles of cytoskeletal and cellular adhesion molecules, and post-synaptic signalling will be addressed in the rest of this thesis, on the cellular and molecular levels.

This study certainly has its limitations. First of all, a power analysis would be necessary to estimate the required sample sizes for particular research questions, however the ability to recruit a larger cohort is limited at present. None of the identified rare candidate variants were over-represented in the current small cohort. A much larger cohort or access to large datasets is required to investigate the relationships between the identified candidate variants or affected pathways and schizophrenia. For example, the frequency of rare damaging *de novo* variants could be calculated and the functional interactions of the affected genes could be investigated to determine if the disruption of certain functional networks during brain development is over-represented in patients. Second, the current study only identified candidate variants that may increase the risk of schizophrenia by estimating the rareness and LoF impacts, there is no proof of a definitive causal relationship between the candidate variants and the clinical phenotypes of patients. To achieve so, much more evidences from the cellular and molecular levels are needed. For example, the rescue of disease-associated cellular phenotypes upon replacing the candidate variants with wild types in patient-derived cells would provide evidences for causal relationship. Third, this study only focused on the coding regions of the genome. Obviously, important regulatory elements from the non-coding regions were not investigated. A whole genome sequencing needs to be done for this purpose

and is planned as one of the future experiments. The identification of disease-associated rare variants relies on the profiling of non-disease associated SNPs. As the knowledge of human non-disease associated SNPs are still growing, even a whole genome sequencing at appropriate depth is likely to still miss some potentially disease-associating rare variants. Last, candidate variants were identified only based on DNA extracted from blood samples, there is a possibility of somatic variants that only present in a subset of tissues. Future experiments should confirm the presence of candidate variants in other tissue types derived from the same donors to confirm that the candidate variants being germline variants. The aims of this part of the study were to identify candidate variants in the present cohort for follow-up biological studies in a long-term. The WES analysis served as a starting place in the bigger picture.

CHAPTER 2 A COMPARISON OF *IN VITRO* BEHAVIOURS OF AN ADULT STEM CELL POPULATION; OLFACTORY ECTO-MESENCHYMAL STEM CELLS, BETWEEN PATIENTS WITH ADOLESCENT-ONSET SCHIZOPHRENIA AND HEALTHY CONTROLS

2.1 Summary

The easily accessible olfactory ecto-mesenchymal stem cells (OE-MSCs) which reside within the nasal cavity provide a fast and cost-effective discovery platform for studying human diseases. They have been used in the past for disease mechanism studies in Alzheimer's disease (AD) (Ghanbari et al., 2004; Johnson et al., 1994; Wolozin, Lesch, Lebovics, & Sunderland, 1993), Parkinson's disease (PD) (Cook et al., 2011; Murrell, Wayne et al., 2008) and adult-onset schizophrenia (English et al., 2015; Fan, Abrahamsen, McGrath, & Mackay-Sim, 2012; Fan et al., 2013; Feron, Perry, Hirning, McGrath, & Mackay-Sim, 1999; McCurdy et al., 2006). OE-MSCs derived from patients with neurodegenerative diseases showed molecular signatures that were consistent with the current hypotheses of the diseases; AD OE-MSCs expressed elevated levels of amyloid precursor proteins while PD OE-MSCs displayed dysregulated gene networks for mitochondrial functions and oxidative stresses. Therefore OE-MSCs offer a platform to study the molecular mechanisms of neurological disorders without extensive *in vitro* manipulations of the primary cells. Here OE-MSCs were used to explore cellular phenotypes associated with adolescent-onset schizophrenia. As a quality control step, OE-MSCs isolated from this cohort were shown to express the same cell identity markers, and were phenotypically similar as described in the literature. Basic stem cell properties, namely self-renewal, proliferation and differentiation remained

indistinguishable between patient cells and control cells, suggesting that potential schizophrenia genetic risk factors did not affect the basic stem cell properties of OE-MSCs. Next, the adhesion and migration ability of the cells were analysed as they were previously reported as aberrant in OE-MSCs derived from patients with adult-onset schizophrenia. Results showed that the cell-to-substrate adhesion of patient cells was significantly reduced compared to that of controls. This result is in line with a previous study using OE-MSCs isolated from adult-onset schizophrenia (Feron et al., 1999). To understand the molecular basis causing the reduced cell adhesion, whole-cell protein lysates from OE-MSCs were analysed with mass spectrometry using the same methods as applied in a previously published proteomic study on OE-MSCs (carried out in the laboratory of Prof. David Cotter, Dublin). Analysing total proteins with statistical and network analysis tools revealed that Eukaryotic initiation factor 2 (EIF2) signalling and global ribosome synthesis were significantly reduced in patient cells, similar to what has been observed in adult schizophrenia. These results showed that OE-MSCs can be used as a disease mechanism discovery platform that offers the unique features of 1) carrying stem cell properties that reflect early developmental processes, 2) being directly isolated from patients so that *in vitro* manipulations could be minimised and 3) retaining high numbers of disease-associated proteins that could be used for mechanistic studies. Future studies will serve to increase the number of biological replicates to increase the power of the observed phenomena.

2.2 Introduction

2.2.1 Adult niche stem cells

Stem cells are present in all multicellular organisms, they differ from other types of cells in the body based on two general properties: 1) they are unspecialised cells that are capable of dividing and renewing themselves for long periods, 2) they can give rise to differentiated cell types. Stem cells can be further classified according to their plasticity and how committed they are to become any particular types of cells. The most versatile stem cell—the totipotent stem cell, is capable of giving rise to all types of cells found in an organism. The fertilised egg is the first totipotent stem cell in the development of an organism, after a few divisions the cells begin to transit into pluripotent stem cells, which retain the ability to form nearly all the tissues but cannot do so independently. During normal development, the pluripotent stem cells further transform into multipotent stem cells that can only give rise to a limited range of cells within an organ. Ultimately, the tissue-specific multipotent stem cells produce progenitor cells that are able to transiently amplify themselves, and differentiate into all cell lineages of the given organ.

Multipotent adult niche stem cells have been successfully isolated and maintained *in vitro* from various regions of the body. Establishment of such *in vitro* cultures have greatly enabled the studies of adult niche stem cell properties; namely proliferation, survival, apoptosis and fate determination. Understanding of these basic stem cell properties facilitate the ability to use patient-derived adult stem cells as an ethical source for disease mechanism study and treatment development, in a disease-relevant, and individualised way.

2.2.2 OE-MSCs in the nasal cavity are adult niche stem cells

Stem cells in olfactory mucosa provide an easily accessible, cost-effective and epigenetically relevant source of cells for studying ongoing human development as environmental factors were shown to leave epigenetic marks on cells (Bird, 2007). The olfactory mucosa is located in the nasal cavity and contains olfactory epithelium (Figure 2.1). Based on evidence from rodent studies, olfactory sensory neurons are made on a daily basis from stem cells that reside in both the olfactory epithelium and the underlying lamina propria (Delorme et al., 2009; Leung, Coulombe, & Reed, 2007). Besides replacing the old olfactory sensory neurons, stem cells residing in the olfactory epithelium also regenerate local surrounding tissue after damage in rodents, suggesting that they are multipotent adult stem cells (Chen, X., Fang, & Schwob, 2004; Leung et al., 2007; Mackay-Sim & Kittel, 1991). Those stem cells exhibit characteristics of both mesenchymal stem cells and neural stem cells; as they are able to self-renewal, proliferate and give rise to osseous cells, chondrocytes, adipocytes and neurons (Delorme et al., 2009; Girard et al., 2011; Matigian et al., 2010) . The observed properties matched those from peripheral olfactory stem cells that originate from neural crest-derived tissues. Therefore, stem cells isolated from olfactory epithelium and lamina propria haven been named ‘olfactory ecto-mesenchymal stem cells’ (OE-MSCs) (Delorme et al., 2009).

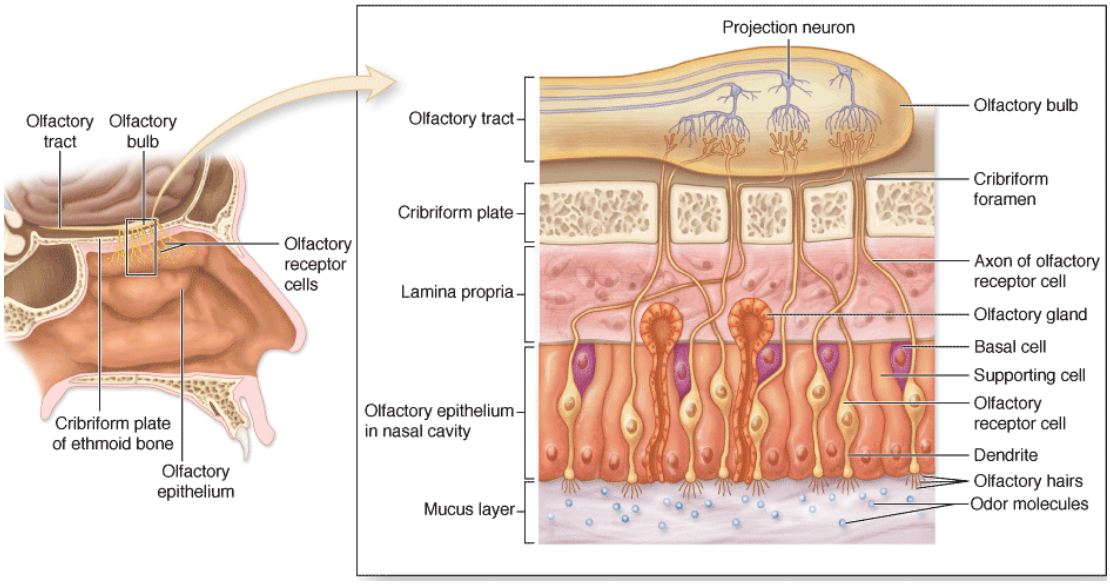


Figure 2.1 The anatomy of the olfactory system. In the nasal cavity, odours are detected by the olfactory receptor cells whose cell bodies reside in the olfactory epithelium and whose axons span to connect with the projection neurons in the olfactory bulb. Figure adapted from (Mescher, 2013).

2.2.3 In vitro characterisation of OE-MSCs

OE-MSCs display specific and consistent properties across species and between individual human subjects. OE-MSCs were firstly isolated and characterised in rodents and humans (Delorme et al., 2009; Girard et al., 2011; Matigian et al., 2010). It was shown that the olfactory epithelium underwent sustained neurogenesis for at least until the age of 72 years in humans (Murrell, W. et al., 1996). OE-MSCs present at multiple locations within the nasal cavity and the locations of isolation affects the yield of obtaining OE-MSCs (Féron, Perry, McGrath, & Mackay-Sim, 1998) . The dorsoposterior part of the nasal septum and the superior turbinate were shown as highly enriched for OE-MSCs (>70% success rate of obtaining OE-MSCs) hence has been routinely used as the location for taking biopsies (Féron et al., 1998). Recently, similar primary cultures of OE-MSCs have been established from mouse, rat, rabbit, sheep, dog, and macaques as a proof-of-concept for future clinical applications (Veron et al., 2018). Across all human individuals and animal species that OE-MSCs were isolated from, cells displayed a highly similar fibroblast-like in adherent culture media. OE-MSCs were consistently highly proliferative and able to generate spheres in the presence of mitogens. The most consistently reported cell identity marker expressed by OE-MSCs across all studies is Nestin, a marker expressed specifically in neural stem/progenitor cells in the central nervous system (CNS), and also expressed in bone-marrow derived mesenchymal stem cells (Delorme et al., 2009; Girard et al., 2011; Lendahl, Zimmerman, & McKay, 1990; Matigian et al., 2010; Méndez-Ferrer et al., 2010; Xie, Zeng, Hu, & Chen, 2015). Nestin belongs to a group of intermediate filament proteins hence is expressed intracellularly (Lendahl et al., 1990). Filament proteins are the major components of cytoskeleton, microtubules and microfilaments. When OE-MSCs were first described, comprehensive transcriptomic

comparison was done between OE-MSCs, neural progenitor cells, hematopoietic stem cells, bone marrow-derived mesenchymal stem cells, synovial fibroblasts and periosteal cells (Delorme et al., 2009) . As summarised in Figure 2.2, OE-MSCs clustered the most closely with bone marrow-derived mesenchymal stem cells after PCA (Delorme et al., 2009). This close clustering matched with the observation that OE-MSCs were able to differentiate into lineages similar to the progeny of mesenchymal stem cells, as well as with the finding that OE-MSCs expressed of several mesenchymal stem cell markers including Nestin, CD105 and CD73 (Matigian et al., 2010). Apart from being similar to mesenchymal stem cells, the expression profile of OE-MSCs was also highly enriched for genes found in neural lineages (Delorme et al., 2009). This is in line with the observation that, depending on the culture method, OE-MSCs showed immunoreactivity to antibodies against various cell identity markers: 1) the astrocytic marker glial fibrillary acidic protein (GFAP). Astrocytes in culture ubiquitously express GFAP, however *in vivo*, GFAP is also expressed by radial glia during embryonic development and by some niche stem cells that are astrocytic in nature at adult neurogenic niches in the CNS; the subventricular zone and dentate gyrus. 2) The neuronal markers microtubule associated protein 2 (MAP2), a general neuronal marker found in all mature neurons but not in other cell types in CNS. However, expression of MAP2 does not translate into electrophysiological maturity of neurons. 3) Microtubule associated protein 5 (MAP5), which is expressed in a wide range of neuronal cells including proliferating neuroblasts (Cheng, Krueger, & Bambrick, 1999), immature neurons and mature neurons. 4) Class III β-tubulin (βIII-tublin, a microtubule element of the tubulin family that is only expressed by neural progenitor cells and neurons in the CNS (Menezes & Luskin, 1994)), as well as 5) the oligodendrocyte marker O4 (an O-antigen expressed on the surface of oligodendrocytes (Sommer & Schachner, 1981)) (Delorme et al., 2009; Girard et al., 2011;

Murrell, Wayne et al., 2005). Taking all this evidence together, the authors argued that OE-MSCs were ‘mesenchymal stem cells in nature but also display neural lineage characteristics’ (Delorme et al., 2009).

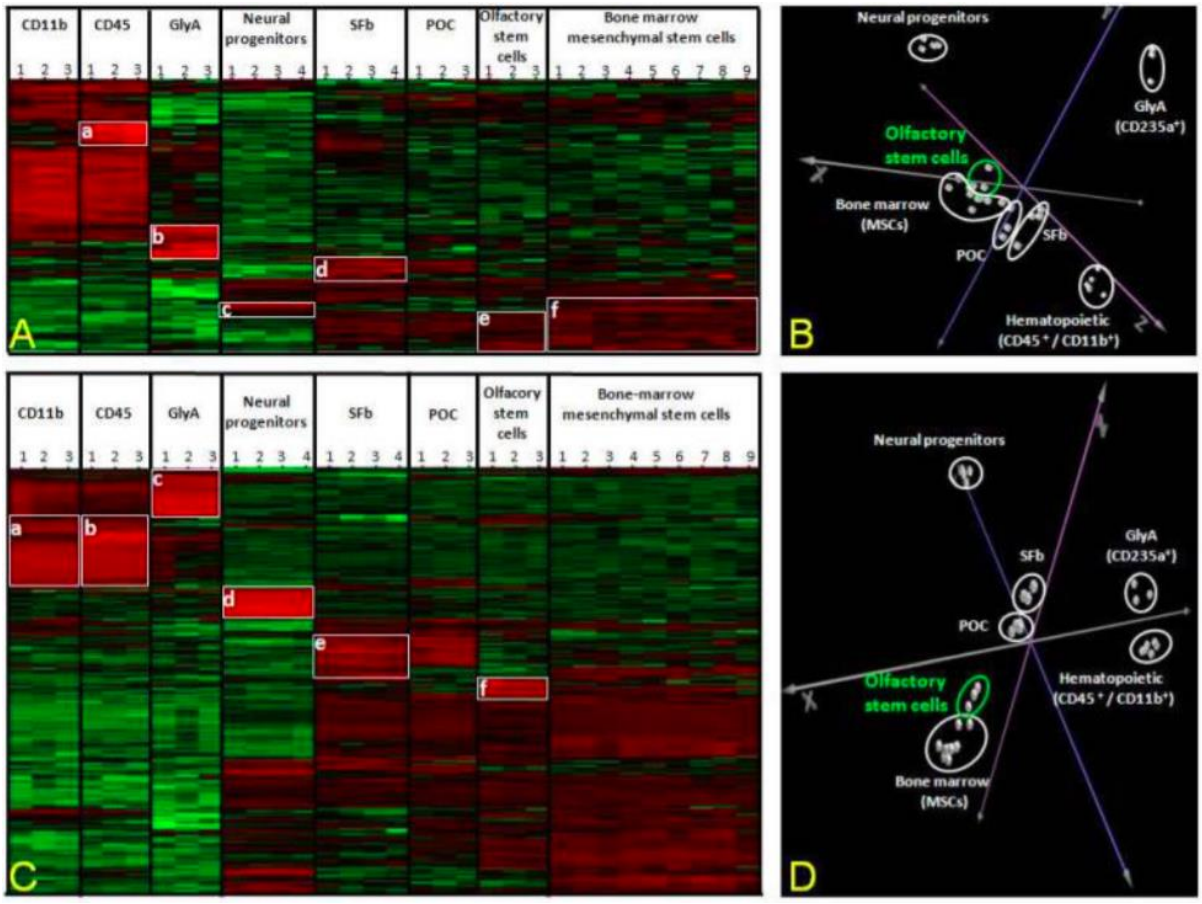


Figure 2.2 Transcriptomic comparison of OE-MSCs with hypothetical relevant cell types in identity. A) Hierarchical clustering of the expression of 147 CDs, using bone marrow-derived mesenchymal stem cells from 9 individuals (n=9), OE-MSCs (shown as 'olfactory stem cells' on the graph, n=3), hematopoietic cells that were CD45+, CD11b+ or CD235a+ (GlyA, n=3), periosteal cells (POC, n=3), synovial fibroblasts (SFb, n=3) and neural progenitor cells (n=4). a=lymphoid clustering; b=erythroid clustering; c=neural clustering; d=synovial fibroblast clustering; e=OE-MSC clustering; f= bone marrow mesenchymal cell clustering. **B)** Principle component analysis (PCA) using expression data on the same set of CDs from the same group of samples. Single profiles are denoted with individual plotted dots. **C)** Hierarchical clustering of the top 50 most upregulated genes and top 50 most downregulated genes in OE-MSCs (n=3), CD45+, CD11b+ or CD235a+ (GlyA) hematopoietic cells (n=3 each), POC (n=3), SFb (n=4), neural progenitor cells (n=4) and bone marrow stem cells (n=9); a=erythroid clustering; b,c=lymphoid clustering; d=neural clustering; e=SFb clustering; f=OE-MSC clustering. **D)** PCA of data shown in Figure C, single profiles are denoted as single plotted dots. Figure adapted from (Delorme et al., 2009).

Throughout this study, OE-MSCs isolated from the lamina propria were used, as they exhibit a relatively higher proliferation rate and less restricted differentiation potential, compared to cells from the olfactory epithelium (Delorme et al., 2009). In previous studies, neuron-like cells differentiated from OE-MSCs using defined media were immunoreactive to antibodies for pan-neuronal markers or dopaminergic neuronal markers, depends on the differentiation media that being used, but lacked expression of synaptic proteins (Delorme et al., 2009; Girard et al., 2011; Murrell et al., 2008; Ohnishi et al., 2015). Thus, caution should be taken when anticipating OE-MSCs as a model for the development of neurons. Rather, OE-MSCs are more relevant as a model for addressing cellular behaviours and the underlying molecular mechanisms of the early development in a stem/progenitor cell system. Especially for a disease that is likely to result from interactions between genes and environment risk factors, the OE-MSCs offer the unique benefits of having been exposed to many aspects of the external environments and carrying the patient's genetic and epigenetic information without extensive *in vitro* manipulations.

2.2.4 OE-MSCs in schizophrenia research

Previous studies using OE-MSCs isolated from patients with adult-onset schizophrenia and age-, gender-matched healthy controls showed cellular and molecular abnormalities (Table 2.1). On the cellular levels, patient cells were more proliferative and less adhesive to culture flasks when compared to cells from controls (Fan et al., 2012; Feron et al., 1999; McCurdy et al., 2006). On the molecular levels, the differentially expressed genes in OE-MSCs derived from patients with adult-onset schizophrenia and healthy controls fall into pathways governing neurodevelopment such as cell adhesion and neurite development, whereas the difference between OE-MSCs derived from patients with Parkinson's disease (PD) and healthy controls fall into pathways linked to mitochondrial function and oxidative stress (Matigian et al., 2010). The most recent work using OE-MSCs to study the molecular basis of schizophrenia showed that there was a significant global reduction of protein synthesis in patient cells, particularly reflected by the down regulation of EIF and mechanistic target of rapamycin (mTOR) signalling pathways (English et al., 2015). However, studies using induced neural progenitor cells observed contradictory results (Topol, A. et al., 2015a). This will be elaborated with my results obtained with the same study design, discussed later in the chapter

Table 2.1 Published OE-MSC studies on schizophrenia.

Year	Sample size	Major findings	Ref
2015	9 patients 9 controls	Patient OE-MSCs had significantly reduced global protein synthesis compared to controls, patient fibroblasts did not. Pathway analysis showed perturbation of eIF2a, eIF4 and mTOR in patient OE-MSCs.	English et al., 2015
2012	9 patients 9 controls	After being synchronised to G1 phase by serum-deprivation, patient OE-MSCs had a larger pool of cycling cells, showed shortened cell cycle periods and increased expression levels of G1/S phase cyclins.	Fan et al., 2012
2010	9 SZ 19 PD 14 controls	SZ OE-MSCs had significantly reduced expression levels of genes related to cell adhesion, neurite development and receptor-mediated signalling while SZ fibroblasts did not. PD OE-MSCs showed altered gene expressions in mitochondrial function and oxidative stress.	Matigian et al., 2010
2006	8 SZ 8 Bipolar 10 controls	SZ patients had more cells in mitosis while bipolar I patients showed more cell death under normal cell culture conditions; gene expression alterations were revealed on cell cycle and phosphatidylinositol signalling for SZ and bipolar I, respectively.	McCurdy et al., 2006
1999	10 patients 10 controls	Patient olfactory biopsies showed reduced ability to adhere to culture flasks and increased proportions of dividing cells. The percentages of apoptotic cells in control cultures were increased while that for patient cultures were decreased upon a treatment of 10 μM dopamine.	Feron et al., 1999

Together, the past studies showed that OE-MSCs 1) are a defined type of adult niche stem cells that is likely to have a neural crest origin, 2) are mesenchymal stem cells in nature but also display characteristics of neural lineages, 3) when maintained *in vitro*, ubiquitously express neural stem cell marker and bone marrow-derive stem cell marker Nestin, 4) behave consistently in their growth and morphology, and 5) show disease-specific cellular and molecular alterations.

2.3 Aims

The primary aims of the OE-MSC study are to investigate whether OE-MSC could be used as a disease-mechanism discovery platform for AOS and if so what the AOS-relevant cellular and molecular phenotypes are.

The aims can be broken down into several steps:

1) To isolate and bank OE-MSCs from patients with adolescent-onset schizophrenia using the same methods as described in previous studies;
2) To confirm the identities of OE-MSCs by assessing their immunoreactivities to the cell identity markers previously described in literature on OE-MSCs;
3) To assess the *in vitro* characteristic behaviours of OE-MSCs, namely being able to be cultured as monolayer in the presence of serum and being able to form spheres in the presence of mitogens;
4) To compare the basic stem cells properties and cellular behaviours that play key role in the development of neurons between patient-derived OE-MSCs and control-derived OE-MSCs;
5) To discover molecular basis that may be responsible for the observed cellular phenotypic differences by using proteomic approaches, which were previously applied on OE-MSCs derived from adult-onset schizophrenia;
6) To compare the results obtained from the current AOS cohort and the previous adult-onset cohort, in order to investigate if the observed cellular and molecular phenotypes are limited to either group.

2.4 My roles in the study and contributions from collaborators

My roles in this part of the study were to 1) dissect biopsies, maintain primary cultures and freeze down expanded cells; 2) carry out characterisation of OE-MSCs and assessment of their cellular behaviours based on past literature; 3) harvest total protein lysates from cells as per described in the adult-onset schizophrenia proteomic study.

Collaborators' roles were to analyse the protein contents of the protein lysates using the same mass spectrometer and all downstream statistical analyses applied to the proteomic dataset.

2.5 Materials and methods

2.5.1 Nasal biopsy processing and primary cultures

Nasal biopsies were taken under local anaesthesia. Nasal mucosae were taken from the posterior part of the septum (Féron et al., 1998). Nasal biopsies were quickly (<10min) transferred while kept in OE-MSC culture medium; Dulbecco's Modified Eagle Medium (DMEM)/HAM F12 with GlutaMax (Gibco 31331), 10% fetal bovine serum (FBS) (Gibco 10270-106), 1% Penicillin-Streptomycin (P/S) (Life Technologies 15140-122) to a sterile dissection flow cabinet. Lamina propria from the nasal mucosae were dissected and plated following a standard protocol (Girard et al., 2011). Briefly, the nasal mucosae were washed in PBS at 37°C incubated in 1 ml of pre-warmed dispase II solution (2.4 IU/ml) (Roche 04942078001) for 1 hour at 37°C. Next, the olfactory epithelium as a transparent sheet was stripped away from the brownish cotton-like lamina propria under a dissection microscope. The lamina propria was washed in medium and cut into 4-6 pieces with each piece inserted into its own well in a 4-well plate (Thermo Scientific 107449) under a round glass coverslip. The OE-MSC culture medium was refreshed every 2-3 days. Two weeks after plating, primary cells usually reached confluency and the cell cultures were passaged with Trypsin/ ethylenediaminetetraacetic acid (EDTA) 0.05%/0.02% in PBS (PAA L11-004) at 37°C. Cells were frozen down at passage 3 in 10% dimethyl sulfoxide (DMSO) (Sigma D2650) in FBS. All cell cultures were kept at 37°C, 5% CO_2 in a sterile humidified incubator. A cell bank of OE-MSCs was maintained as illustrated in Figure 2.3.

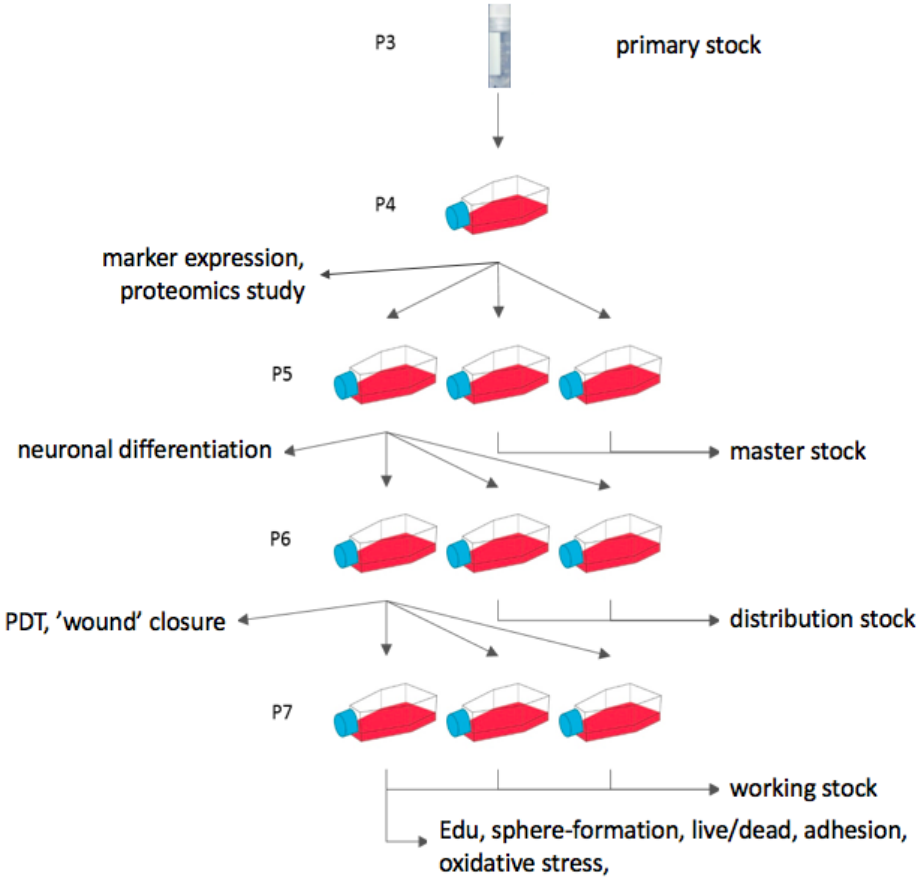


Figure 2.3 The maintenance of a sustainable cell bank of OE-MSCs and a summary of assays done at the corresponding stages. Adherent cultures derived from the laminia propria of nasal biopsies were frozen down at passage 3 (P3) as the primary stock. One vial was thawed into one T75 flask as passage 4 (P4), this passage was used to check cell identity marker expression and to isolate total protein for proteomics study. Two T75 flasks of passage 5 (P5) cells were frozen down as 8 vials of master stock. One flask at P5 was used for neuronal differentiation. Two T75 flasks of passage 6 (P6) were frozen down as 8 vials of distribution stock, one flask at P6 was used for the population doubling time (PDT) assay and 'wound' closure assay. Three T75 flasks were used as the working stock for the EdU proliferation assay, sphere-formation assay, live/dead staining, cell-to-substrate adhesion assay and oxidative stress assay.

2.5.2 Population doubling time assay

Adherently cultured OE-MSCs at passage 6 were harvested using Trypsin/EDTA and plated in three wells of a 6-well plate at a density of 50,000 cells/well. After 24 hours, 48 hours, 72 hours, and 96 hours, respectively, cells were harvested and the total number of cells were determined with a hemocytometer. PDT was calculated using the formula: PDT= $\frac{(t2-t1)*\log(2)}{\log[N(t2)]-\log[N(t1)]}$ (Fan 2012), where t1 is the start point, and t2 is the end point of the exponential growth period, N(t) represents the number of cells at the corresponding time points. The average values from three wells as technical replicates were calculated. Cells derived from 10 patients and 9 controls were used as biological replicates.

2.5.3 EdU incorporation assay

Adherently cultured OE-MSCs at passage 7 were harvested using Trypsin/EDTA and plated on glass coverslips coated with 5 µg/cm^2 poly-L-lysine (PLL, Sigma P6282) in three wells of a 24-well plate at a density of 50,000 cells/well. Next day, half of the medium was removed and replaced with new culture medium with 20 µM EdU (Invitrogen C10339), so that the working concentration of EdU was 10 µM. After incubation with EdU for 2-6 hours at 37°C, cells were fixed with 4% PFA for 15 min at room temperature. After two washes with 10% normal donkey serum (NDS, Bio-Rad C06SBZ) in PBS, cells were permeabilised with 0.5% Triton X-100 (VWR Int. AAA16046-AP) in PBS overnight at 4°C. The incorporation of EdU was visualised with the Click-iT EdU Alexa Fluor 594 Imaging Kit (Bio-Rad C06SBZ) according to the manufacturer instructions. Cell nuclei were stained with 4′,6-diamidino-2-phenylindole (DAPI) 1:1000 in Phosphate-buffered saline (PBS). After three washes with PBS, coverslips were mounted onto glass objective slides and imaging were done using an epi-fluorescence microscope. Ten images were taken per wells, the number of EdU+ cells and DAPI+ cells were counted manually in ImageJ. The average values of EdU+ cell/DAPI+ cells from three wells as technical replicates were calculated. Cells derived from 7 patients and 5 controls were used as biological replicates.

2.5.4 Sphere formation assay

Adherently cultured OE-MSCs at passage 7 were harvested using Trypsin/EDTA and plated in three wells of a 12-well plate coated with 5 µg/cm^2 PLL in sphere formation medium; DMEM/HAM F12 with GlutaMax (Gibco 31331), 1% P/S (Life Technologies 15140-122), 1% Insulin-Transferrin-Selenium (Gibco 41400), 75 ng/ml EGF (Chemicon GF144) and 75 ng/ml fibroblast growth factor 2 (FGF2) (Chemicon GF003). Initial plating density ranging from 7,000-50,000 cells/cm^2 was tested using a few control lines and 15,000 cells/cm^2 allowed most tested lines to generate spheres within a week. Medium was refreshed every day and bright-field images were taken to monitor the progress of sphere formation for each line after medium changes. The number of spheres per well was counted at day 6 and day 8 after plating. Average values from three wells as technical replicates were calculated. Cells derived from 11 patients and 6 controls were used as biological replicates.

2.5.5 Live/dead staining

Adherently cultured OE-MSCs at passage 7 were harvested using Trypsin/EDTA and plated in three wells of a 24-well plate at 50,000 cells/well. The next day, live cells were stained with 1 drop of NucBlue (ThermoFisher Scientific R37605) for live cells and 1 drop of NucGreen (ThermoFisher Scientific R37109) for dead cells, in dark at room temperature for 5 min. Live imaging was performed immediately using a plate scanner (Molecular Device) after staining. The number of green nuclei and blue nuclei was determined by the cell counter function in ImageJ. Ten images were acquired per well and the average values from three wells as technical replicates were used. Cells derived from 8 patients and 5 controls were used as biological replicates.

2.5.6 'Wound closure' assay

Adherently cultured OE-MSCs at passage 6 were harvested using Trypsin/EDTA and plated in three wells of a 12-well plate at 24,000 cells/well in OE-MSC culture medium. After 3-4 days, a confluent monolayer formed. A linear 'wound' was introduced to the monolayer cell culture by scratching through the middle of the well with a 10 µl pipette tip. The remaining cell residues along the 'wound' were removed by gently washing the monolayer twice with warm culture medium. Three square areas along the 'wound', as representative areas to measure the closure, were marked at the bottom of the well under microscope. Bright-field images were taken every 24h at the three marked areas per well till the 'wound' completely closed. The percentage of the 'wound' closure at each day was evaluated from the images using the Wound Healing Tool in ImageJ. The average values from the three measured areas in three wells, as technical replicates, at each day were calculated. Cells derived from 10 patients and 6 controls were used as biological replicates.

2.5.7 Cell-to-substrate adhesion assay

Adherently cultured OE-MSCs at passage 7 were harvested using Trypsin/EDTA and plated in two wells per coating condition of a 24-well plate at 50,000 cells/well in OE-MSC culture medium. The coating conditions used were 10 µg/ml laminin (Sigma, L2020) in PBS 1h at 37°C, 32 µg/ml PLL for 2h at 37°C, 15 µg/ml poly-ornithine overnight at room temperature, and regular tissue culture treated 6-well plate without additional coating. The cell suspension was allowed to settle on these coated culture surfaces for 1h at 37°C. Subsequently, the non-adherent cells were removed by gently washing the cell culture three times with warm PBS. Cells that were able to adhere to the coated cell culture surfaces were fixed with 4% paraformaldehyde (PFA, Sigma P6148-500G) for 15 min at room temperature. DAPI (1:1000 in PBS) nuclear stain at room temperature for 15 min was used to determine the number of attached cells. Ten pictures were taken randomly from each well using an epi-fluorescence microscope and the number of attached cells in each picture was determined by manual counting DAPI+ nuclei in ImageJ. The average values of the numbers of attached cells were calculated from two wells as technical replicates for each coating condition. Cells derived from 7 patients and 5 controls were used as biological replicates.

2.5.8 Oxidative stress assay

Adherently cultured OE-MSCs at passage 7 were harvested using Trypsin/EDTA and plated in a 24-well plate at 50,000 cells/well in OE-MSC culture medium. The next day, medium was replaced with 0 mM, 0.5 mM, 1.0 mM and 2.0 mM H_2O_2 (Sigma H1009) for three wells per condition per line in culture medium to trigger oxidative stress responses. Plates were kept in incubator for 4 hours and bright-field images were taken from each well to compare the degree of membrane blebbing in various lines. After taking live bright-field images, cells were fixed with 4% PFA at room temperature for 15 min. A live/dead staining was performed as described in *the Live/dead assay* and 10 images were taken using a plate scanner (Molecular Device) from each well. The numbers of live cells and the numbers of dead cells were determined using the cell counter function in ImageJ for untreated cells, cells treated with 0.1 mM H_2O_2 and 0.5 mM H_2O_2 as higher concentrations of H_2O_2 resulted in almost 100% cell death for all lines. Average values were calculated from three wells as three technical replicates. Cells derived from 7 patients and 8 controls were used as biological replicates.

2.5.9 Neuronal differentiation

Adherently cultured OE-MSCs at passage 5 were harvested using Trypsin/EDTA and plated in 24-well plates coated with either 32 µg/ml PLL for 2h at 37°C and 1:100 laminin for 1h at 37°C or 15 µg/ml poly-ornithine (PO, Sigma P4957) at room temperature overnight and 1:100 laminin for 1h at 37°C at 25,000 cells/well using 3 different published neuronal differentiation media for OE-MSCs (Table 2.2). At the same time, spheres were derived from passage 4 OE-MSCs as described in *sphere-formation assay* and collected, gently dissociated with accutase (ThermoFisher Scientific A1110501), and plated in 24-well plates coated with either PLL and laminin or PO and laminin as previously described at 25,000 cells/well using 3 different published neuronal differentiation media for OE-MSCs. Neuronal differentiation medium was changed every three days for all conditions. Bright-field images were taken from cells at every medium change to record the morphological changes. Cells were allowed to differentiate for either 14 days or 21 days before fixation in 4% PFA.

Table 2.2 Medium composition of 3 published OE-MSC neuronal differentiation protocols.

No.	Medium composition	Marker expression	Reference
1	Neurobasal (Invitrogen 21103049), GlutaMax, B27 (ThermoFisher Scientific 17504044), 0.025mM L-glutamic acid (Sigma G1251), P/S	MAP2	Delorme2009 Feron2013
2	DMEM/F12, GlutaMax, B27, N2 (ThermoFisher Scientific 17502048), 10% FBS, P/S	Tuj1, MAP2*	Ohnishi2015
3	DMEM, insulin-transferin-selenium, P/S, 25 ng/ml GDNF** (PeproTech 450-10)	TH	Murrell2008

*This MAP2 stain only labelled some 'neurons' and the morphology is not neuronal.

** GDNF=glial cell-derived neurotrophic factor

2.5.10 Immunocytochemistry and microscopy

Cell cultures were fixed in 4% FPA for 15 min at room temperature. After washing with PBS, cells were blocked and permeabilised in PBS with 10% NDS, 0.3% Triton X-100 and 0.01% sodium azide (Sigma S2002) at room temperature for 1 hour or at 4°C overnight. Next, cells were incubated in primary antibodies which were diluted in PBS with 5% NDS, 1% bovine serum albumin (BSA, Sigma 05470), 0.1% Triton X-100 and 0.01% sodium azide at 4°C overnight (Table 2.3). The next day, cells were washed three times, 10 min each, in PBS with 0.3% Triton X-100. Secondary antibodies were diluted in PBS with 5% NDS, 1% BSA and 0.1% Triton X-100 and then left one cells for 90 min at room temperature in dark. After three washes with PBS/0.3% Triton X-100, nuclear staining was done by incubating the cells with 1:1,000 DAPI for 5 min at room temperature. Subsequently, cells were washed once with PBS and coverslips were mounted on glass slides with FluorSave (Life Technologies S36938). Light images were generated with an inverted microscope (Zeiss Axiovert 40) and digital camera (XL imaging Colour CMOS UXGA [2.0 megapixel] USB 2.0 camera). Fluorescence images were generated with a confocal laser scanning microscope (Zeiss LSM 710) and LSM Image Browser (Zeiss).

Table 2.3 Antibodies used in this study.

Primary antibodies		
Source species/antigen	Source	Dilution
Goat α-DCX	Santa Cruz, sc-8066	1:200
Goat α-Iba1	Abcam, ab5076	1:200
Mouse α-Beta-III Tubulin	Abcam, ab78078	1:1000
Mouse α-MAP2	Millipore, 05-346	1:200
Mouse α-Nestin	R&D Systems, MAB1259	1:250
Rabbit α-CD105	Sigma, HPA011862	1:50
Rat α-GFAP	Life Technologies, 130300	1:200
Secondary antibodies		
Source species/antigen/fluophore	Source	Dilution
Donkey α-goat AlexaFluor488	Life Technologies	1:500
Donkey α-goat AlexaFluor568	Life Technologies	1:500
Donkey α-mouse AlexaFluor555	Life Technologies	1:500
Donkey α-rat AlexaFluor488	Life Technologies	1:500
Goat α-rabbit AlexaFluor488	Life Technologies	1:500

2.5.11 Harvesting total protein for proteomics study

Adherently cultured OE-MSCs at passage 4 were harvested using Trypsin/EDTA and plated in a 6-well plate coated with 5 µg/cm^2 at 15,000 cells/cm^2 in sphere formation medium. Daily medium changes with fresh medium was carried out. Free-floating spheres collected from one 6-well plate were re-plated without dissociation in one tissue culture treated T75 flask in OE-MSC culture medium. After 4 days, the cells migrated out of the spheres and became a 90% confluent monolayer in T75. Medium was removed and the cells were washed three times with warm PBS. Flasks were tilted shortly to remove residual PBS as much as possible. Lysis buffer was prepared by dissolving one tablet of proteinase inhibitor (Roche complete, 0469315900) in 10 ml of 1 M triethylamonium bicarbonat (TEAB) lysis buffer (Sigma T7408), and 1ml was added to each T75 flask. Cells were collected with a cell scrapper immediately after adding the lysis buffer. Total cell lysate was collected in a 15ml Falcon tube and subsequently pushed through a 27G needle for 7 times. After an incubation on ice for at least 40 min, the total lysates were centrifuged at 24,000g and 4°C for 30 min. The supernatants, which contained the protein extracts, were carefully removed and stored at -80°C.

2.5.12 Statistics

All statistics apart from the cell-to-substrate adhesion assay the proteomics analysis were done using type 3 two-tail Student's *t*-tests. Statistics for the cell-to-substrate adhesion assay was done using GraphPad Prism repeated measures analysis of variance (RM-ANOVA).

2.6 Results

2.6.1 Banking of OE-MSCs

In order to bank the OE-MSCs as a sustainable resource, cells were grown as adherent cultures up to passage 3 and cryopreserved (Figure 2.4). Upon thawing, 1 vial of cells was plated into 1 T75 flask as passage 4, and cryopreserved at passage 5 as the master stock, at passage 6 as the distribution stock and at passage 7 as the working stock, respectively. Previous characterisation studies on the impact of passage numbers on OE-MSCs showed that the growth speed and sphere formation efficiency remained most stable for the first 12 passages, while the gene expression profile remained stable up to passage 25, and no genomic abnormality was detected with karyotyping in the passage 3-10 (Matigian et al., 2010). Table 1.3 indicates the subjects that OE-MSCs were isolated from. Per subject, usually 20-40 vials of OE-MSCs at passage 3 were cryopreserved.

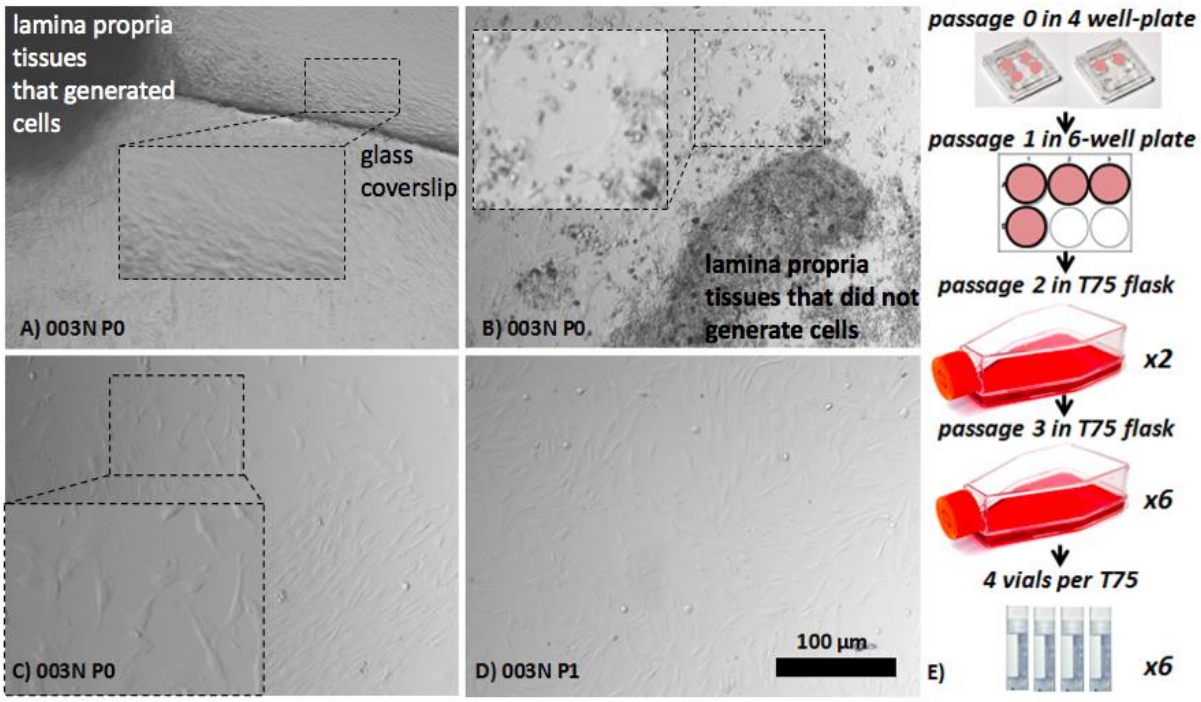


Figure 2.4 Primary cultures from lamina propria and the initial banking strategy. Representative pictures from line 003N showing that: A) Two week after plating the lamina propria under glass coverslips, cells migrated out from the majority of tissue pieces of the dissected lamina propria, proliferated and became abundant in number around the primary tissues (zoom-in view showing 100% confluent cell layer). B) Very rarely, if the pieces of tissue were cut too small some pieces of tissue could fail to generate cells. In this case there was a lack of abundance of cells surrounding the tissues (zoom-in view showing tissue debris and sparse cells). C) Cells migrated from plated tissues of lamina propria to empty culture spaces (zoom-in view showing optimal cell density after 2 week's proliferation and migration) and D) after passaging, cells kept growing and retained the same morphology. E) The initial tissues were plated in 4-well plates and cells were passed to 6-well plates and T75 flasks up to passage 3, at which cells were cryopreserved as 4 vials per T75 flask. Picture A, B and C were taken 16 days after plating the biopsy. 003N: OE-MSC line derived from nasal biopsy from participant 003 (N=nasal). The surface area of 1 picture here is about 0.02% of the surface area of one well in a 6-well plate. Scale bar=100 µm.

2.6.2 OE-MSCs from patients and controls express the same panel of cell identity markers

As the locations where the biopsy is taken from in the nasal cavity affects the success rate of obtaining OE-MSCs (Féron et al., 1998), the cellular composition of all OE-MSC lines was assessed based on immunocytochemistry using a panel of cell identity markers selected from the literature (Figure 2.5) (Matigian et al., 2010; Murrell et al., 2005). The olfactory epithelium in the nasal cavity is constantly exposed to the outer environment and serves as a first layers of defence from the immune system. Therefore, the absence of macrophages in the OE-MSC cultures was confirmed with negative staining results of the microglia/macrophage marker Ionized calcium binding adaptor molecule 1 (Iba1) (Figure 2.5). Next, as the olfactory epithelium exhibits lifelong neurogenesis *in vivo*, I tested for neuroblasts, mature neurons as well as astrocytes. I used the neuroblast marker doublecortin (DCX), which is an early neuronal marker than is expressed by neuroblasts and neurogenic cells that are committed to a neuronal fate, the neuronal marker MAP2 and the astrocytic marker GFAP. I found an absence of expression of these markers for neuroblasts, mature neurons and astrocytes. However, all cells were found to be immunoreactive for the neural stem cell marker and the bone marrow-derive mesenchymal stem cell marker Nestin, and for the general mesenchymal stem cell marker CD105. All cells also were stained positive for βIII-tublin. The same pattern of expression pattern was observed when the OE-MSCs were cultured as spheres in the presence of mitogens and absence of serum (Figure 2.6), as when cultured as monolayers in the presence of serum and absence of mitogens (Figure 2.5). All no primary antibody controls stained negative for all markers and all antibodies were tested previously on positive control cell types (data not shown).

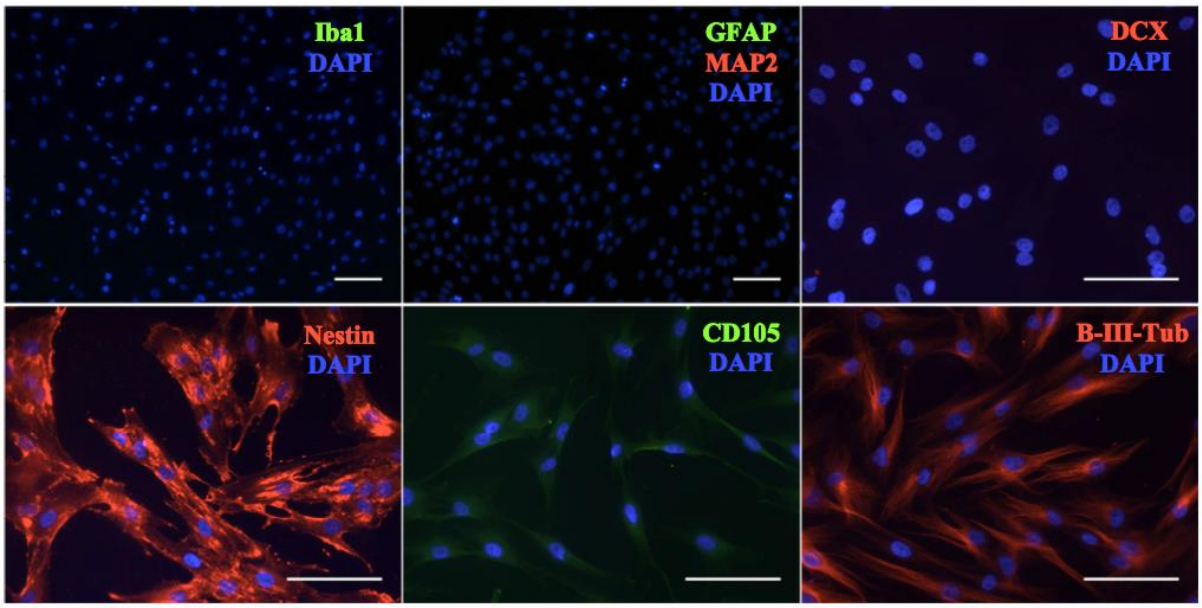


Figure 2.5 Expression patterns of cell identity markers on OE-MSCs when cultured as monolayer. OE-MSCs from all the patients and controls showed the same pattern of cell identity marker immunoreactivity; they all stained negative for macrophage/microglia marker Iba1, astrocyte marker GFAP, neuronal maker MAP2 and neuroblast marker DCX, while all the cells from all the lines stained strongly positive for neural stem cell marker and bone marrow-derived mesenchymal stem cells marker Nestin, weakly positive for general mesenchymal stem cell marker CD105 and neuronal marker βIII-tubulin. Representative pictures from one control subject (010N) were shown. Blue=DAPI nuclear stain. Scale bar=100 µm.

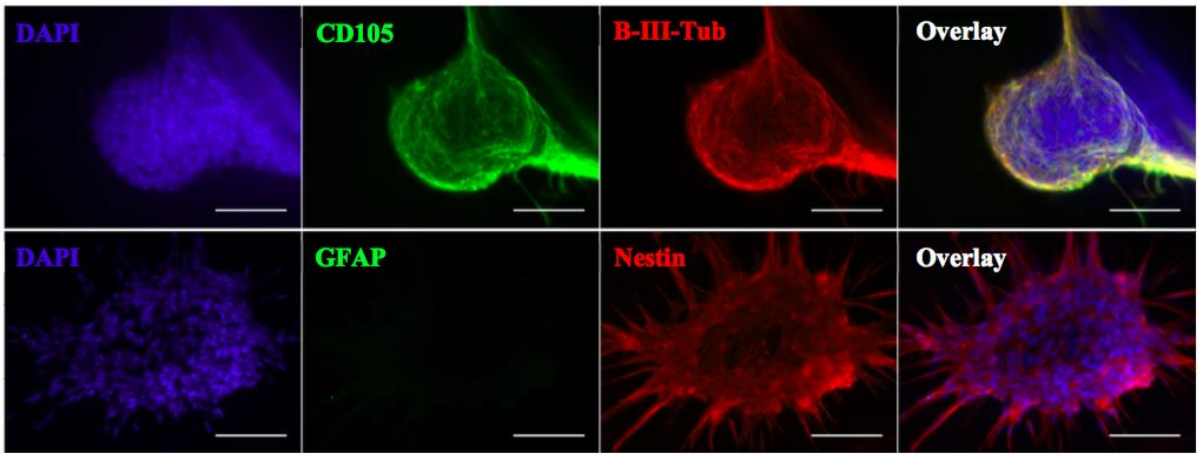


Figure 2.6 Expression patterns of cell identity markers on OE-MSCs when cultured as spheres. OE-MSCs from all the patients and controls showed the same pattern of cell identity marker immunoreactivity, when cultured as spheres; they all stained negative for macrophage/microglia marker Iba1, astrocyte marker GFAP and neuroblast marker DCX, while all the cells from all the lines stained strongly positive for neural stem cell marker and bone marrow-derived mesenchymal stem cell marker Nestin, weakly positive for general mesenchymal stem cell marker CD105 and neuronal marker βIII-tubulin. Representative pictures from one control subject (010N) were shown. Blue=DAPI nuclear stain.
Scale bar=100 μm.

2.6.3 The proliferation rate of OE-MSCs remains the same between patients and controls

One of the key characteristic behaviours of OE-MSCs *in vitro* is being high proliferative, and it was shown by previous studies that, when derived from patients with adult-onset schizophrenia the OE-MSCs proliferated faster than their counterparts from healthy controls (Fan et al., 2012; Feron et al., 1999; McCurdy et al., 2006). Therefore, the rate of proliferation of OE-MSCs derived from patients with adolescent-onset schizophrenia and from healthy controls was compared. Population doubling time (PDT) assays showed the time required for the entire starting cell population to double in number, and Edu (5-ethynyl-2´-deoxyuridine) assays showed the percentage of cells that incorporate Edu—an deoxyribonucleoside analog for DNA synthesis. Therefore, using PDT and Edu assays I broke down the proliferation question to how fast the cells divided as a population, and what percentage of cells were actually dividing. The impact of passage number on the proliferation rate was checked by comparing PDT of adherently cultured OE-MSCs derived from multiple subjects from passage 5 to passage 9. Results showed that PDT increased for all the cell lines as passage number going up, and this increase in PDT could vary significantly between different lines (data not shown); two lines with the same PDT at passage 5 could show considerably different PDT at passage 9. Therefore, passage 6 (as an early passage) OE-MSCs were used to compare all patients and controls for the purpose of reducing noise introduced by extended *in vitro* culturing. As shown in Figure 2.7, both patient cells and control cells showed high within-group variation in the PDT. Overall, no significant between-group difference was observed. The lack of difference in proliferation as seen in the PDT assay was confirmed with results obtained from the Edu assay (Table 2.4). As shown in Figure 2.8, as the exposure time to Edu increasing from 2h to 6h, the percentage of Edu-positive cells also increased. This showed

that Edu worked in a time-sensitive manner. All negative controls without Edu only showed blue DAPI nuclear staining (data not shown), ruling out the possibility of Edu giving false positive signals. Six-hour Edu exposure time was used for all following experiments to avoid comparing low numbers of cells for the purpose of reducing noise from inaccurate cell counting, and to allow for a convenient range of labelled cells from all lines. After 6h incubation with Edu, 50-60% cells of total cells from each line were labelled. However, no between-group difference was observed (Table 2.4). These data showed that OE-MSCs isolated from the current cohort were 1) highly proliferative, same as described in previous studies, 2) equally proliferative when derived from patients or from controls, as neither the speed of dividision on a population level nor the size of the pool of dividing cells was significantly different.

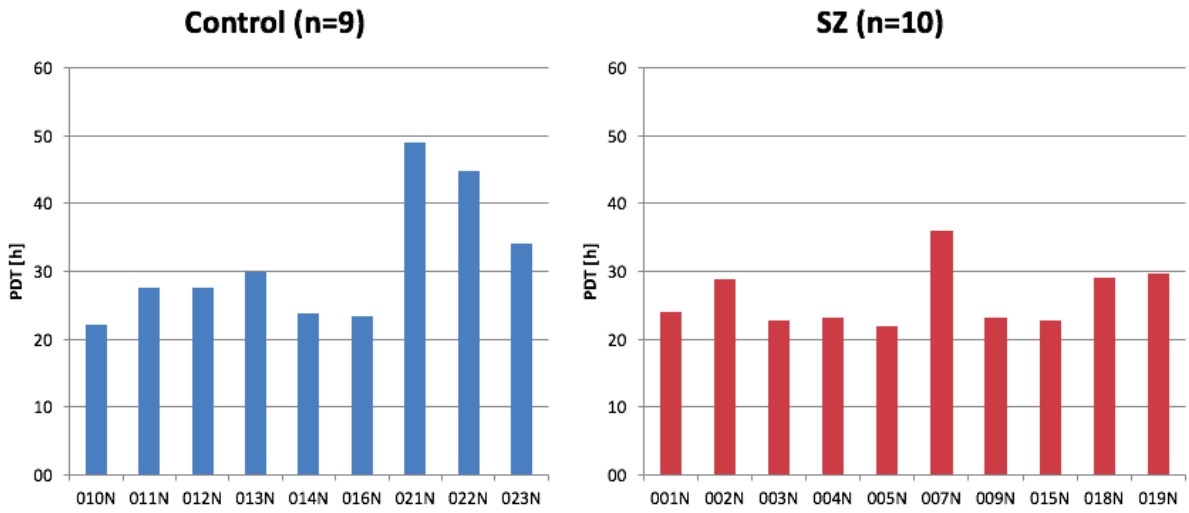


Figure 2.7 Comparison of population doubling time (PDT) between 9 controls and 10 patients (SZ). The number of cells were counted at 24h, 48h, 72h and 96h post-seeding. The time required for the entire cell population to double was calculated and shown on y-axis as PDT in hours (h). Individual PDT for each control line (blue) and patient line (red) was plotted in order to show variations within each group of disease status. No significant difference between patient lines and control lines was observed (2-tail Student's *t*-test, $p>0.05$).

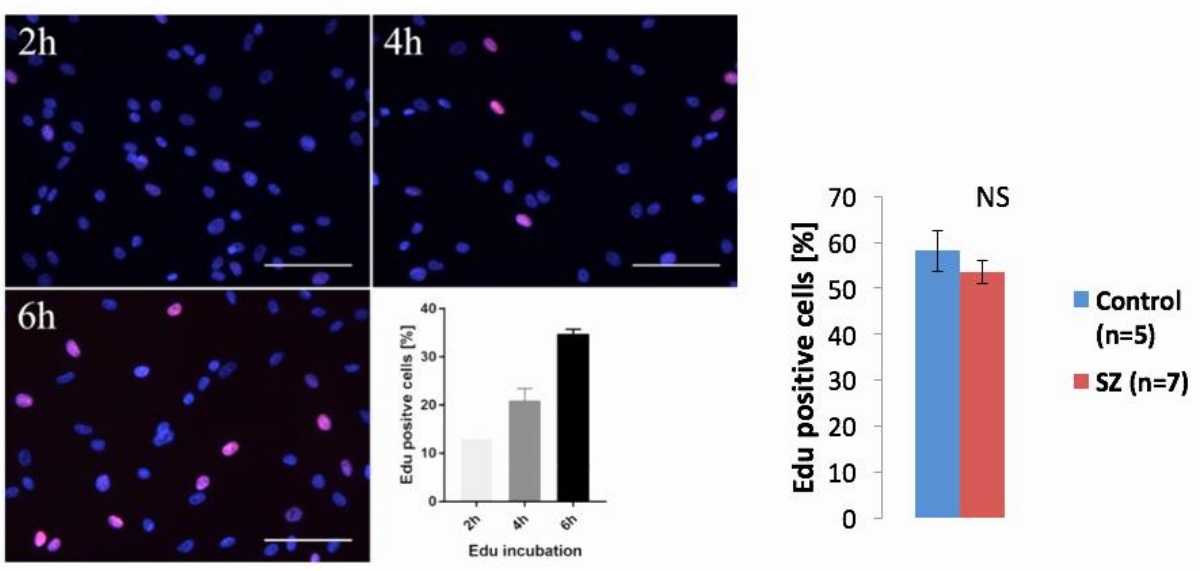


Figure 2.8 Comparison of the percentage of dividing cells using Edu-incorporation as an index between 5 controls and 7 patients (SZ). The amount of Edu-positive (purple) cells among DAPI nuclear stain positive cells (blue) increased as exposing the cells with Edu for 2h (light grey bar), 4h (dark grey bar) and 6h (black grey bar), respectively before fixation. Negative control without Edu only stained blue (data not shown). Six-hour Edu exposure time was used in following experiments. Blue bar represents average percentage of cells that incorporated Edu in 6h among all cells from 5 control lines, and red bar represents that from 7 patient lines. No significant difference was observed between two groups (2-tail Student's *t*-test, $p>0.05$) Error bar=standard error of the mean. Scale bar=100 µm.

Table 2.4 Percentages of Edu-incorporated cells after 6h Edu pause.

Line	Edu+ count	DAPI+ count	Edu/DAPI (%)
control 010N	17.3 ± 0.6	27.8 ± 1.0	62.9 ± 1.4
control 011N	35.6 ± 2.1	86.9 ± 8.1	43.8 ±2.9
control 012N	11.7 ± 0.5	24 ± 1.1	50.1 ± 2.0
control 014N	16.1 ± 0.6	26.8 ± 0.8	60.5 ± 1.6
control 016N	17.3 ± 0.5	25.1 ± 1.1	70.8 ± 2.0
patient 002N	11.2 ± 0.7	27.1 ± 1.7	42.8 ± 2.1
patient 003N	14.3 ± 0.8	23 ± 1.1	61.6 ± 1.5
patient 004N	15.6 ± 0.7	28.9 ± 1.1	54.3 ± 1.5
patient 005N	12.8 ± 0.6	24.0 ± 0.9	53.3 ± 1.6
patient 009N	10.9 ± 0.5	22.5 ± 0.6	48.5 ± 2
patient 015N	15.4 ± 0.5	25.1 ± 0.6	61.4 ± 1.7
patient 019N	10.2 ± 0.6	19.1 ± 0.7	52.9 ± 1.8

2.6.4 Similar sphere-formation ability between patient cells and control cells

The ability for single cells to form spheres over extended period of culture has been generally accepted as an index for self-renewal ability in stem cell researches. OE-MSCs can either be cultured as monolayers in the presence of serum or as spheres in the presence of mitogens. The efficiency of sphere-formation was measured by counting the number of spheres raised from single cell suspension of OE-MSCs in the presence of mitogens. This was to firstly confirm that all the OE-MSCs used in the current study behaved similarly as described in the literature, and secondly to compare the self-renewal ability, as an essential property of all stem cells, between patient cells and control cells. As shown in Figure 2.9, the success of sphere formation was dependent on the initial plating density of OE-MSCs. Based on results obtained from a few test lines, a plating density of 15,000 cells/cm^2 on poly-L-lysine (PLL) coated plates was sufficient to allow sphere-formation in the first 6 days with mitogens for most of the lines (sphere counts listed in Table 2.5). For the other lines, higher plating densities resulted in confluent monolayer without sphere formation (data not shown). However, it is worth noting that although plated as single cells in medium promoting sphere formation, OE-MSCs always underwent an initial growth phase as monolayers before giving rise to spheres, which was in line with previous observations (Matigian et al., 2010). This indicated that OE-MSCs form spheres in a pattern that was fundamentally different from that of neural stem cells, hence caution should be given when interpreting the sphere-formation for OE-MSCs as an index for self-renewal. Rather, the sphere-formation of OE-MSCs is likely a combinatory result from self-renewal, proliferation and cell-cell interaction.

In order to retain the intrinsic properties of OE-MSCs, a relatively early passage number (passage 7) was used for all lines. Same initial plating density and medium refreshment interval was applied for all lines. At day 8, most lines generated spheres with a healthy morphology (Figure 2.10, Table 2.5); clear edge, translucent body and a dark core. However, 2 out of 6 control lines and 4 out of 11 patient lines did not generate any spheres by day 8. Extended period of culture with mitogens showed that they were able to eventually give rise to spheres 1-2 months after seeding. Increasing the initial plating density may allow those slow sphere-generating lines to form spheres quicker (communication with McKay-Sim group). For the lines that were able to give rise to spheres within the first month, the number of spheres was counted from three wells per line at day 6 and day 8. As shown in Figure 2.9, no significant differences were observed between patients and controls. Together, these data showed that 1) all lines were able to generate spheres, 2) sphere-formation of OE-MSCs was plating density-dependent, and 3) different lines varied in the speed and efficiency of generating spheres in a disease-irrelevant manner.

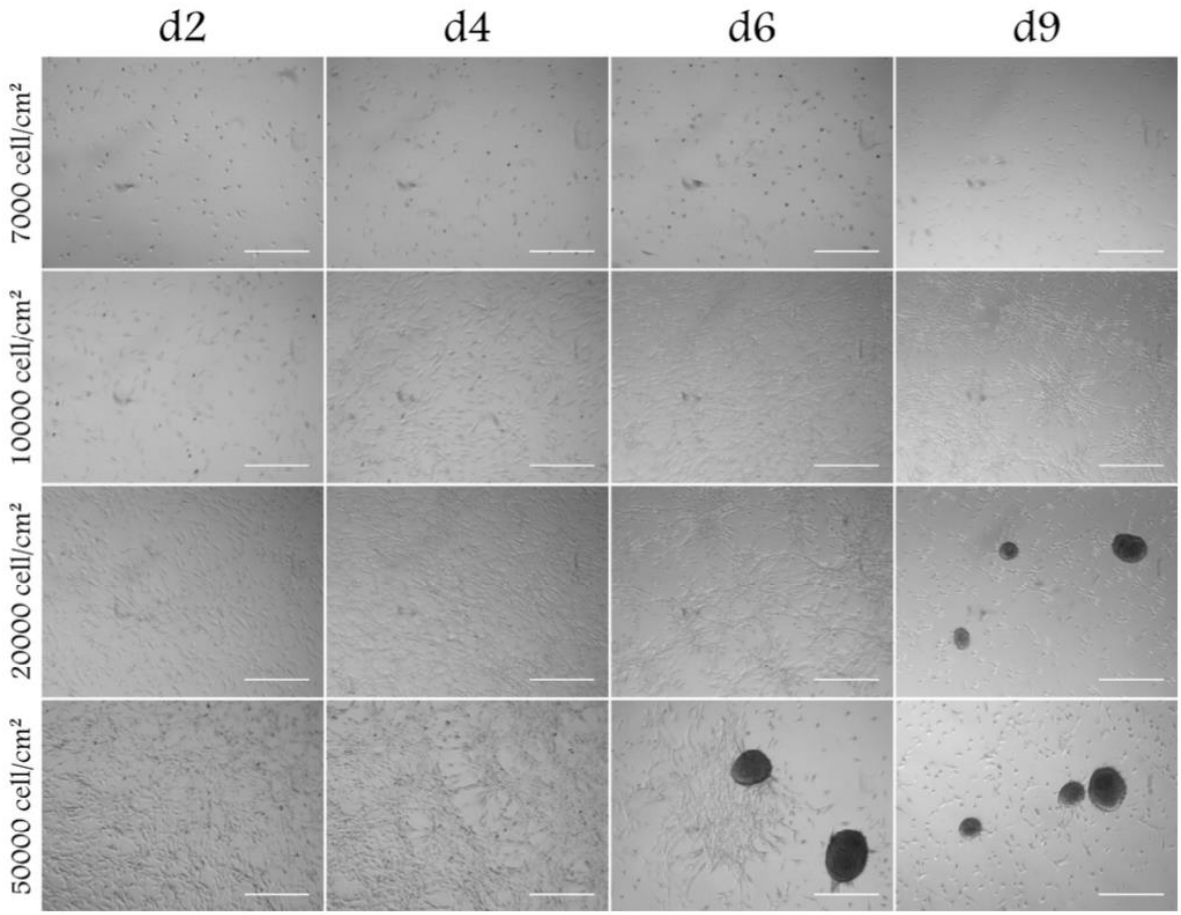


Figure 2.9 sphere formation of OE-MSCs in the presence of mitogen is dependent on the initial seeding density. Passage 10 OE-MSCs from a control line (010N) was seeded at 7,000-50,000 cells/cm^2 on poly-L-lysine (PLL) coated well plates. X-axis=days after seeding. Scale bar=500 µm.

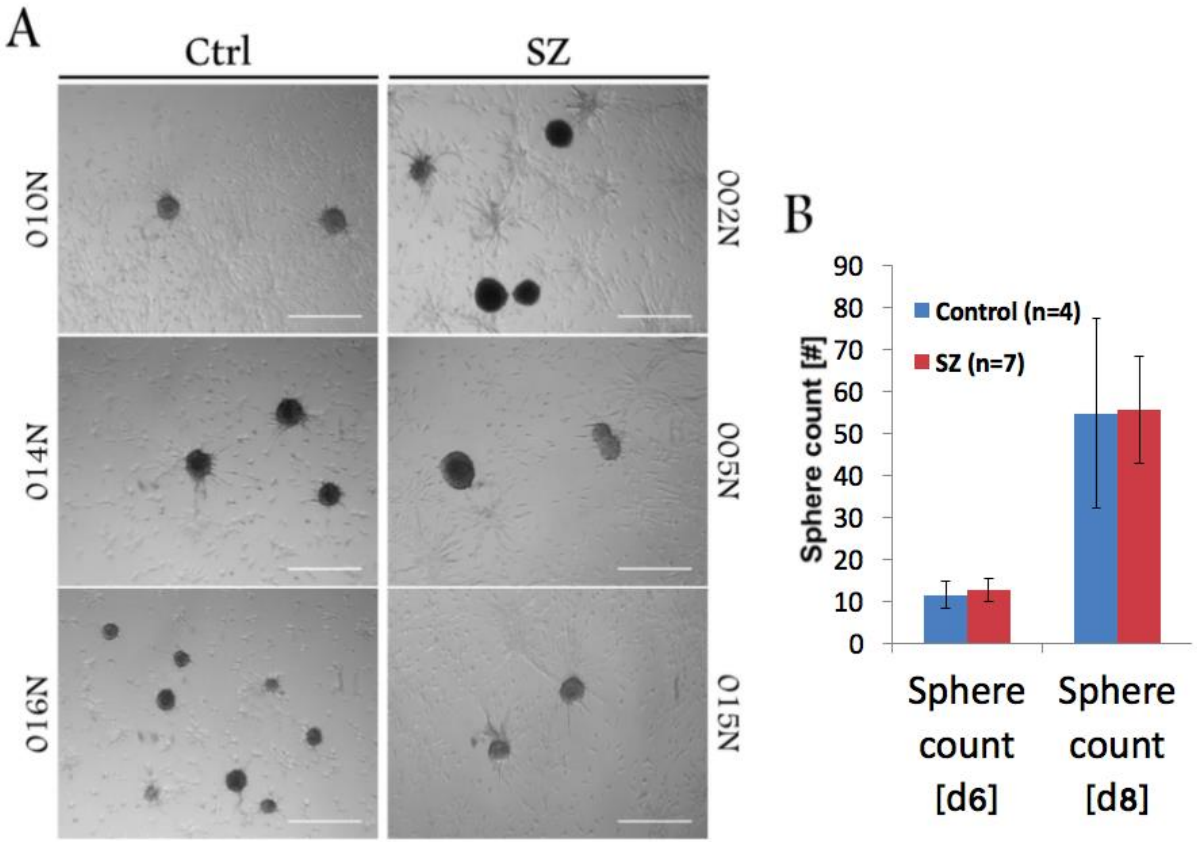


Figure 2.10 Comparison of sphere-formation ability from OE-MSCs derived from 4 controls and 7 patients. A) representative images taken from sphere cultures of 3 control lines (left panel A) and 3 patient lines (right panel A). The number and size of spheres varied in each group but showed no overall difference between groups. B) The number of spheres was counted at day 6 (d6) and day 8 (d8) after seeding cells at 15,000 cells/cm^2. Six control lines and 11 patient lines were initially used, however no spheres were formed based on the tested seeding densities by day 8 for control lines 011N and 013N, patient lines 001N, 006N, 007N and 018N. Higher plating density would be necessary for those lines. Blue bar represents average number of spheres from three technical replicates (3 culture wells) for patient lines 002N, 003N, 004N, 005N, 009N, 015N and 019N. Red bar represents that for control lines 010N, 012N, 014N and 016N. All lines were at passage 7. No significant difference was observed between groups, including or excluding the lines with 0 sphere at day 8 (2-tail Student's *t*-test, $p>0.05$). Error bar=standard error of the mean. Scale bar=500 µm.

Table 2.5 The numbers of spheres raised from single-cell plated OE-MSCs cultured for 6 and 8 days with mitogens.

Line	cells seeded/well	spheres on day 6	spheres on day8
control 010N	57,000	13.7 ± 2.2	35.3 ± 18.9
control 012N	57,000	2.3 ± 1.5	17.3 ± 4.9
control 014N	57,000	13 ± 6	46.7 ± 11.1
control 016N	57,000	17.0 ± 3.5	120.0 ± 5.5
control 011N	57,000	0	0
control 013N	57,000	0	0
patient 002N	57,000	19.7 ± 2.4	106.3 ± 8.1
patient 003N	57,000	8.7 ± 1.3	24.3 ± 2.4
patient 004N	57,000	12.0 ± 2.1	38.3 ± 9.1
patient 005N	57,000	7.3 ± 1.8	99.0 ± 16.3
patient 009N	57,000	22.0 ± 3.8	23.3 ± 4.3
patient 015N	57,000	17.0 ± 1.7	50.7 ± 19.7
patient 019N	57,000	2.0 ± 1.5	46.7 ± 12.4
patient 001N	57,000	0	0
patient 006N	57,000	0	0
patient 007N	57,000	0	0
patient 018N	57,000	0	0

2.6.5 Cell death rate remains the same between patient cells and control cells

As stem cells and progenitor cells undergo apoptosis routinely during development to maintain homeostasis of cell populations, the extent of cell death was compared for OE-MSCs derived from patients and controls. NucBlue is a cell membrane permeant dye that stains the nucleus of both live and dead cells blue, NucGreen is a dye that cannot penetrate the plasma membranes of live cells, hence selectively stains the nucleus of dead cells in green. After co-staining of NucBlue and NucGreen, nuclei of live cells were blue whereas nuclei of dead cells were both green and blue. As shown in Figure 2.11 and Table 2.6, dead cells only account for a minor population in OE-MSC adherent cultures from patient lines and control lines. A positive control of 4-hour treatment with 1mM hydrogen peroxide (H_2O_2) was able to increase the percentage of dead cells to 82% (Figure 2.11). Negative controls showed no staining (data not shown).

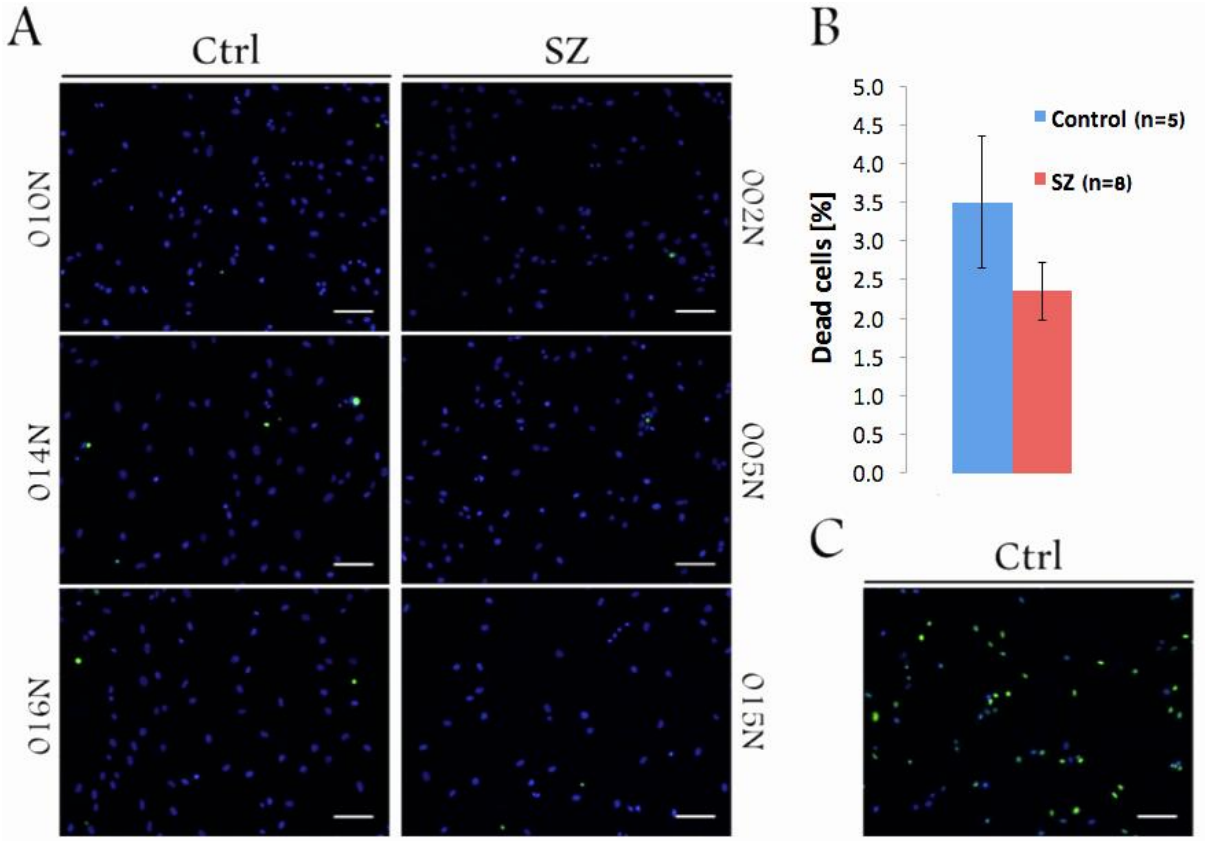


Figure 2.11 Comparison of percentage of dead cells in OE-MSC cultures derived from 5 controls and 8 patients. All lines were at passage 7 as adherent cultures. NucBlue/NucGreen co-stained dead cells whereas NucBlue only stained live cells. A) Representative images taken from 3 control lines and 3 patient lines. B) Cell counting results of percentage of dead cells among all cell populations from 10 fields/line. Both groups showed a very low number of dead cells present in the OE-MSC cultures. No significant difference was shown between groups (2-tail Student's *t*-test, $p>0.05$). C) Positive control of staining using 4 hours treatment of 1mM H_2O_2 elevated the percentage of NucGreen+ cells. Error bar=standard error of the mean. Scale bar=100 µm.

Table 2.6 The numbers of live cells and dead cells present in OE-MSC cultures.

Line	dead cell count	live cell count	dead/total (%)
control 010N	1.9 ± 0.2	103.2 ± 2.7	1.6 ± 0.5
control 011N	3.4 ± 1.0	155.7 ± 43.7	2.4 ± 0.5
control 012N	2.0 ± 0.2	72.3 ± 2.2	2.5 ± 0.4
control 014N	4.1 ± 0.3	58.4 ± 2.2	7.1 ± 1.1
control 016N	3.3 ± 0.3	81.1 ± 2.1	3.6 ± 0.6
patient 002N	1.0 ± 0.1	83.0 ± 2.7	1.4 ± 0.3
patient 003N	1.5 ± 0.2	82.6 ± 5.8	2.3 ± 0.8
patient 004N	1.3 ± 0.2	81.0 ± 4.2	2.4 ± 0.5
patient 005N	1.9 ± 0.4	102.5 ± 3.1	3.4 ± 0.5
patient 009N	2.4 ± 0.2	92.0 ± 3.1	2.4 ± 0.4
patient 015N	2.7 ± 0.3	57.0 ± 2.1	5.0 ± 0.7
patient 018N	6.8 ± 0.8	225.4 ± 33	3.4 ± 0.7
patient 019N	1.9 ± 0.2	86.0 ± 2.3	2.4 ± 0.4

2.6.6 No difference between patients and controls shown in 'wound-closure' assay

Progenitors from stem cells in development often need to migrate to the place where their differentiation reach the final maturity at. *In vitro*, the migration of stem/progenitor cells can be measured using a variety of techniques. The closure of a 'wound' made by a scratch on a confluent cell culture was carried out as an index of the cells ability to both proliferate and migrate into the 'wound'. As the proliferation did not differ between OE-MSCs derived from controls and patients, the rate of such 'wound' closure was used as an index of migration. Prior to the assay, the optimal passage number was determined by comparing the time required for seeded cells to grow confluent and the time required for the entire 'wound' to close; results showed that passage 5-7 gave stable outcomes however at passage 9 the time required in both procedures increased considerably (data not shown). Therefore, a relatively early passage number (passage 6) was used for all lines and the starting plating density was kept constant for all lines. In this assay, one scratch was made per well in a 6-well plate to create a 'wound' of the confluent cell culture and at three fixed locations on the scratch (Figure 2.12, B). Images were taken every 24h for a consecutive 6 days. As shown in Figure 2.12, comparison between 6 control lines and 10 patient lines did not result in significant difference in the 'wound' closure rate over time, suggesting that migration may not be altered in patients. To rule out the possibility of the heterogeneity in proliferation rates contributing to the noises for the 'wound' closure rate, cells were treated with chemical compounds that block proliferation. However, results showed that migration was severely hampered by the compounds at the same time. Therefore, it remained inconclusive whether cell migration of patient OE-MSCs was altered or not.

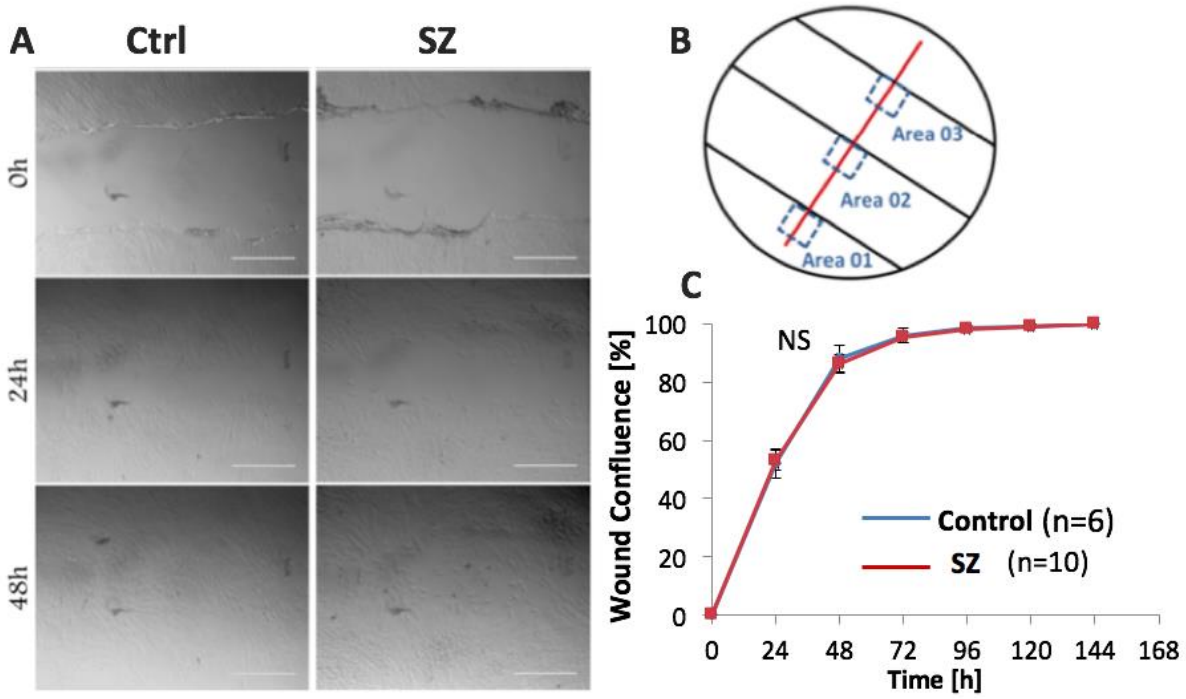


Figure 2.12 Comparison of the 'wound' closure time between 6 control lines and 10 patient lines. OE-MSCs were seeded at the same plating density at passage 6 and allowed to just reach confluency. A scratch was made on the surface of the confluent culture in 6-well plate. The width of the scratch was measured daily for 6 days. A) Representative images showing the 'wound' closure process for a control line (010N) and a patient line (002N). B) One linear 'wound' was made across the centre of a well using a 10 µl pippette tip, bright-field images were taken from three fixed locations per wound every 24h for a period of 6 days. The fixed positions were marked with a grid at the bottom of the culture wells. C) 'Wound' surface area in each bright-field image was analysed with ImageJ. Daily tracking of the 'would' closure showed no significant difference between 6 control lines and 10 patient lines (repeated measure ANOVA, $p>0.05$). Error bar=standard error of the mean. Scale bar=500 µm. NS=non-significant.

2.6.7 Patient cells have reduced cell-to-substrate adhesion ability

Cell adhesion is one of the most important cellular properties for multicellular organisms; it is one of the foundations that allow cells to migrate during development and to interact with each other under physiological conditions. Previous studies of cell adhesion have used static adhesion assays that involves coating culture flasks with components from extracellular matrix, hence measuring the cell-to-substrate adhesion, as well as using flow adhesion assays that usually measure cell-to-cell interactions of blood cell populations, circulating cancer cells and endothelial cells (Khalili & Ahmad, 2015). Cell-to-substrate adhesion was previously shown as hampered in OE-MSCs derived from patients with adult-onset schizophrenia, when compared to age- gender-matched healthy controls (Fan et al., 2013). To investigate whether the same holds true for OE-MSCs derived from this cohort, dissociated OE-MSCs at early passages were exposed to culture flasks that had been pre-coated with several substrates that are routinely used to enhance cell attachment. Poly-L-lysine (PLL), is a naturally occurring polymer of amino acids that carries positive charges on plastic in culture medium, poly-ornithine (PO), is a polymer of synthetic amino acids that also carries a positive charge. Laminins belong to a class of major components of the extracellular matrix that serves as the fundamental protein network for cell differentiation, migration and adhesion (Timpl et al., 1979). A contact period of 1h was used based on results obtained from pilot experiments testing various contact periods. As shown in Figure 2.13, after 1h, the numbers of cells remaining on culture flasks after gentle washing was revealed with DAPI nuclear staining. In general, OE-MSCs derived from patients showed a reduced cell-to-substrate adhesion ability. When analysed with repeated-measures analysis of variance (RM-ANOVA), which compared the mean scores from the patient group with the mean scores from the control group, on the

4 coating conditions, the patient group showed a significant reduction in cell adhesion compared to that of control group (p=0.03), the interactions were not significant. Therefore, the patient OE-MSCs showed overall reduced adhesion ability to adhesive substrates tested. However, the assay may lack the power to reveal significant difference at individual coating condition level, due to the presence of technical errors or the insufficient number of biological replicates.

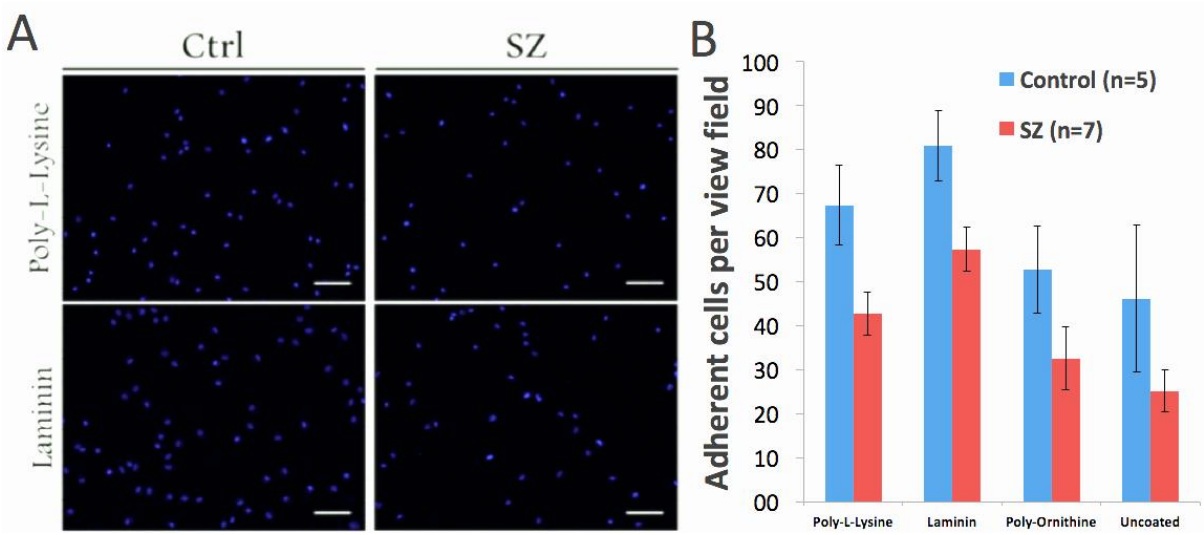


Figure 2.13 Comparison of the cell-to-substrate adhesion ability for OE-MSCs derived from 5 controls and 7 patients. Dissociated OE-MSCs at passage 7 were plated on to untreated culture flasks, as well as culture flasks pre-coated with poly-L-lysine (PLL), poly-ornithine or Laminin. After a contact period of 1h at 37°C, the number of remaining cells after gentle washing was determined by DAPI (blue) nuclear staining and ImageJ cell count function. A) Representative images showing fewer patient cells adhered to PLL-coated and laminin-coated wells. B) Cell counting results based on 10 images per well and 2 wells per line. Repeated-measures ANOVA considering the disease status as variable and the four coating conditions as independent observations showed significant overall reduction in patient group (p=0.03). Error bar=standard error of the mean. Scale bar=100 µm.

2.6.8 Patient cells are more prone to oxidative stress

Oxidative stress has long been implicated in the pathophysiology of schizophrenia (Emiliani, Sedlak, & Sawa, 2014). It results from imbalanced levels of reactive oxygen species (ROS) and enzymatic or non-enzymatic antioxidants. Key mediators of oxidative stress are superoxide and H_2O_2. To test whether OE-MSCs derived from patients have an elevated susceptibility to oxidative stress, OE-MSCs at passage 7 were treated with H_2O_2 at concentrations of 0.1-2.0 mM for 4 hours. As demonstrated in Figure 2.14, membrane blebbing, as a display of protrusions on plasma membranes and an acute cellular response to stress preceding apoptotic cascades (Ambasudhan et al., 2011), occurred in lower doses of H_2O_2 for patient cells than in control cells. Most patient lines showed severe membrane blebbing at 0.5mM H_2O_2 treatment except for one line (004N) while 5 out of 8 control lines did not show membrane blebbing, control line 010N, 012N and 021N showed severe, minor and moderate membrane blebbing, respectively (Figure 2.15, black arrows piont at examples of membrane blebs). However, subsequent assessment of the percentage of dead cells in H_2O_2 treated cell cultures with NucBlue and NucGreen live nuclear staining did not reveal a difference on cell death between patients and controls (Figure 2.14 bottom panel). This could be caused by an accelerated reaction to oxidative stress from patient cells that was reflected by morphological changes-membrane blebbing of the cells. Future experiment should extend the time of H_2O_2 treatment to investigate if eventually control cells and patient cells would show the same levels of membrane blebbing but patient cells react faster to H_2O_2 treatment.

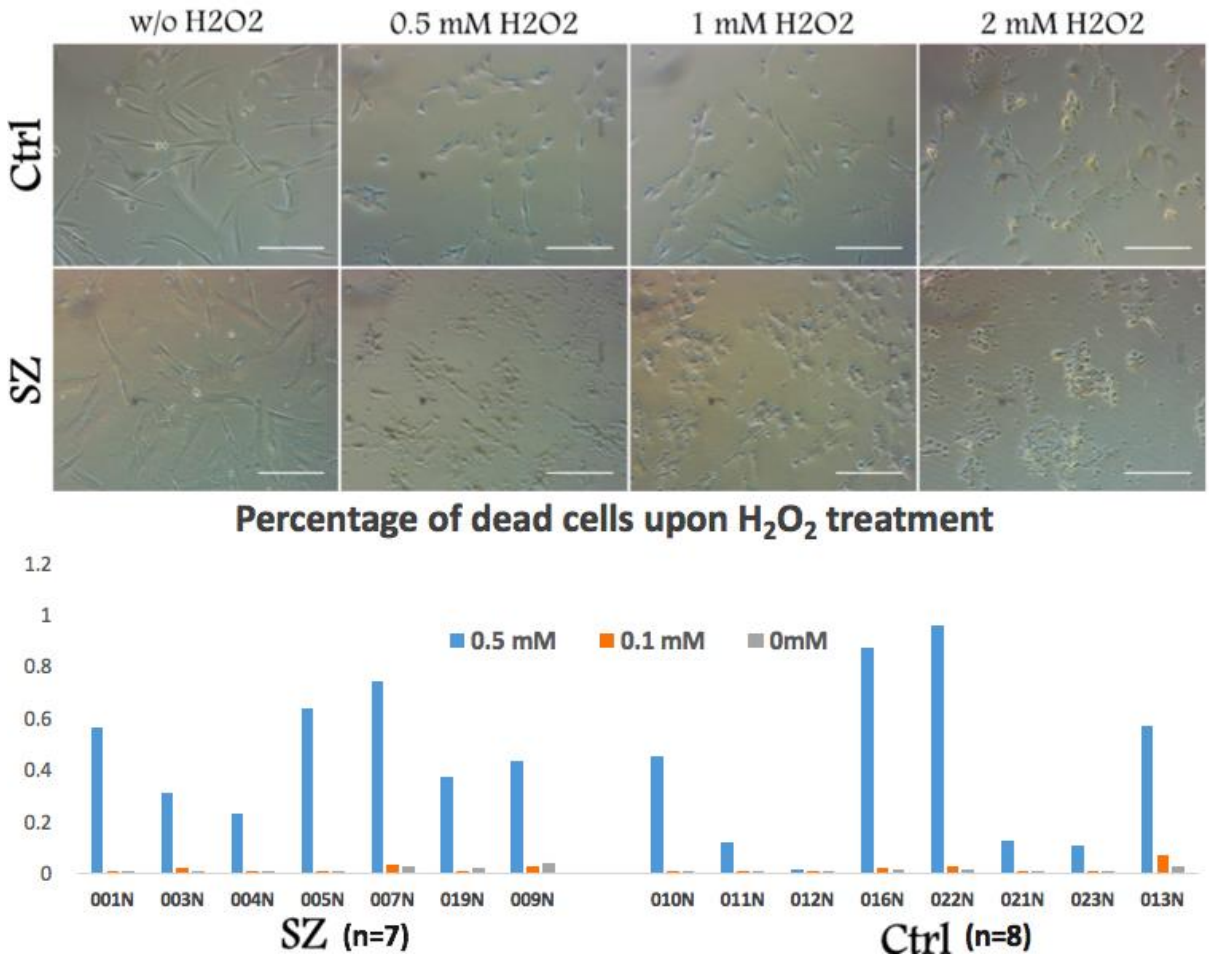
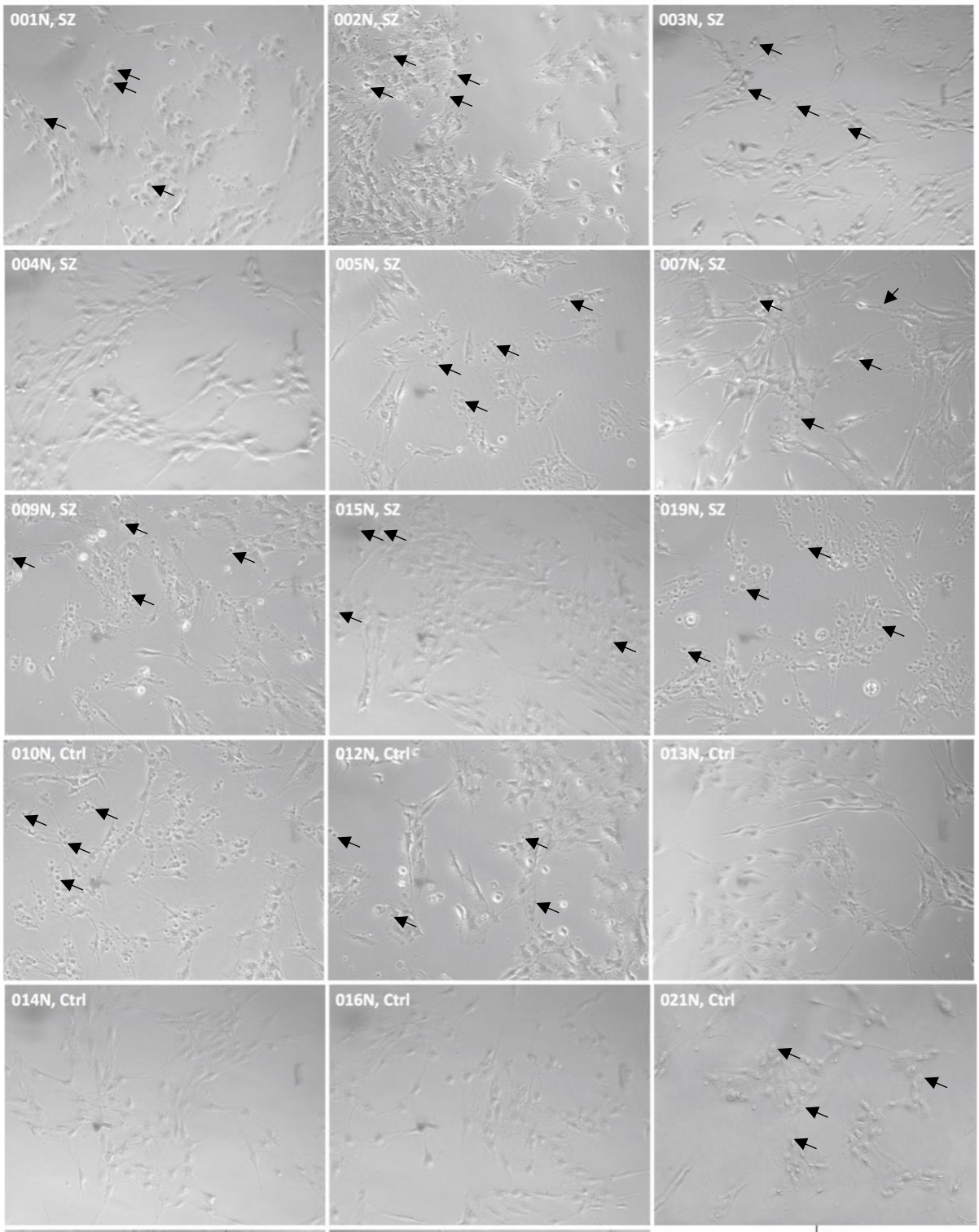


Figure 2.14 Comparison of oxidative stress response from OE-MSCs from 7 patient lines and 8 control lines. OE-MSCs at passage 7 were treated with increasing concentrations of H_2O_2 in culture medium for 4 hours at 37°C. Top panel: representative bright-field images taken from one patient line and one control line right after the 4-hour treatment. Patient cells showed membrane blebbing at lower dose of H_2O_2 treatment than control cells did. Bottom panel: Right after the treatment, live cells were stained with NucBlue that labels live cells and NucGreen that labels dead cells. The percentage of dead cells was calculated based on 15 images per line. No significant difference was detected in the percentage of dead cells present in the OE-MSC cultures after H_2O_2 treatment between patient group and control group (p>0.05). Scale bar=200 μm.



SZ	Ctrl
001N, ++	010N, +++
002N, +++	012N, +
003N, +++	013N, -
004N, -	014N, -
005N, +++	016N, -
007N, ++	021N, ++
009N, +++	022N, -
015N, ++	023N, -
019N, +++	

Figure 2.15 Morphological comparison of membrane blebbing from 9 patient lines and 8 control lines. OE-MSCs at passage 7 were treated with 0.5mM H_2O_2. Bright-field images were taken after 4h of treatment, 5 images were taken each line and the most representative image from each line was shown above. The degree of membrane blebbing was estimated by eye based on 5 images/line and represented with plus signs in bottom right table in which '-'=no membrane blebbing, '+'=minor membrane blebbing, '++'=moderate membrane blebbing, '+++'=severe membrane blebbing. Black arrows denote for blebs. Four examples were given per picture when there was membrane blebs of the cells. Scale bar=200 μm.

2.6.9 OE-MSCs can obtain neuron-like morphology in neuronal differentiation media

In order to investigate whether OE-MSCs could be used as a source for patient-derived neurons, previously published neuronal differentiation protocols for OE-MSCs were tested. Two culture methods have been established for OE-MSC maintenance, one plates down lamina propria in serum containing medium and directly culture the OE-MSCs migrated out as adherent cultures (Delorme et al., 2009), the other plates down lamina propria in serum-containing medium but subsequently cultures the OE-MSCs migrated out in serum-free and mitogen-containing medium to allow sphere formation. The spheres are then dissociated and re-plated in serum-containing medium as adherent culture. The sphere formation step could be preferable to some researchers as it enriched populations that were reactive to mitogens and reduces heterogeneity based on gene expression (Matigian et al., 2010). This method of culturing OE-MSCs was referred to as the sphere-derived monolayer culture. In published differentiation protocols, OE-MSCs were differentiated on culture plates that were either coated sequentially with PLL and laminin or with PO and laminin. Taken together, OE-MSCs cultured as adherent cultures and as sphere-derived monolayers, were differentiated on PLL and laminin coated, or PO and laminin coated culture flasks, using four published neuronal differentiation protocols. OE-MSCs at passage 5 for 3 control lines (021N, 022N and 023N) and 1 patient line (006N) were differentiated for 21 days, cells were fixed at day 14 and day 21, and subjected to immunostaining of pan-neuronal markers. As illustrated by Figure 2.16, cell morphology that was the closest to that of neurons was obtained from a condition using adherently cultured OE-MSCs, PLL and laminin coating and a differentiation medium made of neurobasal medium supplemented with GlutaMax, B27 and 0.025mM L-glutamic acid

(Delorme et al., 2009; Girard et al., 2011). Despite generating cells with morphologies that resembled very early neuronal morphologies (Figure 2.16), the culture did not result into immunoreactivity to any of the neuroblast marker DCX, the young neuron and the mature neuron marker βIII-tublin, the neuronal maker MAP2 or the astrocyte marker GFAP (data not shown).

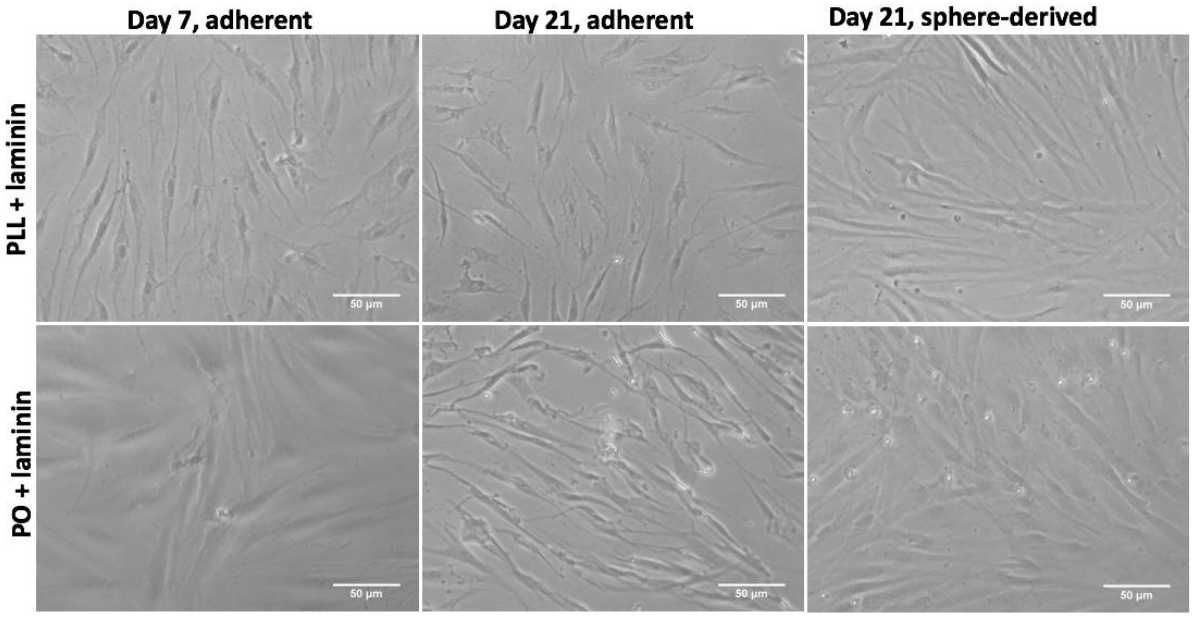


Figure 2.16 Morphological changes of OE-MSCs during neuron differentiation. Representative images were taken from a control line (021N, passage 5) that was differentiated in neurobasal medium supplemented with GlutaMax, B27 and 0.025mM L-glutamic acid (Delorme et al., 2009; Girard et al., 2011). A neuron-like cell morphology could be observed from 7 days onwards in the differentiation using culture flasks coated with poly-L-lysine (PLL) and Laminin. The neuron-like morphology was only observed for the OE-MSCs differentiated on poly-ornithine and laminin coated culture flasks at the end of the 21 day differentiation. Cells cultured as sphere-derived monolayers underwent less morphological changes during the differentiation.

2.6.10 Proteomic expression profiling showed EIF2 signalling was significantly downregulated in patient OE-MSCs

As hypothesis-free methods, transcriptomic and proteomic approaches allow the discovery of disease-associated perturbations based on the total messenger RNAs (mRNAs) and the total proteins that are present in the studied cell populations. While transcriptomic analysis reveals the totality of genes that are transcribed and their expression levels, proteomic analysis directly displays the sum results of genome-wide transcription, total translation and protein degradation, hence showing the pool of proteins that are readily available in the studied cell population. Previously, proteomics approaches have successfully been applied to show altered pathways associated with adult-onset schizophrenia, using sphere-derived monolayer cultures of OE-MSCs (English et al., 2015) and reprogrammed neural progenitor cells (Topol et al., 2015a). In order to investigate if the same pathways would be perturbed in adolescent-onset schizophrenia, passage 3 OE-MSCs from 11 patients and 9 controls were cultured as sphere-derived monolayers and total protein contents were harvested using the same method as previously described (English et al., 2015). As the rates and efficiency of generating spheres in the presence of mitogens vary between lines, in order to rule out possible confounding factors underlying this variability, 6 patient lines and 6 controls lines were eventually harvested for proteomic study as they all generated spheres in a relatively short period of time (within 11-18 days). The rest of the lines generated spheres only after 1 month's culture in serum-free medium with mitogens. The spheres were collected and re-plated as whole spheres in serum-containing medium, cells from all lines (6 patients and 6 controls) migrated out and grew into confluent monolayer in 4 days. Harvested total proteins were stored at -80°C and shipped on dry ice to a collaborator's lab who studies psychiatric

disease using mass spectrometry techniques (laboratory of Prof. David Cotter's, Department of Psychiatry, Royal College of Surgeons in Ireland, all analyses were done by Dr. Melanie Focking). Within the expected range, 1542 proteins were successfully identified in the total 12 samples. As a routine quality control step, 20% of the proteins that were least expressed among all samples were discarded, leaving the dataset with 1336 proteins that were mostly consistently expressed. These were the proteins used in all subsequent statistical and bioinformatics analyses.

First, principle component analysis (PCA) was carried out to identify the possible relatedness between samples. The relative abundance of each individual target proteins compared to total protein contents for the patient and control groups were calculated with R studio. As shown in Figure 2.17, on the two principal components (shown as PC1 and PC2) that explain most of the variances present in the total proteins from all samples (16.89% and 14.49%, respectively), 5 of the patient samples clustered together and 5 of the control samples clustered together closely. One patient sample (015N) and one control sample (023N) were considered as outliers as they did not cluster together with their group defined by disease status. However, OE-MSCs derived from 015N and 023N did not display any unexpected behaviours in the cellular assays. Given that samples from 015N and 023N were the last pair measured with the mass spectrometer, technical errors of the mass spectrometer may account for the discrepancy between observations from peptide counts and observations from cellular behaviours. Inclusion of 015N and 023N did not alter results for the subsequent pathway analyses. Nevertheless, in order to limit the variations within each group when dissecting out proteins that were responsible for distinguishing the patient group and control group, proteins from the 5 patient samples and the 5 control samples that were clustered

together were used for following-up statistical and pathway analyses. Analysis of the 5 patients as a group was done, versus analysing each individual patient, to increase the confidence of discovering disease-associated alterations and to limit the chances of associating protein expression changes to possible confounding factors specific to individual patients.

Next, using Empirical Bayes Statistics for Differential Expression analysis, 127 proteins were found significantly differentially expressed between patient group and control group at a confidence interval of 95%. In permutation-based statistical tests for multiple hypotheses, false positive discovery rate (FDR) describes the possibility of expected rates of false positives among all the claimed positives. In order to discover the most significantly altered pathways, a stringent FDR value of 0.01 was initially applied. No individual protein survived the threshold of significance. To identify disease-associated pathways, a lower-stringency FDR value of 0.05, which was generally used and accepted in the literature, was applied. As a result, 12 proteins survived the FDR of 0.05 (Table 2.7). These proteins represented a range of molecular activities within the cell, including post-translational phosphorylation of proteins, lipid metabolism, endocytosis and ion transport.

In order to identify pathways that most of the significantly expressed proteins from the 1336 total proteins from the 5 patients and the 5 controls fall into, Kyoto Encyclopedia of Genes and Genomes (KEGG) pathway analysis and Ingenuity Pathway Analysis (IPA) analysis were carried out. The KEGG is a collection of databases that contain information on genomes, cellular pathways and their responses to diseases and chemical treatments. It is often used for pathway analysis when interpreting ‘omic data. IPA is an analysis tool for ‘omic data that

can identify relevant signalling pathways and predict their upstream or downstream effects. Table 2.8 and Table 2.9 summarise the most relevant pathways identified with KEGG and IPA, respectively. The most highly significantly implicated cellular processes from KEGG analysis includes ribosomes, biosynthesis of antibiotics, endocytosis, protein processing in endoplasmic reticulum and focal adhesion. IPA results showed the most significantly implicated molecular pathways as the eukaryotic initiation factor 2 (EIF2) signalling, the Farnesoid X receptor (FXR)/FXR activation, Liver X receptor (LXR)/Retinoid X receptor (RXR) activation, tricarboxylic acid (TCA) cycle II and mTOR signalling based on *p*-values. While *p*-values shows the probability of obtaining certain pathways from the analysed dataset based on random observation, z-scores shows the standard deviation of the obtained pathways from a theoretical random pattern which is usually used as the *null* hypothesis in the test. The further the data were from the centre of the normal distribution curve, the smaller the *p*-value will get and the so does the absolute value of the z-score (as z-score can be positive or negative). Hence, the *p*-value and z-score together depict the statistically significant spatial structure of the dataset. As shown in Figure 2.18, the EIF2 signalling came up as the top significantly pathway that was downregulated in patient samples, with the smallest *p*-value and a greatest negative z-score, based on an individualised significance threshold to EIF2 pathway embedded in the IPA software. The second most significantly downregulated pathway was FXR/FXR activation. The only significantly upregulated pathway based on IPA was TCA cycle II (eukaryotic). As a summary, pathway analysis showed signals discriminating the patient group and the control group were highly likely to come from a downregulated EIF2 signalling, a downregulated FXR/FXR activation, as well as an upregulated TCA cycle II in patient OE-MSCs, compared to controls. The most significantly affected cellular components and processes includes ribosomes, endocytosis, post-translational modification and focal

adhesion. It is worth noting that a deficiency of EIF2 signalling in patient samples showed up as the most universally reported result from all analyses performed so far with 15 implicated protein members from the pathway, and with a functional link to ribosomes.

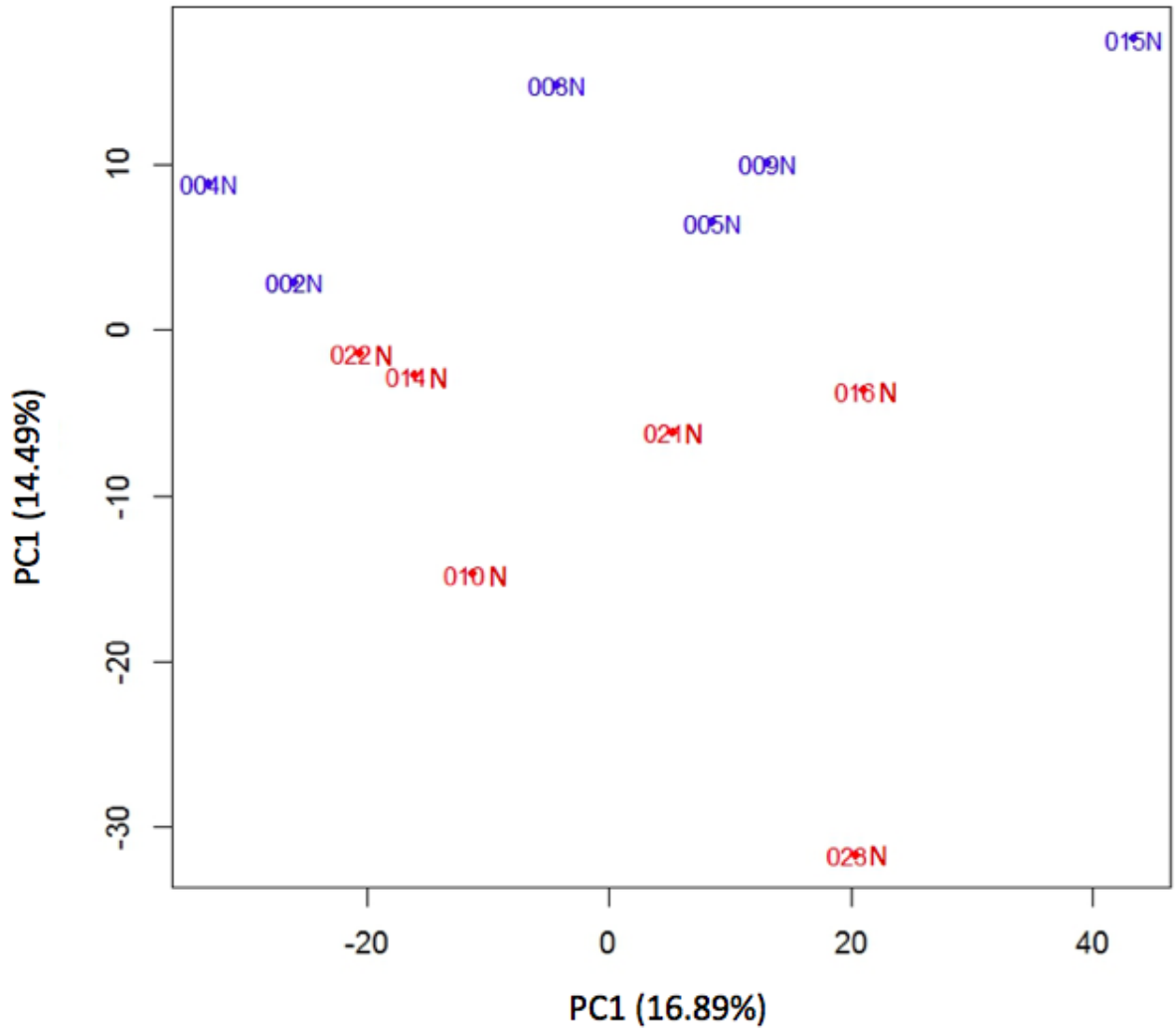


Figure 2.17 Principal component analysis of total proteins from 6 patients (blue) and 6 controls (red). After removing 20% of the least expressed proteins among all samples, 1366 proteins were left and used in the principal component analysis (PCA). On PC1 and PC2, which were the two principal components that best explaining the total variances, 5 patient samples and 5 control samples clustered together according to their group defined as disease status. One patient samples (015N, top right) and one control sample (023N, bottom right) did not cluster with their groupmates hence were considered as outliers. Including 015N and 023N into downstream analysis did not change the results from the subsequent pathway analyses.

Table 2.7 A list of False Discovery Rate positive (FDR) proteins that were significantly differentially expressed between patient group and control group and their corresponding functions.

Protein ID	Protein name	Protein functions
P62633	CNBP, cellular nucleic acid-binding protein	DNA binding protein, sterol-mediated repression, exact function unknown but regulates other genes, required for embryonic development, mostly expressed in muscles
Q5XG92	CES4A, Carboxylesterase 4A	secreted enzyme, may play a role in detoxification of drugs and xenobiotics in neural tissues and cerebrospinal fluid
P04217	A1BG, Alpha-1B-glycoprotein	plasma glycoprotein with unknown function, involved in amyotrophic lateral sclerosis, shared sequence similarities with some immunoglobulin superfamily members
P68871	HBB, Haemoglobin subunit beta	beta chain of the haemoglobin, oxygen delivery to various tissues
P02647	APOA1, Apolipoprotein A-I	promotes cholesterol efflux from tissues, most abundant apolipoprotein in the CSF, has multiple functions involved in immunity, inflammation, apoptosis etc. (protein present in the brain but not mRNA)
P02765	AHSG, Alpha-2-HS-glycoprotein	carrier protein for calcium and phosphate, involved in endocytosis, brain development, formation of bone tissues
P19823	ITIH2, Inter-alpha-trypsin inhibitor heavy chain H2	post-translational protein phosphorylation, regulation of insulin-like growth factor transport and uptake, regulates homeostasis of hyaluronic acid
P02771	AFP, Alpha-fetoprotein	plasma protein, present during fetal development, post-translational protein phosphorylation, regulation of insulin-like growth factor transport and uptake, bind copper or nickel
P02686	MBP, Myelin basic protein	most abundant protein components of the myelin membrane, may also be involved in early brain development before myelination as a member of transcriptional complexes, may be involved in signalling in T-cells and neural cells
P48681	NES, Nestin	required for brain development, intermediate filament protein
P02774	GC, Vitamin D-binding protein	vitamin D transport and storage, scavenging of extracellular G-actin, regulates chemotactic activity of c5 alpha in immunity
P98082	DAB2, Disabled homolog 2	endocytosis of specific proteins (e.g. integrinβ-1, TGFβ receptor), involved in multiple signalling pathways, may be involved in myeloid cell differentiation and macrophage adhesion/spreading. Related with DAB1 which regulates neurodevelopment

Table 2.8 Pathway analysis using Kyoto Encyclopedia of Genes and Genomes (KEGG) of differentially expressed proteins identified with mass spectrometry between OE-MSCs derived from 5 patients and 5 controls.

Term	protein count	% of total protein analysed	*p*-value*
Ribosome	75	5.6	6.3E-35
Biosynthesis of antibiotics	68	5.1	1.7E-15
Endocytosis	59	4.4	2.8E-7
Protein processing in endoplasmic reticulum	52	3.9	3.2E-11
Focal adhesion	49	3.7	1.0E-6
Spliceosome	47	3.5	1.5E-12
Regulation of actin cytoskeleton	47	3.5	1.2E-5
RNA transport	45	3.4	1.8E-7
Carbon metabolism	42	3.1	4.3E-12

**p*-value here describes the rate of identifying the reported pathway as a false-positively when giving the implicated molecules. E.g. the change of discovering ribosome pathways is 6.3E-35 when 75 proteins, which account for 5.6% of the total protein present in the dataset,

Table 2.9 Ingenuity pathway analysis (IPA) of differentially expressed proteins identified with mass spectrometry between OE-MSCs derived from 5 patients and 5 controls.

Pathway	*p*-value	Implicated molecules
EIF2 signalling	4.18E-12	RPL7, RPL21, RPL23, RPL24, RPL28, RPL32, RPL18A, RPS6, RPS8, RPS11, RPS13, RPS26, RPS27L, RPS3A, WARS
FXR/FXR activation	7.00E-07	A1BG, AHSG, APOA1, GC, PCK2, SERPINF1, SERPINF2, VTN
LXR/RXR activation	6.61E-06	A1BG, AHSG, APOA1, GC, PCK2, SERPINF1, SERPINF2, VTN
TCA cycle II	1.03E-05	CS, DLST, MDH2, SDHB
mTOR signalling	2.76E-05	PLD3, RPS6, RPS8, RPS11, RPS13, RPS26, RPS27L, RPS3A

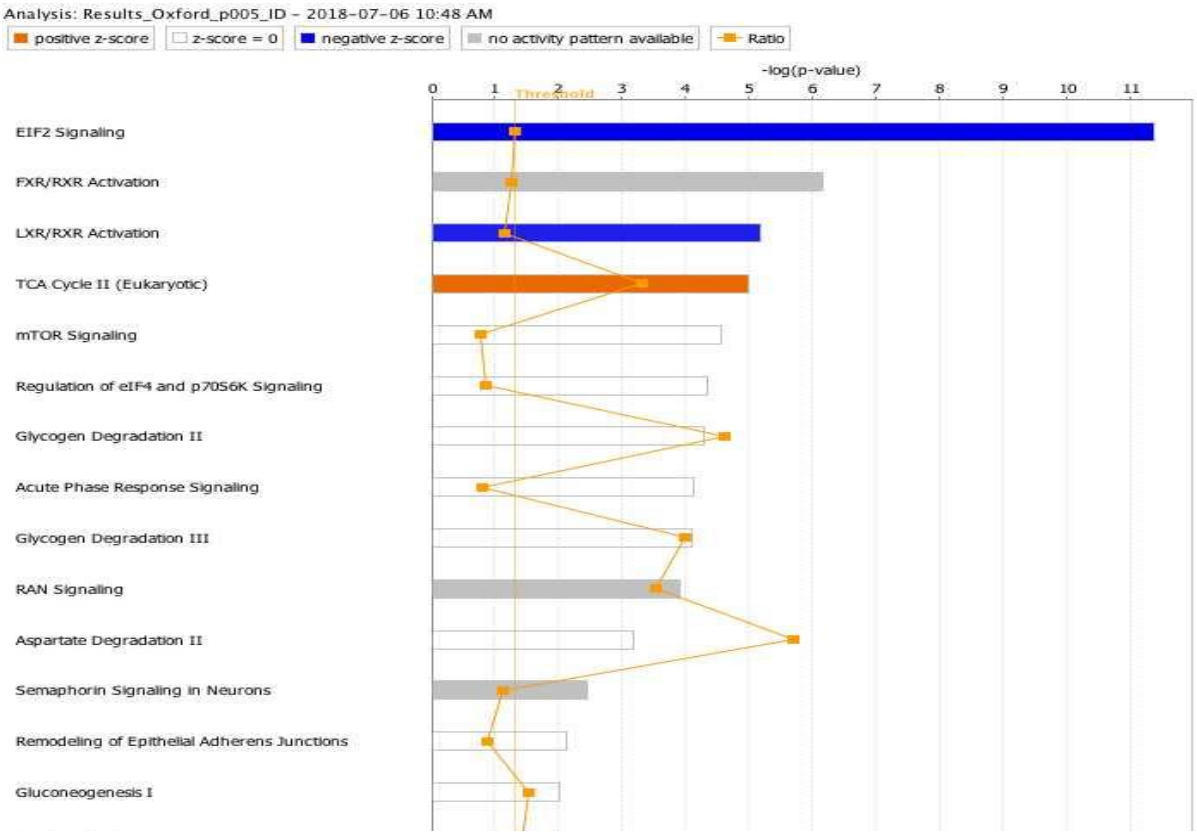


Figure 2.18 Implicated pathways and the directions of changes from Ingenuity Pathway Analysis (IPA) of total proteins from 5 patient samples and 5 control samples. Based on the significantly differentially expressed proteins present in the total proteins, EIF2 signalling pathways and LXR/RXR activation pathway were highly significantly downregulated (blue) in patient group while the TCA cycle II pathway was highly significantly upregulated (orange) in patient group, compared to their corresponding counterparts in control group. Significance threshold was calculated automatically based on online databases available to IPA for individual pathways and was shown in the graph as orange dots connected with orange solid lines. The length of the bars represents the –log(*p*-values) and the colour of the bars represents the value of z-score. Significance was calculated based on the *p*-value that shows the probability of obtaining certain pathway in the analysis merely based on random observation and the z-score, which shows the standard deviation of obtained pathway from theoretical random pattern (null-hypothesis). A z-score>2.5, meaning significantly upregulated, is shown in orange and a z-score<-2.5, meaning significantly downregulated, is shown in blue.

2.7 Discussion

The conservation of fundamental molecular mechanisms governing basic cellular behaviours made it possible to interpret the impact of genetic predisposition to schizophrenia on developmental processes in light of data obtained from OE-MSCs. For example, cell proliferation and apoptosis are tightly regulated by gene regulatory networks that orchestrate molecular activators, inhibitors and check-points. Pathways that surpassed global significance in GWAS studies were often associated with neural development and signalling (Schizophrenia Working Group of the Psychiatric Genomics Consortium, 2014). Given the innate role of OE-MSC in the lamina propria and olfactory epithelium is to renew the olfactory sensory neurons, it is reasonable to view disease-associated changes in OE-MSC cellular behaviours as reflections of the risk gene-driven subcellular mechanisms that can be shared, at least in part, with the development of neurons. In the following subchapters, the observed cellular behaviours and molecular signatures of patient OE-MSCs in contrast with those of control OE-MSCs will be discussed.

2.7.1 Summary of OE-MSC cellular behaviours

In this chapter, OE-MSCs isolated from a AOS cohort were shown to be highly proliferative, and able to generate spheres. They expressed neural stem cell markers, mesenchymal stem cell markers and pan-neuronal markers. These observations on the *in vitro* characteristics of OE-MSCs served as a basis for experiments targeting disease-related cellular phenotypes and the underlying molecular correlates. Firstly, they showed that the cells from this cohort were truly OE-MSCs, and not mixed with other cell types that might be present in the nasal epithelium. Secondly, they showed that the OE-MSCs used in this study was made of a rather homogenous cell population based on their cell identity marker expression patterns, ruling out the possibility of observed differences at the cellular and molecular levels between patients and controls being confounded by different cell populations from either group. This basis allowed meaningful interpretation of following data.

Next, I showed that the basic stem cell properties of OE-MSCs were unchanged between patients and controls. However, appreciable self-renewal and differentiation were not achieved, and thus could not be compared. In a niche environment, stem cells contribute to local tissue homeostasis based on their ability to proliferate, self-renewal, differentiate and undergo apoptosis when necessary. Those essential stem cell properties were measured for OE-MSCs using the following assays: PDT and Edu (proliferation), sphere generation assay (self-renewal), neuronal differentiation and NucBlue/NucGreen (apoptosis). The proliferation rate of OE-MSCs was confirmed as unchanged between patients and controls, by assessing population doubling time and the percentage of diving cells. The percentage of dead cells present in OE-MSC cultures derived from patients or controls also remained highly similar.

However, self-renewal ability and the ability to differentiate into neurons of OE-MSCs remained rather inconclusive due to the limited stemness of OE-MSCs *in vitro*. In the presence of mitogens, single cell OE-MSCs did not give raise to spheres directly. Instead, they underwent a phase of adherent proliferation and subsequently gain contacts with each other to from aggregated cell clusters, which grew larger in size and eventually detached from the adherent culture as spheres. Therefore, the 'sphere formation' in OE-MSC cultures was likely to be a combinatorial result from the initial proliferation (how fast cells grew into the amount that allows detachment), cell-cell contact (when cells aggregated together) and cell-substrate contact (to release the semi-adherently growing OE-MSCs 'islands' into free-floating spheres).

Neuronal differentiation was not achieved based on staining of pan-neuronal markers, following all published OE-MSC neuronal differentiation protocols. This was not surprising as according to unpublished communications with several labs which use OE-MSCs, they could very rarely be differentiated into neurons, unless reprogramming factors towards neuronal fates were introduced to the cells. In summary, the OE-MSCs from this cohorts of patients and controls exhibited stem cell properties, in a highly consistent fashion; which are highly proliferative, minimal presence of dead cells, able to form spheres from cell aggregates.

OE-MSCs derived from patients and controls did not show differences in rates of cell death, even with various degrees of exogenously introduced oxidative stress. This is in line with the lack of cell death phenomena in post-mortem studies, in the human-rodent chimeric model study and in iPSC-based studies (see details and references in the appendix). It is particularly interesting that membrane blebbing appeared at a lower dose of oxidative treatment for most patient cell lines compared to most control cell lines but this did not result in elevated

cell death. Blebbing is an early characteristic signature of apoptosis and injured cells and is also used as an alternative migration mechanism besides lamellipodia-driven migration (Yanase, Carvou, Frohman, & Cockcroft, 2010). The initiation of blebbing arises from a local decreased attachment of the actin-free membrane to the actin cortex of a cell, or a local breakage of the actin cortex itself (Charras & Paluch, 2008). The formation of blebs after the initiation phase is highly dependent on the activity of myosin II via Ca^{2}+ and calmodulin signalling (Blaser et al., 2006; Maugis et al., 2010; Sanz-Moreno & Marshall, 2010; Terayama et al., 2013). Calmodulin in turn activates death kinases to trigger autophagic programmed cell death (Inbal, Bialik, Sabanay, Shani, & Kimchi, 2002). Interestingly, blebbing formation is negatively correlated with actin polymerisation, as a mutant Arp2/3 complex, which is upstream of actin polymerisation, promoted membrane blebbing (Langridge & Kay, 2006). The tendency of increased blebbing in patient OE-MSCs therefore suggests there could be an increase in myosin II signalling or a decrease in actin polymerisation. The exact molecular mechanisms behind the increased blebbing of patient OE-MSCs remain to be studied and its statistical significance confirmed. However, an increased level of pro-apoptotic molecules without increased activated apoptotic events was also observed in post-mortem patient temporal cortices and in patient-derived fibroblasts (Catts et al., 2006; Jarskog, Selinger, Lieberman, & Gilmore, 2004). A previous OE-MSC study addressing adult-onset schizophrenia found higher rates of cell death in patient OE-MSCs compared to control OE-MSCs, suggesting that there might be an upregulation of cell death related pathways in patient cells (Feron et al., 1999). It has been proposed that increased apoptotic susceptibility in schizophrenia neurons could have a restricted effect at the spine and synaptic level, without causing overall cell death, termed synaptic apoptosis (Glantz, Gilmore, Lieberman, & Jarskog, 2006; Mattson, Keller, & Begley, 1998). The neurons are sick but do not die. This is compatible with the

reduced neuropil hypothesis (see appendix for details). In summary, the lack of increased cell death difference under normal culture conditions or with oxidative treatments, but the tendency of an increased membrane blebbing of patient OE-MSCs when compared to controls shows that patient cells might be more reactive to subthreshold cell stresses. This difference may be mediated by increased Ca^2+/ calmodulin/myosin II activity or decreased actin polymerisation, and may manifest in neurons as increased synaptic apoptosis in patient brains. Follow-up experiments should include a time-course of the membrane blebbing and percentage cell death to test whether patient cells were faster in blebbing but eventually would end up with the same amount of membrane blebs as control cells after sufficient reaction time.

OE-MSC data also did not show a difference in cell proliferation between patients and controls. However, previous studies using OE-MSC to address adult-onset schizophrenia did report an increased cell proliferation of patient OE-MSCs when compared to control OE-MSCs (Fan et al., 2012; Feron et al., 1999; McCurdy et al., 2006). The culture methods used in those studies involved a sphere-forming phase right after the initial outgrowth of cells from dissected biopsies and the cells were assessed for cell proliferation shortly after the sphere-formation. Hence it is possible that the sphere-formation step selected cells that were most responsive to mitogens and those cells displayed higher proliferation rates than the population from controls. It is also possible that OE-MSCs from schizophrenia intrinsically had higher proliferation but this property was lost during *in vitro* culturing in my study, however this is unlikely to be the case as a relatively early passage number (passage 6) was used in the present study. Previous OE-MSC papers characterising the impact of passage number on

cellular behaviours and gene expressions of OE-MSCs found the growth speed to be stable in the first 12 passages (Matigian et al., 2010). The most interesting possible explanation would be that the aberrant cell proliferation of OE-MSCs is specific to adult-onset cases. Confounding effects of prolonged antipsychotic medication are difficult to be rule out, as the adult-onset patients generally experienced a much longer treatment history than the adolescent-onset patients recruited in this study. Chronic administration of antipsychotic drugs was shown to increase cell proliferation in hippocampi and prefrontal cortices in rodents (Halim, Weickert, McClintock, Weinberger, & Lipska, 2004; Kodama, Fujioka, & Duman, 2004).

As no difference in cell proliferation or cell death was observed in OE-MSC cultures between controls and AOS patients, it suggests that those basic and critical functions were unlikely to be perturbed by genetic risks. It was possible that schizophrenia-associated risk genes were not expressed or had very low expression levels in OE-MSCs. However, the likelihood of this being the reason behind the similar proliferation and cell death between patient cells and control cells was low. GWAS studies did not reveal genes involved in proliferation or cell death to be associated with schizophrenia (Schizophrenia Working Group of the Psychiatric Genomics Consortium, 2014) . In summary, my current data suggest that cell proliferation machineries were not likely to be affected by the genetic predisposition of the studied patient group and cell death related pathways may be upregulated in patient cells. It remains unclear exactly why patient cells showed more membrane blebs but not higher percentage of dead cells compared to control cells.

2.7.2 Molecular signatures of OE-MSCs and their links with cellular behaviours of OE-MSCs

Proteomics data from AOS OE-MSCs suggest a down-regulated global protein synthesis and this may suggest reduced protein synthesis as a common phenomenon behind AOS and adult-onset schizophrenia. The proteome describes the total proteins that are present in a cell, it is more complex and diverse than the genome or the transcriptome, and reveals the proteins that are ultimately affected by risk genes in schizophrenia. Protein expression profiling of OE-MSCs using mass spectrometry found 127 proteins that were significantly different in their abundance between the patient group and the control group, 14 of those were ribosomal proteins and were down-regulated in the patient group, representing the most significantly impaired pathway—EIF2 signalling.

Protein synthesis in cells is regulated primarily at the initiation step by various eukaryotic initiation factors (EIFs). The role of EIF2 in this process is to control the speed of protein synthesis by regulating the turn-over of the energy source guanosine triphosphate (GTP) (Jackson, Hellen, & Pestova, 2010). The EIF2 pathway is in turn regulated by cellular stresses and by the mTOR pathway so that the global protein synthesis rate drops upon cellular stress and increases when the stress is eliminated. This is an evolutionary conserved mechanism to maintain cellular homeostasis in response to adverse environments such as nutrition deprivation, virus infection and excessive oxidative stress (Pakos-Zebrucka et al., 2016). Interestingly, the mTOR pathway was also significantly downregulated in the patient group, suggesting that patient cells might have a deficiency in global protein translation and an impaired stress response machinery. The finding of downregulated EIF2 signalling and mTOR pathway was previously also reported in OE-MSCs derived from patients with adult-onset

schizophrenia and neural progenitor cells derived from patients with childhood-onset schizophrenia, showing that they likely represent shared mechanisms among diverse patient groups (English et al., 2015; Topol et al., 2015a). Furthermore, it was previously shown that the down-regulated EIF2 pathway, mTOR pathway, as well as EIF4 pathway which was not significantly different between patients and controls in my data, were coupled with a reduction in the total protein in OE-MSCs and reduced size cells (English et al., 2015). Such differences were not found in fibroblasts derived from same cohort, suggesting that global protein synthesis reduction was cell type-specific. The authors further used gene-set enrichment analysis and gene-based association analysis of large GWAS datasets to show that the EIF2, mTOR, EIF4 pathways, as well as two individual members of the EIF2 pathway were significantly associated with schizophrenia. Together, my results and previously published results showed that global protein synthesis reduction, mediated by downregulated EIF2 and mTOR pathways, was a conserved cellular mechanism behind adolescent-onset and adult-onset schizophrenia.

Other significantly downregulated pathways found in patient OE-MSCs include biosynthesis of antibiotics, protein processing in endoplasmic reticulum (ER), cytoskeleton regulation, carbon metabolism and lipid metabolism. The impaired biosynthesis of antibiotics and LXR/RXR activation are particularly relevant for schizophrenia, as infection during pregnancy is a well-known risk factor for developing schizophrenia (Brown, 2012) . LXR is a member of the nuclear receptor family and regulates genes involved in lipid metabolism, however LXR was also shown to modulate both the innate and adaptive immune responses by regulating gene expression in macrophages (Noelia & Castrillo, 2011). The EIF2 signalling pathway is also associated with protein synthesis regulation upon viral infections (Donnelly, Gorman, Gupta,

& Samali, 2013; Rothenburg, Seo, Gibbs, Dever, & Dittmar, 2009). These results suggest that patient cells have aberrant cellular responses to viral infection which may result in insufficient clearance of the virus and dysregulated protein homeostasis upon infections. The impaired protein processing process in ER may further reduce expression levels of physiologically functional proteins, given the already reduced global protein synthesis by down-regulated EIF2 signalling. Dysregulated lipid and glucose metabolism, indicated by significantly down-regulation of FXR/FXR activation (Lambert et al., 2003; Zhang, X. et al., 2006) and LXR/RXR activation (Kalaany & Mangelsdorf, 2006) in schizophrenia patients, can be particularly harmful for neurons whose complex structures and neurotransmitter containing vesicles are made with lipid bilayers. Neurons solely rely on the delivery of glucose from the blood for energy source. Lipid metabolism and glucose metabolism was shown to be upregulated with prolonged antipsychotic treatment in patient cells and animal models (Bowling & Santini, 2016) . Whether this is merely a side-effect of antipsychotic treatment or a biological meaningful mechanism to alleviate symptoms of schizophrenia remain debatable.

The downregulation of focal adhesion and actin cytoskeleton regulation in patient group matched observations that patient OE-MSCs had reduced adhesion ability and may also explain the increased blebbing of patient cells under excessive oxidative stresses. Actin cytoskeleton dynamics allow fundamental cellular processes such as migration and morphogenesis to happen. It does so by forming actin filament networks with the polymerization of monomers at the plasma membrane to provide forces and by forming actomyosin bundles with motor protein myosin II, whose motor domains coordinates the movements, to form contractile structures termed stress fibres (Tojkander, Gateva, &

Lappalainen, 2012). These stress fibres are often connected with each other and anchored to focal adhesions. Focal adhesions are made by transmembrane proteins called integrins that connect the cells to the ECM or adhesion molecules from neighbouring cells (Saif, Sager, & Coyer, 2003). Focal adhesions sense the mechanical forces outside the cells and regulate the growth of stress fibres (Geiger, Spatz, & Bershadsky, 2009; Parsons, Horwitz, & Schwartz, 2010). This is particularly critical for neural progenitor cell migration and neurite outgrowth. When cells migrate, they are able to switch between lamellipodium-driven mode, which involves focal adhesions and actin filaments, to a bleb-driven mode, which involves the formation of actin-free membrane protrusions that are negatively correlated with actin polymerisation (Langridge & Kay, 2006; Yanase et al., 2010). For neurite outgrowth, the growth cone of a developing neuron, containing structures made of actin filament networks called lamellipodium and filopodium, constantly process chemical cues that guide the pathfinding of axons and thus allow the brain as an information processing machine to be built (Dent & Gertler, 2003). Both protein synthesis and actin dynamics play essential roles at synaptic sites, enabling critical functions of neurons such as long-term potentiation (Bramham, 2008). Indeed, molecules taking part in actin dynamics have long been associated with schizophrenia (Barbeau, Liang, Robitalille, Quirion, & Srivastava, 1995; Fan et al., 2013; Mahadik et al., 1994; O'Dushlaine et al., 2011; Zhao, Z. et al., 2015). A previous study that directly exposed OE-MSCs from nasal biopsies to adhesive substrates also found that tissues from patients with adult-onset schizophrenia showed reduced adhesion when compared to controls (Feron et al., 1999). Therefore, the observations of impaired focal adhesion and actin cytoskeleton regulation is in line with the previous literature and may suggest dysregulated adhesion as a common phenomenon shared between AOS and adult-onset schizophrenia.

As a summary, AOS OE-MSCs were less adhesive to cell culture substrates and displayed reduced protein synthesis, mTOR pathway and actin cytoskeleton related pathways. These observations were in line with previous studies using OE-MSCs derived from adult-onset schizophrenia, suggesting that AOS and adult-onset schizophrenia is a continuum and share key cellular and molecular disease-related phenotypes. The field of psychiatry proteomics is relatively small at present, the perturbed protein synthesis and cell adhesion await to be validated by more studies. Limitations of this study include the small N numbers and the depth of protein detecting. Replication of current study with increased numbers of patients and controls should increase the power of the study. The current small N number also makes the results prone to group-effect and other confounding factors such as antipsychotic treatment. However, this is less likely to be true as the results were highly similar to the adult-onset cohort. The proteomic analyses were not likely to cover all proteins. The reported significantly reduced pathways were likely to be the ones that were the easiest to pick up based on the abundance of member proteins—ribosomal pathways and actin cytoskeleton pathways. My current analyses were likely to miss other perturbed pathways in schizophrenia OE-MSCs if the expression levels of protein members were low. Validation experiments using neural progenitor cells or other neural cell types should be done to confirm the hypothesis that protein synthesis is reduced in schizophrenia.

Chapter 3. Phenotypic comparison between reprogrammed neurons derived from patients with adolescent-onset schizophrenia and healthy controls

3.1 Summary

Cellular reprogramming offers the opportunity of studying human disease using patient-derived disease-relevant cell types. In this study, skin fibroblasts from 3 patients with adolescent-onset schizophrenia and 3 controls were reprogrammed to iPSCs, which went through quality control steps to check for downregulation of virus-delivered genes, high expression of pluripotent stem cells markers and genomic integrity. The iPSCs were subsequently converted into induced neurons that resembled prefrontal layer 2/3 glutamatergic projection neurons. This was achieved by introducing overexpression constructs of Neurogenin 2 (*NGN2*) and Reverse tetracycline-controlled transactivator 3 (*rtTA3*) which activates the overexpression of *NGN2* upon binding with doxycycline in iPSCs. Due to the use of viruses and multiple chemical compounds which were all toxic to iPSCs at high doses, it was challenging to produce high quality neurons from all iPSC lines at the same time. Based on live imaging which tracked the conversion of neurons from 2 patient lines and 2 control lines, there were no obvious differences in the conversion processes. However, neurite tracing of day 9 converting neurons showed one line from a patient carrying missense variants in *SYNGAP1* and *SHANK2* had significantly longer neurites than another line from a control subject. Subsequent immunostaining of neuronal makers on day 28 neurons did not reveal morphological differences between the patient and control cells. Due to the lack of power in the present study, the observed line-specific features of converting neurons cannot

be concluded to be a definitive disease-specific phenotype. However, future research will increase the power of the study by including more iPSC lines, as well as carrying the neurons to a more mature stage to address morphology as well as synaptic transmission.

3.2 Introduction

3.2.1 Induced pluripotent stem cells: discovery, characterisations and cautions

Studying human physiology and diseases has been challenging due to the limited amount of human tissue available for research and a lack of model systems that reveal dynamic biological processes that are specific to humans. This is particularly true for neuroscience, which addresses a complex information processing system whose functioning can be modulated by genetic variations, environmental factors, prior knowledge, new experiences and aging and other factors. Powerful research tools have been developed to understand the working mechanisms of brains on each of the above levels. For example, large population-based genetic studies can reveal genetic elements that significantly associate with a certain trait so that the nature of the trait can be revealed by studying the functions of the associated genetic elements. However, the brain is a very sophisticated organ that is composed of numerous types of cells but we do not fully know their diversity, functions and interactions. Therefore, whether research is starting from the level of molecules and seeking their function on the brain, or is starting from a certain cellular function or dysfunction of the brain, the gaps between molecular, cellular, circuitry and whole system levels remain extremely challenging for neuroscientists. The factor of time further complicates the problems in neuroscience. For example, refined post-mortem studies of the brain can faithfully reveal the end products of a brain disorder but cannot offer a clear narrative of how the disorder starts and develops. Therefore, a human-specific research toolset that reveals the diversity, the functions, the spatial and temporal relationships of the cell types in the CNS is highly demanded.

Human embryos have the potential to develop into any cell types and organs in the body, but such versatility cannot be fully restored *in vitro* and the use of human embryos is ethically debatable. The concept of somatic reprogramming was first demonstrated by Sir John Gurdon in 1962 by showing tadpoles can develop from enucleated frog egg cells inserted with the nuclei of frog intestinal epithelial cells (GURDON, 1962). This showed that the genome of a somatic cell can be reprogrammed to behave like a fertilized egg—a totipotent stem cell. 44 years later, Shinya Yamanaka and his team showed mouse somatic cells could be reprogrammed by 4 transcription factors, octamer-binding transcription factor 3/4 (*Oct3/4*), SRY (sex determining region Y)-box 2 (*Sox2*), KLF4 Kruppel like factor 4 (*Klf4*) and MYC proto-oncogene (*c-Myc*), to iPSCs that were indistinguishable from mouse embryonic stem cells on their gene expression profiles and developmental potentials (Takahashi & Yamanaka, 2006). These 4 transcription factors were named 'Yamanaka factors'. Rapidly after this, two protocols for making human iPSCs were published independently (Takahashi et al., 2007; Yu, J. et al., 2007). The human iPSCs made with the original Yamanaka factors expressed human embryonic stem cell (hESC) markers, had active hESC-specific promoters, exhibited high telomerase activity, could be differentiated *in vitro* into the 3 germ layers and formed teratomas *in vivo* (Takahashi et al., 2007; Yu et al., 2007). However, concerns regarding gene expressions that were specific to iPSCs but not hESCs, such as genomic integrity and epigenetic stability were raised.

Table 3.1 summarised recent studies that characterised human iPSCs, mostly done by comparison with isogenic hESCs or multiple hESC lines. The understanding of the limitations and pitfalls of iPSCs has evolved over time. Chin et al., 2009 first compared multiple iPSC lines with hESCs lines and established gene expression, miRNA expression and methylation pattern

differences between iPSCs and hESCs. However, none of those differences are restricted to a certain cellular function and none of the abnormalities were required for successfully making iPSCs. This is important as it tells us reprogramming is imperfect and the genetic components that remains different from hESCs were stochastic in nature. Later on, by analysing large numbers of iPSC lines and using isogenic hESC lines. Genetic imprinting, *in vitro* maintenance, the use of integrating or non-integrating methods for reprogramming (see Table 3.1 for details and references) were identified as key factors to take into consideration when using iPSCs. The study of iPSC reprogramming has evolved to replace oncogenes (e.g. *c-Myc*) with chemical compounds for safer reprogramming, to achieve the naïve state of pluripotency (resembling preimplantation epiblasts) instead of the prime state (resembling post-implantation epiblasts and to eliminate the road blocks of reprogramming to increase the efficiency (Kilens et al., 2018). However, to date, most routinely used iPSC lines in the laboratory are still reprogrammed with the original Yamanaka factors hence the cautions discussed above still hold

Table 3.1 Recent studies that characterised human iPSCs.

Year	Sample size	Major findings	Ref
2009	4 hESC lines 5 iPSC lines 3 fibroblast lines	Gene expression profiles of iPSCs clustered together and away from hESCs; Late-passage (passage 54-61) iPSCs were more similar to hESCs than with early-passage (passage 5-9) iPSCs; Majority of the gene expression difference between iPSCs and hESCs recovered when the passage number of iPSCs increase; Late passage number iPSCs, made with integrating or non-integrating methods, remain a gene expression signature that did not result in any specific pathways in GO analysis; H3K27 methylation patterns on promoter regions were nearly identical for iPSCs and hESCs; Only 1% of the differentially expressed genes between iPSCs and hESCs were methylated in a pattern similar to that of donor fibroblasts; A few microRNAs were differentially expressed between iPSCs and hESCs, not falling into specific functions; No genomic abnormalities were required for successful reprogramming.	Chin et al., 2009
2010	64 iPSC lines and 13 hESCs lines collected from 7 laboratories	Strong correlations between gene expression signatures of the lines and the laboratory in which the lines were derived; Strong impacts of *in vitro* maintenance on the gene expression profiles of iPSC and hESC lines.	Newman & Cooper, 2010

2011	1 hESC line (H9 line, female) 6 isogenic iPSC lines	The expression levels of several imprinted genes, especially including neonatin (*NNAT*) were significantly different between isogenic hESCs and iPSCs.	Teichroeb, Betts, & Vaziri, 2011
2012	20 iPSC lines	IPSCs generated with non-integrating methods cluster closer with hESCs on transcriptomes than the iPSCs generated with integrating methods.	Liu, Cheng, Li, Gao, & Wang, 2012
2012	205 iPSC and hESC lines, 130 somatic samples	Consistent loss of imprinting and loss of XCI in a subset of iPSC and hESC lines; Appropriate methylation patterns at those imprinted loci were not re-gained during differentiation; None of the above aberrations were consistently shared between lines	Nazor et al., 2012
2012	7 iPSC lines	Low-passage female iPSCs retained the appropriate XCI however undergo 'erosion' of XCI as the passage number increases; This erosion of XCI was coupled with a loss of X-inactive specific transcript (*XIST*) expression and H3K27 trimethylation loci, and cannot be reversed by differentiation or another round of reprogramming.	Mekhoubad et al., 2012
2014	1 hESC line (H1 line, male) 3 isogenic iPSC lines	*NNAT* itself was highly variable among different hESC and iPSC lines; previously reported difference on *NNAT* between iPSCs and hESCs could be due to the difference of *in vitro* maintenance of the lines and X-chromosome inactivation (XCI) problems in female lines.	Mallon et al., 2014

H3K27: histone H3 lysine (K)27

3.2.2 Reprogrammed neural cells: directed differentiation and direct conversion

Specific types of neurons and glia have been obtained from iPSCs via 1) directed differentiation using defined media that provide mitogens and morphogens necessary to guide the development of neurons in a time-specific manner, and 2) via direct conversion that uses viruses to directly overexpress transcription factors that play key roles in neurodevelopment in the recipient cells. The benefits of using reprogrammed neurons include 1) they follow the same developmental trajectories when being differentiated as in the brain, 2) they carry genetic predispositions when derived from patients with genetic disorders and show disease-specific cellular phenotypes (Yoshida & Yamanaka, 2017), 3) they can be produced in large numbers to offer a high-throughput human-specific drug screening platform and 4) they have the potential to be transplanted into donor-matched patients as cell therapies. Challenges in using reprogrammed neurons remain for modelling late-onset diseases and interactions with other cell types or organs. These properties of reprogrammed neural cells will be discussed with a focus on neurons in this chapter.

The CNS develops as being instructed by combinations of molecular signals that occur at specific anatomical locations at specific times, resulting in cell populations that are specified with their locations, functions and signalling partners. These molecular signals, including mitogens and morphogens, were used to guide the directed differentiation of iPSCs for obtaining neural cells. The Mothers Against DPP Homolog 1 (*SMAD*) signalling has long been shown to play a crucial role in neural induction *in vivo*. Dual *SMAD* inhibition with noggin, a Bone Morphogenetic Protein (*BMP*) inhibitor, and SB431542, a Transforming Growth Factor Beta (*TGFβ*) inhibitor, can efficiently cause neural induction from iPSCs and generate Paired

Box 6 (*PAX6*)+ neuroepithelial NPCs (Chambers et al., 2009). Gene expression characterisation of this procedure revealed high expression levels of Fibroblast Growth Factor 5 (*FGF5*) and Orthodenticle Homeobox 2 (*OTX2*), both represent the epiblast cell identity, at early stages of neural induction and were followed by upregulation of the neuroepithelial markers including *PAX6* and Zic Family Member 1 (*ZIC1*). These early *PAX6*+ neuroepitehlial cells further developed into anterior NPCs which expressed *OTX2* and Forkhead Box G1B (*FoxG1B*), while the early *PAX6*- (negative) cells developed into neural crest-like cells that expressed Apetala 2 (*AP2*), Beta-1,3-Glucuronyltransferase 1 (*B3GAT1*), Paired Box 7 (*PAX7*) and Nerve Growth Factor Receptor (NGFR). The dual SMAD-induced neuroepithelial NPCs self-rearranged and formed rosettes after re-plating which resembled neural tubes *in vivo*. These neural rosettes were highly polarised, with prominin, Atypical Protein Kinase C (*aPKC*) and Abnormal Spindle Microtubule Assembly (*ASPM*) expression and centrosome locations on the apical side lining a lumen-like cavity (Shi, Kirwan, Smith, Robinson, & Livesey, 2012). Time-lapse imaging showed these cells underwent interkinetic nuclear migration, which is a signature behaviour of neuroepithelial cells. While mitosis mainly happed at the apical surface, a subset of cells also divided at basal sites and were T-box Brain Protein 2 (*TBR2*)+ Marker Of Proliferation Ki-67 (*Ki67*)+ and PAX6-, representing basal progenitor cells. Basal progenitor cells gave rise to the majority of *DCX*+ neuroblasts. Radial glia, which were *PAX6*+, had both apical and basal processes, as well as a single centrosome located at the base of the apical process. Outer radial glia (oRG), which were *TBR2*- *PAX6*+, were identified with single basal process and centrosomes located near the nuclei (Shi et al., 2012). These characterisation studies showed neural induction from iPSCs faithfully resembled neurodevelopmental events that occur *in vivo* (shown in simplified way in Figure 3.1).

The anterior-posterior and dorso-ventral identities of NPCs in rosettes can be patterned with morphogens. In the developing neural tube *in vivo*, Sonic Hedgehog (*SHH*) is secreted in ventral regions while Wingless/Integrated (*WNT*) and Bone Morphogenetic Protein 2 (*BMP2*) are secreted in dorsal regions. Together, their gradients establish dorso-ventral identity. The Fibroblast Growth Factors (FGFs) and Retinoid Acid (RA) together orchestrate anterior-posterior patterning. For example, midbrain neurons and spinal cord neurons were made by introducing the *SHH*, RA and *FGF2* or fibroblast growth factor 8 (*FGF8*) (Chambers et al., 2009; Danjo et al., 2011; Eiraku et al., 2008; Elkabetz et al., 2008). In the differentiation of dorsal forebrain-like rosettes, the emergence of cortical projection neurons representing each of the cortical layers followed a timely order similar that known *in vivo*. The *TBR1*+ and B Cell CLL/Lymphoma 11B (*BCL11B*, also called *CTIP2*)+ layer 5/6 neurons were generated first. This was followed by neurons expressing the layer 2/3 markers POU Domain, Class 3, Transcription Factor 2 (*POU3F2*, also called *BRN2*)+, Homeobox Protein Cut-like 1 (CUX1)+ and DNA-binding Protein SATB2 (*SATB2*)+ (Shi et al., 2012). After a prolonged culture, synaptically functional neurons, astrocytes and oligodendrocytes were detected (Gorris et al., 2015; Shi et al., 2012). These studies showed that the directed differentiation of iPSCs can be manipulated towards various regional specifications and followed well established *in vivo* developmental spatial and temporal patterns.

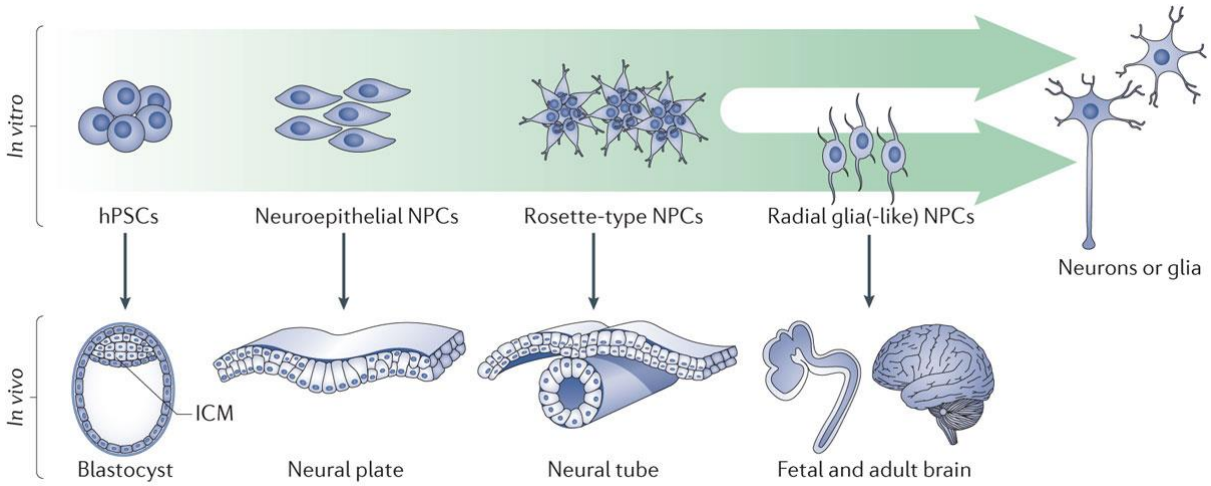


Figure 3.1 Schematic illustration of stages in directed differentiation of neurons, comparing to *in vivo* developmental stages. By using a judicious combination of mitogens and morphogens, induced pluripotent stem cells (iPSCs) can be differentiated to neurons and glia, via a route that resembles *in vivo* development. Neural induction of iPSCs, which are similar to the inner cell mass (ICM), generated neural plate-like neuroepithelial neural progenitor cells (NPCs). The NPCs form rosette-like structures which harbour radial glia, basal progenitors and outer radial glia, and give rise to deep layer neurons before upper layer neurons. As a result, electrophysiologically active neurons, and then glia -astrocytes and oligodendrocytes were generated similar to *in vivo*. Figures adapted from (Mertens, Marchetto, Bardy, & Gage, 2016).

Directed differentiation of iPSCs offers the opportunity to track early human neurodevelopment however requires at least a few months to obtain mature neurons, during which much line-to-line variations can arise. On the other hand, direct conversion, in which key transcription factors governing neuronal development are directly introduced to iPSCs or somatic cells, can bypass several developmental processes and generate the desired neuronal type in fast and reproducible ways. The earliest direct conversion protocols utilised three transcription factors: *BRN2*, Achaete-Scute Family BHLH Transcription Factor 2 (*ASCL2*) and Myelin Transcription Factor 1 Like (*MYT1L*), these three factors were called the BAM factors (Vierbuchen et al., 2010). The successful lineage conversion relies on a hierarchical mechanism that requires sequential actions of transcription factor regulators (Wapinski et al., 2013). *ASCL1* acts as a pioneer transcription factor which enters the nucleus first and allows *BRN2* to bind at the same site, *MYT1L* in turn helps with maturation at a later stage (Wapinski et al., 2013). While NPCs taken through directed differentiation can receive developmental cues for patterning, but there are no such NPCs during direct conversion. Therefore, regional specificity has been achieved by introducing both the pioneer transcription factors that reset the genomic landscapes of recipient cells, as well as lineage-specific transcription factors that further shape gene expression towards specific identities. For example, Forkhead Box A2 (*FOXA2*), LIM Homeobox Transcription Factor 1 Alpha (*LMX1a*), Nuclear Receptor Subfamily 4 Group A Member 2 (*NR4A2*) and Paired Like Homeodomain 3 (*PITX3*), which play essential roles during midbrain development, were used to directly convert fibroblasts into dopaminergic neurons (Ambasudhan et al., 2011; Pfisterer et al., 2011; Xue et al., 2013). However, the direct conversion from fibroblast to neurons generally has a low efficiency, limiting the numbers of neurons that can be studied. Recently, a single transcription factor, *NGN2*, was found to be able to rapidly convert iPSCs directly to layer 2/3 glutamatergic

projection neurons with high efficiencies (Zhang, Y. et al., 2013). *NGN2* is a well-studied basic helix-loop-helix (bHLH) transcription factor that acts as a transcriptional activator for neuronal development and suppresses gliogenesis (Sun, Y. et al., 2001). The induced neurons obtained with *NGN2* overexpression in iPSCs showed high expression levels of markers for telencephalic layer 2/3 excitatory neurons such as *BRN2*, *CUX1* and Forkhead Box G1B (*FOXG1B*), independent of the iPSC/hESC lines used for conversion (Zhang et al., 2013). Importantly, the authors showed that after being co-cultured with mouse glia, the *NGN2*-derived neurons produced robust action potentials and spontaneous synaptic activities that could be blocked by α-amino-3-hydroxy-5-methyl-4-isoxazolepropionic acid (AMPA)-receptor antagonists, suggesting the activation of AMPA-type receptors which mature after N-Methyl-D-aspartic acid (NMDA)-type receptors. When co-cultured with mouse primary cortical neurons, strong inhibitory events were observed, suggesting that *NGN2*-neurons were capable of integrating into the mouse synaptic networks. These data showed that *NGN2* mediated direct conversion is the most efficient neuron-producing protocol to date, and produces glutamatergic excitatory neurons resembling cortical layer 2/3 identity and displaying mature synaptic activities.

3.2.3 Post-synaptic signalling, SYNGAP1 and SHANK2

Cellular reprogramming technologies are powerful tools revealing human-specific developmental processes and disease mechanisms. However, they are limited by their throughput as multiple iPSC clones are usually generated from one donor to counterbalance the line-to-line variability of iPSCs. The line-to-line variability of iPSCs can be due to sporadic mutations that occur during reprogramming or during the *in vitro* maintenance of the lines. Although reprogramming was shown to give rise to cells that were generally genomically and epigenetically stable, subthreshold genetic perturbations are always difficult to rule out, hence research involving cellular reprogramming has adapted to include at least three iPSC lines, derived from 3 individual clones after infecting donor fibroblasts with viruses encoding the Yamanaka factors, to represent one donor.

As discussed in *Chapter 1*, schizophrenia is a polygenic complex disease with a strong genetic basis. The largest GWAS to date implicated loci as significantly associated with schizophrenia that are involved in forebrain development, calcium signalling, glutamatergic neurons, as well as the immune system. Therefore, I decided to derive forebrain glutamatergic neurons from patients and controls, in order to investigate their development and functions *in vitro*. To enrich for genetic components in the patient group that could be studied with cellular reprogramming, 3 adolescent-onset patients (patient 001, patient 002 and patient 007) with family histories of schizophrenia were included in this study. Whole-exome sequencing with trio-design revealed that patient 002 carried a missense point variant in *SYNGAP1* gene, inherited from a father who is likely to suffer from schizoaffective/schizophrenia (AJ). Another missense point variant was found in the *SHANK2* gene, inherited from a neurologically healthy

mother (AJ). Protein products of both genes are involved in the post-synaptic signalling of glutamatergic neurons, which have been heavily implicated in neuropsychiatric disorders (Fromer et al., 2014; Pinto et al., 2014). In this chapter, I will discuss the roles of *SYNGAP1* and *SHANK2* in the context of neurodevelopment and psychiatric diseases.

3.2.3.1 The post-synaptic density

The post-synaptic densities (PSDs) were initially named based on their appearance under electron microscopy (EM): electron-dense structures beneath the postsynaptic membranes of neuronal synapses (PALAY, 1956). Subsequent biochemical studies revealed that PSDs were made of densely packed assemblies of several hundreds of proteins (Cohen, Blomberg, Berzins, & Siekevitz, 1977; Harris & Weinberg, 2012). As illustrated in Figure 3.2, the signal transduction functions of PSD heavily rely on its core feature—the presence of scaffolding proteins. Proteomic studies showed that the PSD scaffolds could be divided into 3 layers: 1) the membrane-associated guanylate kinase (MAGUKs), which are directly connected to glutamate receptors, 2) the disk large associated guanylate-associated proteins (DLGAPs), which connect the top layer MAGUKs with the bottom SH3 And Multiple Ankyrin Repeat Domains (Shank) layer and 3) the Shank family proteins Shank1-3 (Li, J. et al., 2017). Proteomic characterisation of the PSD scaffolding proteins in the developing mouse prefrontal cortices showed that the glutamate receptor subunits already connect to the top layer MAGUKs and the mid-layer DLGAPs at embryonic day 14 (E14). At the same time, Shank proteins already assemble downstream protein components of the PSD separately, without connecting to the top and mid-layer scaffolding proteins until postnatal day 7 (P7). From E14-P14, the top layer of PSD scaffolding proteins continuously recruits proteins whose functions are linked to glutamate receptors, while the mid- and bottom layers continuously recruit proteins with various enzymatic activities (Li et al., 2017). Consistent with this, a separate study reported that PSDs can be reconstituted *in vitro* via liquid-liquid phase transition of the core scaffolding proteins independent of the order in which the core scaffolding proteins are introduced into the system (Zeng et al., 2018). The authors further showed that dropout of individual core

scaffolding proteins directly reduced the amount of its interactors in PSDs. For example, removal of the Shank3 protein resulted in more than half reduction in the amount of GKAP (a member of DLGAPs) and Homer3, which belonged to the mid-layer and the bottom layer, respectively, but did not cause obvious reductions in the glutamate receptor, SynGAP (protein product of *SYNGAP1* gene) or PSD-95 (a subfamily of MAGUKs), which co-localised with the top layer. The later study confirmed that PSD scaffolding proteins selectively enrich the presence of glutamate receptors and synaptic enzymes, promote actin bundle formations and expel proteins associated with inhibitory synapses. These studies showed that the PSD was a hub of postsynaptic signal transduction via protein-protein interactions that were enabled by the scaffolding proteins.

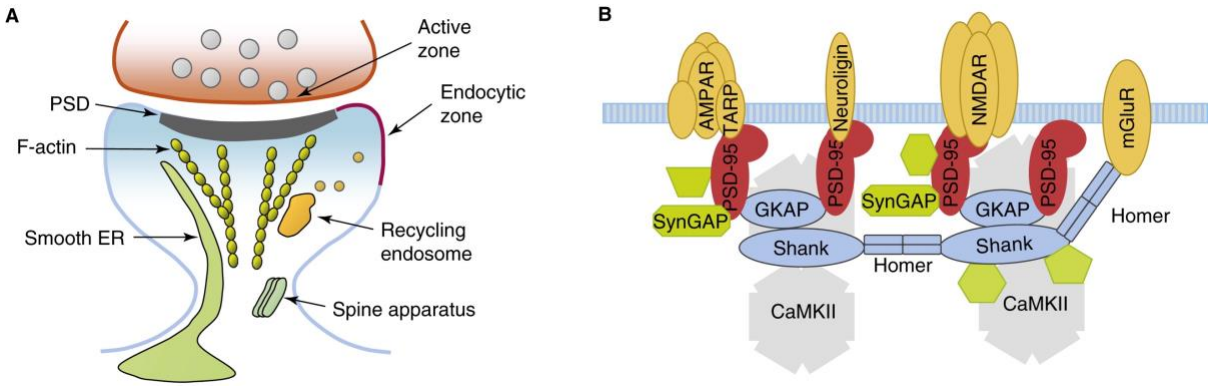


Figure 3.2. Simplified schematic illustration of the synapsis and the molecular composition of the postsynaptic density. A) On the synapse of a dendritic spine, the PSD is located directly underneath the presynaptic active zone which releases neurotransmitters. PSD receives neurotransmitter and process them into signals in the postsynaptic neuron. PSD is attached to components of the actin-cytoskeleton (e.g. actin bundles) and is in close proximity to the endocytic zone, the smooth endoplasmic reticulum (ER) and recycling endosomes that coordinate protein turnover. **B)** Scaffolding proteins at the PSD, including PSD-95, GKAP, Shank and Homer, form dense protein networks and transduce signals from the synaptic cleft via transmembrane proteins such as glutamate receptors (AMPAR, NMDAR) and cell adhesion molecules (neuroligin) to downstream signal transducers such as the Calcium/calmodulin-dependent protein kinase type II (CaMKII). Figure adapted from (Kim, E. & Sheng, 2009).

3.2.3.2 SYNGAP1

Protein products of the *SYNGAP1* gene are at the core of the PSD and play essential roles in glutamate receptor mediated signalling (Bayés et al., 2012; Chen, H., Rojas-Soto, Oguni, & Kennedy, 1998; Kim, J. H., Liao, Lau, & Huganir, 1998). LoF variants of *SYNGAP1* are associated with a number of neuropsychiatric disorders including intellectual disability (ID), autism spectrum disorder (ASD) and schizophrenia (Hoischen, Krumm, & Eichler, 2014; Zhu et al., 2014). A recent study surveying more than 60,000 neurologically healthy subjects did not find any damaging *SYNGAP1* variants based on the LoF-intolerance metric pLI (Kosmicki et al., 2017). Given that LoF *SYNGAP1* variants can explain up to 1% of all ID cases (Berryer et al., 2013; Deciphering Developmental Disorders Study, 2017), pathogenic LoF variants of *SYNGAP1* thus are highly penetrant (Kosmicki et al., 2017).

SYNGAP1 plays important roles in PSD formation, spine development and neuroplasticity (Walkup IV et al., 2016; Zeng, Bai, & Zhang, 2017; Zeng et al., 2018). The understanding of *SYNGAP1* functions comes largely from rodent studies. While complete knock-out of *SYNGAP1* is lethal in rodents, haploinsufficient *SYNGAP1* mice (*SYNGAP1*$^{+/-}$) had reduced brain volumes but larger cortical pyramidal neuronal sizes, accelerated rates of spine development, increased spine volume, more mushroom-shaped dendritic spines and impaired excitatory/inhibitory balance. *SYNGAP1*$^{+/-}$ mice displayed various disruptions in learning and memory, including spatial learning and contextual memory consolidation (Aceti et al., 2015; Guo et al., 2009; Kilinc et al., 2018; Komiyama et al., 2002; Muhia, Yee, Feldon, Markopoulos, & Knuesel, 2010; Ozkan et al., 2014). It was proposed that Ca^{2+}/calmodulin-dependent protein kinase II (CaMKII) regulates long term potentiation (LTP) via the action of protein

products from *SYNGAP1* (Wang, Held, & Hall, 2013). LTP is believed to be a core cellular process enabling learning and memory (Lynch, Rex, & Gall, 2007; Nicoll, 2017) and CaMKII has a well-established role in regulating LTP, it is a downstream effector of NMDARs, with increased levels of CaMKII leading to decreased AMPAR-mediated spontaneous and evoked activities (Barria & Malinow, 2005; Pi, Otmakhov, Lemelin, De Koninck, & Lisman, 2010).

SynGAP (protein product of *SYNGAP1* a1 isoform protein) is a synaptic ras GTPase activating protein, it directly binds with the PSD95/DLG/ZO1 (PDZ) domain of PSD-95 and negatively regulates Ras and Rap activities (Kim et al., 1998) . At basal levels of neuronal activity, SynGAP is phosphorylated and thereby suppressed by CaMKII, thus maintaining normal levels of Ras activity (Chen et al., 1998). Ras in turn, is upstream of Mitogen-activated Protein Kinase (MAPK, also called ERK) signalling, which through Mammalian Target Of Rapamycin (mTOR) signalling, can increase local protein synthesis to increase AMPARs levels on postsynaptic membranes (Di Cristo et al., 2001; Gobert et al., 2008; Schmitt, Guire, Saneyoshi, & Soderling, 2005; Tsokas, Ma, Iyengar, Landau, & Blitzer, 2007; Ying et al., 2002). However, upon strong NMDAR-mediated signals, SynGAP is released from CaMKII hence becoming active, and resulting in reduced ERK/mTOR activity and reduced local protein synthesis for AMPAR incorporation (Krapivinsky, Medina, Krapivinsky, Gapon, & Clapham, 2004). Interestingly, SynGAP was shown to physically move out of the PSD when strong NMDAR signals occurred, allowing synaptic strengthening via increased AMPARs (Yang, Tao-Cheng, Reese, & Dosemeci, 2011). Therefore, there are at least two mechanisms involving SynGAP to modulate the synaptic strength of glutamatergic neurons, phosphorylation by CaMKII or transient physical absence. *SYNGAP1* was also proposed to coordinate with GluN2B to regulate neural development. During normal development, reduced levels of NMDARs is necessary for

increasing AMPAR signalling and the subunits GluN2B present in NMDARs during early development are gradually replaced with the GluN2A subunit (Adesnik, Li, During, Pleasure, & Nicoll, 2008; Gray et al., 2011; Hall, B. J. & Ghosh, 2008; Wang et al., 2011) . SynGAP was found to preferentially bind with GluN2B containing NMDARs than with the GluN2A containing NMDARs (Chen et al., 1998; Kim et al., 1998; Wang et al., 2013). Therefore, it was hypothesized that, by recruitment of SynGAP, GluN2B containing NMDARs during early development suppressed the ERK/mTOR signalling cascade to suppress local protein synthesis necessary for AMPAR incorporation. Later in development, when the GluN2B subunits were replaced by GluN2A subunits, this inhibition is released by reduced levels of SynGAP in the PSD (Wang et al., 2013). Taking all these studies together, it was shown that SynGAP had a critical role for synapse development, homeostasis and plasticity. However, it remains unexplained how *SYNGAP1*$^{+/-}$ could result in impaired E/I balance and/or reduced brain volumes.

3.2.3.3 SHANK2

Mutations in the Shank family were previously associated with ASD and ID (Berkel et al., 2010; Kumar, 2010; Leblond et al., 2012) . Recently, the *SHANK2* gene was shown for the first time to be associated with schizophrenia (Peykov et al., 2015). A significant increase in the number of *SHANK2* missense variants with minor allele frequencies <1% was found in patients with schizophrenia compared to controls (Peykov et al., 2015). The Shank family is composed of three members based on current knowledge: Shank1, Shank2 and Shank3, whose full-length versions share structural similarities and hence functional similarities (Sheng & Kim, 2000). They are all scaffolding proteins at excitatory PSDs and mainly localise at the bottom layers of the PSDs (Naisbitt et al., 1999; Yao et al., 1999). They are also abundantly present in growth cones of developing neurons, suggesting roles in axonal pathfinding and dendritic development (Du, Weed, Xiong, Marshall, & Parsons, 1998; Naisbitt et al., 1999). While the vast majority of mRNAs are usually localised in the soma, mRNAs of the Shank family were found at dendritic spines, suggesting local protein synthesis of Shank for synapse development and functioning (Kiebler & DesGroseillers, 2000; Schuman, 1999; Worley, 1998). The locations of Shank family proteins share similarities. Shank2 was found highly abundant in the brain and less so the in liver and the kidney (Du et al., 1998). Shank3 is highly expressed in heart but moderately expressed in brain and spleen (Lim et al., 1999). While Shank2 was found in almost all brain regions, Shank3 was found mainly in the cerebral cortex and hippocampus in rodents (Boeckers et al., 1999). Furthermore, the homogenous Shank2 distribution in the brain remained stable during rodent postnatal development (Boeckers et al., 1999).

Rodent studies showed that Shank2 function is linked to NMDAR signalling (Schmeisser et al., 2012; Won et al., 2012). Mouse models that carried double copies of *SHANK2* microdeletions in exon 6 and exon 7, resulting in frame shifts, displayed behavioural phenotypes that resembled ASD (Won et al., 2012). When Shank2 levels were undetectable, there was no compensatory increase in either *SHANK1* or *SHANK3* expression. The levels of glutamate receptors, PSD scaffolding proteins and signalling adaptors, including PSD-95, Discs large homolog 1 (DLG1), GKAP, SynGAP and Homer1, were also unchanged in the Shank2 mutants. Also, PDS morphology and the numbers of excitatory synapses remained the same. Patch-clamp experiments using CA1 pyramidal neurons showed normal basal excitatory transmissions and membrane excitability. However, LTP was severely impaired and long-term depression (LTD) was abolished in CA1 pyramidal neurons but not in medial prefrontal neurons. Given the roles of NMDARs and AMPARs in LTP and LTD, the authors carefully dissected the source of the altered LTP and LTD and found that AMPR-mediated transmission was unchanged, while the NMDAR-mediated transmission was reduced. This was confirmed by the observations that NMDAR agonist administration fully rescued reduced NMDAR-mediated transmission, LTP, LDP and ASD-like behaviours. Analysis of total protein profiles of brains showed that the levels of phosphorylated CaMKII, Erk and p38 were significantly reduced, while the levels of phosphorylated mTOR remained unchanged. The levels of GluN1 were increased, and may result from a compensatory mechanism. This study clearly showed that a lack of Shank2 proteins reduces NMDAR signalling, not via PSD assembly but possibly via reduced levels of phosphorylated CaMKII, Erk and p38 (Won et al., 2012). How the reduction in NMDAR signalling arose and how such a reduction did not result in increased AMPR signalling remains to be further elucidated. Another rodent study that created mouse

models with double copies of deleted exon 7 of *SHANK2* also found ASD-like behaviours, but with reduced numbers of spines, reduced basal transmissions and increased NMDAR-mediated currents, which contrasted with the mouse model that had exon 6 and 7 deletions (Schmeisser et al., 2012). It is unclear how various deletions in *SHANK2* result in the difference of spine numbers and signalling patterns of neurons. However, a recent *in vitro* study introduced four *SHANK2* missense variants found in schizophrenia patients (S610Y, R958S, P1119T and A1371S) into rodent hippocampal neurons and did not find reduced spine volumes or numbers, nor altered presynaptic or postsynaptic terminal numbers. They did find reduced presynaptic contacts of Shank2+ puncta for all 4 variants, reduced ability to increase spine volumes for 2 variants (S610Y, P1119T) and reduced Shank2 PSD clustering for 1 variant (A1371S). Taken together, these studies showed that *SHANK2* variants found in ASD and schizophrenia could lead to reduced NMDAR signalling, impaired dynamic spine volume regulation and reduced pre- and post-synaptic contacts.

3.3 Aims

The primary aims of the iPSC study are to model the development of glutamatergic pyramidal neurons in schizophrenia using cellular reprogramming and to discover cellular phenotypic differences between AOS patients and controls.

The aims can be broken down into several steps:

1) To generate iPSCs from 3 AOS patients with family histories of schizophrenia, as this is likely to enrich for the genetic causal components which are more realistic to study with iPSCs, and from 3 healthy controls;

2) To derive cortical glutamatergic neurons from the induced pluripotent stem cells for the 3 AOS patients with family histories of schizophrenia and the 3 healthy controls;

3) To compare the growth of neurites during the neuronal conversions between patients and controls;

4) To compare the morphology of mature neurons between patients and controls;

5) To compare the maturity and the functions of the induced glutamatergic pyramidal neurons, based on the expressions of glutamate receptors and the PSD components.

3.4 My roles in the study and contributions from collaborators

My roles in this study were to reprogram fibroblasts into iPSCs and characterise the iPSCs, as well as to induced and study glutamatergic pyramidal neurons using the NGN2 protocol. All work presented in this chapter were done by myself except for the analysis of Chip array data in the genomic integrity assay, which was done by a collaborator (Sally Cowley) due to limited access to the analysis software.

3.5 Materials and methods

3.5.1 Skin biopsy processing and primary cultures

A 3- to 4-mm cylindrical skin biopsy containing the epidermis, dermis and subcutaneous fat was made on the inside of the upper arm with a skin punch instrument (carried out by ENT specialist Dr. Pable Devesa). The skin biopsy was kept in fibroblast culture medium; Advanced DMEM (Life Technologies 12491-023), 10%FBS, 1%P/S for 10-20 min at room temperature during transportation. The plating of skin biopsies and handling of fibroblasts followed a standard operation procedure developed by Oxford University's STEMBANCC project (SOP13 Fibroblast Culture from Skin Biopsy for StemBANCC v1.0). Briefly, the subcutaneous fat was removed and the remaining tissue was cut into 15-20 small cubes, which were subsequently placed in two wells in a 6-well plate (Corning 3516) with a sterile 22*m*m x22*m*m glass coverslip (Fisher Scientific 13206778) on top. The initial outgrowth of keratinocytes and fibroblasts usually occurred within the first 3-5 days. When the cell culture became confluent, fibroblasts were detached with a 5 min exposure to Trypsin/EDTA 0.05%/0.02% in PBS at 37°C which was insufficient to detach keratinocytes. Fibroblast culture medium was renewed every 2-3 days. Fibroblasts were frozen down at passage 2 in 10% DMSO in fibroblast culture medium and stored in liquid nitrogen. All cell culture was kept at 37°C, 5% CO_2 in a sterile humidified environment.

3.5.2 Reprogramming

Fibroblasts were reprogrammed to iPSCs by transfecting cells with Sendai viruses (CytoTune®-iPS 2.0 Sendai Reprogramming Kit, Invitrogen A16517) that encode the reprogramming factors, *Oct4 c-Myc, Klf4* and *Sox2*. The transfected cells were plated on mouse embryonic fibroblast (MEF) feeder cells to allow the initial appearance of iPSC clones. Picked clones were expanded on Matrigel (BD Bioscience/Corning 354277) with mTeSR1 medium (Stem Cell Technologies 05850), 1% P/S. Three banked iPSC lines per subject had to pass quality control steps. If banked lines failed the quality control, back-up lines would be banked and taken through quality control.

On day 1, fibroblasts were plated in a 12-well plate at 12.5K, 25K, 50K, 75K and 100K cells/well. On day 3, an aliquot of the mixed CytoTune Sendai viruses suitable for infecting 150K cells was thawed and gently mixed with 1ml of pre-warmed fibroblast culture medium without P/S, and loaded on a well 70% confluent with fibroblasts. The next day, medium was renewed and thereafter renewed every other day. MEF conditioned medium was prepared for supporting the growth of iPSC colonies when the feeder cells became too old and insufficient (around day 18). Per individual, 12 million deactivated MEF were seeded in three T75 flasks that were coated with 0.1% gelatin. From the day after seeding onwards, 45 ml of hES medium (no P/S or FGF2) that had been left on MEF for 24 hours were collected from three flasks consecutively for 7 days. Next, the pooled conditioned medium was filtered through a 0.22 µm filter and stored at -20°C. On day 9, deactivated MEFs were seeded on three 6-well plates at 0.44 million cells/well. One well was left blank as a no-MEF control. On day 10, the CytoTune-transduced fibroblasts were gently dissociated with TryplE (Gibco

1723937). TryplE was washed away with 9 ml pre-warmed fibroblast culture medium and 5 min, 1000 rpm centrifugation. The cell pellet was re-plated onto two MEF plates at 8,000 cells per well and one MEF plate at 12,000 cells per well (this high density plate contains one no-MEF control well). Re-plated cells were left in fibroblast medium overnight and cultured in hES medium without P/S or FGF2—Knockout-DMEM (Life Technologies 10829-018), 20% Knock-out serum replacement (Life Technologies 10828-028), 100 µM non-essential amino acids (NEAA) (Gibco 1605380), 2 mM GlutaMax (Gibco 35050), 1% P/S, afterwards for 6 days with daily medium refreshment. The cultures were thereafter observed closely for the appearance of iPSC colonies. Starting on day 17, the medium was refreshed with 1ml of MEF conditioned medium with 1% P/S and 10 ng/ml FGF2 (PeproTech 100-18B). When a colony had grown to appropriate sizes for transfer, it was cut with sterile needles into 3-5 pieces under a dissection microscope and transferred into one well of a 12-well plate coated with Matrigel. Per reprogramming, 12 colonies were picked to select for the best three as working lines and the second best three lines as back-ups. The best three iPSC clones were the clones that grew at normal speed (1:3 split, one split per 3 day) and showed the least spontaneous differentiation in mTeSR medium. Under feeder-free condition, the picked iPSCs were grown in mTeSR medium/1%P/S with daily medium refreshment. Cells were purified by manually removing the differentiated parts under a dissection microscope and passaged every 3-4 days. The top three lines were expanded to passage 13 and cryopreserved from six 10cm dishes into 30 vials as the master stock whereas the top six lines were frozen down at passage 4, 5 and 6 as early passage back-ups. Master stocks had to pass quality control procedures which included 1) growth after thawing, 2) CytoTune clearance assay, 3) flowcytometry analysis of pluripotency markers, and 4) SNP analysis of genomic integrity.

3.5.3 Freezing and thawing of iPSCs

To freeze iPSCs, cells were washed once with pre-warmed PBS and once with pre-warmed 0.5 mM EDTA (Life Technologies 15575-038) in PBS, then treated with 0.5 mM EDTA/PBS for 5min at 37°C. EDTA/PBS was gently removed without disturbing the loose monolayer of iPSCs. Cells were gently resuspended in one volume of mTeSR medium and finally mixed with another volume of 2x iPSC freezing medium; 60% ES-qualified FBS (Life Technologies 10439-024/15141-079), 20% DMSO and 20% knock-out DMEM (KO-DMEM). Usually, cells from one well in a 6-well plate were cryopreserved in one vial and cells from one 10 cm culture dish were cryopreserved in five vials. To thaw iPSCs, a cryopreserved sample was defrosted in a warm water bath until only a small piece of ice was still visible. Cells were gently mixed with PBS and centrifuged at 400g for 5 min. The pellet was resuspended in pre-warmed mTeSR with 10 µM ROCK inhibitor (AbCam Ab120-129) in order to minimise single cell death and left in one well of a 6-well plate overnight. Next day, the medium was refreshed without ROCK inhibitor.

3.5.4 Flow cytometry

Cells were harvested from one well in a 6-well plate by 5 min treatment with 1 ml of TrylE at 37°C and centrifuged with 9 ml of PBS at 400g for 5 min. The pellet was resuspended in 1 ml of cold 2% paraformaldehyde diluted in fluorescence activated cell sorting (FACS) buffer. After 10 min incubation at room temperature, the fixed cells were pelleted down and resuspended in 1 ml ice cold pure methanol. Next, cells were permeabilized by incubating in methanol for at least 30 min at -20°C. Methanol was removed by washing the cells in 5 ml of FACS buffer and centrifugation at 400g for 5 min. Per iPSC line, two reactions were done; one staining with 1:100 *TRA-1-60* 488 (Biolegend B119983) mixed with 1:150 NANOG647 (Cell Signalling 5448S) and the other staining with 1:100 Immunoglobulin M (IgM)-488 (Biolegend 401617) mixed with 1:150 Immunoglobulin G (IgG)-647 (Cell Signalling 5448S) as isotype controls for background signal. Antibodies were diluted in FACS buffer and per reaction 200,000 cells were mixed with 50 µl of antibody mixture. Even staining was ensured by incubation on a rocker at room temperature for 40-60 min in the dark. The reaction was washed with 200 µl of FACS buffer and then analysed with a flow cytometer (FACScalibur Becton Dickinson). Operation of the flow cytometer and downstream analysis with FlowJo software was done with help from a trained post-doctoral researcher (WH).

3.5.5 RNA extraction and qRT-PCR

To check the clearance of viruses in the iPSC master stock, expression levels of viral backbone and the reprogramming factors were measured in the total RNA extract with real time quantitative reverse transcription polymerase chain reaction (qRT-PCR). RNeasy® Mini Kit (QIAGEN 74104) was used to isolate RNA following standard protocol. Essentially, cell lysates were applied onto the column. DNA was digested and washed away while RNA was retained on the membrane and subsequently eluted with water. The yield of RNA extraction was measured with Nanodrop. Reverse transcription was done with Superscript III Kit (Life Technologies) using 2 µg template RNA in a total reaction volume of 20 µl. 10 µl of 1:10 diluted cDNA product was used in a PCR reaction of 20 µl total volume using Power SYBR® Green PCR Mastermix (Applied Biosystem 4367659). Primers are provided with the reprogramming kit. QRT-PCR was done by 40 cycles of 58°C for 60 sec, 72°C for 30 sec and 95°C for 15 sec on an Applied Biosystem StepOne Plus Real Time PCR machine. Melting curves were included to check the specificity of amplification products.

3.5.6 DNA extraction and genome integrity assay

DNA was extracted from iPSC master stock and primary fibroblasts following the standard protocol of DNeasy Blood and Tissue kit (QIAGEN 69506). The integrity of the genome was assessed by detecting about 300,000 signature SNPs of the genome, using an Illumina Human CytoSNP-12v2.1 beadchip array. Data generated from iPSC lines and the primary fibroblasts were compared using GenomeStudio and KaryoStudio software (Illumina). The beadchip array and downstream analysis was done by experienced scientist (SC).

3.5.7 Generation of lentiviruses

Plasmid pTet-O-Ngn2-puro and pLV-hEF1a-rtTA3 were gifts from Prof. Zameel Cader (Nuffield Department of Clinical Neuroscience). All other plasmids were purchased from Addgene (Table 3.2). Plasmid isolation was done using EndoFree Plasmid Maxi Kit (Qiagen 12362). Briefly, 250 ml overnight bacteria cultures in Lysogeny broth (LB) medium with 100 μg/ml ampicillin were harvested by centriguation at 6000 g for 20 min. The bacteria pellets were used for plasmid isolation following the manufacturer's instructions. The concentrations of plasmids were measured with Nanodrop. For infection, Human embryonic kidney 293 (with large T antigen) (HEK293T) cells (CloneTech) were cultured in DMEM (D6421), 10% FBS and 5% P/S 0.1% gelatin coated 10cm tissue culture dishes. When the HEK293T cells reached 90% confluency, the culture media were refreshed with opti-MEM (ThermoFisher Scientific) with 2% serum, no P/S, 1h prior to the transfection. Per 10cm dish, 88 μl of 1mg/ml PEI (added this to opti-MEM first and waited for 5min), 4.4 μg of virual genomes, 4.4 μg of each of the 3rd generation lenti-virus packing plasmids: pMDLg/pRRE, pRSV-Rev and pMD2.G were added to 1.8 ml of opti-MEM. Master mix per 10 dishes was made and 1396 μl of the master mix was added per dish to the HEK293T cultures gently and drop-by-drop. Next day, 6.5 ml of fresh HEK293T culture media were refreshed per dish. The culture media were collected after 24h as the first harvest of the virus suspension and 6.5 ml culture medium was refreshed. Another 24h later the media were collected as the second harvest. All virus suspensions were filtered through 0.45 μm synringe filters and condensed with Lenti-X (CloneTech) concentrator overnight in cold room. Virus pellets were obtained by centrifugation at 1,500 g at 4°C for 45 min. Supernatants were discarded but 200-300 μl of the supernatants were left for virus resuspension. The pellets were gently resuspended, aliquoted and stored at -80°C.

Table 3.2 Summaries of plasmids used in the *NGN2* protocol.

Name	Addgene ID	Competent E.coli	Bacterial resistance
pLV-hEF1a-rtTA3	61472	Stbl3	ampicillin
pMDLg/pRRE	12251	DH5alpha	ampicillin
pTet-O-Ngn2-puro	52047	Stbl3	ampicillin
pRSV-Rev	12253	DH5alpha	ampicillin
pMD2.G	12259	NEB stable	ampicillin
Tet-O-FUW-EGFP	30130	Stbl3	ampicillin
pLV-TetO-hNGN2-eGFP-Puro	79823	NEB stable	ampicillin
pLV-TetO-hNGN2-Puro	79049	NEB stable	ampicillin

3.5.8 Inducing neurons with NGN2 overexpression

The optimal concentrations of *NGN2* and *rtTA3* viruses were determined by titering on iPSCs. Prior to the virus infection, iPSCs were seeded at line-specific densities (*Results*) in mTeSR (StemCell Techonologies) with Ri (Tocris Bioscience 1254) in 24-well plates coated with geltrex (LifeTechnologies A1413302). Next day, old media on iPSCs were discarded and viruses (usually 5 μl of *NGN2* viruses and 4 μl of *rtTA3* viruses) were added with 8 μg/ml polybrene in 500 μl mTeSR with Ri per well. Next day, media were refreshed with 500 μl mTeSR with Ri per well. The next day, cells were re-plated onto 24-well plates that were coated with 32 μg/ml PLL for 24h and 1:100 mouse laminin for at least 2h at 37°C in mTeSR with Ri. 5h later, media were changed to DMEM/F12 with the N2 medium: GlutaMax (Gibco 31331), 1% NEAA (LifeTech 11140-050), 1% N2 supplements (ThermoFisher Scientific 17502048) and 1% P/S, 10ng/mL brain-derived neurotrophic factor (BDNF) (PeproTech), 10ng/mL Neurotrophin-3 (NT-3) (PeproTech) and 1 μg/ml doxycycline (CloneTech 631311). Next day, no action was taken, this day was marked as day 1 in the protocol. On day 2, the N2 media were supplemented with Ri, 1 μg/ml puromycin and Growth Factor Reduced (GFR) Matrigel (VWR 47743-722) at 33 μl/10ml total medium. On day 3, the B27 medium: neurobasal (Invitrogen 21103049) with 1% GlutaMax, 2% B27 supplement (ThermoFisher Scientific 17504044), 1% P/S, 10ng/mL BDNF, 10ng/mL NT-3 and 1 μg/mL doxycycline was added with 1 μg/ml puromycine and 33 μl/10ml GFR matrigel. Primary mouse glia were added at the ratio of 1 confluent T25 glia for one 24-well plate on day 4 in the B27 medium with 1 μM ara-c and 33 μl/10ml GFR matrigel. On day 7, medium was refreshed with the B27 medium with 33 μl/10ml GFR matrigel. On day 9, half medium change was done with the BrainPhys medium: BrainPhys without phenol red (StemCell technologies 5791) with 2% B27,

1% P/S, 10ng/mL BDNF and 10ng/mL NT-3, supplemented with 1 μg/ml doxycycline and 33 μl/10ml GFR matrigel. On day 11, a full medium change was done with the BrainPhys medium (no doxycycline). From day 13 onwards, half medium change was done with the BrainPhys medium with 2.5% FBS every other day. GFR matrigel was added every 4 days.

3.5.9 Immunocytochemistry and microscopy

Same methods and secondary antibodies were used as described in *Chapter 2*. Antibodies used specifically in the iPSC study are summarised in Table 3.3.

Table 3.3 Primary antibodies used in the iPSC study.

Primary antibodies		
Name	Source	Dilution
Chicken α-MAP2	Abcam, ab5392	1:2000
Rat α-GFAP	Life Technologies, 130300	1:200
Mouse α-synapsin	Synaptic System 106011	1:500
Rabbit α-vGlut1	Synaptic System 135303	1:500
Rabbit α-SynGAP	Sigma HPA038373	1:30
Alexa Fluo™ 647 Phalloidin (binds with F-actin)	ThermoFisher Scientific	1:1000

3.6 Results

3.6.1 SYNGAP1 and SHANK2 variants in patient 002

Whole exome sequencing revealed genetic variants of the studied cohort in coding regions (*Chapter 1*). Patient 002 carried candidate variants in *SYNGAP1* and *SHANK2*, the protein products of which play essential roles in post-synaptic signalling. To find out if the variants were *de novo* or inherited, the parents of patient 002 were subsequently recruited. WES analysis showed that the *SYNGAP1* variant in patient 002 was inherited from the father, who had schizoaffective disorder or schizophrenia (AJ) and the *SHANK2* variant was inherited from the mother, who was neurologically healthy. Patient 001 and patient 007 were not whole exome sequenced due to the priority of the trio study (*Chapter 1*). Table 3.4 summarised the locations of the genetic variants and their predicted impacts on transcripts and proteins. Both the low allele frequency for the *SHANK2* variant (0.0001934) and the non-documented *SYNGAP1* variant on gnomAD, which is a database of exome sequencing data from 123,126 individuals and whole genome sequencing data on 15,496 individuals, showed that the variants patient 002 carried is rare. The patient *SYNGAP1* variant was in exon 15 and theoretically would affect all transcripts (Figure 3.3). At the protein level, the variant did not fall into any defined structural domain of SynGAP (Figure 3.3). However, the *SHANK2* variant, located in exon 11, was adjacent to the Src homology (SH3) domain which links Shank with AMPAR and actin-cytoskeletons (Figure 3.4).

Table 3.4 Summaries of *SYNGAP1* and *SHANK2* variants in patient 002.

	SYNGAP1	***SHANK2***
Genomic location	chr6:33411081 C to T	chr11:70666733 G to A
Minor allele frequency	N/A on gnomAD	0.0001934
Exon	15	11
Impact on the longest protein product	Ala918Thr	Thr411Met
predicted impact on transcripts by gnomAD	N/A on gnomAD (theoretically affecting all transcripts)	ENST00000338508: Thr411Met Polyphen: probably damaging; SIFT: deleterious ENST00000294018: Thr41Met Polyphen: benign; SIFT: deleterious ENST00000423696: Thr31Met Polyphen: benign; SIFT: deleterious ENST00000425049 Arg58Cys Polyphen: unknown; SIFT: unknown

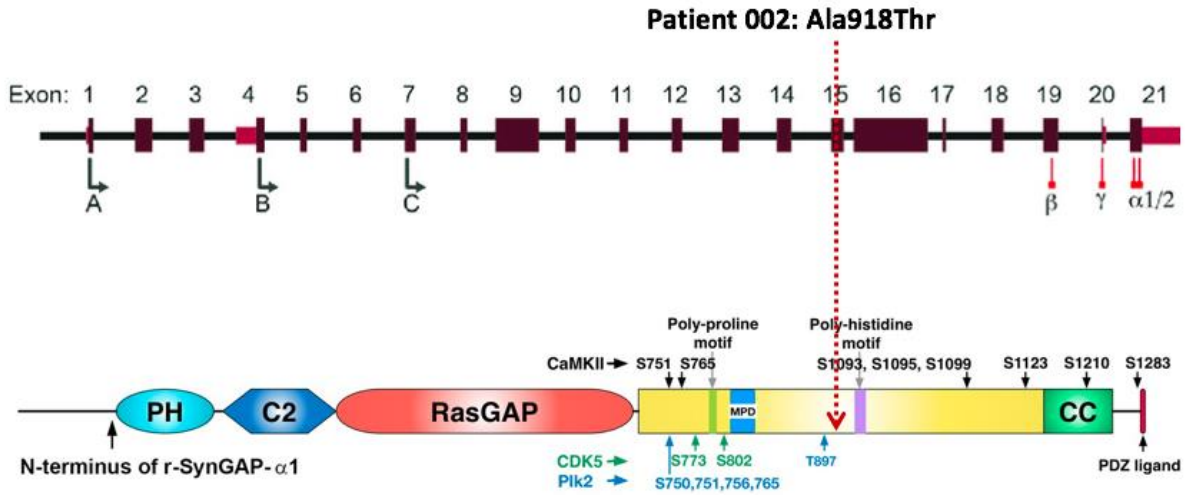


Figure 3.3 Illustration of the *SYNGAP1* variant in patient 002 at the gene and protein levels. Top panel: transcript variants from *SYNGAP1* gene, the combinations of multiple start sites (A, B and C) with multiple endpoints (β, γ, and α1/2) result in many *SYNGAP1* transcripts whose functions are not well understood. Bottom panel: The most well studied transcript of *SYNGAP1* is the longest form α1 whose protein product is called SynGAP. There are several well-documented structures on SynGAP. The Pleckstrin homology (PH) domain is used for binding with phosphatidylinositol lipids, the C2 domain facilitates protein binding to cell membranes and the RasGAP domain activates ras GTPase. The poly-proline motif often forms secondary structures with its neighbouring enzymatic domains and is believed to play essential roles in the liquid-liquid phase transition (LLPS) of proteins, the membrane proximal domain (MPD) acts as a potentiator for membrane-fusion. The poly-histidine motif has been linked with nuclear speckle binding. The Coiled-coil (CC) domain allows SynGAP to form coiled-coil structures. The PDZ ligand which is on the very C-terminal of SynGAP can bind to the PDZ-domain on the PSD scaffolding protein PSD-95. Sites on SynGAP that can be phosphorylated by Ca^{2+}/calmodulin-dependent protein kinase II (CaMKII), cyclin-dependent kinase 5 (CDK5) and Phosphatidylinositol 3-kinase 2 (PIk2) are denoted with arrow heads in black, green and blue, respectively. Dashed red line indicates the location of the *SYNGAP1* variants in patient 002. Figure adapted from (Kilinc et al., 2018; Walkup IV et al., 2016).

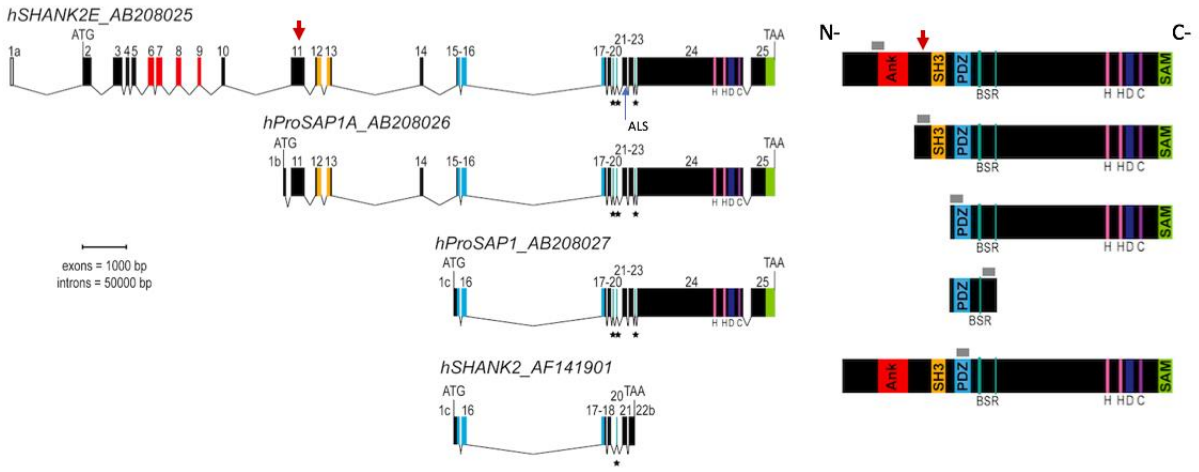


Figure 3.4 Illustration of the *SHANK2* variant in patient 002 at the transcript and protein levels. Left panel: the *SHANK2* gene has multiple transcript products, 4 of which are documented in humans. The variant in patient 002 is located in exon 11, which is only present in the longest two transcripts documented so far. Right panel: Five protein products have been documented for *SHANK2*, the longest protein product contains multiple domains, brain-specific regions (BRS) and modification sites. The Ankyrin repeat domain (Ank) domain promotes protein-protein interaction. The Src homology (SH3) domain links Shank with AMPAR and actin-cytoskeleton. The PSD95/DLG/ZO1 (PDZ) domain is a proline-rich region that can bind SynGAP. The sterile alpha motif (SAM) domain is a putative protein-interactive module and is believed to be important for the oligomerisation of Shank. Upstream of SAM is a long proline-rich region. The locations of the *SHANK2* variants in patient 002 are denoted with a dashed red line. Figure adapted from (Leblond et al., 2012).

3.6.2 Generation of induced pluripotent stem cells

Skin biopsies were obtained from the inner upper arms of all participants and dissected in a sterile flow cabinet under a dissection microscope. For skin biopsies, fibroblasts and keratinocytes rapidly grew out from the plated pieces of biopsies (Figure 3.5). Fibroblasts were isolated from the primary culture by treating the cells with Trypsin/EDTA; the fibroblasts detached within 5-7 mins while the keratinocytes required longer than 10min. Passage 2 fibroblasts were cryopreserved in liquid nitrogen tanks.

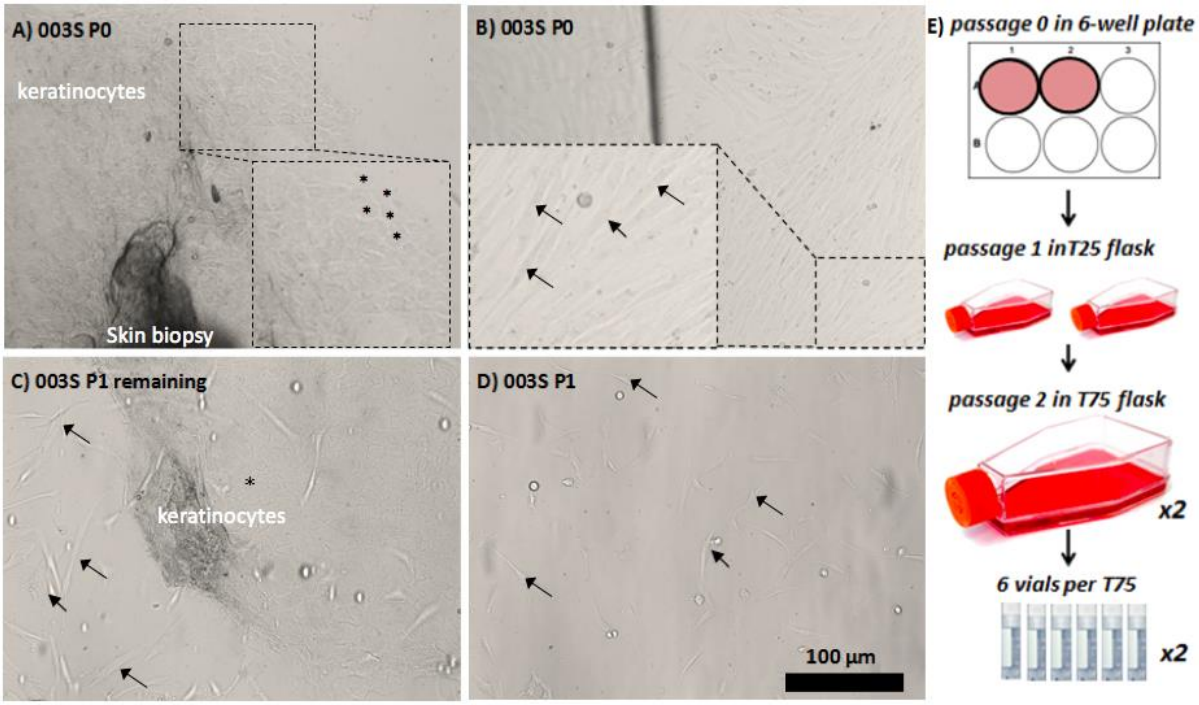


Figure 3.5 Primary cultures from skin biopsies and the banking strategy. Representative pictures from 003S showing that A) keratinocytes grew from the biopsy first and form colony-like monolayer (only keratinocytes are present in A), B) fibroblasts migrated out later and grew confluent, the morphology of fibroblasts (arrows) was significantly different from that of keratinocytes (asterisks). After the first passage, C) keratinocytes (asterisk) remained on the plate as a colony-like monolayer, as well as a few fibroblasts (arrows), while D) sufficient amount of fibroblasts were transferred to the new plate where the culture was purely fibroblasts and no more keratinocytes. E) The initial tissues were plated in a 6-well plate and cells were passed to T25 and T75 flasks and brought up to passage 2, at which cells were cryopreserved as 6 vials per T75 flask. Pictures A, B and C were taken from the same well. 003S: Skin fibroblasts from participant 003.

Fibroblasts from the primary master stocks and Sendai viruses encoding the four Yamanaka factors were used to generate iPSC lines according to the manufacturer's instructions. Cells underwent morphological changes during this procedure (Figure 3.6). Based on the morphologies of the iPSCs and their behaviours in cell cultures—cells grew as tightly packed monolayers; no single cells migrated out from patches of iPSCs and cells remained small and homogenous. The best three iPSC lines were chosen for the three patient fibroblast lines; 001S, 002S & 007S and the three control fibroblast lines; 010S, 011S and 014S. Three iPSC lines per individual were expanded to passage 13 and cryopreserved as iPSC master stocks. As summarised in Table 3.5, all iPSC master stocks grew normally after thawing; showed clearance of Sendai viruses (table 3.6); and highly expressed pluripotency markers Homeobox Protein NANOG (*Nanog*) and *TRA-1-60* (Figure 3.7). However, lines 001S-1 and 001S-4 showed large triplicated segments of chromosomes in the genetic integrity assay, hence they were excluded from the study (Figure 3.8). All other lines passed the genomic integrity test.

Table 3.5. Summaries of the status of all iPSC lines generated in this study.

Participant	Line code	Growth after thaw	Sendai virus	Pluripotency markers	Genomic integrity	Master stock (p12)
001S (patient)	001S-1*	normal	cleared	high	fail	terminated
	001S-4	normal	cleared	high	fail	terminated
	001S-7	normal	cleared	high	pass	30 vials
	001S-5	normal	cleared	high	pass	30 vials
	001S-9	normal	cleared	high	pass	30 vials
002S (patient)	002S-2	normal	cleared	high	pass	30 vials
	002S-9	normal	cleared	high	pass	30 vials
	002S-10	normal	cleared	high	pass	30 vials
007S (patient)	007S-8	normal	cleared	high	pass	30 vials
	007S-16	normal	cleared	high	pass	30 vials
	007S-21	normal	cleared	high	pass	30 vials
Participant	**Line code**	**Growth after thaw**	**Sendai virus**	**Pluripotency markers**	**Genomic integrity**	**Status**
010S (control)	010S-1	normal	cleared	high	pass	30 vials
	010S-7	normal	cleared	high	pass	30 vials
	010S-8	normal	cleared	high	pass	30 vials
011S (control)	011S-2	normal	cleared	high	pass	30 vials
	011S-8	normal	cleared	high	pass	30 vials
	011S-16	normal	cleared	high	pass	30 vials
014S (control)	014S-3	normal	cleared	high	pass	30 vials
	014S-5	normal	cleared	high	pass	30 vials
	014S-10	normal	cleared	high	pass	30 vials

**001S-1: the first colony picked from transduced 001S (skin fibroblasts from participant 001).*

Table 3.6 Ct values from qRT-PCR Sendai virus clearance assay.

Ct values	SeV	*Klf4*	KOS	*c-Myc*	β-actin
001S-day 7*	17.57	20.60	23.39	26.15	21.36
001S-1 p5*	25.93	29.16	28.97	27.65	26.93
001S-1 p7*	35.61	34.58	31.35	34.95	25.04
001S-1 p13	undetermined	34.79	29.97	34.30	21.63
001S-4 p13	undetermined	34.59	29.96	34.24	21.47
001S-7 p13	undetermined	34.32	30.21	34.51	21.82
002S-2 p13	undetermined	35.00	29.94	36.37	21.53
002S-9 p13	undetermined	35.08	30.69	34.92	22.31
002S-10 p13	undetermined	35.74	31.12	34.80	23.02

**001S-day7: 7 days after transducing 001S, cells were harvested as a positive control for qPCR clearance assay. All other iPSC lines displayed similar values.*

Same applies to 001S-1 at passage 5 and passage 7.

Red=detected. SeV=backbone of Sendai virus.

KOS=a vector containing Klf4, Oct4 and Sox2.

β-actin was used as the house keeping gene.

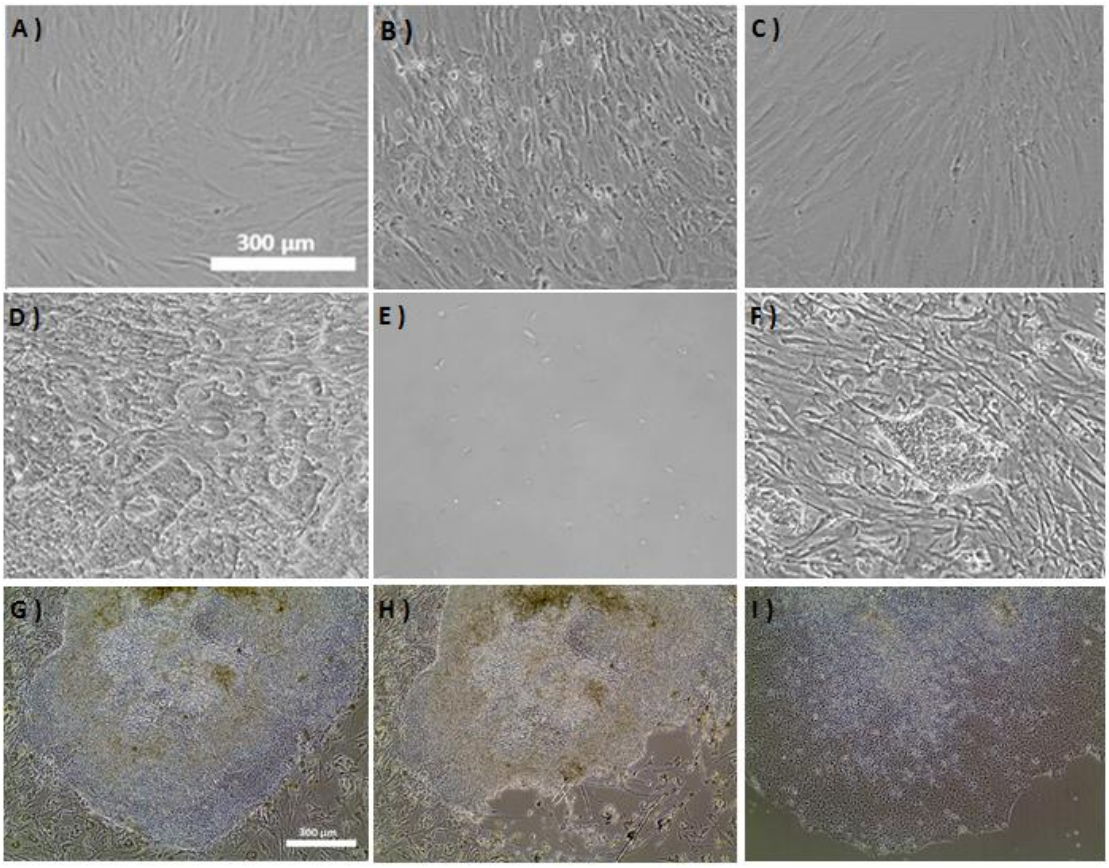


Figure 3.6 Morphological changes during generation of induced pluripotent stem cells.
Representative pictures from the reprogramming of 002S are shown. Before transduction, fibroblasts were about 70% confluent (**A**). Two days after transduction, cells became much smaller (**B**) compared to the un-transduced control (**C**). One week after transduction, cells formed irregular colonies (**D**) and were re-plated on mouse embryonic fibroblasts (MEFs) feeders to allow growth of individual colonies. The re-plating density can be seen on a well without MEFs (**E**). Small colonies appeared one week after re-plating on MEFs (**F**) and were closely watched to be picked when large enough (**G**). Colonies with clearly defined edges and containing regular monolayer regions were picked (**H**, either the entire colony or the regular parts of a colony). The picked parts from one colony were transferred to feeder-free matrigel-coated wells and expanded (**I**). Per fibroblast line, 12-20 colonies were picked and the best three were expanded to passage 13. Differentiated parts of iPSCs were removed before passaging to purify the iPSC lines. Figure A-F, scale bar=300 µm. Figure G-I, scale bar=300 µm.

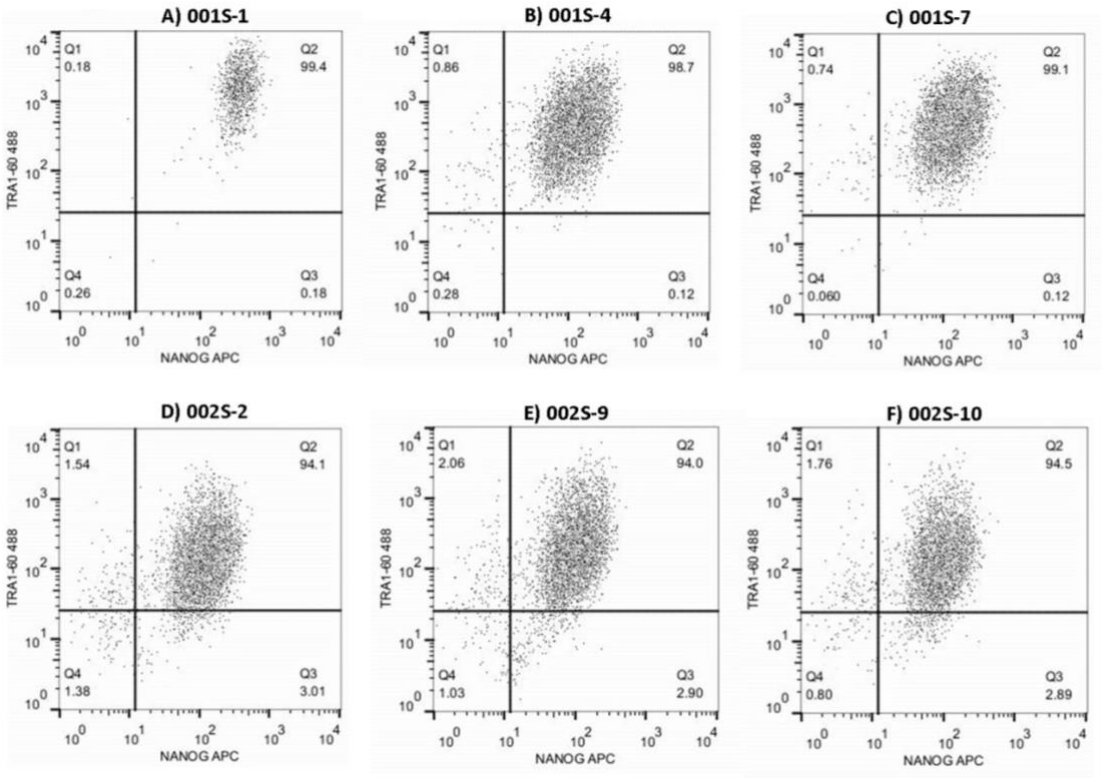


Figure 3.7 Vast majority of cells in iPSC master stocks highly express pluripotency markers. Results from flow cytometry analysis for expression of *Nanog* and *TRA-1-60* in iPSC master stocks of 001S and 002S are shown as examples. All other lines displayed highly similar results. X-axis shows the signal from *Nanog* (APC) and Y-axis shows the signal from *TRA-1-60* (488). Quadrants are defined by letting isotopic controls fall into Q4 (data not shown).

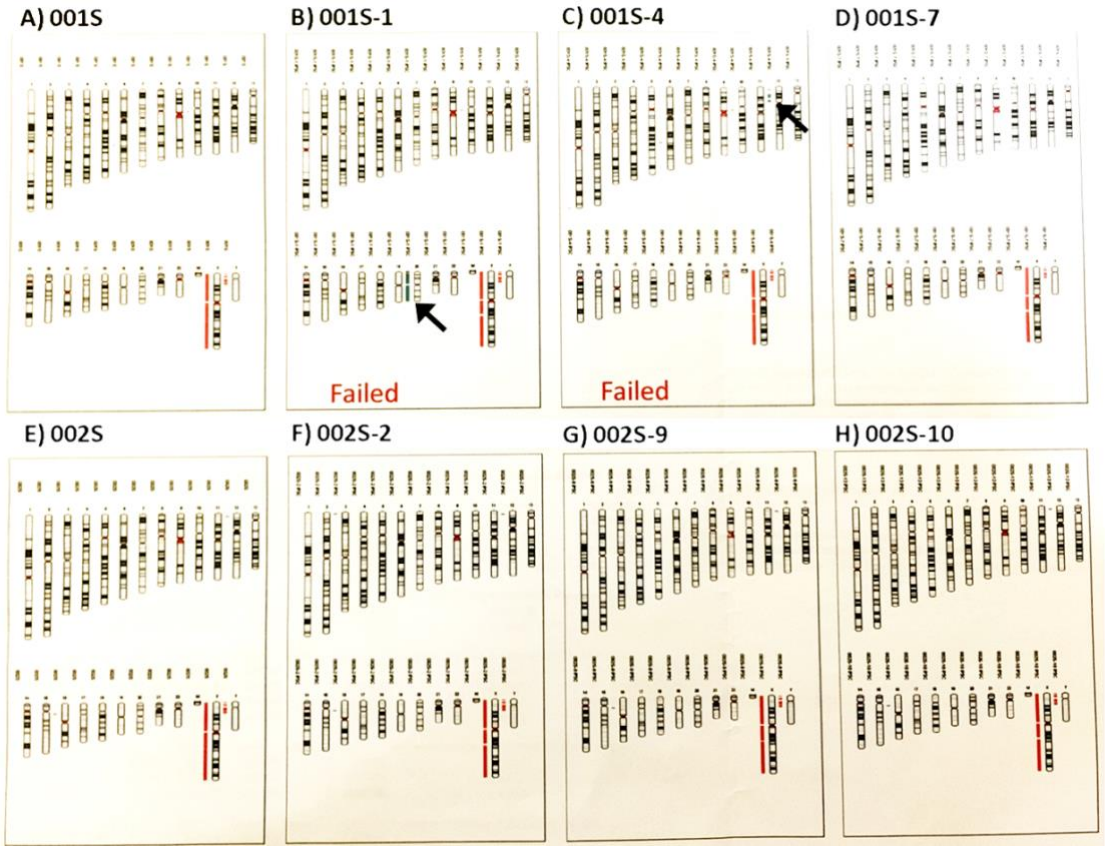


Figure 3.8 Genomic integrity test results. Results are based on SNP analysis of total DNA. The genomes of iPSC lines were compared with their parental fibroblasts. Line 001S-1 (B) and 001S-4 (C) harboured large segments of triplication mutations (green bars) hence were excluded from the study. All other lines passed the genomic integrity check. Results from 001S and 002S are shown as examples. Genomic integrity test results for other lines were incuded in appendix. Arrows indicate the sites of mutation.

3.6.3 Generation of cortical glutamatergic neurons

3.6.3.1 NGN2 protocol optimisation

The overexpression of *NGN2* gene was found to efficiently convert iPSCs into cortical layer 2/3 glutamatergic projection neurons (Zhang et al., 2013). The doxycycline inducible *NGN2* overexpression was achieved by using lenti-viruses encoding *rtTA3* and *NGN2*, or *NGN2-EGFP*. The *rtTA3* is a protein created by random mutagenesis on the tetracycline repressor to achieve inducible activation of the tet response element (TRE) upstream of *NGN2*. Third generation lenti-viruses encoding *rtTA3*, the human *NGN2*, *NGN2-EGFP* and the mouse *Ngn2* were made using plasmids shown in table 3.7. After maxi-prep from *E.coli* cultures for isolating plasmids, all plasmid identities were confirmed with sequencing. The enhanced green fluorescent protein (*EGFP*) gene following *NGN2* allowed live observation of neuronal morphology based on green fluorescence. The puromycin-resistant gene insert distal to *NGN2* or *NGN2-EGFP* allowed selection of cells that successfully incorporated and expressed the construct. However, the doses of *rtTA3*, *NGN2*/*NGN2-EGFP* and puromycin selection to obtain pure populations of neurons for each iPSC line were unexpectedly different. Therefore, various combinations of viruses and the chemical compounds required for the protocol were tested. Although all iPSC lines in this study were generated with the same method, the initial plating density required to survive the virus infection and the doxycycline induction varied. Table 3.8 shows the optimal plating density for all lines. Table 3.9 summarises testing results of chemical compounds required for the *NGN2*-mediated neuronal conversion. The initial plating density seemed to be the most critical parameter of all; low plating density resulted in complete cell death after virus infection or after doxycycline induction while high plating

density prevented some cells from receiving sufficient concentration of virus. The cells that did not receive enough virus became non-converting cells whose presence was problematic because they over-populated the cultures and prevented proper neurite development. Non-converting cells also required higher doses of puromycin and cytarabine (ara-c, a chemical compound used to stop cell proliferation) treatment, which was toxic to converting cells from some lines. Re-plating the infected cells before doxycycline induction was important for subsequent neuronal development; as both being sparse or being overpopulated (resulting from different levels of cell death after virus infection), when the *NGN2* overexpression was turned on by doxycycline, prevented formation of good neurite morphology (confirmed with Kristen Brennand, unpublished communication).

Table 3.7 Nanodrop results of plasmids for making *NGN2*-neurons.

Nr.	plasmid name	ng/µl	260/280	260/230	Volume (µl)
1	pLV-hEF1a-rtTA3	3429.8	1.91	2.26	130
2	pMDLg/pRRE	2746.2	1.91	2.35	130
3	pTet-O-Ngn2-puro (mouse)	3652.4	1.87	2.22	130
4	pRSV-Rev	3244.3	1.91	2.29	130
5	pMD2.G	2260.4	1.93	2.42	300
6	Tet-O-FUW-EGFP	3084.2	1.92	2.34	300
7	pLV-TetO-NGN2-eGFP-Puro (human)	2517.3	1.94	2.32	300
8	pLV-TetO-NGN2-Puro (human)	2406.6	1.94	2.33	300

Table 3.8 The optimal plating densities for *NGN2* induction varies between iPSC lines*.

Ranking	iPSC line	plating density
Robust lines	<u>007S-21, patient</u> 007S-16, patient 007S-8, patient 001S-7, patient 010S-1, control	160,000 cells/well in 24-well plates
Standard lines	010S-8, control 010S-7, control <u>002S-10, patient</u> 002S-9, patient	200,000 cells/well in 24-well plates
Fragile lines	<u>014S-5, control</u> 014S-3, control <u>011S-16, control</u> 011S-2, control 002S-2, patient	250,000 cells/well in 24-well plates
Extremely fragile lines	011S-8, control 014S-10, control	280,000 cells/well in 24-well plates

* These are the plating densities aiming for infection 20h after plating. The densities are only accurate when passaging the iPSCs (not directly thawed) with StemPro Accutase and culturing in mTeSR medium. Infection after 20h plating requires lower plating density and alternative passaging (EDTA methods) or culturing (E8 medium) requires higher plating density. The material of coating does not matter for cells surviving the infection and induction.
The lines converted the best were underlined (002S-10, 007S-21, 011S-16 and 014S-5).

Table 3.9 Summary of testing results for key chemical compounds.

Name	Function	Optimal dose	Note
polyethylenimine (PEI)	introduce plasmids to HEK293T cells for virus production	1 μg total DNA 4 μg total PEI	commonly used at 1:3 1:4 increased the number *NGN2-EGFP*+ cells
polybrene (pb)	increase efficiency of viruses entering iPSCs for infection	8 μg/μl in virus master mix	8 μg/μl pb alone or viruses alone were toxic to fragile lines (medium should be changed 8-12h post-infection), however when combined together worked better than 2-48 μg/μl
rock inhibitor (Ri)	inhibit single cell death for iPSCs	before and after infection	leaving Ri in medium after infection and during dox induction increased survival greatly
doxycycline	induce NGN2 overexpression	1 μg/μl	4 μg/μl used in original protocol, toxic to fragile lines, 1 μg/μl is sufficient to induce strong *NGN2-EGFP* for all iPSC lines in this study
puromycin	kill cells that did not receive NGN2	1 μg/μl	tested 0.4-4 μg/μl from various protocols, 0.4-0.8 μg/μl not sufficient to kill non-converting cells; 1.2-4 μg/μl reduced the number of *NGN2-EGFP*+ cells
ara-c	stop primary glia and non-converting cells from proliferation	1 μM	1.5-2 μM killed lines from 007S. Higher dose is required if non-converting cells were not killed by puromycin

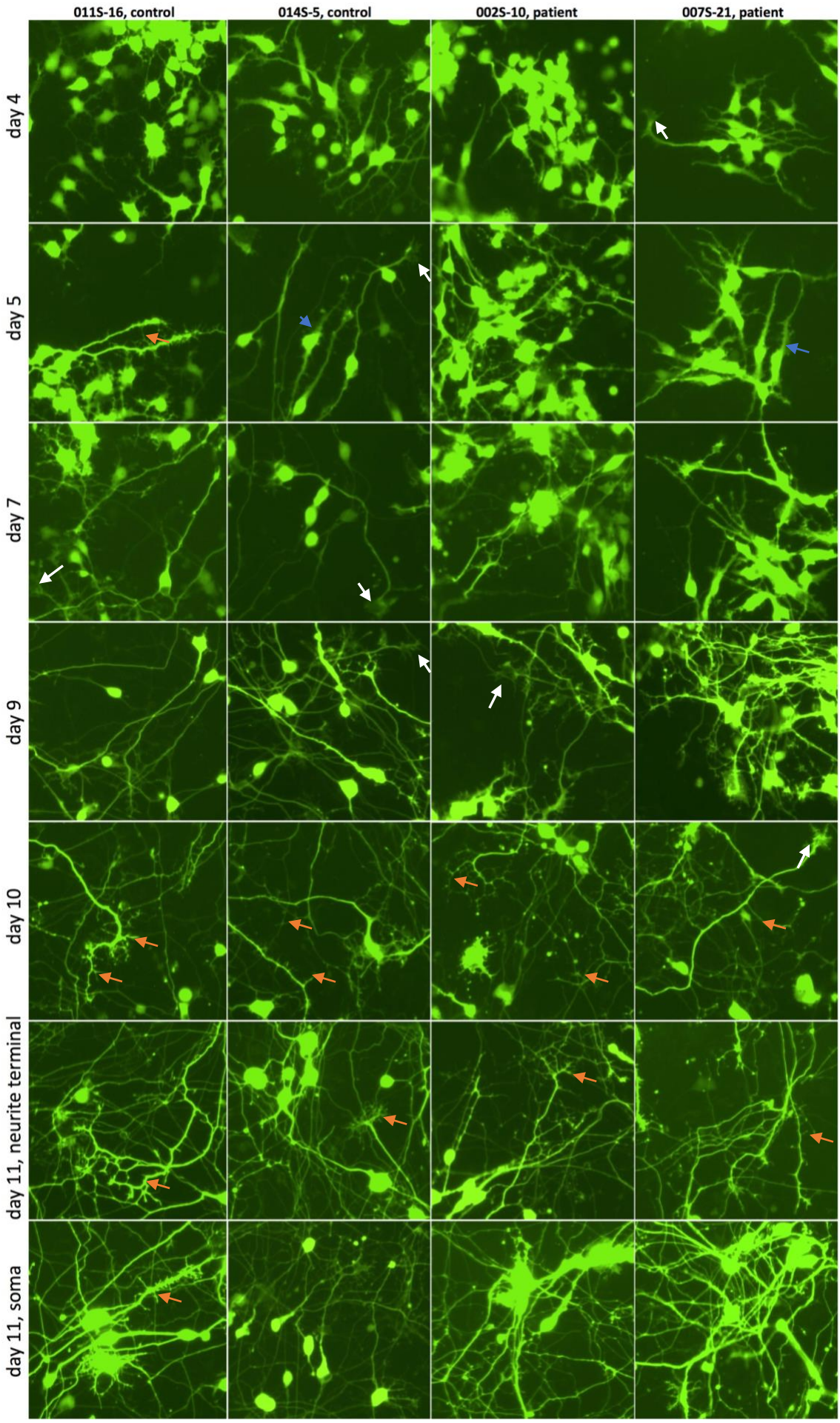
3.6.3.2 Live imaging of induced neurons

All iPSC lines generated in this study, except for 001S-1 and 001S-4 which did not pass the genomic integrity test, were subjected to NGN2-mediated neuronal conversions. Out of the 16 lines, only 4 lines eventually resulted in satisfactory conversions at the same time. The other lines either became too sparse or overly crowded in the first week of conversion due to variable degrees of cell death and cell proliferation after the virus infections and doxycycline inductions. For example, most cells in patient line 002S-2 gradually died after the doxycycline inductions, regardless of high plating densities having been applied. The remaining 11 lines all showed various degrees of overgrowth after induction, suggesting that further testing on the optimal re-plating densities should be done for each line. A re-plating step 4 hours prior to doxycycline induction allowed equal contact of single cells to doxycycline and puromycin. Cells after infection that were not re-plated often grew as clusters hence harbouring non-converting cells that later over populated the cell cultures. Previously, the initial plating density was optimised for each line, and a 1:1 ratio was used for re-plating before induction. However, the iPSC lines after induction survived and grew at different speed, resulting in variations of the densities of neurons.

Based on the 4 lines that had optimal densities to allow proper neurite development, longitudinal live tracking of the cell morphologies based on *NGN2-EGFP* expression (Figure 3.9) did not reveal any obvious difference in the speed or extent of neurite development between lines. However, some line-specific features were present. As shown in Figure 3.9, control line 011S-16 showed structures that resembled secondary neurites as early as day 5, while other lines still had lamellipodium-like structures along the primary neurites. Control

line 014S-5 showed growth cones as early as day 5-7. The growth cones of converting neurons from 014S-5 could still be seen at day 9. Complex neurite terminal structures that likely to be formed by the collapse of growth cones could be seen on 014S-5 from day 11 onwards. By day 13, complex structures around the soma of neurons made of primary protrusions were observed in the two control lines, however no such structures were observed for patient line 002S-10 and only one field with such structure was observed from patient line 007S-21.

Close observations of the conversion processes revealed day 5-13 as the window in which the most dramatic morphological changes occurred. Images were taken at 20x to reveal the fine structures of converting cells. However due to limited access to high-throughput fast whole well scanning equipment, the 20x images could not be used for whole neuron analysis. To track the neurite length dynamics, a separate live imaging experiment was performed applying a whole-well fast scanning method at low magnification. This allowed the whole well to be scanned within 5 minutes, which was considered tolerable for live cells. Images were stitched automatically after scanning and the neurite length was manually measured using Simple Neurite Tracer in ImageJ. Although images were obtained on day 9, 12 and 16, the total neurite length could not be accurately traced for day 12 and day 16 due to the complexity of neurites. Tracking results from day 9 showed a significant increase (22% increase, p=0.04) of the total neurite length on patient line 002S-9 when compared to control line 011S-16 (Figure 3.10).


011S-16, control
014S-5, control
002S-10, patient
007S-21, patient
day 4
day 5
day 7
day 9
day 10
day 11, neurite terminal
day 11, soma

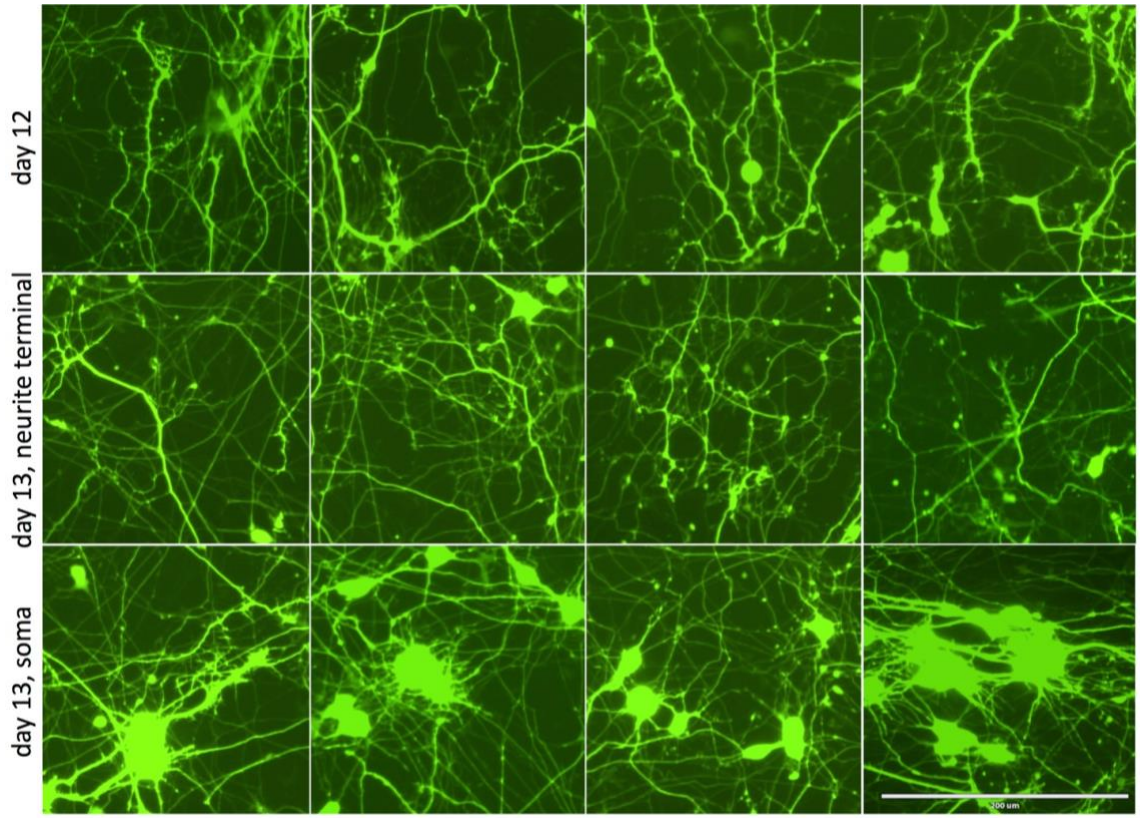


Figure 3.9 Morphological changes during the neuronal conversions mediated by *NGN2-EGFP* overexpression in induced pluripotent stem cells. Live images were taken from all lines during the first 13 days of conversions. Only pictures from the best converted lines were shown. Per day per line, 10 images were taken targeting areas with the most complex neuronal morphologies. Areas that showed the most complex neuronal morphologies were cropped and shown above to represent the best neurite development from a line. Lines that were not included showed hampered neurite development due to being too sparse or overly crowed (but all lines converted). Note that the two control lines generally showed neuronal soma with abundant primary neurites at day 13 while no such morphology could be found for patient line 002S-10 and only field with such morphology could be found for patient line 007S-21. Pictures were over-exposed in order to reveal fine structures on neurites. Orange arrows point at examples of secondary neurites (neurites that directly branched from primary neurites). Blue arrows point at examples of lamellipodium-like structures (branches from primary neurites that were not yet spiny). White arrows point at examples of growth cones. Scale bar=200 μm.

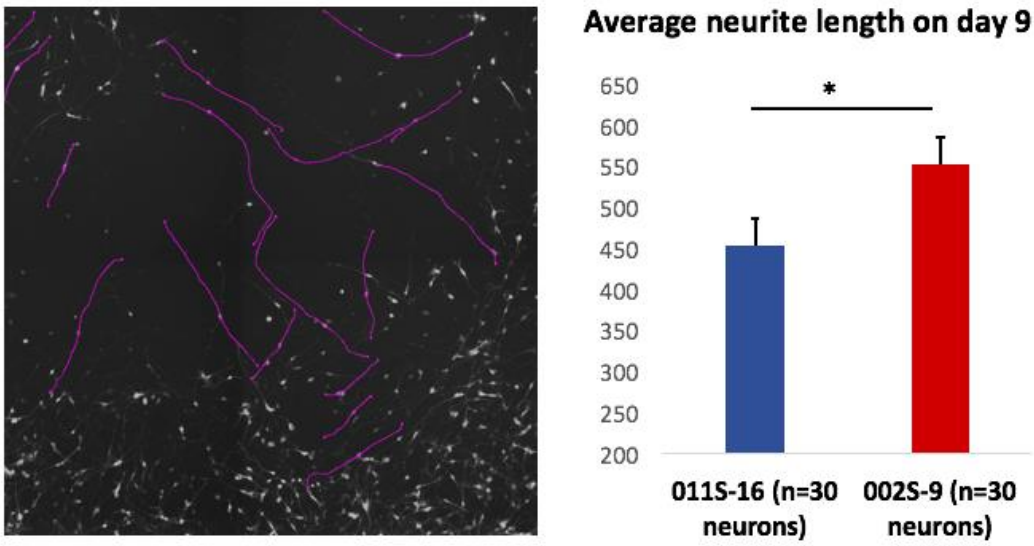


Figure 3.10 Neurite tracing results showed significant longer neurites on converting neurons from patient line 002S-9 than from control line 011S-16. Whole-well stitched images were used in ImageJ Simple Neurite Tracer to manually trace neurite lengths. Left panel: converting cells that were clearly isolated were measured for total neurite lengths. Purple lines are semi-manually labelled neurites using ImageJ Simple Neurite Tracer. Right panel: on day 9, the average value of neurite lengths, represented by total pixel count on y-axis, for 002S-9 (553.1±33.8 pixels) was significantly greater than that for 011S-16 (453.9±33.1 pixels, p=0.04, 2-tail type 3 Student's t-test).

3.6.3.3 Staining of NGN2-neurons and RNA sequencing

I next confirmed the neuronal identity of the induced neurons. Day 28 neurons from control line 011S-16 and patient line 002S-9 were stained with phalloidin to visualise F-actin, antibodies against human Microtubule-associated Protein 2 (MAP2, a pan-neuronal neurite marker), Vascular Glutamate Transporter 1 (vGlut1, a marker for presynaptic terminals), Synapsin (a presynaptic marker for mature neurons), SynGAP and antibodies against mouse GFAP when the neurons were co-cultured with mouse primary glia. F-actin was used to help visualise the morphologies of neurons at low magnification. During development of spines in vivo, F-actins populate the spine-like protrusions before microtubules. F-actin and MAP2 co-staining at high magnification was used to reveal the stages of spine development. All neurons were MAP2+ and vGlut1+ at day 28, no morphological differences were observed between control line 011S-16 and patient line 002S-9 at low or high magnification (Figure 3.11). It was noticed that when co-cultured with primary mouse glia, neurons grew larger and displayed multiple spine-like protrusions mainly on the primary neurites when compared to neurons that were not co-cultured with primary mouse glia (Figure 3.11, bottom panel). These spine-like protrusions were already MAP2+. No neurons expressed detectable synapsin or SynGAP immunoreactivity at day 28. Staining of adult mouse brain sections showed positive immunoreactivity of these two antibodies (Figure 3.12).

To explore possible perturbations of gene expression profiles in patient induced neurons compared with control induced neurons, RNAs from pure induced neuron cultures were extracted and subjected to bulk RNA-seq.

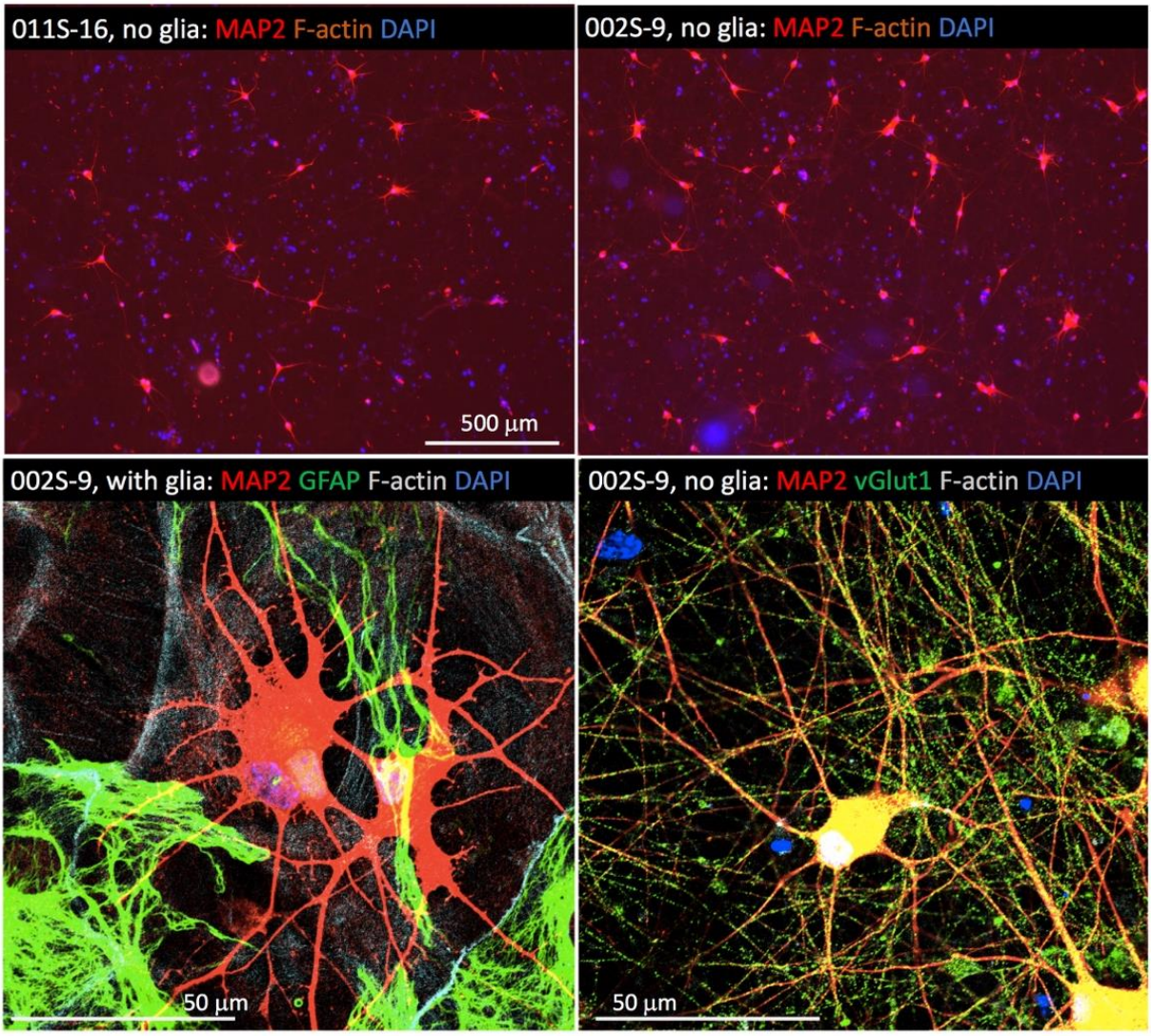


Figure 3.11 Immunostaining characterisation of *NGN2*-neurons at day 28. Top panel: overview of neuronal morphology did not reveal morphological differences, or levels of marker expression, between control line 011S-16 and patient line 002S-9. Bottom panel: at day 28, all neurons were positive for the pan-neuronal marker Microtubule-Associated Protein 2 (MAP2) and Vesicular Glutamate Transporter 1 (vGlut1). Bottom left image showed when co-cultured with mouse primary glia, which were labelled with Glial Fibrillary Acidic Protein (GFAP), neurons displayed spine-like structures on primary neurites. Bottom right image showed when not co-cultured with mouse primary glia, no MAP2+ spine-like structures were observed and the neurons were smaller than the ones co-cultured with mouse primary glia.

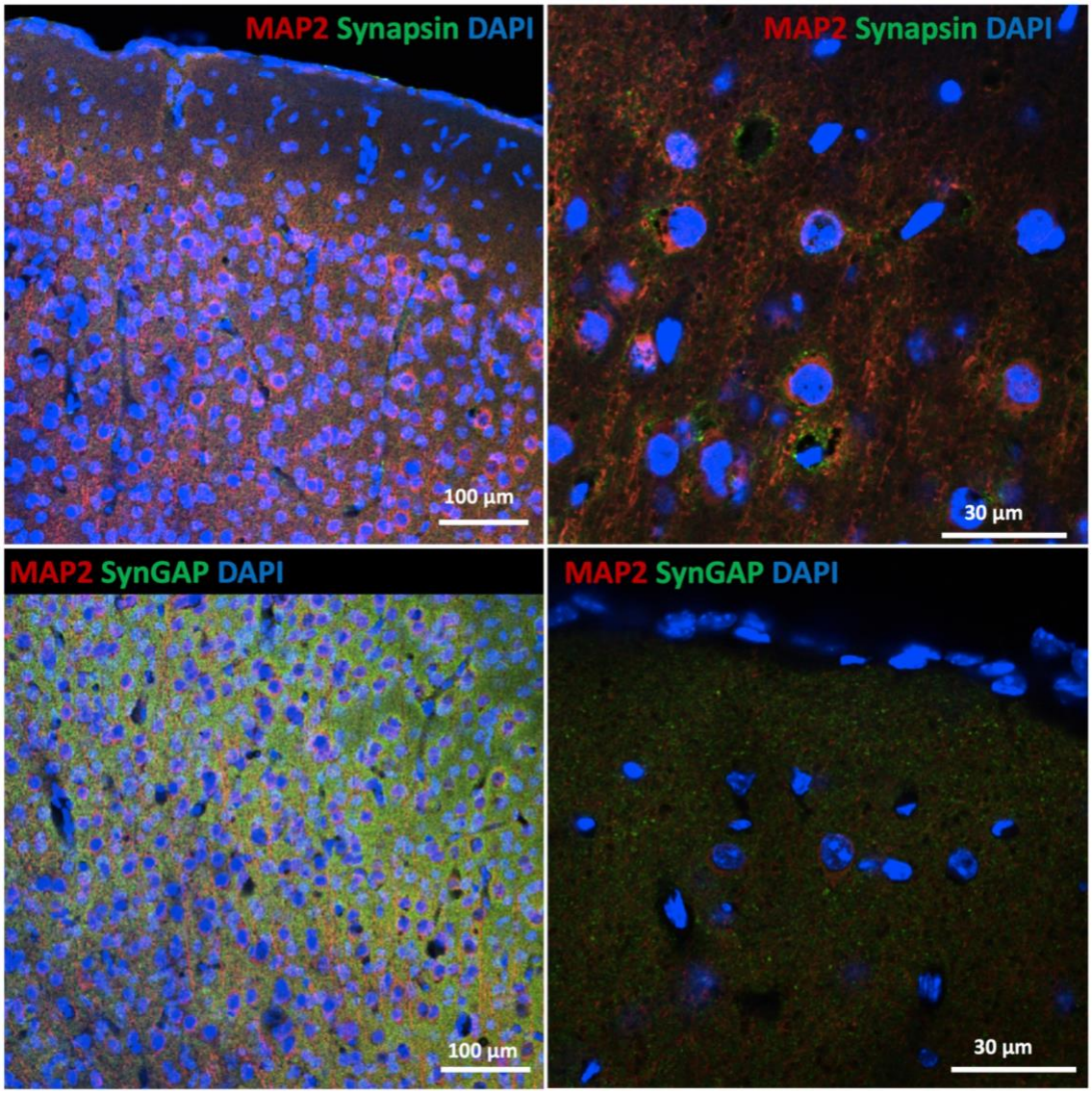


Figure 3.12 Immunostaining of synapsin and SynGAP on adult mouse brain whole-mount sections. Antibodies that react to both human and mouse were used. Adult mouse brain coronal sections showed high immunoreactivities to the pan-neuronal marker Microtubule-Associated Protein 2 (MAP2), pre-synaptic marker synapsin and the synaptic GTPase activating protein (SynGAP) which play important roles in the post-synaptic densities.

3.7 Discussion

This aims of this study were to generate iPSCs from fibroblasts derived from 3 patients and 3 controls, as well as to convert iPSCs to cortical glutamatergic neurons for comparing the processes involved in neuronal development. Both iPSCs and induced neurons were successfully generated however several technical challenges were encountered and resulted in significantly reduced power of the study. The technical challenges, the biological meaning of the obtained results and suggestions for future research for this study will be discussed in the following subchapters.

3.7.1 Technical challenges in cellular reprogramming

The iPSC lines generated from this study were free from Sendai viruses that were used to deliver the Yamanaka factors, expressed high levels of the pluripotency markers *Nanog* and *TRA-1-60*. Out of the 18 iPSC lines generated (3 lines per patient/control), 16 retained highly similar genome structures from the donor fibroblasts. This was assessed by a genome integrity assay on all iPSC lines generated (Illumina Human CytoSNP-12v2.1 beadchip array, results on page 183,273-274). However, two iPSC lines harboured abnormal genomic rearrangements, hence were excluded from the study. The rate of obtaining genomic abnormalities during reprogramming in my study was 11% (2 out of 18), which is within the range of what is commonly found in iPSC research (~20%, Sally Cowley, James Martin Stem Cell Facility, unpublished communications). Research to understand the mechanisms of reprogramming are still under way. Cellular tumour antigen p53 (*TP53*) was found to limit the reprogramming efficiency and to guard genomic stability of the transforming cells (Kawamura et al., 2009; Marión et al., 2009). However, it is unclear why some cells during reprogramming to become iPSC can evade the surveillance of p53 and obtain genomic abnormalities. Research trying to improve cellular reprogramming are also ongoing. For example, The Zinc Finger And SCAN Domain Containing 4 (*ZSCAN4*) gene and *ZSCAN10* genes were found to improve genomic stabilities of reprogramming by regulating the DNA damage responses (Jiang et al., 2013; Skamagki et al., 2017). Understanding the mechanisms of cellular reprogramming and introducing factors that alleviate problems occurred during reprogramming may help to reduce the rate of genomic abnormalities in the future.

Manipulating cell fates after iPSC reprogramming can also be challenging. Overexpression of *NGN2* was used to more rapidly obtain cortical neurons, as this protocol allowed a pure population of cortical neurons that resembled the telencephalic layer2/3 glutamatergic neurons to be generated. However, in practice, generation of a pure population of induced neurons was not straightforward. The challenges present in this study mainly came from balancing between obtaining the desired effects from several chemical compounds used in the *NGN2* protocol and avoiding excessive toxic effects on cells. In order to not introduce technical variations on biological samples, hence to avoid false positive observations, the doses of all chemical compounds were kept the same for all lines. However, a dose that was tolerable to one line could be toxic to another. The layers of variations in the *NGN2* protocol included 1) the initial plating density of the cells, 2) the doses of viruses used for infection, 3) the re-plating density of infected cells prior to doxycycline induction, 4) the doses of doxycycline used for *NGN2* overexpression induction, 5) the doses of puromycin used to kill the cells that did not receive enough virus (non-converting cells) and 6) the doses of ara-c used to stop the proliferation of mouse primary glia and the non-converting cells. Although low plating density, high load of viruses or high doses of chemical compound could kill all iPSC lines, the optimal reaction ranges of each iPSC line on these 6 layers of variables turned out to be slightly different. This reflected the line-to-line variation problem of iPSC research, which describes the varying behaviours of iPSCs that did not come from a biologically meaningful basis. Another related problem is the variations caused by *in vitro* maintenance of cells. A recent paper that compared large numbers of iPSC-derived neurons, from which iPSCs were derived in different laboratories, showed that the top distinguishing factor on the transcriptomes of the iPSC-neurons was the laboratory in which the iPSCs were generated, instead of disease-status of the donor (e.g. Alzheimer's disease versus healthy) (Volpato et

al., 2018). To reduce the variations introduced by *in vitro* maintenance, all iPSC lines were thawed and experiments were conducted at the same time, except for virus tittering on iPSCs. Using the same amount of viruses for all lines was intended, as scaling the amount of viruses based on the initial plating densities of iPSCs resulted in excessive cell death for lines that required high plating densities (data not shown). To address the line-to-line variability on the virus infection and chemical treatments, future research should test each individual iPSC line before conducting cohort experiments. Alternatively, stable lines could be created, in which the doxycycline inducible overexpression constructs are inserted into safe harbours of the host iPSC genomes with gene editing technologies. The use of stable lines bypasses the problems of initial plating densities, virus infections and puromycin treatments, hence reducing the degrees of variables by a large extent.

As a summary, eliminating genomic abnormalities and obtaining differentiated cell types from iPSCs with minimal technical variations remains a major unsolved problem of the field. Although iPSCs have been widely used to study diseases owning to their ability to offer human-specific disease modelling, the field of cellular reprogramming is still relatively young and the available technologies are certainly still imperfect. Besides driving research to improve current methods of cellular reprogramming, the presence of these challenges also cautions researchers to take quality control measures when applying cellular reprogramming methods.

3.7.2 Biological meaning of the obtained data

Based on live imaging of the converting cells from 2 patient lines (002 and 007) and 2 control lines (011 and 014), there was no obvious differences, during elaboration of complex neuronal morphologies, that could distinguish the patient group from the control group. Although some line-to-line variations existed in the timing of spine-like protrusions to appear on primary neurites, the duration for the growth cones to be present at the end of the neurites and the degrees of complexities on terminal structures and around the neuronal soma. More lines will be needed to investigate whether these features are enriched in the patient group. Control line 014S-5 was derived from the control subject 014, who turned out to carry a CNV associated with schizophrenia (one of the 108 loci), regardless of being neurologically healthy. The risk of this individual, who was 15 years old when recruited, to developing psychosis in the future remains unknown. It was noticed that on day 19 both control lines showed neurons with complex primary protrusions at the soma, however this was not found for patient line 002S-9 and was very sparse for patient line 007S-21. On the contrary, another batch of *NGN2*-conversions showed on day 28, when co-cultured with primary mouse glia (which was the case for the live imaging), both the patient line 002S-9 and the control line 011S-16 showed complex neurite structures on the soma. Therefore, whether the results from the live imaging were one-time observations or reproducible phenotypes associated with patient 002, who carried missense variants in two important players at the PSD, *SYNGAP1* and *SHANK2*, remains to be validated. Neurite tracking on day 9 showed a significantly increased neurite length (denoted with purple lines on Figure 3.10) for 002S-9, compared to control line 011S-16. Neurite tracing was not possible after day 9 due to the complexities of neuronal networks in the cell cultures. Future experiments will need to re-plate small numbers of *NGN2-EGFP*

converted neurons with abundant *NGN2*-converted neurons (as being too sparse or overly crowed both could hamper neurite development) in order to clearly distinguish the corresponding soma for a neurite. Using machine learning based image analysis methods for neurite recognition (with the laboratory of Prof. Jens Rittscher, the Oxford Institute of Biomedical Engineering) was attempted but was very challenging. Images generated from sparsely plated *NGN2-EGFP*+ neurons with non-fluorescent *NGN2*+ neurons on the background should serve as a pool of good training data. Repeated experiments with all three iPSC lines from patient 002, together with more control lines were required to confirm the observation that converting neurons from patient 002 bear longer neurites. As a summary, current data suggested some trends of altered neurite development in patient-derived cells but significantly lacked power to draw a conclusion.

Neurite development is particular relevant to schizophrenia and is easier to access *in vitro* for disease mechanism studies and drug screening. As discussed in *Appendix*, many post-mortem studies of schizophrenia showed evidence to support the reduced neuropil hypothesis. Neurite development has long been known to be influence both by cell-intrinsic factors such as genes and cell-extrinsic factors such as growth factors. Altered neurite development is one of the possible cellular mechanisms that link genetic risks to reduced neuropil. For example, the two well-studied schizophrenia-associated genes: disrupted-in-schizophrenia 1 (*DISC1*) and neuregulin-1 (*NRG1*) were both associated with neurite development (Miyoshi et al., 2003). *DISC1* was shown to directly interact with the elongation protein zeta-1 (*FEZ1*), and indirectly with F-actin in the growth cones of developing neurons, and regulates axon outgrowth and fasciculation (Kamiya et al., 2005; Miyoshi et al., 2003; Ozeki et al., 2003). *DISC1* served as an interesting example of how the same genes could contribute to diverse

processes in neuronal development and functioning. Although its roles were not fully understood, it may be that its' associations with cytoskeleton dynamics enabled *DISC1* to affect neurite outgrowth, neurite fasciculation and synaptic transmission (Miyoshi et al., 2003). NRG1 protein is a cell adhesion molecule on axons and was also shown to directly promote neurite outgrowth by activating the Receptor Tyrosine-protein Kinase erbB (erbB) family receptors (Bermingham-McDonogh, McCabe, & Reh, 1996; Gamett et al., 1995). Interestingly, NRG1 also played a role in synaptic transmission and LTP via its interactions with the erbB family receptors (Kwon, Longart, Vullhorst, Hoffman, & Buonanno, 2005; Li, B., Woo, Mei, & Malinow, 2007).

It is unknown why evolution has made neurite outgrowth and synaptic transmission employ the same or similar molecules to some extent. Similarly, the Shank family proteins are canonically associated with the PSD, yet are also found abundantly present in growth cones (Du et al., 1998). Another PSD protein—Homer regulates the turning of growth cones by interacting with calcium signalling (Gasperini, Choi-Lundberg, Thompson, Mitchell, & Foa, 2009). Glutamate was known to regulate neurite development, the close associations of Shank and Homer with glutamate receptors hence made it plausible that neurons may apply similar mechanisms to process and to react with signals from glutamate during development and functioning. On a practical level, cellular model-based schizophrenia research often reports very fine phenotypes at electrophysiological levels. If earlier developmental processes would be affected by similar mechanisms that perturbed the normal electrophysiological functions of a neuron, the readouts for disease mechanism studies and for drug development would become more accessible and scalable.

3.7.3 Previous studies on schizophrenia using iPSCs

Previous studies on schizophrenia using iPSC-derived neurons as models converged on several themes (Table 3.10). First, reprogrammed neurons from patients showed reduced neurites, reduced neuronal connections and reduced functional synapses. The first iPSC study of schizophrenia, using 1 childhood-onset idiopathic case and 3 adult-onset familial cases, showed reduced neuronal connectivity based on rabies virus trans-neuronal tracing in immature neurons. They also found reduced primary neurite numbers and reduced expression levels of the *PSD-95* gene in patient derived neuronal cultures that contained mostly glutamatergic neurons but also some dopaminergic neurons. However, the electrophysiological properties of single mature neurons remained indistinguishable between patients and controls (Brennand et al., 2011). The normal electrophysiological properties assessed by patch-clamping suggested that post-synaptic function was not affected under their experimental settings. Therefore, the reduced rabies virus retrograde tracing in patient-derived neurons could result from deficits in presynaptic signals. Due to lack of knowledge of the exact mechanisms of rabies virus transmission between synapses, the conclusion that there was a deficiency in presynaptic signals for patient neurons remains indirect. It will be more conclusive to test the presynaptic functions of pure populations of patient-derived neurons. A subsequent paper using the same 4 patients reported reduced gene expression levels of *NEUROD1*, *PROX1* and *TBR1* in patient-derived dentate gyrus granule neuron progenitors, normal electrophysiological properties based on whole cell patch-clamp, reduced percentage of active neurons based on calcium imaging and reduced levels of spontaneous neurotransmitter release in mature patient-derived dentate gyrus granule neurons, when compared to their counterparts derived from controls (Yu et al., 2014). These

results suggested that deficits during hippocampal granule neuron development were already present at the neural progenitor cell (NPC) stage and these deficits led to reduced connectivity between neurons. As the patch-clamp recording showed normal action potentials of patient-derived granule neurons, it is again suggested that the presynaptic signals were deficient. Another study using iPSCs derived from patients from a family with a *DISC1* frameshift mutation showed that forebrain-specific glutamatergic neurons had reduced levels of functional glutamatergic synapses based on SV2 staining and deficient presynaptic neurotransmission based on electrophysiological recording and live imaging of synaptic vesicle release (Wen et al., 2014). Taken together, these results suggest that patients with different genetic backgrounds could show similar deficits in the development of glutamatergic neurons and hippocampal granule neurons. Interestingly, in the first paper, a reduced level of post-synaptic protein PSD-95 was coupled with a likely presynaptic signal deficit. It is known that post-synaptic proteins, especially PSD-95, can modulate the levels of presynaptic maturation and neurotransmitter release probability (El-Husseini, Schnell, Chetkovich, Nicoll, & Bredt, 2000; Futai et al., 2007; Kim, S. et al., 2006). Hence, it remains unknown if the observed presynaptic deficits could be a result from transient deficits in the development of post-synaptic terminals. Future research pairing the development of pre-synaptic neurons derived from patients with the development of post-synaptic neurons derived from healthy controls should be able to offer a clearer answer.

Second, reprogrammed neural cells from patients showed abnormal energy metabolism. Neural precursor cells isolated from neural rosettes that were differentiated from iPSCs derived from an adult-onset clozapine-resistant patient using RAs showed 2-fold higher extra-mitochondrial oxygen consumption levels and ROS levels (Paulsen et al., 2012). The elevated

levels of ROS in patient neural precursor cells could be reduced to the level of controls upon treatment with the mood stabiliser valproic acid. Such differences were not observed in iPSCs or fibroblasts, indicating that the disease mechanisms were selectively affecting neural precursor cells in this case and resulted in increased oxidative stress levels (Paulsen et al., 2012). However, it was unclear in this study what impact the increased oxidative stress levels had on neural precursor cells generating mature neurons. Another study that differentiated iPSCs derived from 3 related-patients with family histories of schizophrenia reported impaired abilities of patient iPSCs to differentiate into glutamatergic neurons and dopaminergic neurons when compared to control iPSCs. Reduced levels of synaptic proteins and glutamate turnover were observed in patient neural progenitor cells, however, this was not surprising as the neural differentiation was not successful for patient-iPSCs. The authors also found dissipation of mitochondrial membrane potentials, which indicated the activity of oxidative phosphorylation, and perturbations in mitochondria connectivity that resulted in an uneven distribution of mitochondria in patient cells along the differentiation process (Robicsek et al., 2013).

These results showed that under specific experimental settings, the three related-patients' reprogrammed glutamatergic progenitors were affected by impaired mitochondrial functions, and could not be differentiated fully to functional neurons. The *in vitro* differentiation procedures in this study may have revealed cell-intrinsic vulnerability of neural progenitor cells derived from this specific family, as the cells grown *in vitro* had lost support or compensation mechanisms that were available *in vivo*. Taken together, these 2 studies showed perturbed cellular processes that were related to the energy metabolism of neural progenitor cells. Although it is plausible that aberrant energy metabolism of progenitor cells

during neural development may result in neurons with reduced volume, a direct causal relationship still needs to be prooved with experiments that perturb energy metabolism of cells derived from healthy individuals in similar ways as observed in the patient-derived neural progenitor cells, and/or rescue experiments that alleviate the energy metabolism abnormalities in patient-derived cells. Dysregulated synaptic development in neurons and aberrant energy metabolism in neural progenitor cells are two examples of how research using patient-derived cells could elucidate cellular events that may contribute to the reduction of neuropil in patient brains.

Third, problems in cellular polarity and progenitor migration were also reported for patient-derived cells (Brennand et al., 2015; Lee et al., 2015; Stachowiak et al., 2017; Topol et al., 2016; Yoon et al., 2014). The mechanisms behind aberrant migration phenotypes were different; ranging from down regulation of microRNA expression levels (Topol et al., 2016) to dysregulated WAVE complex (Yoon et al., 2014). Although multiple studies suggest that neural progenitor cell migrations were dysregulated in schizophrenia, the exact mechanisms still remain unclear. Other findings on schizophrenia using iPSCs as model systems reported glia phenotypes, gene expression and microRNA expression dysregulations, WNT signalling defects, transposable elements insertion dysregulation, global protein synthesis upregulation and aberrant reactions to environmental disturbances (see details in Table 3.10). Given the high heterogeneity in genetic predisposition of schizophrenia and the current low-throughput of reprogramming technologies, these studies are likely to all reflect disease mechanisms in the subset of patients that they used. How these cellular phenotypes contribute to schizophrenia remains to be addressed in future studies

Table 3.10. Recent published studies on schizophrenia using iPSCs grouped according to major findings.

Group1: neurite development, synaptic maturation and neurotransmission

Year	Patients	Cell types	Major disease-phenotypes	Ref
2014	4 members from a family with frameshift DISC1	Forebrain neurons	Synaptic vesicle release deficits; Mutant DISC1 depletes wildtype DISC1 and dysregulates genes related to synapses and psychiatric disorders;	Wen et al., 2014
2014	1 childhood onset 3 familial	Hippocampal NPCs	Deficient in DG granule neuron generation from patient; Reduced neuronal activity; Reduced spontaneous neurotransmitter release;	Yu et al., 2014
2014	3 familial	neurons	Changes in catecholamine secretion; Increased percentage of TH-positive neurons	Hook et al., 2014
2011	1 childhood onset 3 familial	glutamatergic neurons	Reduced neuronal connectivity, neurite number, PSD-95 protein level, glutamate receptor expression; Altered gene expression in cAMP and WNT signalling pathways	Brennand et al., 2011

Group2: energy metabolism

Year	Patients	Types of cells	phenotypes	Reference
2015	4 adolescent patients	forebrain NPCs	Abnormal gene expression in cytoskeletal remodelling and oxidative stress; Aberrant migration and increased oxidative stress;	Brennand et al., 2015
2013	3 patient	dopaminergic neurons and glutamatergic neurons	Perturbations in neural differentiation and mitochondrial function	Robicsek et al., 2013
2012	1 patient (clozapine resistant)	neural precursor cells	2-fold increased O_2 consumption in SZ NPC compared to control NPC (no such effect in fibroblasts or iPSCs);	Paulsen et al., 2012

Group3: polarity & migration

Year	Patients	Types of cells	phenotypes	Reference
2017	3 patients (1 child-onset, 1 AOS, 1 adult-onset)	cerebral organoids	Lack of Tbr1+ and Reelin+ neurons in schizophrenia cortex in organoids; proliferating cells dispersed through intermediate zones and cortical plates in patient organoids; accumulation of neurons in subcortical regions.	Stachowiak et al., 2017
2016	1 childhood onset 3 familial; 10 childhood onset	NPCs	Downregulated miR-9 in a subset of SZ NPCs; miR-9 impacts neural migration;	Topol et al., 2016
2015	4 adolescent patients	forebrain NPCs	Abnormal gene expression in cytoskeletal remodelling and oxidative stress; Aberrant migration and increased oxidative stress;	Brennand et al., 2015
2015	2 patients with CNTNAP2 deletion	NPCs, neurons and OPCs	Reduced distance of NPC migration	Lee et al., 2015
2014	3 childhood onset with 15q11.2del	neural precursor cells	Disrupted apical polarity and adherens junction; Reduced WAVE complex expression;	Yoon et al., 2014

Group4: others

Year	Patients	Types of cells	phenotypes	Reference
2019	3 patients from the same family	forebrain NPCs and OPCs	OPCs from 3 patients that shared the same candidate variant in CSPG4 gene showed abnormal post-translational processing and subcellular locations of NG2 protein; reduced OPC viability and myelination potential for patients.	de Vrij et al., 2019
2018	4 patients	NPCs Ngn2 neurons	Increased $STEP_{61}$ protein level; (likely means reduced ubiquitination and degradation); inhibition of STEP prevents loss of NMDAR in mice	Xu et al., 2018
2017	5 juvenile onset patients	glial progenitor cells	Patient-derived glial progenitor cells gave rise to morphological aberrant astrocytes and hypomyelination	Windrem et al., 2017
2016	4 patients	neurons	Activity-dependent changes of gene expression between SZ and controls	Roussos et al., 2016
2016	2 patients with DISC1 mutation	NSC	Upregulation of miR-219; reduced of TLX expression; reduced cell proliferation;	Murai et al., 2016

2015	3 with 22q11del, 2 childhood onset	mixed population of glutamatergic neurons and GABAergic neurons	Different miRNA expression; Whose mRNA targets enrich for neurological disease and psychological disorders	Zhao, D. et al., 2015
2015	1 childhood onset 3 familial	forebrain NPCs	Increased total protein level; Increased ribosomal and translation initiation and elongation factor proteins	Topol et al., 2015a
2015	4 adolescent patients	forebrain NPCs	Altered WNT signalling in iPSC-NPC	Topol et al., 2015b
2014	22q11.2 deletion	neurons	Increased L1 retrotransposition insertion in SZ and synapse related genes; Increased L1 copy number after immune activation;	Bundo et al., 2014
2014	1 childhood onset 3 familial	NPC	NPCs are more susceptible to environmental disturbances than neurons; Higher heat-shock factor 1 level variability in patient iPSC-NPCs;	Hashimoto-Rorii et al., 2014

3.7.4 Suggestions for future research

In the present study, an attempt to model early developmental processes with *NGN2*-overexpression-driven induced neurons was made. Future research should validate the status of early converting neurons. Growth cones were observed in the conversion processes, however direct lineage conversions do not go through the classic developmental processes of a neuron (normal processes were summarised in Figure 1). It was unclear where exactly in the developmental processes did early converting neurons in the *NGN2* protocol enter. During normal development, obtaining a neuronal identity is orchestrated by numerous signals. It was believed that cellular reprogramming forced the recipient cells to upregulate key signals, which in turn caused waves of downstream signalling events and eventually shaped the genomes and epigenomes as the desired cell identity. Therefore, it is important to confirm the stages of development that the early converting neurons have entered in order to associate observed phenotypes with real human brain development.

Due to lack of power, the current study did not link the cellular features displayed by any line with the disease status. Future research should increase both the number of clones per individual and the numbers of individuals in order to discover disease-associated phenotypes. Correcting the *SYNGAP1* and *SHANK2* mutations in patient 002 with gene editing technologies would enable future research to discover gene-associated phenotypes. Combining the disease-associated phenotypes with the gene-associated phenotypes, future research would also be able to discover other 'hits' in the genome of the patient using gene inactivating/activating screening. Trio recruitment and genome sequencing should be done for patient 001 and patient 007 in order to dissect the genetic risk factors and to design

relevant experiments. As shown in table 3.10, previous studies using iPSCs to address schizophrenia found phenotypes related to glial cells. Isogenic microglia, astrocytes and oligodendrocytes should be derived from the iPSC lines and their interactions with isogenic neurons or non-isogenic neurons should be studied. Finally, due to the limits of time, neurons were not carried to a fully mature state. This was indicated by the lack of synapsin and SynGAP expression. Induced neurons should be cultured with glia for an extended period of time to allow full maturation. Patch-clamp or even calcium imaging experiments should be done to assess the electrophysiological properties of patient and control neurons. To study the pre-synaptic functions of neurons and their developmental dynamics, patient-derived induced neurons should be co-cultured with rodent neurons. Introducing opto-genetic actuators, which turn light signals to electrical signals on membranes, in human neurons, and opto-genetic sensors, which turn electrical signals on membranes into light signals in rodent neurons should be able to measure the dynamics of presynaptic signals released by human neurons.

GENERAL DISCUSSION

The aims of my study were to study phenotypic differences between AOS patients and control subjects, on cellular and molecular levels. Three types of patient-derived biomaterials were applied; blood samples for WES, for characterising the genetic candidate variants and for identifying patients to be included in the iPSC study; nasal biopsies for OE-MSCs, for discovering disease-relevant cellular and molecular signatures of schizophrenia; and finally skin biopsies for iPSCs, for modelling the neurodevelopmental processes. In *Chapters 1-3*, the genetic variants, the cellular behaviours and their possible molecular basis, and neurite development of induced neurons were discussed separately. This chapter aims to give an integrated discussion based on the key findings from each study.

The WES study resulted in the identification of rare variants that can be assigned to several functional groups, including the post-synaptic signalling pathways and the cell adhesion pathways. However, due to lack of power in this study, it is still hard to draw conclusion on any of the rare variants or genes identified. Nevertheless, the data can still be used to prioritise AOS patients who should be included in the iPSC study. From the WES analysis, genetic variants that fell into pathways directly associated with cytoskeleton and cell adhesion molecules were 006, 019, 025, 026 and 027, all of which were AOS patients. In the cell-to-substrate adhesion assay, OE-MSCs derived from 7 patients (002N, 003N, 004N, 005N, 009N, 015N and 019N) and 5 controls were compared for the numbers of cells that adhered to cell cultures plates coated with various coating materials. The lowest adhesion among all

patient cells and control cells came from patient line 019N on TC-treated plates without extra coating, which was consistent with that fact that genetic variants in adhesion molecules were found in this patient. Among all the patients included for the adhesion assay, patient 019 was the only one who carried a genetic variant in genes encoding cell adhesion molecules or cytoskeleton regulators. The identified variant in patient 019 was a heterozygous *de novo* mutation in the exon located in the 3 prime untranslated region (3'UTR) of Cadherin 11 (*CDH11*). Cadherin 11 is a cell adhesion molecule that was shown to co-localise with focal adhesions and facilitate cell-to-substrate adhesion (Langhe et al., 2016). The 3'UTR is a region downstream of the transcription termination codon and contains elements for the post-transcriptional regulation of mRNA (Mazumder, Seshadri, & Fox, 2003). The functional impacts of this 3' UTR variant remain to be investigated. Missense mutations in the 3'UTR of *MECP2* were found to be significantly enriched in ASD (Shibayama et al., 2004). A partial LoF of the gene was proposed (Amir et al., 1999). Therefore, it is plausible to hypothesize that genetic variants located in the 3'UTR of *CDH11* could reduce the expression level of *CDH11* and lead to partial LoF. This made patient 019 the next candidate to be reprogrammed and studied in detail.

Taking all the patients in the adhesion assay together, they all showed reduced cell-to-substrate adhesion when compared to controls, yet only one of them carried a WES-detectable genetic variant directly associated with cell adhesion. This suggests that reduced cell adhesion might be a common disease-associated phenotype, rather than a gene-associated phenotype. Whole protein expression profiling of OE-MSCs from 5 patients and 5 controls showed reduced global protein synthesis, downregulated mTOR activity and reduced cytoskeleton and adhesion molecules in patient cells. None of the patients included in this

experiment carried identified genetic variants in cytoskeleton regulation or adhesion molecules. This again suggested that the observed molecular changes might be disease-specific rather than gene-specific. It is possible that the reduced global protein synthesis also contributed to the reduced adhesion, as cell adhesion was achieved solely on the interactions of abundant adhesion proteins and cytoskeleton interactors. Therefore, a reduction in global protein synthesis in OE-MSCs may result in a reduced numbers of adhesion molecules which individually were minimal but which in aggregate contribute to the adhesion phenotypes. Highly similar cellular and molecular phenotypes were previously discovered from OE-MSCs derived from patients with adult-onset schizophrenia. This showed that reduced cell adhesion and reduced global protein synthesis may be shared cellular pathology of schizophrenia.

Combining results from the WES study and the OE-MSC study, a key question emerged: how could this shared dysregulation in cell adhesion and global protein synthesis raise from the diverse genetic predispositions that patients carry? For example, OE-MSCs from patient 002, who carried missense variants in *SYNGAP1* and *SHANK2*, showed the worst adhesion to laminin-coated plates among all cell lines. Both Syngap1 and Shank2 are associated with PSD assembly and signalling and interact with the actin cytoskeleton in dendritic spines (*Chapter 3*), but they have not been associated with cell adhesion. Hence it remains confusing how variants in *SYNGAP1* and *SHANK2* could possibly impair cell adhesion and protein synthesis. Experiments are now planned to use gene editing to correct these genetic variants and test their effects on adhesion. Furthermore, neurite tracing of *NGN2*-induced neurons showed 002S-9, an iPSC line derived from patient 002, had significantly longer neurites than a control line. Laminin was known to have a positive effect on neurite outgrowth by increasing the association between neurites and extracellular matrix, as well as activating cell surface

integrin receptors (Kiryushko, Berezin, & Bock, 2004). Therefore, it is unexpected that the isogenic OE-MSCs showed reduced cell adhesion to laminins while the induced neurons showed accelerated neurite development. Many interesting questions arise from these rather preliminary observations; Could a dysregulated mTOR pathway be responsible for both the reduced protein synthesis and the seemingly accelerated neurite development? Is global protein synthesis also dysregulated during the *in vitro* conversion of neurons? The current filed of using OE-MSCs to study schizophrenia remains small. Previous results and my results both suggested reduced cell adhesion and reduced global protein synthesis as common disease mechanisms. However, much future research still need to be done to dissect the pathways leading to these cellular and molecular phenotypes. The expression levels of genes in which candidate variants were identified should be determined so that one could know if the identified candidate variants contributed to the reduced cell adhesion and reduced global protein synthesis at all. Whole genome sequencing still needs to be done so that the impacts from variants in non-coding elements could be included. Most importantly, to date no one has compared to direct proteomes of OE-MSCs to any proteomes of neural lineages. It is critical to investigate how much of the proteins used in neurons or their progenitors would also be present in OE-MSCs. If OE-MSC proteome is missing the vast majority of proteins necessary for neurons or their progenitors, any data obtained using OE-MSCs should be questioned for their relevance to brain diseases. Current research in the Szele lab includes comparing the proteome of OE-MSCs to publically available databases of gene expression and proteomes in neural lineages.

The iPSC study remains incomplete and inconclusive. Previous studies on schizophrenia using iPSCs have identified cellular and molecular phenotypes associated with cell polarity, cell migration, energy metabolism, neurite development, synaptic maturation, gene expression regulation and microRNA expression regulation. My iPSC study attempted to address the neurite development and synaptic maturation using 3 patients and 3 controls. No conclusive disease-associated morphological differences during neurite development were observed. Induced neurons co-cultured with rodent glia were not synaptically mature. Much more future experiments were still needed for this part of the study; which at least includes 1) an optimal conversion method needs to be applied for all lines so that at least 3 clones per patient and at least 3 patients could be included to compare the dynamic process of neurite development and synaptic maturation, and 2) induced neurons need to be co-cultured with rodent glia for extended period of time for the maturation of synapses. Future directions also include combining cellular reprogramming with gene editing so that the candidate variants identified in patients could be corrected to wildtypes. In this way, it could be determined if the observed cellular phenotypes are truly caused by candidate variants identified in the patients. To finally validate the bona fide glutamatergic neuronal identity of the induced neurons, engraftment into development rodent brains should be done. The synaptic partners of induced neurons in *in vivo* environments should be investigated to verify the functions of the induced neurons. *In vivo* developmental environments also could be used to investigate the outcomes of pathological phenotypes that patient-derived induced neurons would lead to. In summary, the contribution of my iPSC study to the field of modelling schizophrenia with iPSCs still relies on more future experiments.

CONCLUSIONS

The aims of this study were to use OE-MSCs and induced neurons derived from patients with adolescent-onset schizophrenia, whose genetic variants were characterised with WES, to study disease-associated cellular phenotypes. WES revealed that each patient carried a different set of genetic variants. Several candidate *de novo* variants were identified. Candidate variants in 6 patients were associated with cell adhesion and cytoskeleton regulation, representing the most variant-enriched cellular process in this cohort. The cell proliferation, cell death and cell migration of OE-MSCs were not significantly different under normal culture conditions between patients and controls. This contrasted with the increased cell proliferation and cell migration found for OE-MSCs isolated from patients with adult-onset schizophrenia. Cell-to-substrate adhesion was significantly reduced for patient cells, consistent with the reduced adhesion from OE-MSCs from adult-onset cases. Whole protein expression profiling revealed the most significantly downregulated cellular process as EIF2 signalling, resulting in reduction of ribosomal proteins. Pathways related to cellular response to virus infection, metabolic regulation, focal adhesion and actin dynamics were also significantly downregulated in patient OE-MSCs. This is highly in line with previous findings from a proteomic study using adult-onset OE-MSCs. Together, these data suggest that reduced adhesion and downregulated global protein synthesis are common mechanisms behind adolescent-onset and adult-onset schizophrenia. The deficits in cytoskeleton regulation observed from patient OE-MSCs may manifest as impaired neural progenitor cell migration, axon pathfinding or synaptic development in patient brains. The reduced global protein synthesis may impact on critical mechanisms underlying normal neuron functions such as local synaptic protein synthesis for strengthening the synaptic connections. The

induced neurons from 2 patients and 2 controls did not show any obvious difference in the conversion processes. Due to the lack of power in this study, the observed feature cannot be associated with disease status. Future research should increase the power of the study by including more lines. In general, reduced cell adhesion and global protein synthesis in OE-MSCs are proposed as a general disease-associated cellular phenotype for schizophrenia.

REFERENCE

References

1000 Genomes Project Consortium. (2010). A map of human genome variation from population-scale sequencing. *Nature, 467*(7319), 1061.

1000 Genomes Project Consortium. (2012). An integrated map of genetic variation from 1,092 human genomes. *Nature, 491*(7422), 56.

Aceti, M., Creson, T. K., Vaissiere, T., Rojas, C., Huang, W., Wang, Y., . . . Rumbaugh, G. (2015). Syngap1 haploinsufficiency damages a postnatal critical period of pyramidal cell structural maturation linked to cortical circuit assembly. *Biological Psychiatry, 77*(9), 805-815.

Adesnik, H., Li, G., During, M. J., Pleasure, S. J., & Nicoll, R. A. (2008). NMDA receptors inhibit synapse unsilencing during brain development. *Proceedings of the National Academy of Sciences of the United States of America, 105*(14), 5597-5602. doi:10.1073/pnas.0800946105 [doi]

Ambasudhan, R., Talantova, M., Coleman, R., Yuan, X., Zhu, S., Lipton, S. A., & Ding, S. (2011). Direct reprogramming of adult human fibroblasts to functional neurons under defined conditions. *Cell Stem Cell, 9*(2), 113-118.

American Psychiatric Association. (2013). *Diagnostic and statistical manual of mental disorders (DSM-5®)* American Psychiatric Pub.

Amir, R. E., Van den Veyver, Ignatia B, Wan, M., Tran, C. Q., Francke, U., & Zoghbi, H. Y. (1999). Rett syndrome is caused by mutations in X-linked MECP2, encoding methyl-CpG-binding protein 2. *Nature Genetics, 23*(2), 185.

Auer, P. L., & Lettre, G. (2015). Rare variant association studies: Considerations, challenges and opportunities. *Genome Medicine, 7*(1), 16.

Barbeau, D., Liang, J. J., Robitalille, Y., Quirion, R., & Srivastava, L. K. (1995). Decreased expression of the embryonic form of the neural cell adhesion molecule in schizophrenic brains. *Proceedings of the National Academy of Sciences of the United States of America, 92*(7), 2785-2789.

Barria, A., & Malinow, R. (2005). NMDA receptor subunit composition controls synaptic plasticity by regulating binding to CaMKII. *Neuron, 48*(2), 289-301.

Bayés, À, Collins, M. O., Croning, M. D., van de Lagemaat, Louie N, Choudhary, J. S., & Grant, S. G. (2012). Comparative study of human and mouse postsynaptic proteomes finds high compositional conservation and abundance differences for key synaptic proteins. *PloS One, 7*(10), e46683.

Berkel, S., Marshall, C. R., Weiss, B., Howe, J., Roeth, R., Moog, U., . . . Pinto, D. (2010). Mutations in the SHANK2 synaptic scaffolding gene in autism spectrum disorder and mental retardation. *Nature Genetics, 42*(6), 489.

Bermingham-McDonogh, O., McCabe, K. L., & Reh, T. A. (1996). Effects of GGF/neuregulins on neuronal survival and neurite outgrowth correlate with erbB2/neu expression in developing rat retina. *Development (Cambridge, England), 122*(5), 1427-1438.

Berryer, M. H., Hamdan, F. F., Klitten, L. L., Møller, R. S., Carmant, L., Schwartzentruber, J., . . . Neugnot-Cerioli, M. (2013). Mutations in SYNGAP1 cause intellectual disability, autism, and a specific form of epilepsy by inducing haploinsufficiency. *Human Mutation, 34*(2), 385-394.

Bird, A. (2007). Perceptions of epigenetics. *Nature, 447*(7143), 396.

Blaser, H., Reichman-Fried, M., Castanon, I., Dumstrei, K., Marlow, F. L., Kawakami, K., . . . Raz, E. (2006). Migration of zebrafish primordial germ cells: A role for myosin contraction and cytoplasmic flow. *Developmental Cell, 11*(5), 613-627.

Boeckers, T. M., Kreutz, M. R., Winter, C., Zuschratter, W., Smalla, K. H., Sanmarti-Vila, L., . . . Gundelfinger, E. D. (1999). Proline-rich synapse-associated protein-1/cortactin binding protein 1 (ProSAP1/CortBP1) is a PDZ-domain protein highly enriched in the postsynaptic density. *The Journal of Neuroscience : The Official Journal of the Society for Neuroscience, 19*(15), 6506-6518.

Bowling, H., & Santini, E. (2016). Unlocking the molecular mechanisms of antipsychotics–a new frontier for discovery. *Swiss Med Wkly, 146*, w14314.

Bramham, C. R. (2008). Local protein synthesis, actin dynamics, and LTP consolidation. *Current Opinion in Neurobiology, 18*(5), 524-531.

Brennand, K. J., Simone, A., Jou, J., Gelboin-Burkhart, C., Tran, N., Sangar, S., . . . Yu, D. (2011). Modelling schizophrenia using human induced pluripotent stem cells. *Nature, 473*(7346), 221.

Brennand, K., Savas, J. N., Kim, Y., Tran, N., Simone, A., Hashimoto-Torii, K., . . . Ladran, I. (2015). Phenotypic differences in hiPSC NPCs derived from patients with schizophrenia. *Molecular Psychiatry, 20*(3), 361.

Brown, A. S. (2012). Epidemiologic studies of exposure to prenatal infection and risk of schizophrenia and autism. *Developmental Neurobiology, 72*(10), 1272-1276.

Bundo, M., Toyoshima, M., Okada, Y., Akamatsu, W., Ueda, J., Nemoto-Miyauchi, T., . . . Kakita, A. (2014). Increased l1 retrotransposition in the neuronal genome in schizophrenia. *Neuron, 81*(2), 306-313.

Catts, V. S., Catts, S. V., McGrath, J. J., Féron, F., McLean, D., Coulson, E. J., & Lutze-Mann, L. H. (2006). Apoptosis and schizophrenia: A pilot study based on dermal fibroblast cell lines. *Schizophrenia Research, 84*(1), 20-28.

Chambers, S. M., Fasano, C. A., Papapetrou, E. P., Tomishima, M., Sadelain, M., & Studer, L. (2009). Highly efficient neural conversion of human ES and iPS cells by dual inhibition of SMAD signaling. *Nature Biotechnology, 27*(3), 275.

Charras, G., & Paluch, E. (2008). Blebs lead the way: How to migrate without lamellipodia. *Nature Reviews Molecular Cell Biology, 9*(9), 730.

Chen, H., Rojas-Soto, M., Oguni, A., & Kennedy, M. B. (1998). A synaptic ras-GTPase activating protein (p135 SynGAP) inhibited by CaM kinase II. *Neuron, 20*(5), 895-904.

Chen, X., Fang, H., & Schwob, J. E. (2004). Multipotency of purified, transplanted globose basal cells in olfactory epithelium. *Journal of Comparative Neurology, 469*(4), 457-474.

Cheng, A., Krueger, B. K., & Bambrick, L. L. (1999). MAP5 expression in proliferating neuroblasts. *Developmental Brain Research, 113*(1-2), 107-113.

Cohen, R. S., Blomberg, F., Berzins, K., & Siekevitz, P. (1977). The structure of postsynaptic densities isolated from dog cerebral cortex. I. overall morphology and protein composition. *The Journal of Cell Biology, 74*(1), 181-203.

Conrad, D. F., Pinto, D., Redon, R., Feuk, L., Gokcumen, O., Zhang, Y., . . . Campbell, P. (2010). Origins and functional impact of copy number variation in the human genome. *Nature, 464*(7289), 704.

Cook, A. L., Vitale, A. M., Ravishankar, S., Matigian, N., Sutherland, G. T., Shan, J., . . . Mellick, G. D. (2011). NRF2 activation restores disease related metabolic deficiencies in olfactory neurosphere-derived cells from patients with sporadic parkinson's disease. *PloS One, 6*(7), e21907.

Curtis, D., Coelewij, L., Liu, S., Humphrey, J., & Mott, R. (2018). Weighted burden analysis of exome-sequenced case-control sample implicates synaptic genes in schizophrenia aetiology. *Behavior Genetics, 48*(3), 198-208.

Dahoun, T., Trossbach, S. V., Brandon, N. J., Korth, C., & Howes, O. D. (2017). The impact of disrupted-in-schizophrenia 1 (DISC1) on the dopaminergic system: A systematic review. *Translational Psychiatry, 7*(1), e1015.

Danjo, T., Eiraku, M., Muguruma, K., Watanabe, K., Kawada, M., Yanagawa, Y., . . . Sasai, Y. (2011). Subregional specification of embryonic stem cell-derived ventral telencephalic tissues by timed and combinatory treatment with extrinsic signals. *The Journal of*

Neuroscience : The Official Journal of the Society for Neuroscience, 31(5), 1919-1933. doi:10.1523/JNEUROSCI.5128-10.2011 [doi]

Davis, J., Eyre, H., Jacka, F. N., Dodd, S., Dean, O., McEwen, S., . . . Amminger, P. (2016). A review of vulnerability and risks for schizophrenia: Beyond the two hit hypothesis. *Neuroscience & Biobehavioral Reviews, 65*, 185-194.

de Vrij, F. M., Bouwkamp, C. G., Gunhanlar, N., Shpak, G., Lendemeijer, B., Baghdadi, M., . . . Quadri, M. (2019). Candidate CSPG4 mutations and induced pluripotent stem cell modeling implicate oligodendrocyte progenitor cell dysfunction in familial schizophrenia. *Molecular Psychiatry, 24*(5), 757.

Deciphering Developmental Disorders Study. (2017). Prevalence and architecture of de novo mutations in developmental disorders. *Nature, 542*(7642), 433-438. doi:10.1038/nature21062 [doi]

Delorme, B., Nivet, E., Gaillard, J., Häupl, T., Ringe, J., Devèze, A., . . . Roman, F. S. (2009). The human nose harbors a niche of olfactory ectomesenchymal stem cells displaying neurogenic and osteogenic properties. *Stem Cells and Development, 19*(6), 853-866.

Dent, E. W., & Gertler, F. B. (2003). Cytoskeletal dynamics and transport in growth cone motility and axon guidance. *Neuron, 40*(2), 209-227.

Di Cristo, G., Berardi, N., Cancedda, L., Pizzorusso, T., Putignano, E., Ratto, G. M., & Maffei, L. (2001). Requirement of ERK activation for visual cortical plasticity. *Science (New York, N.Y.), 292*(5525), 2337-2340. doi:10.1126/science.1059075 [doi]

Donnelly, N., Gorman, A. M., Gupta, S., & Samali, A. (2013). The eIF2α kinases: Their structures and functions. *Cellular and Molecular Life Sciences, 70*(19), 3493-3511.

Drake, R. E., & Cotton, P. G. (1986). Depression, hopelessness and suicide in chronic schizophrenia. *The British Journal of Psychiatry, 148*(5), 554-559.

Du, Y., Weed, S. A., Xiong, W. C., Marshall, T. D., & Parsons, J. T. (1998). Identification of a novel cortactin SH3 domain-binding protein and its localization to growth cones of cultured neurons. *Molecular and Cellular Biology, 18*(10), 5838-5851.

Eiraku, M., Watanabe, K., Matsuo-Takasaki, M., Kawada, M., Yonemura, S., Matsumura, M., . . . Sasai, Y. (2008). Self-organized formation of polarized cortical tissues from ESCs and its active manipulation by extrinsic signals. *Cell Stem Cell, 3*(5), 519-532.

El-Husseini, A. E., Schnell, E., Chetkovich, D. M., Nicoll, R. A., & Bredt, D. S. (2000). PSD-95 involvement in maturation of excitatory synapses. *Science (New York, N.Y.), 290*(5495), 1364-1368. doi:9001 [pii]

Elkabetz, Y., Panagiotakos, G., Al Shamy, G., Socci, N. D., Tabar, V., & Studer, L. (2008). Human ES cell-derived neural rosettes reveal a functionally distinct early neural stem cell stage. *Genes & Development, 22*(2), 152-165. doi:10.1101/gad.1616208 [doi]

Emiliani, F. E., Sedlak, T. W., & Sawa, A. (2014). Oxidative stress and schizophrenia: Recent breakthroughs from an old story. *Current Opinion in Psychiatry, 27*(3), 185-190. doi:10.1097/YCO.0000000000000054 [doi]

English, J. A., Fan, Y., Föcking, M., Lopez, L. M., Hryniewiecka, M., Wynne, K., . . . Mackay-Sim, A. (2015). Reduced protein synthesis in schizophrenia patient-derived olfactory cells. *Translational Psychiatry, 5*(10), e663.

Etherton, M. R., Blaiss, C. A., Powell, C. M., & Südhof, T. C. (2009). Mouse neurexin-1α deletion causes correlated electrophysiological and behavioral changes consistent with cognitive impairments. *Proceedings of the National Academy of Sciences, 106*(42), 17998-18003.

Fan, Y., Abrahamsen, G., McGrath, J. J., & Mackay-Sim, A. (2012). Altered cell cycle dynamics in schizophrenia. *Biological Psychiatry, 71*(2), 129-135.

Fan, Y., Abrahamsen, G., Mills, R., Calderon, C. C., Tee, J. Y., Leyton, L., . . . Mackay-Sim, A. (2013). Focal adhesion dynamics are altered in schizophrenia. *Biological Psychiatry, 74*(6), 418-426.

Feron, F., Perry, C., Hirning, M. H., McGrath, J., & Mackay-Sim, A. (1999). Altered adhesion, proliferation and death in neural cultures from adults with schizophrenia. *Schizophrenia Research, 40*(3), 211-218.

Féron, F., Perry, C., McGrath, J. J., & Mackay-Sim, A. (1998). New techniques for biopsy and culture of human olfactory epithelial neurons. *Archives of Otolaryngology–Head & Neck Surgery, 124*(8), 861-866.

Fromer, M., Pocklington, A. J., Kavanagh, D. H., Williams, H. J., Dwyer, S., Gormley, P., . . . Ruderfer, D. M. (2014). De novo mutations in schizophrenia implicate synaptic networks. *Nature, 506*(7487), 179.

Futai, K., Kim, M. J., Hashikawa, T., Scheiffele, P., Sheng, M., & Hayashi, Y. (2007). Retrograde modulation of presynaptic release probability through signaling mediated by PSD-95–neuroligin. *Nature Neuroscience, 10*(2), 186.

Gamett, D. C., Greene, T., Wagreich, A. R., Kim, H. H., Koland, J. G., & Cerione, R. A. (1995). Heregulin-stimulated signaling in rat pheochromocytoma cells. evidence for ErbB3 interactions with neu/ErbB2 and p85. *The Journal of Biological Chemistry, 270*(32), 19022-19027.

Gasperini, R., Choi-Lundberg, D., Thompson, M. J., Mitchell, C. B., & Foa, L. (2009). Homer regulates calcium signalling in growth cone turning. *Neural Development, 4*(1), 29.

Geiger, B., Spatz, J. P., & Bershadsky, A. D. (2009). Environmental sensing through focal adhesions. *Nature Reviews Molecular Cell Biology, 10*(1), 21.

Genovese, G., Fromer, M., Stahl, E. A., Ruderfer, D. M., Chambert, K., Landén, M., . . . Sullivan, P. F. (2016). Increased burden of ultra-rare protein-altering variants among 4,877 individuals with schizophrenia. *Nature Neuroscience, 19*(11), 1433.

Ghanbari, H. A., Ghanbari, K., Harris, P. L., Jones, P. K., Kubat, Z., Castellani, R. J., . . . Perry, G. (2004). Oxidative damage in cultured human olfactory neurons from alzheimer's disease patients. *Aging Cell, 3*(1), 41-44.

Gilmore, J. H., Kang, C., Evans, D. D., Wolfe, H. M., Smith, J. K., Lieberman, J. A., . . . Gerig, G. (2010). Prenatal and neonatal brain structure and white matter maturation in children at high risk for schizophrenia. *American Journal of Psychiatry, 167*(9), 1083-1091.

Gilmore, J. H., Schmitt, J. E., Knickmeyer, R. C., Smith, J. K., Lin, W., Styner, M., . . . Neale, M. C. (2010). Genetic and environmental contributions to neonatal brain structure: A twin study. *Human Brain Mapping, 31*(8), 1174-1182.

Girard, S. D., Deveze, A., Nivet, E., Gepner, B., Roman, F. S., & Feron, F. (2011). Isolating nasal olfactory stem cells from rodents or humans. *Journal of Visualized Experiments : JoVE, (54). pii: 2762. doi*(54), 10.3791/2762. doi:10.3791/2762 [doi]

Glantz, L. A., Gilmore, J. H., Lieberman, J. A., & Jarskog, L. F. (2006). Apoptotic mechanisms and the synaptic pathology of schizophrenia. *Schizophrenia Research, 81*(1), 47-63.

Gobert, D., Topolnik, L., Azzi, M., Huang, L., Badeaux, F., DesGroseillers, L., . . . Lacaille, J. (2008). Forskolin induction of late-LTP and up-regulation of 5′ TOP mRNAs translation via mTOR, ERK, and PI3K in hippocampal pyramidal cells. *Journal of Neurochemistry, 106*(3), 1160-1174.

Gogtay, N., Greenstein, D., Lenane, M., Clasen, L., Sharp, W., Gochman, P., . . . Rapoport, J. (2007). Cortical brain development in nonpsychotic siblings of patients with childhood-onset schizophrenia. *Archives of General Psychiatry, 64*(7), 772-780.

Gogtay, N., Lu, A., Leow, A. D., Klunder, A. D., Lee, A. D., Chavez, A., . . . Rapoport, J. L. (2008). Three-dimensional brain growth abnormalities in childhood-onset schizophrenia visualized by using tensor-based morphometry. *Proceedings of the National Academy of Sciences,*

Gogtay, N., Vyas, N. S., Testa, R., Wood, S. J., & Pantelis, C. (2011). Age of onset of schizophrenia: Perspectives from structural neuroimaging studies. *Schizophrenia Bulletin, 37*(3), 504-513.

Gorris, R., Fischer, J., Erwes, K. L., Kesavan, J., Peterson, D. A., Alexander, M., . . . Karus, M. (2015). Pluripotent stem cell-derived radial glia-like cells as stable intermediate for efficient generation of human oligodendrocytes. *Glia, 63*(12), 2152-2167.

Gray, J. A., Shi, Y., Usui, H., During, M. J., Sakimura, K., & Nicoll, R. A. (2011). Distinct modes of AMPA receptor suppression at developing synapses by GluN2A and GluN2B: Single-cell NMDA receptor subunit deletion in vivo. *Neuron, 71*(6), 1085-1101.

Grayton, H. M., Missler, M., Collier, D. A., & Fernandes, C. (2013). Altered social behaviours in neurexin 1α knockout mice resemble core symptoms in neurodevelopmental disorders. *PloS One, 8*(6), e67114.

Greenstein, D., Lerch, J., Shaw, P., Clasen, L., Giedd, J., Gochman, P., . . . Gogtay, N. (2006). Childhood onset schizophrenia: Cortical brain abnormalities as young adults. *Journal of Child Psychology and Psychiatry, 47*(10), 1003-1012.

Guo, X., Hamilton, P. J., Reish, N. J., Sweatt, J. D., Miller, C. A., & Rumbaugh, G. (2009). Reduced expression of the NMDA receptor-interacting protein SynGAP causes behavioral abnormalities that model symptoms of schizophrenia. *Neuropsychopharmacology, 34*(7), 1659.

GURDON, J. B. (1962). The developmental capacity of nuclei taken from intestinal epithelium cells of feeding tadpoles. *Journal of Embryology and Experimental Morphology, 10*, 622-640.

Halim, N. D., Weickert, C. S., McClintock, B. W., Weinberger, D. R., & Lipska, B. K. (2004). Effects of chronic haloperidol and clozapine treatment on neurogenesis in the adult rat hippocampus. *Neuropsychopharmacology, 29*(6), 1063.

Hall, B. J., & Ghosh, A. (2008). Regulation of AMPA receptor recruitment at developing synapses. *Trends in Neurosciences, 31*(2), 82-89.

Hall, J., Trent, S., Thomas, K. L., O'Donovan, M. C., & Owen, M. J. (2015). Genetic risk for schizophrenia: Convergence on synaptic pathways involved in plasticity. *Biological Psychiatry, 77*(1), 52-58.

Hao, Y., Yan, Q., Liu, H., Xu, L., Xue, Z., Song, X., . . . Shan, B. (2009). Schizophrenia patients and their healthy siblings share disruption of white matter integrity in the left prefrontal cortex and the hippocampus but not the anterior cingulate cortex. *Schizophrenia Research, 114*(1-3), 128-135.

Harris, K. M., & Weinberg, R. J. (2012). Ultrastructure of synapses in the mammalian brain. *Cold Spring Harbor Perspectives in Biology, 4*(5), 10.1101/cshperspect.a005587. doi:10.1101/cshperspect.a005587 [doi]

Hashimoto-Torii, K., Torii, M., Fujimoto, M., Nakai, A., El Fatimy, R., Mezger, V., . . . Brennand, K. J. (2014). Roles of heat shock factor 1 in neuronal response to fetal environmental risks and its relevance to brain disorders. *Neuron, 82*(3), 560-572.

Hatzikotoulas, K., Gilly, A., & Zeggini, E. (2014). Using population isolates in genetic association studies. *Briefings in Functional Genomics, 13*(5), 371-377.

Hoischen, A., Krumm, N., & Eichler, E. E. (2014). Prioritization of neurodevelopmental disease genes by discovery of new mutations. *Nature Neuroscience, 17*(6), 764.

Hook, V., Brennand, K. J., Kim, Y., Toneff, T., Funkelstein, L., Lee, K. C., . . . Gage, F. H. (2014). Human iPSC neurons display activity-dependent neurotransmitter secretion: Aberrant catecholamine levels in schizophrenia neurons. *Stem Cell Reports, 3*(4), 531-538.

Hoptman, M. J., Nierenberg, J., Bertisch, H. C., Catalano, D., Ardekani, B. A., Branch, C. A., & DeLisi, L. E. (2008). A DTI study of white matter microstructure in individuals at high genetic risk for schizophrenia. *Schizophrenia Research, 106*(2-3), 115-124.

Iafrate, A. J., Feuk, L., Rivera, M. N., Listewnik, M. L., Donahoe, P. K., Qi, Y., . . . Lee, C. (2004). Detection of large-scale variation in the human genome. *Nature Genetics, 36*(9), 949.

Inbal, B., Bialik, S., Sabanay, I., Shani, G., & Kimchi, A. (2002). DAP kinase and DRP-1 mediate membrane blebbing and the formation of autophagic vesicles during programmed cell death. *The Journal of Cell Biology, 157*(3), 455-468. doi:10.1083/jcb.200109094 [doi]

International Schizophrenia Consortium. (2009). Common polygenic variation contributes to risk of schizophrenia and bipolar disorder. *Nature, 460*(7256), 748.

Ishizuka, K., Paek, M., Kamiya, A., & Sawa, A. (2006). A review of disrupted-in-schizophrenia-1 (DISC1): Neurodevelopment, cognition, and mental conditions. *Biological Psychiatry, 59*(12), 1189-1197.

Jackson, R. J., Hellen, C. U., & Pestova, T. V. (2010). The mechanism of eukaryotic translation initiation and principles of its regulation. *Nature Reviews Molecular Cell Biology, 11*(2), 113.

Jarskog, L. F., Selinger, E. S., Lieberman, J. A., & Gilmore, J. H. (2004). Apoptotic proteins in the temporal cortex in schizophrenia: High bax/bcl-2 ratio without caspase-3 activation. *American Journal of Psychiatry, 161*(1), 109-115.

Jiang, J., Lv, W., Ye, X., Wang, L., Zhang, M., Yang, H., . . . Liu, L. (2013). Zscan4 promotes genomic stability during reprogramming and dramatically improves the quality of iPS cells as demonstrated by tetraploid complementation. *Cell Research, 23*(1), 92.

Johnson, G. S., Basaric-Keys, J., Ghanbari, H. A., Lebovics, R. S., Lesch, K. P., Merril, C. R., . . . Wolozin, B. (1994). Protein alterations in olfactory neuroblasts from alzheimer donors. *Neurobiology of Aging, 15*(6), 675-680.

Kalaany, N. Y., & Mangelsdorf, D. J. (2006). LXRS and FXR: The yin and yang of cholesterol and fat metabolism. *Annu.Rev.Physiol., 68*, 159-191.

Kamiya, A., Kubo, K., Tomoda, T., Takaki, M., Youn, R., Ozeki, Y., . . . Okawa, M. (2005). A schizophrenia-associated mutation of DISC1 perturbs cerebral cortex development. *Nature Cell Biology, 7*(12), 1167.

Kaufman, J., Birmaher, B., Brent, D., Rao, U., Flynn, C., Moreci, P., . . . Ryan, N. (1997). Schedule for affective disorders and schizophrenia for school-age children-present and lifetime version (K-SADS-PL): Initial reliability and validity data. *Journal of the American Academy of Child & Adolescent Psychiatry, 36*(7), 980-988.

Kawamura, T., Suzuki, J., Wang, Y. V., Menendez, S., Morera, L. B., Raya, A., . . . Belmonte, J. C. I. (2009). Linking the p53 tumour suppressor pathway to somatic cell reprogramming. *Nature, 460*(7259), 1140.

Kay, S. R., Flszbein, A., & Opfer, L. A. (1987). The positive and negative syndrome scale (PANSS) for schizophrenia. *Schizophrenia Bulletin, 13*(2), 261.

Khalili, A. A., & Ahmad, M. R. (2015). A review of cell adhesion studies for biomedical and biological applications. *International Journal of Molecular Sciences, 16*(8), 18149-18184.

Kiebler, M. A., & DesGroseillers, L. (2000). Molecular insights into mRNA transport and local translation in the mammalian nervous system. *Neuron, 25*(1), 19-28. doi:S0896-6273(00)80868-5 [pii]

Kilens, S., Meistermann, D., Moreno, D., Chariau, C., Gaignerie, A., Reignier, A., . . . Nedellec, S. (2018). Parallel derivation of isogenic human primed and naive induced pluripotent stem cells. *Nature Communications, 9*(1), 360.

Kilinc, M., Creson, T., Rojas, C., Aceti, M., Ellegood, J., Vaissiere, T., . . . Rumbaugh, G. (2018). Species-conserved SYNGAP1 phenotypes associated with neurodevelopmental disorders. *Molecular and Cellular Neuroscience,*

Kim, E., & Sheng, M. (2009). The postsynaptic density. *Current Biology : CB, 19*(17), 723. doi:10.1016/j.cub.2009.07.047 [doi]

Kim, J. H., Liao, D., Lau, L., & Huganir, R. L. (1998). SynGAP: A synaptic RasGAP that associates with the PSD-95/SAP90 protein family. *Neuron, 20*(4), 683-691.

Kim, S., Burette, A., Chung, H. S., Kwon, S., Woo, J., Lee, H. W., . . . Kim, E. (2006). NGL family PSD-95–interacting adhesion molecules regulate excitatory synapse formation. *Nature Neuroscience, 9*(10), 1294.

Kirov, G., Gumus, D., Chen, W., Norton, N., Georgieva, L., Sari, M., . . . Ropers, H. (2007). Comparative genome hybridization suggests a role for NRXN1 and APBA2 in schizophrenia. *Human Molecular Genetics, 17*(3), 458-465.

Kirov, G., Pocklington, A. J., Holmans, P., Ivanov, D., Ikeda, M., Ruderfer, D., . . . Georgieva, L. (2012). De novo CNV analysis implicates specific abnormalities of postsynaptic signalling complexes in the pathogenesis of schizophrenia. *Molecular Psychiatry, 17*(2), 142.

Kirov, G., Rujescu, D., Ingason, A., Collier, D. A., O'donovan, M. C., & Owen, M. J. (2009). Neurexin 1 (NRXN1) deletions in schizophrenia. *Schizophrenia Bulletin, 35*(5), 851.

Kiryushko, D., Berezin, V., & Bock, E. (2004). Regulators of neurite outgrowth: Role of cell adhesion molecules. *Annals of the New York Academy of Sciences, 1014*(1), 140-154.

Kodama, M., Fujioka, T., & Duman, R. S. (2004). Chronic olanzapine or fluoxetine administration increases cell proliferation in hippocampus and prefrontal cortex of adult rat. *Biological Psychiatry, 56*(8), 570-580.

Komiyama, N. H., Watabe, A. M., Carlisle, H. J., Porter, K., Charlesworth, P., Monti, J., . . . Grant, S. G. (2002). SynGAP regulates ERK/MAPK signaling, synaptic plasticity, and learning in the complex with postsynaptic density 95 and NMDA receptor. *The Journal*

of Neuroscience : The Official Journal of the Society for Neuroscience, 22(22), 9721-9732. doi:22/22/9721 [pii]

Kosmicki, J. A., Samocha, K. E., Howrigan, D. P., Sanders, S. J., Slowikowski, K., Lek, M., . . . Roeder, K. (2017). Refining the role of de novo protein-truncating variants in neurodevelopmental disorders by using population reference samples. *Nature Genetics, 49*(4), 504.

Krapivinsky, G., Medina, I., Krapivinsky, L., Gapon, S., & Clapham, D. E. (2004). SynGAP-MUPP1-CaMKII synaptic complexes regulate p38 MAP kinase activity and NMDA receptor-dependent synaptic AMPA receptor potentiation. *Neuron, 43*(4), 563-574.

Kryukov, G. V., Shpunt, A., Stamatoyannopoulos, J. A., & Sunyaev, S. R. (2009). Power of deep, all-exon resequencing for discovery of human trait genes. *Proceedings of the National Academy of Sciences of the United States of America, 106*(10), 3871-3876. doi:10.1073/pnas.0812824106 [doi]

Kumar, R. A. (2010). SHANK2 redemption: Another synaptic protein for mental retardation and autism. *Clinical Genetics, 78*(6), 519-521.

Kwon, O. B., Longart, M., Vullhorst, D., Hoffman, D. A., & Buonanno, A. (2005). Neuregulin-1 reverses long-term potentiation at CA1 hippocampal synapses. *The Journal of Neuroscience : The Official Journal of the Society for Neuroscience, 25*(41), 9378-9383. doi:25/41/9378 [pii]

Lambert, G., Amar, M. J., Guo, G., Brewer, H. B.,Jr, Gonzalez, F. J., & Sinal, C. J. (2003). The farnesoid X-receptor is an essential regulator of cholesterol homeostasis. *The Journal of Biological Chemistry, 278*(4), 2563-2570. doi:10.1074/jbc.M209525200 [doi]

Langhe, R. P., Gudzenko, T., Bachmann, M., Becker, S. F., Gonnermann, C., Winter, C., . . . Franz, C. M. (2016). Cadherin-11 localizes to focal adhesions and promotes cell–substrate adhesion. *Nature Communications, 7*, 10909.

Langridge, P. D., & Kay, R. R. (2006). Blebbing of dictyostelium cells in response to chemoattractant. *Experimental Cell Research, 312*(11), 2009-2017.

Leblond, C. S., Heinrich, J., Delorme, R., Proepper, C., Betancur, C., Huguet, G., . . . Rastam, M. (2012). Genetic and functional analyses of SHANK2 mutations suggest a multiple hit model of autism spectrum disorders. *PLoS Genetics, 8*(2), e1002521.

Lee, I. S., Carvalho, C. M., Douvaras, P., Ho, S., Hartley, B. J., Zuccherato, L. W., . . . Malhotra, D. (2015). Characterization of molecular and cellular phenotypes associated with a heterozygous CNTNAP2 deletion using patient-derived hiPSC neural cells. *NPJ Schizophrenia, 1*, 15019.

Lendahl, U., Zimmerman, L. B., & McKay, R. D. (1990). CNS stem cells express a new class of intermediate filament protein. *Cell, 60*(4), 585-595.

Leonenko, G., Richards, A. L., Walters, J. T., Pocklington, A., Chambert, K., Al Eissa, M. M., . . . Bass, N. J. (2017). Mutation intolerant genes and targets of FMRP are enriched for nonsynonymous alleles in schizophrenia. *American Journal of Medical Genetics Part B: Neuropsychiatric Genetics, 174*(7), 724-731.

Leucht, S., Samara, M., Heres, S., Patel, M. X., Furukawa, T., Cipriani, A., . . . Davis, J. M. (2015). Dose equivalents for second-generation antipsychotic drugs: The classical mean dose method. *Schizophrenia Bulletin, 41*(6), 1397-1402. doi:10.1093/schbul/sbv037 [doi]

Leung, C. T., Coulombe, P. A., & Reed, R. R. (2007). Contribution of olfactory neural stem cells to tissue maintenance and regeneration. *Nature Neuroscience, 10*(6), 720-726.

Levinson, D. F., Duan, J., Oh, S., Wang, K., Sanders, A. R., Shi, J., . . . Amin, F. (2011). Copy number variants in schizophrenia: Confirmation of five previous findings and new evidence for 3q29 microdeletions and VIPR2 duplications. *American Journal of Psychiatry, 168*(3), 302-316.

Li, B., Woo, R., Mei, L., & Malinow, R. (2007). The neuregulin-1 receptor erbB4 controls glutamatergic synapse maturation and plasticity. *Neuron, 54*(4), 583-597.

Li, D., Lewinger, J. P., Gauderman, W. J., Murcray, C. E., & Conti, D. (2011). Using extreme phenotype sampling to identify the rare causal variants of quantitative traits in association studies. *Genetic Epidemiology, 35*(8), 790-799.

Li, J., Zhang, W., Yang, H., Howrigan, D. P., Wilkinson, B., Souaiaia, T., . . . Tudor, J. C. (2017). Spatiotemporal profile of postsynaptic interactomes integrates components of complex brain disorders. *Nature Neuroscience, 20*(8), 1150.

Lim, S., Naisbitt, S., Yoon, J., Hwang, J., Suh, P., Sheng, M., & Kim, E. (1999). Characterization of the shank family of synaptic proteins multiple genes, alternative splicing, and

differential expression in brain and development. *Journal of Biological Chemistry, 274*(41), 29510-29518.

Loh, P., Bhatia, G., Gusev, A., Finucane, H. K., Bulik-Sullivan, B. K., Pollack, S. J., . . . Kendler, K. S. (2015). Contrasting genetic architectures of schizophrenia and other complex diseases using fast variance-components analysis. *Nature Genetics, 47*(12), 1385.

Lynch, G., Rex, C. S., & Gall, C. M. (2007). LTP consolidation: Substrates, explanatory power, and functional significance. *Neuropharmacology, 52*(1), 12-23.

Mackay-Sim, A., & Kittel, P. (1991). Cell dynamics in the adult mouse olfactory epithelium: A quantitative autoradiographic study. *The Journal of Neuroscience : The Official Journal of the Society for Neuroscience, 11*(4), 979-984.

Mahadik, S. P., Mukherjee, S., Wakade, C. G., Laev, H., Reddy, R. R., & Schnur, D. B. (1994). Decreased adhesiveness and altered cellular distribution of fibronectin in fibroblasts from schizophrenic patients. *Psychiatry Research, 53*(1), 87-97. doi:0165-1781(94)90097-3 [pii]

Maher, B. (2008). Personal genomes: The case of the missing heritability. *Nature News, 456*(7218), 18-21.

Manolio, T. A., Collins, F. S., Cox, N. J., Goldstein, D. B., Hindorff, L. A., Hunter, D. J., . . . Chakravarti, A. (2009). Finding the missing heritability of complex diseases. *Nature, 461*(7265), 747.

Marión, R. M., Strati, K., Li, H., Murga, M., Blanco, R., Ortega, S., . . . Blasco, M. A. (2009). A p53-mediated DNA damage response limits reprogramming to ensure iPS cell genomic integrity. *Nature, 460*(7259), 1149.

Matigian, N., Abrahamsen, G., Sutharsan, R., Cook, A. L., Vitale, A. M., Nouwens, A., . . . Mackay-Sim, A. (2010). Disease-specific, neurosphere-derived cells as models for brain disorders. *Disease Models & Mechanisms, 3*(11-12), 785-798. doi:10.1242/dmm.005447 [doi]

Mattai, A. A., Weisinger, B., Greenstein, D., Stidd, R., Clasen, L., Miller, R., . . . Gogtay, N. (2011). Normalization of cortical gray matter deficits in nonpsychotic siblings of patients with childhood-onset schizophrenia. *Journal of the American Academy of Child & Adolescent Psychiatry, 50*(7), 697-704.

Mattson, M. P., Keller, J. N., & Begley, J. G. (1998). Evidence for synaptic apoptosis. *Experimental Neurology, 153*(1), 35-48.

Maugis, B., Brugues, J., Nassoy, P., Guillen, N., Sens, P., & Amblard, F. (2010). Dynamic instability of the intracellular pressure drives bleb-based motility. *Journal of Cell Science, 123*(Pt 22), 3884-3892. doi:10.1242/jcs.065672 [doi]

Mazumder, B., Seshadri, V., & Fox, P. L. (2003). Translational control by the 3'-UTR: The ends specify the means. *Trends in Biochemical Sciences, 28*(2), 91-98.

McCurdy, R. D., Féron, F., Perry, C., Chant, D. C., McLean, D., Matigian, N., . . . Mackay-Sim, A. (2006). Cell cycle alterations in biopsied olfactory neuroepithelium in schizophrenia

and bipolar I disorder using cell culture and gene expression analyses. *Schizophrenia Research, 82*(2-3), 163-173.

McGrath, J. J., Féron, F. P., Burne, T. H., Mackay-Sim, A., & Eyles, D. W. (2003). The neurodevelopmental hypothesis of schizophrenia: A review of recent developments. *Annals of Medicine, 35*(2), 86-93.

Mednick, S. A., Machon, R. A., Huttunen, M. O., & Bonett, D. (1988). Adult schizophrenia following prenatal exposure to an influenza epidemic. *Archives of General Psychiatry, 45*(2), 189-192.

Méndez-Ferrer, S., Michurina, T. V., Ferraro, F., Mazloom, A. R., MacArthur, B. D., Lira, S. A., . . . Frenette, P. S. (2010). Mesenchymal and haematopoietic stem cells form a unique bone marrow niche. *Nature, 466*(7308), 829.

Menezes, J. R., & Luskin, M. B. (1994). Expression of neuron-specific tubulin defines a novel population in the proliferative layers of the developing telencephalon. *The Journal of Neuroscience : The Official Journal of the Society for Neuroscience, 14*(9), 5399-5416.

Mertens, J., Marchetto, M. C., Bardy, C., & Gage, F. H. (2016). Evaluating cell reprogramming, differentiation and conversion technologies in neuroscience. *Nature Reviews Neuroscience, 17*(7), 424.

Mescher, A. L. (2013). *Junqueira's basic histology: Text and atlas* Mcgraw-hill.

Messias, E. L., Chen, C., & Eaton, W. W. (2007). Epidemiology of schizophrenia: Review of findings and myths. *Psychiatric Clinics of North America, 30*(3), 323-338.

Missler, M., Zhang, W., Rohlmann, A., Kattenstroth, G., Hammer, R. E., Gottmann, K., & Südhof, T. C. (2003). A-neurexins couple ca 2 channels to synaptic vesicle exocytosis. *Nature, 423*(6943), 939.

Miyoshi, K., Honda, A., Baba, K., Taniguchi, M., Oono, K., Fujita, T., . . . Tohyama, M. (2003). Disrupted-in-schizophrenia 1, a candidate gene for schizophrenia, participates in neurite outgrowth. *Molecular Psychiatry, 8*(7), 685.

Moberg, P. J., Agrin, R., Gur, R. E., Gur, R. C., Turetsky, B. I., & Doty, R. L. (1999). Olfactory dysfunction in schizophrenia: A qualitative and quantitative review. *Neuropsychopharmacology, 21*(3), 325-340.

Muhia, M., Yee, B. K., Feldon, J., Markopoulos, F., & Knuesel, I. (2010). Disruption of hippocampus-regulated behavioural and cognitive processes by heterozygous constitutive deletion of SynGAP. *European Journal of Neuroscience, 31*(3), 529-543.

Murray, R. M., & Lewis, S. W. (1987). Is schizophrenia a neurodevelopmental disorder? *British Medical Journal (Clinical Research Ed.), 295*(6600), 681-682.

Murray, R. M., Bhavsar, V., Tripoli, G., & Howes, O. (2017). 30 years on: How the neurodevelopmental hypothesis of schizophrenia morphed into the developmental risk factor model of psychosis. *Schizophrenia Bulletin, 43*(6), 1190-1196.

Murrell, W., Bushell, G. R., Livesey, J., McGrath, J., MacDonald, K. P., Bates, P. R., & Mackay-Sim, A. (1996). Neurogenesis in adult human. *Neuroreport, 7*(6), 1189-1194.

Murrell, W., Féron, F., Wetzig, A., Cameron, N., Splatt, K., Bellette, B., . . . Mackay-Sim, A. (2005). Multipotent stem cells from adult olfactory mucosa. *Developmental Dynamics, 233*(2), 496-515.

Murrell, W., Wetzig, A., Donnellan, M., Féron, F., Burne, T., Meedeniya, A., . . . Silburn, P. (2008). Olfactory mucosa is a potential source for autologous stem cell therapy for parkinson's disease. *Stem Cells, 26*(8), 2183-2192.

Naisbitt, S., Kim, E., Tu, J. C., Xiao, B., Sala, C., Valtschanoff, J., . . . Sheng, M. (1999). Shank, a novel family of postsynaptic density proteins that binds to the NMDA receptor/PSD-95/GKAP complex and cortactin. *Neuron, 23*(3), 569-582.

Ng, S., Lin, L., Soh, B. S., & Stanton, L. W. (2013). Long noncoding RNAs in development and disease of the central nervous system. *Trends in Genetics, 29*(8), 461-468.

Nguyen, A. D., Shenton, M. E., & Levitt, J. J. (2010). Olfactory dysfunction in schizophrenia: A review of neuroanatomy and psychophysiological measurements. *Harvard Review of Psychiatry, 18*(5), 279-292.

Nicoll, R. A. (2017). A brief history of long-term potentiation. *Neuron, 93*(2), 281-290.

Noelia, A., & Castrillo, A. (2011). Liver X receptors as regulators of macrophage inflammatory and metabolic pathways. *Biochimica Et Biophysica Acta (BBA)-Molecular Basis of Disease, 1812*(8), 982-994.

O'Dushlaine, C., Kenny, E., Heron, E., Donohoe, G., Gill, M., Morris, D., & Corvin, A. (2011). Molecular pathways involved in neuronal cell adhesion and membrane scaffolding

contribute to schizophrenia and bipolar disorder susceptibility. *Molecular Psychiatry, 16*(3), 286.

Ohnishi, Y., Iwatsuki, K., Ishihara, M., Shikina, T., Shinzawa, K., Moriwaki, T., . . . Kishima, H. (2015). Isolation of human adult olfactory sphere cells as a cell source of neural progenitors. *Stem Cell Research, 15*(1), 23-29.

Ozeki, Y., Tomoda, T., Kleiderlein, J., Kamiya, A., Bord, L., Fujii, K., . . . Snyder, S. H. (2003). Disrupted-in-schizophrenia-1 (DISC-1): Mutant truncation prevents binding to NudE-like (NUDEL) and inhibits neurite outgrowth. *Proceedings of the National Academy of Sciences, 100*(1), 289-294.

Ozkan, E. D., Creson, T. K., Kramár, E. A., Rojas, C., Seese, R. R., Babyan, A. H., . . . Noebels, J. L. (2014). Reduced cognition in Syngap1 mutants is caused by isolated damage within developing forebrain excitatory neurons. *Neuron, 82*(6), 1317-1333.

Pakos-Zebrucka, K., Koryga, I., Mnich, K., Ljujic, M., Samali, A., & Gorman, A. M. (2016). The integrated stress response. *EMBO Reports, 17*(10), 1374-1395. doi:embr.201642195 [pii]

PALAY, S. L. (1956). Synapses in the central nervous system. *The Journal of Biophysical and Biochemical Cytology, 2*(4 Suppl), 193-202.

Pantelis, C., Velakoulis, D., McGorry, P. D., Wood, S. J., Suckling, J., Phillips, L. J., . . . Soulsby, B. (2003). Neuroanatomical abnormalities before and after onset of psychosis: A cross-sectional and longitudinal MRI comparison. *The Lancet, 361*(9354), 281-288.

Pantelis, C., Yücel, M., Wood, S. J., Velakoulis, D., Sun, D., Berger, G., . . . McGorry, P. D. (2005). Structural brain imaging evidence for multiple pathological processes at different stages of brain development in schizophrenia. *Schizophrenia Bulletin, 31*(3), 672-696.

Pardiñas, A. F., Holmans, P., Pocklington, A. J., Escott-Price, V., Ripke, S., Carrera, N., . . . Hamshere, M. L. (2018). Common schizophrenia alleles are enriched in mutation-intolerant genes and in regions under strong background selection. *Nature Genetics, 50*(3), 381.

Parsons, J. T., Horwitz, A. R., & Schwartz, M. A. (2010). Cell adhesion: Integrating cytoskeletal dynamics and cellular tension. *Nature Reviews Molecular Cell Biology, 11*(9), 633.

Patruno, A., Tran, N., Abdelrahim, M., & Brennand, K. (2014). Investigating the mechanisms involved in aberrant neurosphere migration in schizophrenia (784.2). *The FASEB Journal, 28*(1_supplement), 784.2.

Paulsen, B. d. S., Maciel, R. d. M., Galina, A., da Silveira, M. S., Souza, C. d. S., Drummond, H., . . . Massuda, R. (2012). Altered oxygen metabolism associated to neurogenesis of induced pluripotent stem cells derived from a schizophrenic patient. *Cell Transplantation, 21*(7), 1547-1559.

Peykov, S., Berkel, S., Schoen, M., Weiss, K., Degenhardt, F., Strohmaier, J., . . . Nöthen, M. M. (2015). Identification and functional characterization of rare SHANK2 variants in schizophrenia. *Molecular Psychiatry, 20*(12), 1489.

Pfisterer, U., Kirkeby, A., Torper, O., Wood, J., Nelander, J., Dufour, A., . . . Parmar, M. (2011). Direct conversion of human fibroblasts to dopaminergic neurons. *Proceedings of the National Academy of Sciences of the United States of America, 108*(25), 10343-10348. doi:10.1073/pnas.1105135108 [doi]

Pi, H. J., Otmakhov, N., Lemelin, D., De Koninck, P., & Lisman, J. (2010). Autonomous CaMKII can promote either long-term potentiation or long-term depression, depending on the state of T305/T306 phosphorylation. *The Journal of Neuroscience : The Official Journal of the Society for Neuroscience, 30*(26), 8704-8709. doi:10.1523/JNEUROSCI.0133-10.2010 [doi]

Pinto, D., Delaby, E., Merico, D., Barbosa, M., Merikangas, A., Klei, L., . . . Wang, Z. (2014). Convergence of genes and cellular pathways dysregulated in autism spectrum disorders. *The American Journal of Human Genetics, 94*(5), 677-694.

Pocklington, A. J., Rees, E., Walters, J. T., Han, J., Kavanagh, D. H., Chambert, K. D., . . . Kirov, G. (2015). Novel findings from CNVs implicate inhibitory and excitatory signaling complexes in schizophrenia. *Neuron, 86*(5), 1203-1214.

Purcell, S. M., Moran, J. L., Fromer, M., Ruderfer, D., Solovieff, N., Roussos, P., . . . Kähler, A. (2014). A polygenic burden of rare disruptive mutations in schizophrenia. *Nature, 506*(7487), 185.

Qureshi, I. A., Mattick, J. S., & Mehler, M. F. (2010). Long non-coding RNAs in nervous system function and disease. *Brain Research, 1338*, 20-35.

Rapoport, J. L., Giedd, J. N., & Gogtay, N. (2012). Neurodevelopmental model of schizophrenia: Update 2012. *Molecular Psychiatry, 17*(12), 1228.

Rapoport, J. L., Addington, A. M., Frangou, S., & Psych, M. (2005). The neurodevelopmental model of schizophrenia: Update 2005. *Molecular Psychiatry, 10*(5), 434-449.

Redon, R., Ishikawa, S., Fitch, K. R., Feuk, L., Perry, G. H., Andrews, T. D., . . . Chen, W. (2006). Global variation in copy number in the human genome. *Nature, 444*(7118), 444.

Rees, E., Walters, J. T., Georgieva, L., Isles, A. R., Chambert, K. D., Richards, A. L., . . . McCarroll, S. A. (2014). Analysis of copy number variations at 15 schizophrenia-associated loci. *The British Journal of Psychiatry, 204*(2), 108-114.

Ripke, S., Neale, B. M., Corvin, A., Walters, J. T., Farh, K., Holmans, P. A., . . . Huang, H. (2014). Biological insights from 108 schizophrenia-associated genetic loci. *Nature, 511*(7510), 421.

Robicsek, O., Karry, R., Petit, I., Salman-Kesner, N., Müller, F. J., Klein, E., . . . Ben-Shachar, D. (2013). Abnormal neuronal differentiation and mitochondrial dysfunction in hair follicle-derived induced pluripotent stem cells of schizophrenia patients. *Molecular Psychiatry, 18*(10), 1067.

Rothenburg, S., Seo, E. J., Gibbs, J. S., Dever, T. E., & Dittmar, K. (2009). Rapid evolution of protein kinase PKR alters sensitivity to viral inhibitors. *Nature Structural & Molecular Biology, 16*(1), 63.

Roussos, P., Guennewig, B., Kaczorowski, D. C., Barry, G., & Brennand, K. J. (2016). Activity-dependent changes in gene expression in schizophrenia human-induced pluripotent stem cell neurons. *JAMA Psychiatry, 73*(11), 1180-1188.

Rujescu, D., Ingason, A., Cichon, S., Pietiläinen, O. P., Barnes, M. R., Toulopoulou, T., . . . Bramon, E. (2008). Disruption of the neurexin 1 gene is associated with schizophrenia. *Human Molecular Genetics, 18*(5), 988-996.

Saha, S., Chant, D., Welham, J., & McGrath, J. (2005). A systematic review of the prevalence of schizophrenia. *PLoS Medicine, 2*(5), e141.

Saif, M. T. A., Sager, C. R., & Coyer, S. (2003). Functionalized biomicroelectromechanical systems sensors for force response study at local adhesion sites of single living cells on substrates. *Annals of Biomedical Engineering, 31*(8), 950-961.

Sanders, A. R., Duan, J., Levinson, D. F., Shi, J., He, D., Hou, C., . . . Olincy, A. (2008). No significant association of 14 candidate genes with schizophrenia in a large european ancestry sample: Implications for psychiatric genetics. *American Journal of Psychiatry, 165*(4), 497-506.

Sanz-Moreno, V., & Marshall, C. J. (2010). The plasticity of cytoskeletal dynamics underlying neoplastic cell migration. *Current Opinion in Cell Biology, 22*(5), 690-696.

Schizophrenia Working Group of the Psychiatric Genomics Consortium. (2014). Biological insights from 108 schizophrenia-associated genetic loci. *Nature, 511*(7510), 421-427.

Schmeisser, M. J., Ey, E., Wegener, S., Bockmann, J., Stempel, A. V., Kuebler, A., . . . Spilker, C. (2012). Autistic-like behaviours and hyperactivity in mice lacking ProSAP1/Shank2. *Nature, 486*(7402), 256.

Schmitt, J. M., Guire, E. S., Saneyoshi, T., & Soderling, T. R. (2005). Calmodulin-dependent kinase kinase/calmodulin kinase I activity gates extracellular-regulated kinase-dependent long-term potentiation. *The Journal of Neuroscience : The Official Journal of the Society for Neuroscience, 25*(5), 1281-1290. doi:25/5/1281 [pii]

Schuman, E. M. (1999). mRNA trafficking and local protein synthesis at the synapse. *Neuron, 23*(4), 645-648. doi:S0896-6273(01)80023-4 [pii]

Sebat, J., Lakshmi, B., Troge, J., Alexander, J., Young, J., Lundin, P., . . . Chi, M. (2004). Large-scale copy number polymorphism in the human genome. *Science, 305*(5683), 525-528.

Sheng, M., & Kim, E. (2000). The shank family of scaffold proteins. *Journal of Cell Science, 113 (Pt 11)*(Pt 11), 1851-1856.

Shi, Y., Kirwan, P., Smith, J., Robinson, H. P., & Livesey, F. J. (2012). Human cerebral cortex development from pluripotent stem cells to functional excitatory synapses. *Nature Neuroscience, 15*(3), 477-486.

Shibayama, A., Cook Jr, E. H., Feng, J., Glanzmann, C., Yan, J., Craddock, N., . . . Sommer, S. S. (2004). MECP2 structural and 3'-UTR variants in schizophrenia, autism and other psychiatric diseases: A possible association with autism. *American Journal of Medical Genetics Part B: Neuropsychiatric Genetics, 128*(1), 50-53.

Singh, T., Kurki, M. I., Curtis, D., Purcell, S. M., Crooks, L., McRae, J., . . . Breen, G. (2016). Rare loss-of-function variants in SETD1A are associated with schizophrenia and developmental disorders. *Nature Neuroscience, 19*(4), 571.

Skamagki, M., Correia, C., Yeung, P., Baslan, T., Beck, S., Zhang, C., . . . Giunta, S. (2017). ZSCAN10 expression corrects the genomic instability of iPSCs from aged donors. *Nature Cell Biology, 19*(9), 1037.

Sommer, I., & Schachner, M. (1981). Monoclonal antibodies (O1 to O4) to oligodendrocyte cell surfaces: An immunocytological study in the central nervous system. *Developmental Biology, 83*(2), 311-327.

Stachowiak, E. K., Benson, C. A., Narla, S. T., Dimitri, A., Chuye, L. B., Dhiman, S., . . . Brennand, K. J. (2017). Cerebral organoids reveal early cortical maldevelopment in schizophrenia—computational anatomy and genomics, role of FGFR1. *Translational Psychiatry, 7*(11), 6.

Sun, D., Phillips, L., Velakoulis, D., Yung, A., McGorry, P. D., Wood, S. J., . . . Cannon, T. D. (2009). Progressive brain structural changes mapped as psychosis develops in 'at risk'individuals. *Schizophrenia Research, 108*(1-3), 85-92.

Sun, Y., Nadal-Vicens, M., Misono, S., Lin, M. Z., Zubiaga, A., Hua, X., . . . Greenberg, M. E. (2001). Neurogenin promotes neurogenesis and inhibits glial differentiation by independent mechanisms. *Cell, 104*(3), 365-376.

Takahashi, K., Tanabe, K., Ohnuki, M., Narita, M., Ichisaka, T., Tomoda, K., & Yamanaka, S. (2007). Induction of pluripotent stem cells from adult human fibroblasts by defined factors. *Cell, 131*(5), 861-872.

Takahashi, K., & Yamanaka, S. (2006). Induction of pluripotent stem cells from mouse embryonic and adult fibroblast cultures by defined factors. *Cell, 126*(4), 663-676.

Takata, A., Ionita-Laza, I., Gogos, J. A., Xu, B., & Karayiorgou, M. (2016). De novo synonymous mutations in regulatory elements contribute to the genetic etiology of autism and schizophrenia. *Neuron, 89*(5), 940-947.

Terayama, K., Kataoka, K., Morichika, K., Orii, H., Watanabe, K., & Mochii, M. (2013). Developmental regulation of locomotive activity in X enopus primordial germ cells. *Development, Growth & Differentiation, 55*(2), 217-228.

Timpl, R., Rohde, H., Robey, P. G., Rennard, S. I., Foidart, J. M., & Martin, G. R. (1979). Laminin--a glycoprotein from basement membranes. *The Journal of Biological Chemistry, 254*(19), 9933-9937.

Tojkander, S., Gateva, G., & Lappalainen, P. (2012). Actin stress fibers--assembly, dynamics and biological roles. *Journal of Cell Science, 125*(Pt 8), 1855-1864. doi:10.1242/jcs.098087 [doi]

Topol, A., English, J. A., Flaherty, E., Rajarajan, P., Hartley, B. J., Gupta, S., . . . Friedman, L. (2015). Increased abundance of translation machinery in stem cell–derived neural progenitor cells from four schizophrenia patients. *Translational Psychiatry, 5*(10), e662.

Topol, A., Zhu, S., Hartley, B. J., English, J., Hauberg, M. E., Tran, N., . . . Johnson, J. (2016). Dysregulation of miRNA-9 in a subset of schizophrenia patient-derived neural progenitor cells. *Cell Reports, 15*(5), 1024-1036.

Topol, A., Zhu, S., Tran, N., Simone, A., Fang, G., & Brennand, K. J. (2015). Altered WNT signaling in human induced pluripotent stem cell neural progenitor cells derived from four schizophrenia patients. *Biological Psychiatry, 78*(6), e34.

Tsokas, P., Ma, T., Iyengar, R., Landau, E. M., & Blitzer, R. D. (2007). Mitogen-activated protein kinase upregulates the dendritic translation machinery in long-term potentiation by controlling the mammalian target of rapamycin pathway. *The Journal of Neuroscience : The Official Journal of the Society for Neuroscience, 27*(22), 5885-5894. doi:27/22/5885 [pii]

Velakoulis, D., Wood, S. J., McGorry, P. D., & Pantelis, C. (2000). Evidence for progression of brain structural abnormalities in schizophrenia: Beyond the neurodevelopmental model. *Australian and New Zealand Journal of Psychiatry, 34*(sup2), S126.

Veron, A. D., Bienboire-Frosini, C., Feron, F., Codecasa, E., Deveze, A., Royer, D., . . . Chabaud, C. (2018). Isolation and characterization of olfactory ecto-mesenchymal stem cells from eight mammalian genera. *BMC Veterinary Research, 14*(1), 17.

Vierbuchen, T., Ostermeier, A., Pang, Z. P., Kokubu, Y., Südhof, T. C., & Wernig, M. (2010). Direct conversion of fibroblasts to functional neurons by defined factors. *Nature, 463*(7284), 1035.

Volpato, V., Smith, J., Sandor, C., Ried, J. S., Baud, A., Handel, A., . . . Whiteley, E. (2018). Reproducibility of molecular phenotypes after long-term differentiation to human iPSC-derived neurons: A multi-site omics study. *Stem Cell Reports, 11*(4), 897-911.

Walkup IV, W. G., Mastro, T. L., Schenker, L. T., Vielmetter, J., Hu, R., Iancu, A., . . . Kennedy, M. B. (2016). A model for regulation by SynGAP-α1 of binding of synaptic proteins to PDZ-domain'slots' in the postsynaptic density. *Elife, 5*, e16813.

Walterfang, M., McGuire, P. K., Yung, A. R., Phillips, L. J., Velakoulis, D., Wood, S. J., . . . Soulsby, B. (2008). White matter volume changes in people who develop psychosis. *The British Journal of Psychiatry, 193*(3), 210-215.

Wang, C., Held, R. G., Chang, S., Yang, L., Delpire, E., Ghosh, A., & Hall, B. J. (2011). A critical role for GluN2B-containing NMDA receptors in cortical development and function. *Neuron, 72*(5), 789-805.

Wang, C., Held, R. G., & Hall, B. J. (2013). SynGAP regulates protein synthesis and homeostatic synaptic plasticity in developing cortical networks. *PloS One, 8*(12), e83941.

Wapinski, O. L., Vierbuchen, T., Qu, K., Lee, Q. Y., Chanda, S., Fuentes, D. R., . . . Neff, N. F. (2013). Hierarchical mechanisms for direct reprogramming of fibroblasts to neurons. *Cell, 155*(3), 621-635.

Wechsler, D. (1999). *Wechsler abbreviated scale of intelligence* Psychological Corporation.

Weinberger, D. R. (1987). Implications of normal brain development for the pathogenesis of schizophrenia. *Archives of General Psychiatry, 44*(7), 660-669.

Wen, Z., Nguyen, H. N., Guo, Z., Lalli, M. A., Wang, X., Su, Y., . . . Zhang, C. (2014). Synaptic dysregulation in a human iPS cell model of mental disorders. *Nature, 515*(7527), 414-418.

White, T., Ho, B., Ward, J., O'Leary, D., & Andreasen, N. C. (2006). Neuropsychological performance in first-episode adolescents with schizophrenia: A comparison with first-episode adults and adolescent control subjects. *Biological Psychiatry, 60*(5), 463-471.

Windrem, M. S., Osipovitch, M., Liu, Z., Bates, J., Chandler-Militello, D., Zou, L., . . . Miller, R. H. (2017). Human iPSC glial mouse chimeras reveal glial contributions to schizophrenia. *Cell Stem Cell, 21*(2), 208. e6.

Wolozin, B., Lesch, P., Lebovics, R., & Sunderland, T. (1993). Olfactory neuroblasts from alzheimer donors: Studies on APP processing and cell regulation. *Biological Psychiatry, 34*(12), 824-838.

Won, H., Lee, H., Gee, H. Y., Mah, W., Kim, J., Lee, J., . . . Cho, Y. S. (2012). Autistic-like social behaviour in Shank2-mutant mice improved by restoring NMDA receptor function. *Nature, 486*(7402), 261.

Worley, P. (1998). Making proteins at the synapse: Activity-regulated translation and CPEB. *Neuron, 21*(5), 936-938. doi:S0896-6273(00)80609-1 [pii]

Xie, L., Zeng, X., Hu, J., & Chen, Q. (2015). Characterization of nestin, a selective marker for bone marrow derived mesenchymal stem cells. *Stem Cells International, 2015*, 762098. doi:10.1155/2015/762098 [doi]

Xue, Y., Ouyang, K., Huang, J., Zhou, Y., Ouyang, H., Li, H., . . . Bi, Y. (2013). Direct conversion of fibroblasts to neurons by reprogramming PTB-regulated microRNA circuits. *Cell, 152*(1), 82-96.

Yanase, Y., Carvou, N., Frohman, M. A., & Cockcroft, S. (2010). Reversible bleb formation in mast cells stimulated with antigen is Ca2 /calmodulin-dependent and bleb size is regulated by ARF6. *Biochemical Journal, 425*(1), 179-193.

Yang, Y., Tao-Cheng, J., Reese, T. S., & Dosemeci, A. (2011). SynGAP moves out of the core of the postsynaptic density upon depolarization. *Neuroscience, 192*, 132-139.

Yao, I., Hata, Y., Hirao, K., Deguchi, M., Ide, N., Takeuchi, M., & Takai, Y. (1999). Synamon, a novel neuronal protein interacting with synapse-associated protein 90/postsynaptic density-95-associated protein. *The Journal of Biological Chemistry, 274*(39), 27463-27466.

Ying, S. W., Futter, M., Rosenblum, K., Webber, M. J., Hunt, S. P., Bliss, T. V., & Bramham, C. R. (2002). Brain-derived neurotrophic factor induces long-term potentiation in intact adult hippocampus: Requirement for ERK activation coupled to CREB and upregulation of arc synthesis. *The Journal of Neuroscience : The Official Journal of the Society for Neuroscience, 22*(5), 1532-1540. doi:22/5/1532 [pii]

Yoon, K., Nguyen, H. N., Ursini, G., Zhang, F., Kim, N., Wen, Z., . . . Park, Y. (2014). Modeling a genetic risk for schizophrenia in iPSCs and mice reveals neural stem cell deficits associated with adherens junctions and polarity. *Cell Stem Cell, 15*(1), 79-91.

Yoshida, Y., & Yamanaka, S. (2017). Induced pluripotent stem cells 10 years later: For cardiac applications. *Circulation Research, 120*(12), 1958-1968.

Yu, D. X., Di Giorgio, F. P., Yao, J., Marchetto, M. C., Brennand, K., Wright, R., . . . Grasmick, J. M. (2014). Modeling hippocampal neurogenesis using human pluripotent stem cells. *Stem Cell Reports, 2*(3), 295-310.

Yu, J., Vodyanik, M. A., Smuga-Otto, K., Antosiewicz-Bourget, J., Frane, J. L., Tian, S., . . . Thomson, J. A. (2007). Induced pluripotent stem cell lines derived from human somatic cells. *Science (New York, N.Y.), 318*(5858), 1917-1920. doi:1151526 [pii]

Zarrei, M., MacDonald, J. R., Merico, D., & Scherer, S. W. (2015). A copy number variation map of the human genome. *Nature Reviews Genetics, 16*(3), 172.

Zeng, M., Bai, G., & Zhang, M. (2017). Anchoring high concentrations of SynGAP at postsynaptic densities via liquid-liquid phase separation. *Small GTPases,* , 1-9.

Zeng, M., Chen, X., Guan, D., Xu, J., Wu, H., Tong, P., & Zhang, M. (2018). Reconstituted postsynaptic density as a molecular platform for understanding synapse formation and plasticity. *Cell, 174*(5), 1187. e16.

Zhang, X., Klueber, K. M., Guo, Z., Cai, J., Lu, C., Winstead, W. I., . . . Roisen, F. J. (2006). Induction of neuronal differentiation of adult human olfactory neuroepithelial-derived progenitors. *Brain Research, 1073*, 109-119.

Zhang, Y., Pak, C., Han, Y., Ahlenius, H., Zhang, Z., Chanda, S., . . . Covy, J. (2013). Rapid single-step induction of functional neurons from human pluripotent stem cells. *Neuron, 78*(5), 785-798.

Zhao, D., Lin, M., Chen, J., Pedrosa, E., Hrabovsky, A., Fourcade, H. M., . . . Lachman, H. M. (2015). MicroRNA profiling of neurons generated using induced pluripotent stem cells derived from patients with schizophrenia and schizoaffective disorder, and 22q11. 2 del. *PLoS One, 10*(7), e0132387.

Zhao, Z., Xu, J., Chen, J., Kim, S., Reimers, M., Bacanu, S., . . . Wang, Q. (2015). Transcriptome sequencing and genome-wide association analyses reveal lysosomal function and actin cytoskeleton remodeling in schizophrenia and bipolar disorder. *Molecular Psychiatry, 20*(5), 563.

Zhu, X., Need, A. C., Petrovski, S., & Goldstein, D. B. (2014). One gene, many neuropsychiatric disorders: Lessons from mendelian diseases. *Nature Neuroscience, 17*(6), 773.

Appendix I: Speculations on the links between basic stem cell properties and the cellular neuropathology of schizophrenia

Grey matter volume reductions and white matter connectivity reductions are the most reproducible macroscopic neuropathology of schizophrenia. Recent evidences from multiple lines suggest the brain volume reductions associated with schizophrenia are rooted in early brain development and are not likely caused by confounding factors (see the chapter *General Introduction* for details and review paper Rapoport et al., 2012 for further reading). Microscopically, the most consistent neuropathological findings are reduced neuron volume and spine/synapsis density in the prefrontal regions and the hippocampi (see recent review Bakhshi & Chance, 2015 for details). The exact mechanisms behind the brain volume reductions in schizophrenia remain completely unknown. In this chapter, an attempt of bridging stem cell properties and the origins of neuropathology of schizophrenia is given, with the aims of identifying plausible hypotheses and next steps of study.

From a cell biology perspective, what could be the cellular causes of the widely observed brain volume reductions? Theoretically, the possibilities largely are: 1) increased cell death in the brain, 2) reduced cell proliferation in the brain, 3) reduced volume of individual cells in the brain associated with neurite atrophy. The molecular basis behind the possible cellular causes of reduced brain volume will be discussed later.

Could brain volume reduction in schizophrenia be caused by increased cell death?

First, increased cell death is not likely to be the cause of reduced brain volume. Several studies using post-mortem brains addressed this question; most of them used small sample sizes and reported regional reduction in neuronal number which did not reach significance (Dorph-Petersen, Pierri, Wu, Sampson, & Lewis, 2007; Falkai, Bogerts, & Rozumek, 1988; Krimer et al., 1997; Pakkenberg, 1993; Schmitt, A. et al., 2009; Stark, Uylings, Sanz-Arigita, & Pakkenberg, 2004; Thune, Uylings, & Pakkenberg, 2001). Furthermore, regional reductions in the numbers of excitatory or inhibitory neurons are insufficient to explain global brain volume reduction. Indeed, a study that examined global cortical neuron numbers in post-mortem brains from patients with schizophrenia did not find any significant difference in neuron numbers between patients and controls (Dorph-Petersen et al., 2007). However, to what extent glial populations may contribute to volume reduction is unclear. Evidence so far is limited to small groups of patients. For example, decreased numbers of oligodendrocytes were reported from a group of patients who committed suicide (Honer et al., 1999). In a separate study, a reduced number of oligodendrocytes was observed in the prefrontal cortex and its underlying white matter (Black et al., 2004; Hof et al., 2003). Most studies also reported no change in the number of astrocytes (Bakhshi & Chance, 2015), further suggesting that neurodegeneration-induced inflammation is not seen in schizophrenia. A post-mortem study that directly measured the level of caspase-3 also did not find significant differences between patients and controls in the temporal cerebral cortex (Jarskog, Selinger, Lieberman, & Gilmore, 2004). On the contrary, a recent study using human reprogrammed glial progenitor cells implanted in myelination-deficient mice showed significant reduction in the number of oligodendrocytes that remain in white matter (Windrem et al., 2017). As well

myelination levels and astrocyte maturation, decreased when using glial progenitor cells derived from patients with child-onset schizophrenia, compared to healthy controls (Windrem et al., 2017). The authors further showed that the patient-derived glial progenitor cells failed to recognise local stop signals in the developing white matter, in a cell-autonomous manner, hence prematurely migrating into the cortex and resulting in a hypomyelination of central nervous system white matter structures. This hypomyelination was worsened by the hampered astrocytic maturation However, the question of why the global glia phenotypes observed in this rodent-human chimeric model was not reflected by global abnormalities of glia in post-mortem brains remains to be elucidated. Future research addressing the impact of signals from human neuronal and microglia populations during development on human glia progenitor cells in the context of schizophrenia may fill this gap. Taken together, the widely observed brain volume reduction in schizophrenia is not likely to be a result of increased neuronal death. Insightful new findings from a rodent-human chimeric model suggests a reduced number of oligodendrocytes during brain development, however future studies are still necessary to thoroughly validate oligodendrocytes in a human system.

Could brain volume reduction in schizophrenia be caused by decreased cell proliferation?

The second hypothetical cellular cause for reduced brain volume in schizophrenia is reduced cell proliferation. Based on evidence from post-mortem studies, the total number of cortical neurons was not reduced in schizophrenia (Dorph-Petersen et al., 2007). Nor were overall differences observed in the number of astrocytes or oligodendrocytes. Therefore, if reduced cell proliferation in the brain is responsible for the reduced brain volume, is it not likely to happen during embryonic development, during which the vast majority of brain cells are generated in humans. If that were the case, there should be an overall reduction in cell numbers in patient brains. Apart from embryonic neurogenesis and gliogenesis, two niches in human brains continue to generate new neurons throughout life; the subventricular zone (SVZ) lining the lateral walls of lateral ventricles (Ernst et al., 2014; Sanai et al., 2011) and the subgranular zone (SGZ) in the hippocampus (Santos, Southon, Griffin, Beaupre, & Druffel, 2007; Spalding et al., 2013). The functional purpose and duration of post-natal human SVZ neurogenesis has not reached a final agreement at present, although studies suggested new born neurons migrated into prefrontal regions and the striatum (Ernst et al., 2014; Sanai et al., 2011). Studies of adult neurogenesis in schizophrenia therefore have been focusing on the SGZ. A recent study using post-mortem hippocampus tissues from 10 patients and 16 matched controls showed that the density of Marker Of Proliferation Ki-67 (Ki67), a cell proliferation marker, was significantly reduced in patients, and this reduction was not correlated with age (Allen, Fung, & Shannon Weickert, 2016). The study included the dentate gyrus and hilus, the former of which contains a well-established adult neurogenesis niche (Toni et al., 2008; van Praag et al., 2002). This is in line with the previous notion that reduced adult neurogenesis in in hippocampus is associated with schizophrenia (Barbeau, Liang,

Robitalille, Quirion, & Srivastava, 1995; Reif et al., 2006). However, a subgroup of glial cells in the brain, named nerve/glia antigen 2 (NG2) glia, are also present in this region in rodents and are able to proliferate during adulthood (Aguirre, A. & Gallo, 2004; Aguirre, A. A., Chittajallu, Belachew, & Gallo, 2004; Nishiyama, Komitova, Suzuki, & Zhu, 2009; Passlick et al., 2013). Indeed, a study using surgical brain tissues showed almost all cycling cells in the adult human brain co-expressed NG2 and Olig2, indicating that NG2 glia account for a significant proportion of cycling cells even in the dentate gyrus (Geha et al., 2010). It is thus so far unclear to what extend NG2 glia may have contributed to the reduced Ki67 labelling in dentate gyrus of patients with schizophrenia. Nevertheless, the implication of reduced number of cycling cells in the dentate gyrus of adult schizophrenia patients points to interactions between stem cell biology, disease durations and antipsychotic treatments. Although several studied showed that antipsychotic medication can increase, rather than decrease, hippocampal neurogenesis (Keilhoff, Fusar-Poli, & Becker, 2012), it remains difficult at present to determine whether the reduced number of cycling cells is part of the disease aetiology or a result of the disease.

Recently technological developments allow reprogramming of skin cells to stem cells and then differentiation into neural cells from patients to help reveal early developmental events. These cells carry the genetic predispositions of the patients but do not carry the epigenetic marks resulting from environmental insults, prolonged disease durations or antipsychotic treatments. Therefore, reprogrammed neural cells may be used as powerful tools to study causal relationships between strong genetic variances and cellular phenotypes (Dolmetsch & Geschwind, 2011). A recent study used such reprogrammed neural progenitor cells, that resembled *in vivo* first trimester fetal brain tissue. They were derived from a patient with

child-onset schizophrenia, and three patients with adult-onset schizophrenia and did not show any differences in cell proliferation between patients and controls, nor between child-onset cases and adult-onset cases (Brennand, K. et al., 2014). On the contrary, another study using reprogrammed neural stem cells derived from two patients with truncated *DISC1* genes showed reduced proliferation rates of reprogrammed neural stem cells (Murai et al., 2016). However, *DISC1* itself has an essential role in cortical development and is highly expressed during all stages of hippocampal development (Austin, Ky, Ma, Morris, & Shughrue, 2004; Kamiya et al., 2005; Kamiya et al., 2006; Miyoshi et al., 2003; Ozeki et al., 2003; Schurov, Handford, Brandon, & Whiting, 2004). Therefore, the results from two schizophrenia patients with truncating mutations of *DISC1* may not represent the same disease aetiology for a broader patient group. These two studies addressed the question of neural stem/progenitor cell proliferation in 2-dimensional environments, where cell-cell contact was diminished. Instead, cerebral organoids derived from induced pluripotent stem cells offer the opportunity to examine early brain development processes in 3-dimensional, cell-cell contact enriched environments. Cerebral organoids derived from 4 patients with schizophrenia all showed increased number of, and more dispersed patterns of, Ki67+ neural progenitor cells in the equivalent regions of ventricle/subventricle zones in organoids, when compared to that of controls (Stachowiak et al., 2017). These dysregulated neural progenitor cells subsequently migrated prematurely into the equivalent of subcortical regions in organoids, leaving the upper cortical regions a lack of mature neurons. Taken together, evidence from reprogrammed neural stem/progenitor cells remains contradictory. This might be due to the specificity of patient groups used in the studies and the difference between 2-dimensional and 3-dimensional cell culture systems. Importantly, the impact of some important cell types in the brain, including microglia and oligodendrocytes, were not considered due to current

technical limitations. Future methods that allow astrocytes, oligodendrocytes, microglia and blood vessels to interact in physiological patterns in cerebral organoids are necessary to provide comprehensive models of human neurodevelopment.

These results showed that the genetic predispositions patients carry do not always impact on the proliferation of neural stem/progenitor cells, contrasting data that has consistently shown patient brain volumes are reduced. Indeed, meta-analysis of data obtained from post-mortem schizophrenia tissues did not result in any significant universal loss of neurons in any specific brain structures or at the whole brain level (Bakhshi & Chance, 2015). If the reduced number of cycling cells in patient dentate gyrus was indeed due to reduced neurogenesis, what were the molecular mechanisms that pardoned the embryonic neural progenitors cells from reduced proliferation? On the other hand, if the reduced number of cycling cells in patient's dentate gyrus was due to reduced NG2 glia, which serve as stem cells for oligodendrocytes and astrocytes (Dimou & Götz, 2014), why was there no global reduction in the number of glia in patient brains? Furthermore, if embryonic neurogenesis was affected in patients, why were the patients mentally healthy before the first symptoms emerged? These confusing questions reflect the difficulties of studying schizophrenia without a good model. In animal models of schizophrenia, risk genes were usually knocked-down or knocked-out. Several studies have shown associations between the reduced expression of risk genes and hampered adult hippocampal neurogenesis in rodent models (Kang, Wen, Song, Christian, & Ming, 2016). However, the genetic risks born by patients are polygenic and are generally SNPs or CNVs (*Chapter 1*). Removing single risk genes in rodents is likely to simplify the disease processes and over-represent the effects from single genes, therefore leaving the results difficult to interpret in the context of patient disease development. As a summary, so far there

is a lack of concordant evidence showing reduced cell proliferation being associated with reduced volumes of schizophrenia brains.

Could brain volume reduction in schizophrenia be caused by reduced cell volume?

The last hypothetical reason for reduced brain volume in schizophrenia is reduced individual cell volumes. The 'reduced neuropil' hypothesis proposes that the reduced space between neurons, including axons, dendrites and synapses, is responsible for the reduced brain volume in schizophrenia (Selemon & Goldman-Rakic, 1999). The reduced space between neurons could be further broken down to reduced cell sizes, reduced numbers and/or volumes of neurites, reduced spine densities, and reduced synaptic densities.

Neuronal size reduction was reported in the hippocampis and the frontal regions of patient brains. The size of pyramidal neurons was reduced in the hippocampus in three post-mortem studies (Arnold et al., 1995; Benes, McSparren, Bird, SanGiovanni, & Vincent, 1991; Zaidel, Esiri, & Harrison, 1997). Reduced neuronal size was also reported for pyramidal neurons in the dorsal lateral prefrontal cortices of patients, especially for the large layer III neurons (Rajkowska, Selemon, & Goldman-Rakic, 1998). This finding was later replicated (Pierri, Volk, Auh, Sampson, & Lewis, 2001). Pyramidal neurons were also found to be smaller in the auditory association cortices in post-mortem schizophrenia brains (Sweet, Pierri, Auh, Sampson, & Lewis, 2003). Another study that 3-D reconstructed Golgi-stained prefrontal pyramidal neurons found the number of basilar dendrites was significantly reduced in patient neurons compared to control neurons, while the apical dendrites remained the same (Kalus, Muller, Zuschratter, & Senitz, 2000). Apart from excitatory neurons, the number of axon terminals of parvalbumin-immunoreactive interneurons was greatly reduced in the dorsolateral prefrontal cortices and the dorsolateral and medial prefrontal cortices of post-mortem patient brains (Lewis, 2000). Another study reported reduced densities of

parvalbumin-immunoreactive interneurons in dorsolateral prefrontal cortices and the medial temporal cortices of patient brains (Reynolds, Beasley, & Zhang, 2002). Neuronal sizes in other cortical regions such as the visual cortex and the motor cortex were found to be unchanged in patient brains and control brains (Harrison & Weinberger, 2005), indicating that the neuronal size reduction was region-specific. Although the overall neuronal number was not reduced in patient cortices (as previously discussed), reduced numbers of neurons were found in the dorsomedial nuclei and the anteroventral nuclei in patient brains (Danos et al., 1998; Pakkenberg, 1990). Both nuclei mainly project to the prefrontal cortex, raising the possibility of projection loss and therefore neuropil reduction between the nucleus and the prefrontal cortex. This could contribute to the loss of volume in the prefrontal cortex. In summary, size reduction for some pyramidal neurons was found in patient hippocampi and prefrontal regions, neurite number reduction and cell number reduction were found for parvalbumin-immunoreactive interneurons in patient prefrontal regions, and cell loss was found in the deep white matter nuclei that mainly projects to prefrontal regions in patient brains.

Dendritic and synaptic density reduction was reported in hippocampi and frontal regions of patient brains. In patient hippocampi, reduced expression of the neuron-specific dendritic protein MAP2 was shown in some subfields, suggesting the presence of dendritic abnormalities (Arnold, Lee, Gur, & Trojanowski, 1991; Cotter, Kerwin, Doshi, Martin, & Everall, 1997). Imaging studies using proton magnetic resonance spectroscopy showed that the neuronal marker N-acetyl-aspartate (NAA) was significantly reduced in patient hippocampi and DLPFCs (Bertolino, Nawroz, Mattay, & Barnett, 1996; Deicken, R. F., Zhou, Corwin, Vinogradov, & Weiner, 1997; Deicken, Raymond F., Zhou, Schuff, Fein, & Weiner,

1998; Maier, Ron, Barker, & Tofts, 1995). A reduced concentration of NAA in the superior temporal cortices was also found in patient post-mortem brains (Nudmamud, Reynolds, & Reynolds, 2003). The reduced NAA signal was previously reported in medication-free (Bertolino et al., 1998) and first-episode (Renshaw, Yurgelun-Todd, Tohen, Gruber, & Cohen, 1995) patients, suggesting that the cytoarchitectural abnormalities observed in post-mortem patient brains were likely to reflect the disease itself, rather than antipsychotic treatment or prolonged psychosis. Similar to the locations where neuronal size reduction was seen in patient brains, dendritic spine density was found to be specifically reduced in the deep layer III and layer V pyramidal neurons of the prefrontal cortex (Black et al., 2004; Garey et al., 1998; Glantz & Lewis, 2000; Rosoklija et al., 2000). Due to the difficulty of obtaining electron microscopy data on a large scale in the analysis of synapses in schizophrenia brains, the abundance of certain synaptic proteins was used for quantitative analyses. Those synaptic proteins were usually enriched at either pre- or post-synaptic terminals. Synaptophysin is a major presynaptic protein and has been shown as an accurate index of synaptic densities (Calhoun et al., 1996). A recent meta-analysis on synaptic protein expression using post-mortem data showed a significant reduction of synaptophysin in the hippocampi and the frontal regions in patient brains (Osimo, Beck, Marques, & Howes, 2018). Protein abundance of other pre- and post-synaptic proteins was also found to be reduced in patient hippocampi and frontal regions, however the reduction did not reach significance (Harrison & Weinberger, 2005; Osimo et al., 2018). Reductions of synaptic densities were found in other brain regions such as the thalamus and the caudate nucleus in the striatum (Harrison, 1999). However, those regions were thought to be more severely affected by antipsychotic treatments, making it difficult to draw a conclusion based on the limited amount of data.

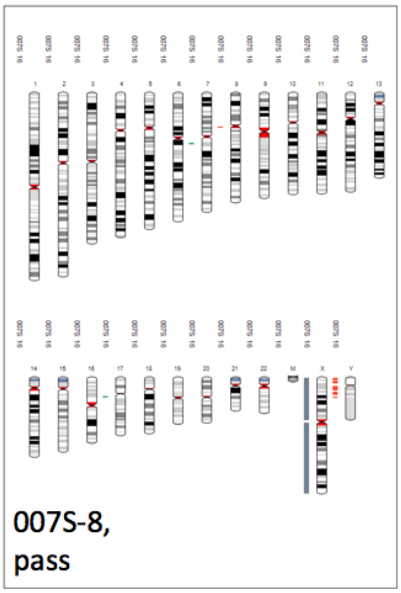
Nevertheless, they generally support the notion that altered synaptic organisation is involved in schizophrenia.

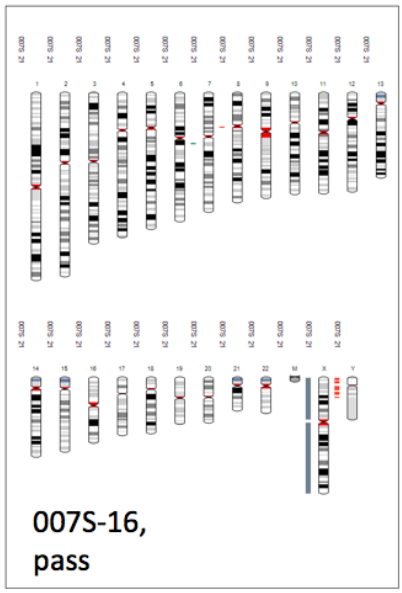
Taken together, the locations of the microscopic findings (reduced neuronal sizes, reduced spine densities and loss of synapses) in post-mortem patient brains interestingly matched with the two well-established locations of macroscopic brain volume reduction in schizophrenia—the hippocampus and the frontal lobe. It is promising to connect the reduced neuropil hypothesis with reduced brain volume findings, however evidence pointing in other directions are still present. For example, two studies examined neuron sizes in the hippocampus and the DLPFC did not find significant difference between patients and controls (Cotter et al., 2002; Highley, Walker, McDonald, Crow, & Esiri, 2003). This suggests that sub-group effects could still be present even though multiple lines of evidence indicated that reduced neuropils should be largely in charge of reduced brain volume. Nevertheless, current results overall support the notion that reduced neuropil could be an important contributing factor, at the cellular level, to the brain volume loss in schizophrenia. Finally, although fairly convincing evidence is available from post-mortem studies, the reduced neuropil hypothesis still needs to be further refined.

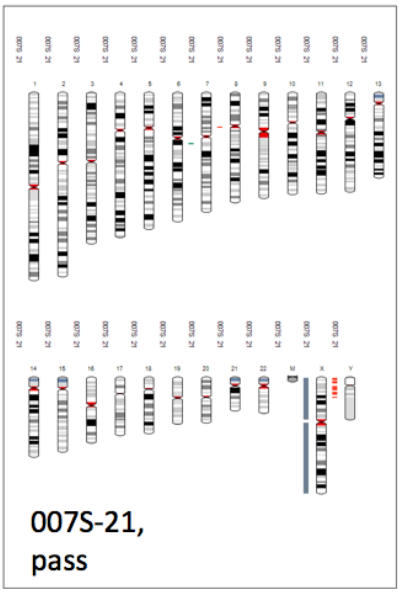
Combining data from real patients based on neuroimaging studies and post-mortem studies, it is becoming more and more encouraging to see the merging of large bodies of evidence in the field of schizophrenia pathology, which was previously considered to be a ‘graveyard of neuropathologists’ (Plum, 1972). However, the question remains of how the microscopic and macroscopic abnormalities in patient brains, particularly in prefrontal regions and hippocampi, could raise and manifest, from apparent ‘healthy’ new-born babies to the time

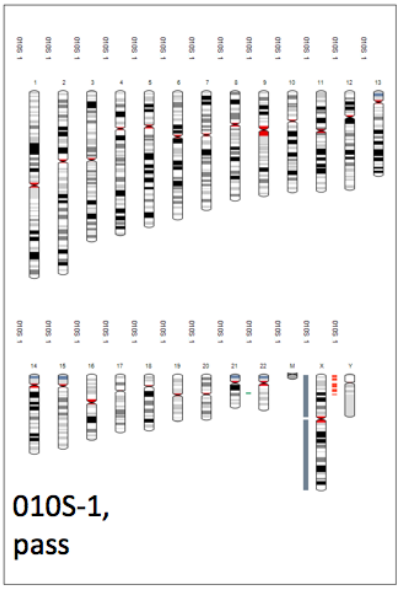
of onset, and eventually to end-point evidences in post-mortem brains. These questions remain to be addressed by studies using multiple approaches that allow patient-relevant disease modelling in temporal- and spatial-relevant manners.

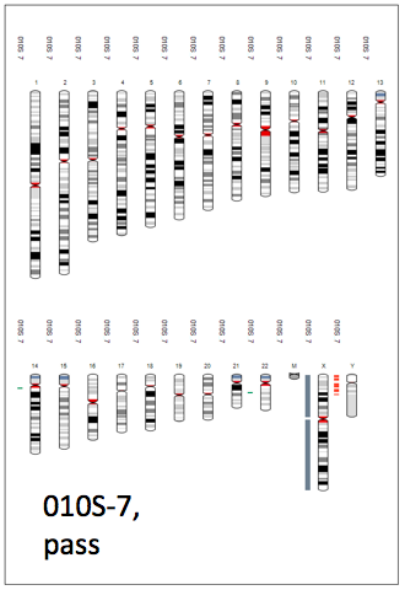
Appendix II: Additional results for genomic integrity assay

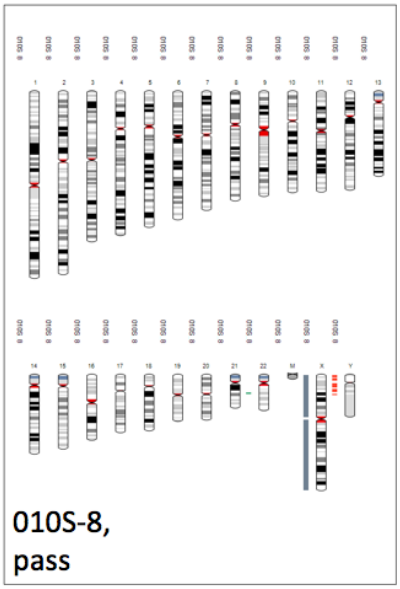












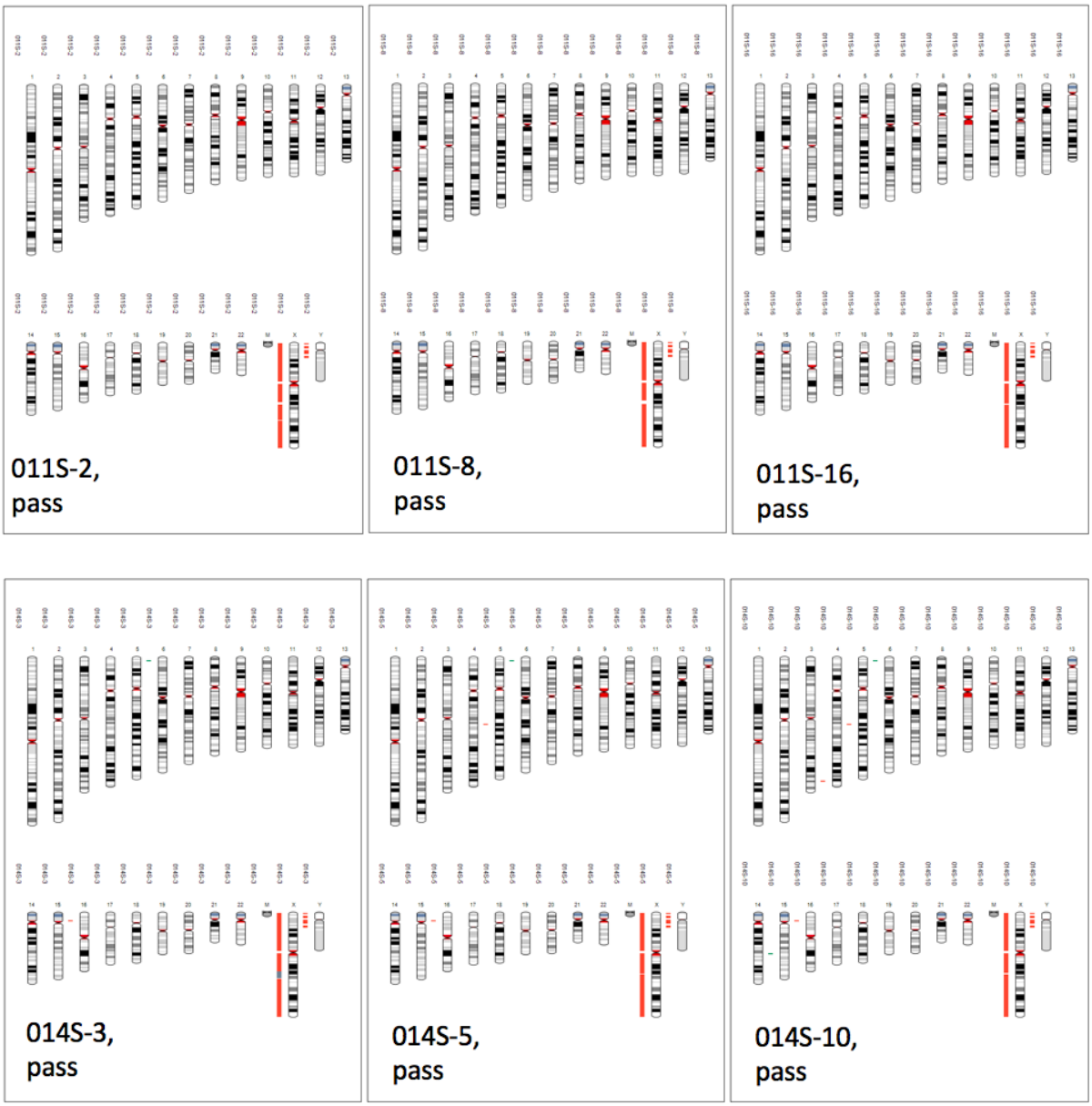


Figure II.1 Additional genomic integrity test results. Results are based on SNP analysis of total DNA. The genomes of iPSC lines were not compared with their parental fibroblasts but compared with isogenic clones. All lines shown here passed the genomic integrity check. Note that the names assigned to individual genomes for 007S-8 and 007S-16 were labelled incorrectly (small letters above each chromosome). Due to the limited access to the analysis software, results with correct labelling were not obtained.

Appendix III: short description of clinical phenotypes (from Anthony James)

Patient ID	Descriptions
001	A-18-year old boy with a 3-year history of schizophrenia with persistent unremitting auditory hallucinations, paranoid delusions and very limited insight. His symptoms improved but did not remain fully on clozapine. He lives in residential care. CGAS score 30.
002	a 17-year-old boy with schizophrenia and experiencing auditory hallucinations of command nature and paranoid beliefs that he was going to be electrocuted. He was admitted to and adolescent psychiatric unit and at one point not eating or drinking due to paranoid beliefs. Improved considerably on clozapine. CGAS on discharge 45.
003	A 17-year-old girl admitted to a psychiatric inpatient unit following behavioral disturbance in response to paranoid beliefs about her family and continuous command hallucinations. She remained violent and unresponsive to 2 courses of antipsychotic medication but responded well to clozapine allowing discharge to home, CGAS on discharge 50.
004	17-year-old girl who was detained in forensic adolescent service because of severe non-response schizophrenia associated with violence. Treated with a combination of clozapine and a course of ECT but required prolonged admission to adult psychiatric services. CGAS on discharge 35.
005	17-year-old girl with paranoid symptoms and some auditory hallucinations of a mild nature which remitted with antipsychotic medication. CGAS on discharge 55.
006	15-year-old girl with paranoid symptoms and auditory hallucinations, which remitted with antipsychotic medication. CGAS on discharge 55.

009 17-year-old girl with FEP diagnosed as having schizophrenia. CGAS on discharge 50.

015 14-year-old boy with schizophrenia who had persistent auditory command hallucinations who responded well to amisulpride. CGAS on discharge 53.

017 17-year-old boy with schizophrenia, experiencing auditory hallucinations of a command nature and paranoid beliefs. On admission to an adolescent psychiatric unit he was treated and had a good response to clozapine and he was discharged home. CGAS on discharge 48.

018 16-year-old girl with schizophrenia who responded well to treatment with clozapine CGAS on discharge 50.

019 17-year-old boy with schizophrenia who responded well to treatment with clozapine CGAS on discharge 52.

020 16-year-old boy with childhood onset schizophrenia and continuous command hallucinations and borderline intellectual functions who responded to clozapine. He was discharged to a specialist day school. CGAS on discharge 40.